frontiers | Research Topics

SARS-cov-2 variants, B lymphocytes, and autoreactivity

Edited by
Moncef Zouali and Marko Radic

Published in
Frontiers in Immunology

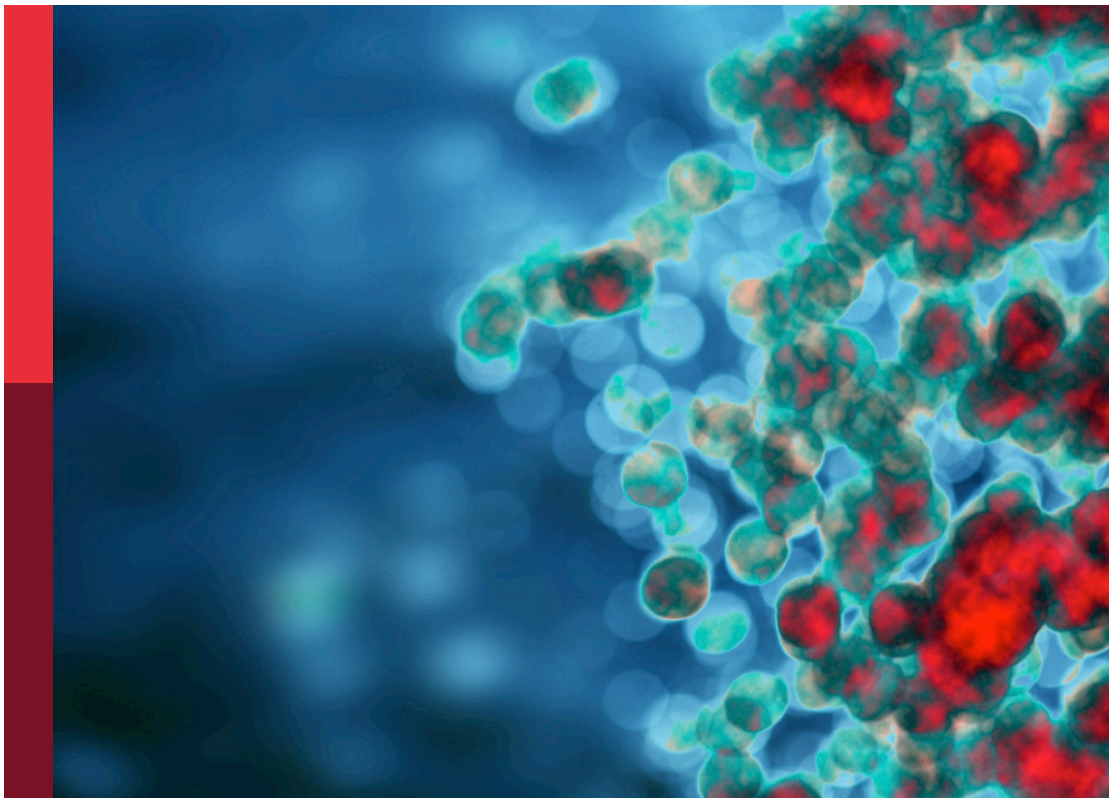

ISSN 1664-8714
ISBN 978-2-83251-430-6
DOI 10.3389/978-2-83251-430-6

About Frontiers

Frontiers is more than just an open access publisher of scholarly articles: it is a pioneering approach to the world of academia, radically improving the way scholarly research is managed. The grand vision of Frontiers is a world where all people have an equal opportunity to seek, share and generate knowledge. Frontiers provides immediate and permanent online open access to all its publications, but this alone is not enough to realize our grand goals.

Frontiers journal series

The Frontiers journal series is a multi-tier and interdisciplinary set of open-access, online journals, promising a paradigm shift from the current review, selection and dissemination processes in academic publishing. All Frontiers journals are driven by researchers for researchers; therefore, they constitute a service to the scholarly community. At the same time, the *Frontiers journal series* operates on a revolutionary invention, the tiered publishing system, initially addressing specific communities of scholars, and gradually climbing up to broader public understanding, thus serving the interests of the lay society, too.

Dedication to quality

Each Frontiers article is a landmark of the highest quality, thanks to genuinely collaborative interactions between authors and review editors, who include some of the world's best academicians. Research must be certified by peers before entering a stream of knowledge that may eventually reach the public - and shape society; therefore, Frontiers only applies the most rigorous and unbiased reviews. Frontiers revolutionizes research publishing by freely delivering the most outstanding research, evaluated with no bias from both the academic and social point of view. By applying the most advanced information technologies, Frontiers is catapulting scholarly publishing into a new generation.

What are Frontiers Research Topics?

Frontiers Research Topics are very popular trademarks of the *Frontiers journals series*: they are collections of at least ten articles, all centered on a particular subject. With their unique mix of varied contributions from Original Research to Review Articles, Frontiers Research Topics unify the most influential researchers, the latest key findings and historical advances in a hot research area.

Find out more on how to host your own Frontiers Research Topic or contribute to one as an author by contacting the Frontiers editorial office: frontiersin.org/about/contact

SARS-CoV-2 variants, B lymphocytes, and autoreactivity

Topic editors

Moncef Zouali — Institut National de la Santé et de la Recherche Médicale (INSERM), France

Marko Radic — University of Tennessee College of Medicine, United States

Citation

Zouali, M., Radic, M., eds. (2023). *SARS-CoV-2 variants, B lymphocytes, and autoreactivity*. Lausanne: Frontiers Media SA. doi: 10.3389/978-2-83251-430-6

Table of contents

frontiers | Frontiers in Immunology

TYPE Editorial
PUBLISHED 10 January 2023
DOI 10.3389/fimmu.2022.1125732

OPEN ACCESS

EDITED AND REVIEWED BY
Annalisa Ciabattini,
University of Siena, Italy

*CORRESPONDENCE
Moncef Zouali
moncef.zouali@wanadoo.fr
Marko Z. Radic
mradic@uthsc.edu

SPECIALTY SECTION
This article was submitted to B Cell Biology, a section of the journal Frontiers in Immunology

RECEIVED 16 December 2022
ACCEPTED 22 December 2022
PUBLISHED 10 January 2023

CITATION
Radic MZ and Zouali M (2023) Editorial: SARS-CoV-2 variants, B lymphocytes, and autoreactivity. *Front. Immunol.* 13:1125732. doi: 10.3389/fimmu.2022.1125732

Editorial: SARS-CoV-2 variants, B lymphocytes, and autoreactivity

Marko Z. Radic[1]* and Moncef Zouali[2]*

[1]University of Tennessee, College of Medicine, Memphis, TN, United States, [2]Graduate Institute of Biomedical Sciences, China Medical University, Taichung City, Taiwan

KEYWORDS

B cell, COVID - 19, memory, antibody repertoire analysis, variable gene selection

Editorial on the Research Topic
SARS-CoV-2 variants, B lymphocytes, and autoreactivity

Since its identification in 2019, SARS-CoV-2 has caused the ongoing COVID-19 pandemic that resulted in over six 6 million deaths worldwide. Similar to other Coronaviruses, infections with SARS-CoV-2 progresses in a multistep manner that involves cleavage and rearrangement of the surface spike protein (S) that uses the receptor binding domain (RBD) to engage angiotensin-converting enzyme 2 (ACE2) on target cells (1). The rapid evolution of SARS-CoV-2 and the emergence of variants of concern (VOC), such as the omicron (B.1.1.529) mutant, represent challenges for the immune system, with implications for designing potent vaccines and developing therapeutic antibodies. Articles in this Research Topic shine a light on the B cell responses mounted by the immune system to cope with infection to, and vaccination against SARS-CoV-2.

Antigenic cartography and dynamic changes

SARS-CoV-2 variants exhibit characteristic mutations in the S protein, including the RBD, which represents an immunodominant part of the S protein and is targeted by a large proportion of neutralizing antibodies (2, 3). Several S protein-based serological assays have been developed to profile the anti-SARS-CoV-2 humoral immune response and to analyze its dynamic changes, including ELISA assays, peptide microarrays, and antibody binding epitope mapping (Chen et al.). More recently, flow cytometric approaches have been introduced using cells expressing native S proteins in the same orientation and a glycosylation pattern similar to that found on the viral membrane. In this collection, Vesper et al. describe a flow cytometric assay that, in combination with a color-coded barcoding method, allow comparison of binding of S proteins or RBD mutants to soluble ACE2-Ig molecules, or antibodies of different classes in the sera of vaccinated or infected subjects. This new assay should be valuable for further evaluations of the humoral response to SARS CoV-2 variants.

Understanding the mechanism underlying viral evasion from the immune response is important for designing effective vaccines and therapeutics. Thus, the Omicron variant

(B.1.1.529.1) exhibits 34 mutations in its S protein, including 15 changes in the RBD, compared with the original Wuhan SARS-CoV-2 strain reported in 2019. These mutations could facilitate viral internalization through binding to ACE2 on target cells and promote the increased immune evasion potential of VOC. Comparison of the sequences of SARS-CoV-2 proteins from multiple ancestral strains, including Omicron variants (BA.1, BA2, BA3, BA.4, BA.5, BQ.1 and BBX.1), and the previously circulating Alpha, Beta, Gamma, and Delta strains, revealed that Omicron and it's sub-variants exhibit a bias toward Asparagine to Lysine transitions within the S protein (Boer et al.). This mutation could lead to conformational changes, thereby potentially reducing the activity of neutralizing antibodies in infected subjects.

Mining antibody genes

Initial surveys of antibody repertoire in COVID-19 patients noted a polyclonal response associated with high numbers of circulating plasmablasts and low-levels of somatic mutations (4). Further analysis of RBD-specific antibodies from convalescent subjects revealed that the acquisition of somatic mutations and affinity maturation could impart protection against diversifying SARS-CoV-2 variants (5). In this collection, two cohorts of not previously infected patients were used to probe somatic hypermutation at distinct points after vaccination (Paschold et al.). After the priming vaccinations, B lineage evolution and somatic hypermutation were low. With booster vaccinations, antigen-experienced B cell clones were mobilized to further rapid somatic hypermutation, suggesting that affinity maturation may account for the increased protection of booster injections against SARS-CoV-2 variants, such as the Omicron variant B.1.1.529.

Taking a different research angle, Stewart et al. compared the antibody repertoire during pandemic, epidemic and endemic viral disease by tracking the V-D-J sequences in the context of antibody subclasses in B cell responses to COVID-19, Ebola virus disease survivors from West Africa and the UK, volunteers challenged with Respiratory Syncytial Virus, and samples from healthy donors. They report that, while features of B cell responses are specific for particular infections, the immunoglobulin repertoire can exhibit similarities across very different diseases, such as a general increase of IGHV4-39 gene used in response to SARS-CoV-2 and Ebola virus infection.

B lymphocyte population dynamics

In an in-depth commentary, Rossi et al. present an overview of IgM memory B cells with a focus on human secondary lymphoid structures in the spleen and list evidence for the protective role of IgM and IgA antibodies to SARS-CoV-2. Most notably, the authors cite the observation that patients, who were infected with SARS-CoV-2 but showed reduced or depleted levels of the IgM memory B cell subset, experienced more severe or fatal infections. The authors thus argue for the benefit of a close assessment of the immune status in newly infected individuals, such that prophylactic or therapeutic measures could be administered in a timely manner.

Taking a closer look at the risk of administering the B cell depleting anti-CD20 monoclonal antibody, Rituximab, as a therapy for the autoimmune disease rheumatoid arthritis, to patients, who also required protection from SARS-CoV-2 by standard mRNA vaccination against the virus, Stefanski et al. observed that the efficacy of a third vaccine dose was preserved, if Rituximab was given 1-2 months after the second dose of the vaccine. The conclusion was reached that generation of anti-SARS-CoV-2 memory B cells, protective antibodies, and spike-specific CD4 T cells, prior to CD20 B cell depletion, allows further boost of anti-viral responses and elicits a particularly strong IgA B cell population.

SARS-CoV-2 infection and autoreactive B cells

The parallel observations that inflammatory cytokines, such as TNF–α, IL-1β and IFN-γ, favor the development of so-called double-negative CD27- IgD- (DN) B cells, a likely precursor population driving the production of autoantibodies in lupus, and the separate finding that SARS-CoV-2 infection may promote the expression of autoantibodies, prompted Castleman et al. to examine the relative abundance of DN B cells in COVID-19. The original discoveries reported in this paper included the diminished frequencies of DN1 B cells and elevated numbers of DN2 and DN3 B cells in severe COVID-19. Along with cytokine imbalances induced by the viral infection, the authors observed a notable expansion of DN3 B cells and the appearance of autoreactive antibodies within the pro-inflammatory milieu.

The induction of autoreactivities in a set of 31 individuals exposed to SARS-CoV-2 in the healthcare setting was also examined by Moody et al. The authors noted the presence of a set of antibodies to 11 autoantigens. Strikingly, the analysis, using an autoantigen array approach, identified the autoreactivity to calprotectin, a complex of the mammalian proteins S100A8 and S100A9, in one fourth of the analyzed plasma samples that persisted for eight months following the SARS-CoV-2 infection and correlating with complete recovery from the viral infection.

Conclusions

In sum, the articles presented in this Research Topic represent a valuable set of diverse and innovative research that has been sparked by the COVID-19 pandemic. With determination and vigorous collaborative efforts, the scientific community is responding to the challenge and yielded numerous new insights into the pathogenesis of SARS-CoV-2 infections and immune responses, including humoral responses, alterations in B lymphocyte population dynamics, and effects on antibody repertoire profiles. Many of the newly emerging concepts will retain lasting impact, long beyond the current health emergency.

Author contributions

Both authors listed have made a substantial, direct, and intellectual contribution to the work and approved it for publication.

Funding

MZ is supported by China Medical University (Taichung, Taiwan) and by a Senior Jade Mountain Award (Ministry of Education, Taipei, Taiwan).

Conflict of interest

The authors declare that the research was conducted in the absence of any commercial or financial relationships that could be construed as a potential conflict of interest.

Publisher's note

All claims expressed in this article are solely those of the authors and do not necessarily represent those of their affiliated organizations, or those of the publisher, the editors and the reviewers. Any product that may be evaluated in this article, or claim that may be made by its manufacturer, is not guaranteed or endorsed by the publisher.

References

1. Jackson CB, Farzan M, Chen B, Choe H. Mechanisms of SARS-CoV-2 entry into cells. *Nat Rev Mol Cell Biol* (2022) 23:3–20. doi: 10.1038/s41580-021-00418-x

2. Piccoli L, Park YJ, Tortorici MA, Czudnochowski N, Walls AC, Beltramello M, et al. Mapping neutralizing and immunodominant sites on the SARS-CoV-2 spike receptor-binding domain by structure-guided high-resolution serology. *Cell* (2020) 183:1024–1042.e21. doi: 10.1016/j.cell.2020.09.037

3. Walls AC, Park YJ, Tortorici MA, Wall A, McGuire AT, Veesler D. Structure, function, and antigenicity of the SARS-CoV-2 spike glycoprotein. *Cell* (2020) 181:281–292.e6. doi: 10.1016/j.cell.2020.02.058

4. Kreer C, Zehner M, Weber T, Ercanoglu MS, Gieselmann L, Rohde C, et al. Longitudinal isolation of potent near-germline SARS-CoV-2-Neutralizing antibodies from COVID-19 patients. *Cell* (2020) 182:843–854.e12. doi: 10.1016/j.cell.2020.06.044

5. Muecksch F, Weisblum Y, Barnes CO, Schmidt F, Schaefer-Babajew D, Wang Z. Affinity maturation of SARS-CoV-2 neutralizing antibodies confers potency, breadth, and resilience to viral escape mutations. *Immunity* (2021) 54:1853–1868.e7. doi: 10.1016/j.immuni.2021.07.008

frontiers in Immunology

ORIGINAL RESEARCH
published: 23 September 2021
doi: 10.3389/fimmu.2021.730766

A Barcoded Flow Cytometric Assay to Explore the Antibody Responses Against SARS-CoV-2 Spike and Its Variants

*Niklas Vesper[1,2], Yaneth Ortiz[1,2], Frauke Bartels-Burgahn[1,2], Jianying Yang[1,2], Kathrin de la Rosa[3], Matthias Tenbusch[4], Sebastian Schulz[5], Stephanie Finzel[6], Hans-Martin Jäck[5], Hermann Eibel[6,7], Reinhard E. Voll[6,7] and Michael Reth[1,2]**

[1] Institute of Biology III, Faculty of Biology, University of Freiburg, Freiburg, Germany, [2] Research Centres Bioss, Centre for Biological signal studies, CIBSS, Centre for Integrative Biological Signalling Studies, University of Freiburg, Freiburg, Germany, [3] Department of Cancer and Immunology, Max-Delbrück-Center for Molecular Medicine in the Helmholtz Association (MDC), Berlin, Germany, [4] Institute of Clinical and Molecular Virology, University Hospital Erlangen, Friedrich-Alexander University Erlangen-Nuremberg, Erlangen, Germany, [5] Division of Molecular Immunology, Internal Medicine III, Nikolaus-Fiebiger-Center of Molecular Medicine, Friedrich-Alexander University Erlangen-Nuremberg, Erlangen, Germany, [6] Department of Rheumatology and Clinical Immunology, Medical Center – University of Freiburg, Faculty of Medicine, University of Freiburg, Freiburg, Germany, [7] Center for Chronic Immunodeficiency, Medical Center, University of Freiburg, Freiburg, Germany

OPEN ACCESS

Edited by:
Moncef Zouali,
Institut National de la Santé et de la Recherche Médicale (INSERM), France

Reviewed by:
Bruce David Mazer,
Research Institute of the McGill University Health Center (RI-MUHC), Canada
Wayne Marasco,
Dana–Farber Cancer Institute, United States

***Correspondence:**
Michael Reth
michael.reth@bioss.uni-freiburg.de

Specialty section:
This article was submitted to B Cell Biology, a section of the journal Frontiers in Immunology

Received: 25 June 2021
Accepted: 03 September 2021
Published: 23 September 2021

Citation:
Vesper N, Ortiz Y, Bartels-Burgahn F, Yang J, de la Rosa K, Tenbusch M, Schulz S, Finzel S, Jäck H-M, Eibel H, Voll RE and Reth M (2021) A Barcoded Flow Cytometric Assay to Explore the Antibody Responses Against SARS-CoV-2 Spike and Its Variants. Front. Immunol. 12:730766. doi: 10.3389/fimmu.2021.730766

The SARS-CoV-2 pandemic has spread to all parts of the world and can cause life-threatening pneumonia and other severe disease manifestations known as COVID-19. This health crisis has resulted in a significant effort to stop the spread of this new coronavirus. However, while propagating itself in the human population, the virus accumulates mutations and generates new variants with increased fitness and the ability to escape the human immune response. Here we describe a color-based barcoded spike flow cytometric assay (BSFA) that is particularly useful to evaluate and directly compare the humoral immune response directed against either wild type (WT) or mutant spike (S) proteins or the receptor-binding domains (RBD) of SARS-CoV-2. This assay employs the human B lymphoma cell line Ramos, transfected for stable expression of WT or mutant S proteins or a chimeric RBD-CD8 fusion protein. We find that the alpha and beta mutants are more stably expressed than the WT S protein on the Ramos B cell surface and/or bind with higher affinity to the viral entry receptor ACE2. However, we find a reduce expression of the chimeric RBD-CD8 carrying the point mutation N501Y and E484K characteristic for the alpha and beta variant, respectively. The comparison of the humoral immune response of 12 vaccinated probands with 12 COVID-19 patients shows that after the boost, the S-specific IgG class immune response in the vaccinated group is similar to that of the patient group. However, in comparison to WT the specific IgG serum antibodies bind less well to the alpha variant and only poorly to the beta variant S protein. This is in line with the notion that the beta variant is an immune escape variant of SARS-CoV-2. The IgA class immune response was more variable than the IgG response and

higher in the COVID-19 patients than in the vaccinated group. In summary, we think that our BSFA represents a useful tool to evaluate the humoral immunity against emerging variants of SARS-CoV-2 and to analyze new vaccination protocols against these variants.

Keywords: COVID-19, coronavirus, SARS-CoV-2, virus variants, spike protein, RBD, humoral immunity, flow cytometry

INTRODUCTION

Since December 2019, the severe acute respiratory syndrome coronavirus 2 (SARS-CoV2) has been spreading in the human population as a pathogen causing the coronavirus disease 2019 (COVID-19) associated with severe pneumonia (1). The rapid spread of this pandemic virus and the severity of this worldwide health crisis is associated with three features (2). First, SARS-CoV-2 is a new member of the beta-coronavirus family and hence there is no human immunity against this emerging virus (3). Second, SARS-CoV-2 enters the cells *via* the angiotensin-converting enzyme 2 (ACE2), a receptor widely expressed in human mucosal tissues of the nose and mouth and particularly abundant in the lung (4, 5). Third, SARS-CoV-2 is a positive-strand RNA virus and can thus rapidly generate mutations (6). The virus binds to the ACE2 entry receptor *via* the trimeric spike (S) protein prominently expressed on the viral membrane (7). Upon binding to ACE2, the S protein undergoes a conformational change. It is cleaved by cellular proteases into an S1 and S2 portion, with the latter inducing a fusion reaction between the viral and cellular membrane, thereby starting the infection cycle (8). The RBD, that directly binds to ACE2 is located within the S1 portion. The structure of the SARS-CoV-2 trimeric S protein has been determined by cryo-electron microscopy at the atomic level. It has revealed that the RBD can assume a closed (down) or open (up) conformation, with only the latter being able to interact with the ACE2 entry receptor (9).

The trimeric S protein of SARS-CoV-2 is a prominent target of the humoral immune response (9–11). In particular, RBD-specific antibodies can inhibit the binding of the S protein to ACE2 and thus function as neutralizing antibodies that block viral entry into the target cells (4). Indeed, it has been found that the RBD is an immunodominat structure of the S protein and targeted by more than 90% of the neutralizing antibodies (12). Several specific monoclonal antibodies (mAb) have been generated and are used in the clinic as therapeutic reagents to treat acute COVID-19. These mAb can be directed to the full-length S protein or the RBD domain. A co-crystallization of Fab fragments of anti-RBD mAb with the RBD resulted in their classification in ACE2-blocking or non-blocking antibodies (9, 12). The S protein or its encoding mRNA are used for the rapid development of vaccines that counteract the spread of the SARS-CoV-2. In particular, mRNA vaccines could be rapidly produced and play an essential role in the worldwide vaccination programs counteracting the spread of the virus. However, these efforts may be compromised by the appearance of SARS-CoV-2 variants that start to spread in different parts of the world (6). The SARS-CoV-2 variants carry characteristic mutations in the RBD and other parts of the S protein. According to the World Health Organization's recommendations (WHO), they are now classified as Greek letters (13). They are usually characterized by their increased infectivity, their ability to multiply more rapidly in an infected host and to escape recognition by at least some neutralizing antibodies generated against the S protein of WT SARS-CoV-2. Hence, the virus variants represent "fitness" and/or "immune evasion" mutants (14).

Many S protein-based serological assays have been developed to evaluate the success of the diverse vaccination programs and determine the anti-SARS-CoV-2 humoral immune status of a human population. These are based on linear peptides or the full-length S protein and frequently use the ELISA technique (15). Recently also flow cytometric techniques have been introduced (16–18). The advantage of these assays is that they use cells expressing native S proteins with the same orientation and a glycosylation pattern similar to that found on the viral membrane. This also applies to a cell-based enzyme-linked immunosorbent assay used for the detection of a HIV or SARS-CoV-2 infection (19, 20). Here we describe a flow cytometric assay that allows comparison of the humoral immune response of vaccinated and infected persons in terms of its reactivity towards the S protein and RBD of either WT or the variants of SARS-CoV-2.

MATERIALS AND METHODS

Participants

Four female and eight male COVID-19 patients (n=12) with mean ages of 65 and 62 years were recruited at the Medical Center University of Freiburg. Written informed consent was obtained from all participants in this study. Convalescent plasma was collected according to the FDA recommendation. Donors met routine FDA-established blood donor eligibility requirements and had previous SARS-CoV-2 infection documented by laboratory testing for the virus during illness or antibodies to the virus after recovery from suspected illness. In addition, six female and six male subjects (n=12) vaccinated with BioNTech/Pfizer Comirnaty were recruited with a mean age of 49.33 and 44.83 years, respectively at the Medical Center – University of Freiburg. Written informed consent was obtained from all participants. The study was approved by the Ethical Committee of the University of Freiburg (EK-Freiburg no 315/10). Serum and plasma samples were aliquoted and stored at−80°C.

Cloning

The retroviral expression vectors encoding the WT, alpha or beta variant S protein of SARS-CoV-2 are based on the pMIG vector backbone (pMIG was a gift from William Hahn [Addgene plasmid # 9044; http://n2t.net/addgene:9044; RRID: Addgene_9044)]. The cDNA of the relevant S protein genes was amplified by PCR with primers containing the proper extensions to be ligated into the linearized pMIG vector by a Gibson assembly-like method, namely the In-Fusion cloning protocol from ClonTech. To connect the PCR fragments, we designed them so that they have a 15 base pair overlap. The cDNA encoding the WT S protein is derived from the plasmid pVAX1-SARS2-S with a codon-optimized sequence of the S protein gene of SARS-CoV-2 (21). The alpha and beta S protein cDNA were synthesized in ITD gBlocks. The retroviral expression vector encoding the RBD-CD8 chimeric const ruct is based on the pMIG-CD8 vector containing the murine CD8 gene cDNA. The cDNA encoding the RBD of the WT S protein was amplified by PCR and ligated into the linearized pMIG-CD8 vector so that the RBD was placed in between the leader peptide and the extracellular Ig domain of CD8. The point mutations in the RBD-CD8 construct were generated by site-directed mutagenesis. For the design of primers and plasmids, we used Geneious 9.0.5 software. The component mixture used for the PCR and the PCR program was set up according to CloneAmp HIFI PCR Premix. All generated vectors were sequenced (Eurofins Genomics) and the sequencing results were analyzed by Geneious software

Cell Culture

Ramos B cells were cultured in RPMI medium supplemented with 10% fetal bovine serum (FBS), 1% penicillin-streptomycin and 0.12% β-mercaptoethanol (RPMI+). The Ramos B cell cultures were split every 2 days.

Retroviral Production in Phoenix Cells and Transduction of Ramos B Cells

Phoenix cells were cultured in iscove basal medium (IBM) supplemented with 10% FBS and 1% penicillin streptomycin (IBM+). Cells were split every 2 days by diluting them 1/10. One day before the transfection with the retrovirus producing plasmids pKAT and pMIG, $5x10^5$ Phoenix cells at 70 % confluency were pipetted into a coated 6-well plate. Afterward, the cells were supplemented with 2 ml of IBM+. Between 18 and 24 hours later, the transfection was performed on cells at 70% confluency, using Polyjet transfection reagent, according to the manufacturer's instructions. After 2 days of culture, the virus-containing supernatant was collected and filtered through a 0.45 µm filter. Afterward, Polybrene was added at a concentration of 1 µl/ml. Ramos-null B cells were split the day before the transduction, $6x10^5$ Ramos-null cells were resuspended in 1 ml of the transduction mixture and then centrifuged for 3 h at 400xg and 37°C. After this step, the viral supernatant was replaced with RPMI+. The cells were then transferred to a 12-well plate in a total volume of 2.5 ml of medium.

Barcoding

For barcoding, 10^6 Ramos B cells were resuspenden in 1 ml of DPBS alone or with different concentrations of the cell proliferation tracer CytoTell blue (1:250, 1:1250, 1:10.000). The cells were incubated for 30 min in the dark at room temperature, washed twice with DPBS and then combined in one test tube for further staining.

Cell Surface Staining and Subsequent Analysis

The following flow cytometry antibodies were obtained from BioLegend: anti human IgG (M1310G05), anti human IgA (HP6123), anti mouse CD8 (53-6.7), anti mouse kappa light chain (RMK-12). For primary staining, barcoded cells were incubated with the binding reagent for 30 min at 4 °C in the dark. After incubation, the cells were washed twice with DPBS. Secondary staining was performed under the same conditions using appropriate fluorescent label secondary antibodies. The cells were washed resuspended in DPBS for FACS analysis on a ThermoFisher Attune NxT flow cytometer. Filters used 440/50, 530/30, 585/16 and 670/14. Flow cytometry data were analyzed with FlowJo v10 (Tristart). The mean fluorescent intensity (MFI) values from each cell line were then normalized to the MFI from the control Null cell line within each barcoded sample, and the resulting normalized MFI was used for comparison of binding to different Spikes or RBDs variants.

ACE-Ig Reagent and mAb

ACE2-Ig was cloned by fusing the human *ACE2* Q18-V739 fragment to the human IgG1-Fc portion (E99-K330 portion, where 1st amino acid is G encoded by J-CH1 fusion) of the expression vector from Oxford Genetics (pSF-CMV-HuIgG1). Cloning constructs were used to transfect FreeStyle 293-F cells that were grown in suspension using FreeStyle 293 expression medium (Life Technologies) at 37°C in a humidified 8% CO2 incubator rotating at 125 rpm. Cells were grown to a density of 2.5 million cells per mL, transfected using PEI (4 µg/mL in cell suspension) and DNA (1200 ng/ml in cell suspension), and cultivated for 3 days. The supernatants were harvested and ACE2-Ig was purified by protein G SpinTrap columns according to manufacturer's instructions (Cytiva, 28903134).

The isolation of monoclonal TRES antibodies is described in (22). Briefly, TRIANNI C57/Bl6 mouse line HHKKLL (Patent US 2013/0219535 A1) was primed with a plasmid encoding wild type SARS-COV-2 spike protein and boosted twice intramuscularly with stabilized trimeric S protein of SARS-CoV-2 adjuvanted with Monophosphoryl Lipid A (MPLA) liposomes (Polymun Scientific GmbH, Klosterneuburg, Austria). Spleen cells were fused with Sp2/0 cells, and hybridoma clones were screened for spike-binding antibodies with a flow-based assay as described by (17). Positive clones were subcloned by the limiting dilution method. Rearranged VH and VL exons were cloned by the 5' Race method and sequenced.

Anti-SARS-CoV-2-ELISA IgG

Sera of vaccinated persons, diluted 1/100, were tested for anti-spike IgG antibodies by ELISA, using the EI 2601-9601 G SARS-CoV-2 Spike IgG kit from Euroimmun applying the reagents and the protocol provided by the manufacturer. The CE certified assay is widely used to determine the presence of SARC-COV-2 specific antibodies (23). According to the manufacturer, the assay's sensitivity is 94,4% and the specificity 99.8%

RESULTS

Setting Up the Spike Flow Cytometric Assay

The human Burkitt lymphoma cell line Ramos is a valuale tool of immunological research (24). These cells can be propagated efficiently in cell cultures and modified by the CRISPR/Cas9 technique (25). In our study, we used a Ramos-null line lacking all four components of the B cell antigen receptor (BCR), namely heavy chain, light chain, Igα and Igβ (26). Although the Ramos-null cells grow more slowly than Ramos wild type (WT), they can be maintained in culture and expanded to large cell numbers. Furthermore, the Ramos-null cells also carry on their surface a receptor for ecotropic retroviruses (ecoR) that allows the efficient transduction of these cells with murine retroviral vectors (**Figure 1A**). For the expression of different S constructs on the surface of Ramos-null cells, we used a pMIG vector carrying after the LTR promoter the construct sequence, an internal ribosome entry site (IRES) and the sequence coding for the green fluorescent protein (GFP) (**Figure 1B**). This vector system allows us to detect and enrich the transduced (GFP-positive) Ramos-null cells and correlate to some extent the expression of the S protein with that of GFP. The different retroviral vectors were used to express either the S protein of SARS-CoV-2 or a chimeric protein carrying the isolated RBD of the S protein in front of the murine CD8 molecule.

Furthermore, we also expressed the S protein of two SARS-CoV-2 mutants, namely the alpha variant (B1.1.7) and the beta variant (B.1.351) (**Figure 1C**). These mutant S proteins differ from the WT SARS-CoV-2 sequence at 8-10 amino-acid positions (**Figure 1D**). In the RBD sequence, the mutant S proteins carry critical amino acid exchange mutations that influence the binding of the S protein to the ACE2 target and its detection by neutralizing antibodies (6, 27). These are an asparagine to tyrosine exchange (N501Y) in the alpha variant and the same mutation in combination with a glutamate to lysine (E484K) exchange mutation in the beta variant. In addition, the S proteins expressed on the Ramos cell surface carry a deletion of four amino acids (RRAR) at the border between the S1 and S2 domains, preventing their cleavage by cellular proteases.

To directly compare Ramos cells expressing different S protein constructs in their binding of either a soluble ACE2 or anti-SARS-CoV-2 antibodies, we developed a color-based barcoded spike protein flow cytometric assay (BSFA). To this end, we first incubated Ramos cells with PBS alone or with different concentrations of the cell proliferation tracer *CytoTell* blue. The Ramos cells are then washed and combined in one sample tube (**Figure 2A**) before being stained with different binding reagents. Finally, the combined Ramos cells are separated by a flow cytometric gate using the blue fluorescent

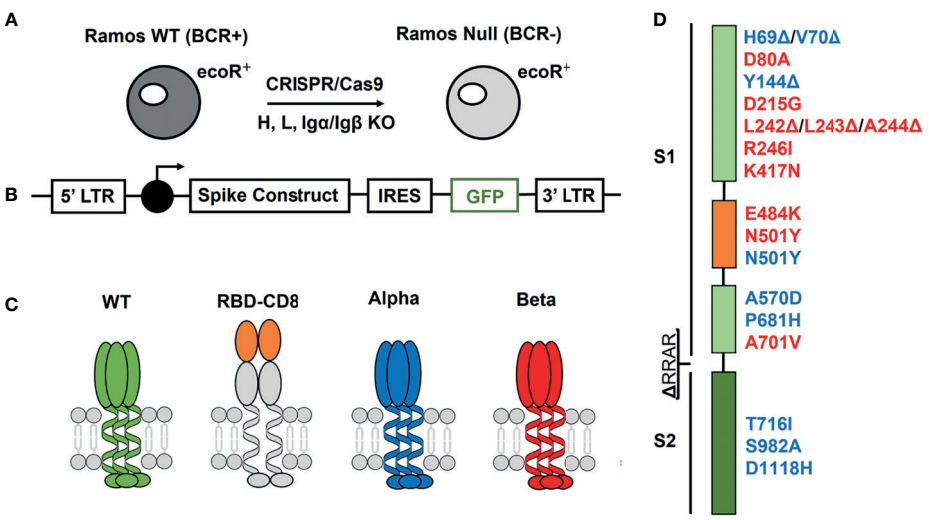

FIGURE 1 | Expression system for the generation of Ramos-null B cells carrying on their surface WT or variant spike proteins of SARS-CoV-2. **(A)** Generation of the Ramos-null cells lacking functional genes for the four components (heavy chain, light chain, Igα, Igβ) of the IgM-BCR by the CRISPR/Cas9 technique. These cells also carry the ecoR receptor for efficient retroviral transfection. **(B)** Retroviral vector used for the linked expression of the spike protein and GFP using an internal ribosome entry site (IRES) sequence in front of the GFP cDNA. **(C)** Schematic drawing of the expressed S proteins with the WT (green), the receptor binding domain (RBD) (orange) attached to the murine CD8 protein (grey), the alpha variant B.1.1.7 (blue) and the beta variant B.1.3.5.1 (red). **(D)** Location of the amino acid exchange or deletion mutations in the S1 and S2 domain of the S protein. Alterations in the S protein of the alpha variant are indicated in blue and those of the beta variant in red.

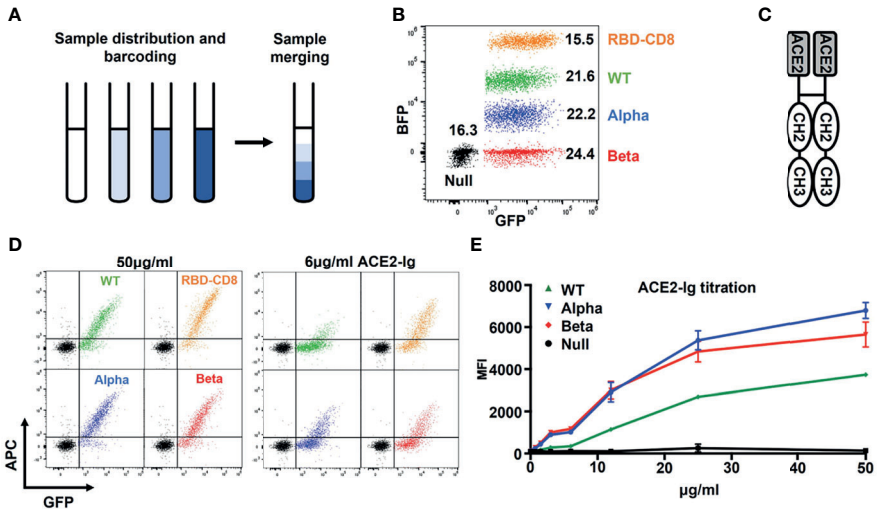

FIGURE 2 | Establishment of the color-based barcoded spike flow assay (BSFA). **(A)** Labeling of four different Ramos cell populations by exposure to different concentrations (0, 1:250, 1:1250, 1:10.000) of *CytoTell* blue for further analysis in one test tube. **(B)** Gating strategy for the analysis of four different Ramos cell populations by flow cytometry. The *CytoTell* blue -loaded Ramos cells are separated by the blue fluorescent protein (BFP) gate. **(C)** Structural model of the chimeric ACE2-Ig molecule used for the detection of the S protein or the RBD-CD8 chimera on transfected Ramos cells. **(D)** Analysis of Ramos cells expressing the WT (green), alpha variant (blue), beta variant (red) S protein or the RBD-CD8 construct (orange). The cells were exposed to either 50 or 6 ug/ml of ACE2-Ig, washed, stained with APC-coupled anti-human IgG antibodies and then analyzed by flow cytometry. Shown is the dot plot depicting the GFP and APC fluorescence form each one of the variants overlay with the Ramos-Null (GFP-) control cell line. **(E)** Titration of the ACE2-Ig binding to the four indicated Ramos cell populations. As negative control we used Ramos cells without S protein (black). The mean values of three different experiments are shown.

protein (BFP) channel (**Figure 2B**). To test for the expression of the different S constructs, we used an ACE2-immunoglobulin (ACE2-Ig) chimeric protein carrying at the C-terminus instead of the TM region of ACE2 the CH2 and CH3 domains of human IgG1 (**Figure 2C**). The different Ramos cells were first incubated with increasing concentrations of ACE2-Ig, washed, stained with allophycocyanin (APC)-coupled anti-human IgG antibodies and then analyzed for APC and GFP fluorescence by flow cytometry (**Figure 2D**). We found that Ramos cells expressing the RBD-CD8 construct show the most robust ACE2-Ig binding. This is in line with a structural analysis showing that only a minority of the trimeric S proteins display the RBD in an open (ACE2-binding) conformation (9, 28), whereas as part of the RBD-CD8 construct, the RBD should be fully accessible for ACE2 binding. The directed comparison of Ramos cells expressing the WT S constructs or the alpha and beta variants shows that the variants display a stronger ACE2-Ig binding (**Figure 2D**). This is particularly visible at the lower (6 ug/ml) concentration of ACE2-Ig and confirmed by a more detailed titration experiment (**Figure 2E**). These data show that the BSFA can be used to evaluate the expression and binding activity of WT and mutant SARS-CoV-2 S proteins to ACE2.

Evaluation of Anti-S Antibodies and Sera

We next incubated the four different Ramos cell lines with 1 ug/ml of monoclonal antibodies (mAb) generated against the WT trimeric S protein of SARS-CoV-2. These TRIANNI-Erlangen anti-SARS-CoV-2- Spike (TRES) mAb are either directed against the hACE2 binding site (TRES224, TRES6) or the N-terminal domain (TRES328) of the S protein (22). The BSFA showed that the TRES224 and TRES6 antibodies are indeed directed against the RBD of the S protein whereas TRES328 hardly binds this structure (**Figure 3A**). A strong RBD binding was also found when using the therapeutic anti-SARS-Cov-2 antibody R10987 characterized as a class 3 RBD binder (9). The RBD-specific mAb TRES224, TRES6 and R10987 also bind well to the alpha and beta variant S proteins, which is not true for TRES328. Interestingly, the titration of the three RBD-specific mAb shows that they bind even better to Ramos cells expressing the variant than those expressing the WT S proteins (**Figure 3B**). These data demonstrate that on the Ramos cell surface the variant S proteins are expressed as well as or even better than the WT S protein and that the BSFA can be used to evaluate the fine specificity of anti-SARS-CoV-2 antibody response.

Having demonstrated that the BSFA works well in the evaluation and characterization of anti-S antibodies, we next analyzed sera from 12 persons (V1-V12) who had been vaccinated with the BioNTech/Pfizer mRNA vaccine (Comirnaty®). For each person, we obtained sera before or shortly after vaccination, 10-14 days after the first and 10-15 days after the second vaccination (**Table 1**). As an example, for the human humoral response after vaccination, we show a BSFA study for S-specific IgG and IgA antibodies in the sera of a 47-year-old female (V7) taken either 1 day before or 12 days after the first and 10 days after the secondary (boost) vaccination (**Figure 4**). No S-specific antibodies were found before immunization, and that was the case for all analyzed sera (**Supplementary Figure 1**). After the first vaccination,

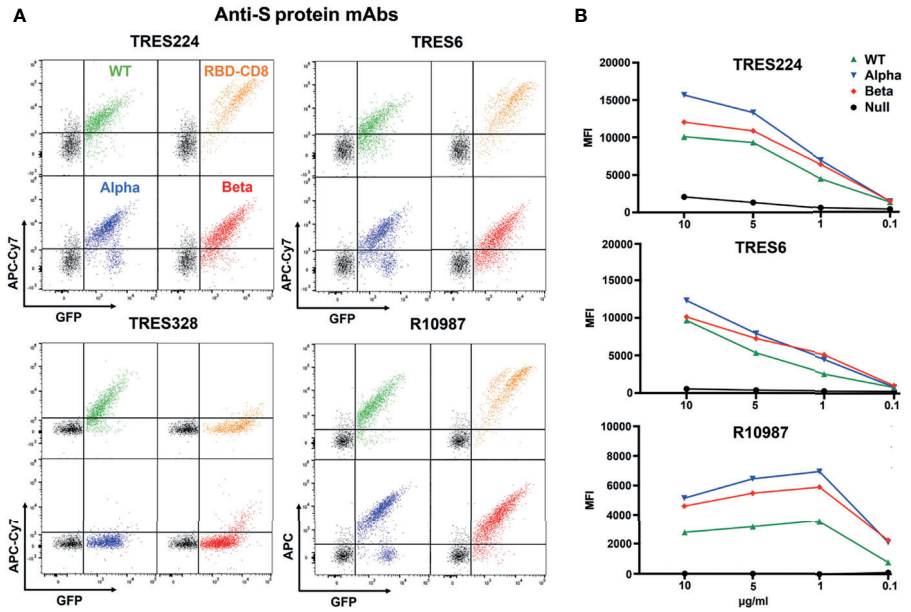

FIGURE 3 | BSFA study of the binding of four monoclonal antibodies (mAb) to S protein- expressing Ramos cells. **(A)** Ramos cells carrying the WT (green), alpha variant (blue), beta variant (red) S protein or the RBD-CD8 construct (orange) cells were incubated with 1 ug/ml of the mAb TRES224, TRES6, TRES328 and R10987. After washing, the cells were stained with either APC-Cy7-coupled anti-mouse IgG antibodies (for TRES224, TRES6, TRES328) or APC-coupled anti-human IgG antibodies (for R10987) and analyzed for the APC-Cy7/APC and GFP color by flow cytometry. **(B)** Titration of the mAb TRES224, TRES6 and R10987 to Ramos cells carrying the indicated S proteins. As negative control we used Ramos cells without S protein (black). The mean values of three different experiments are shown.

TABLE 1 | Demographic data of SARS-CoV-2 infected patients.

Patient cohort	Days between diagnose and sampling	Sex	Age
C1	51	M	59
C2	94	M	53
C3	39	M	67
C4	28	M	61
C5	19	F	78
C6	8	M	74
C7	48	F	66
C8	34	F	50
C9	26	F	68
C10	46	M	65
C11	16	M	63
C12	19	M	56

Median age: 64+/- 8,18 years; M, male; F, female.

the serum of V7 contained specific IgG antibodies directed against the WT and RBD-CD8 but not against the alpha and beta variant S proteins. The primary IgA antibody response of V7 is also predominantly directed towards the WT but not the variant S proteins. After the secondary immunization, the amount of IgG antibodies directed against the WT S protein and RBD has increased. The sera now also contain IgG antibodies binding to the alpha and beta variant S proteins. However, in contrast to the previously tested mAb, the serum antibodies of V7 recognize the WT better than the alpha and beta variants' S proteins. (**Figure 4**, outer right panel). The secondary IgA antibody response did not improve much compared to the primary response. Only a few IgA antibodies bound to the Ramos cells expressing high amounts of the alpha and beta variants' S proteins.

The analysis of sera from all 12 vaccinated persons confirms these findings (**Figures 5A, B**). The S-specific IgG antibody response is in most cases higher in the secondary than in the primary sera. The secondary sera also contain IgG antibodies against the alpha and beta variants S proteins, albeit at a lower level. This is in line with a study showing that the protective antibody respose of mRNA vaccinated person is sufficient but lower in the case of the alpha mutant (29). Four of the 12 vaccinated persons (V1, V2, V4 and V10) already had a high anti-S primary IgG response that did not improve substantially after the secondary immunization. The S-specific IgA antibody response is more variable from person to person and is not always improved in the secondary response. Most sera of the vaccinated group had IgA antibodies that bind more strongly to Ramos cells expressing the WT than those expressing the alpha and beta variants' S proteins. For comparison we also studied the blood samples of the 12 vaccinated persons with an ELISA detecting IgG antibodies directed against the S1 part of the WT S protein (**Supplementary Figure 2**). This assay also shows that in most cases the IgG antibody response is higher in the secondary than in the primary response. However, there are some discrepancies in the variability of the primary response and the secondary response of V7 that may be due to the detection of different epitopes on the isolated S1 part of the

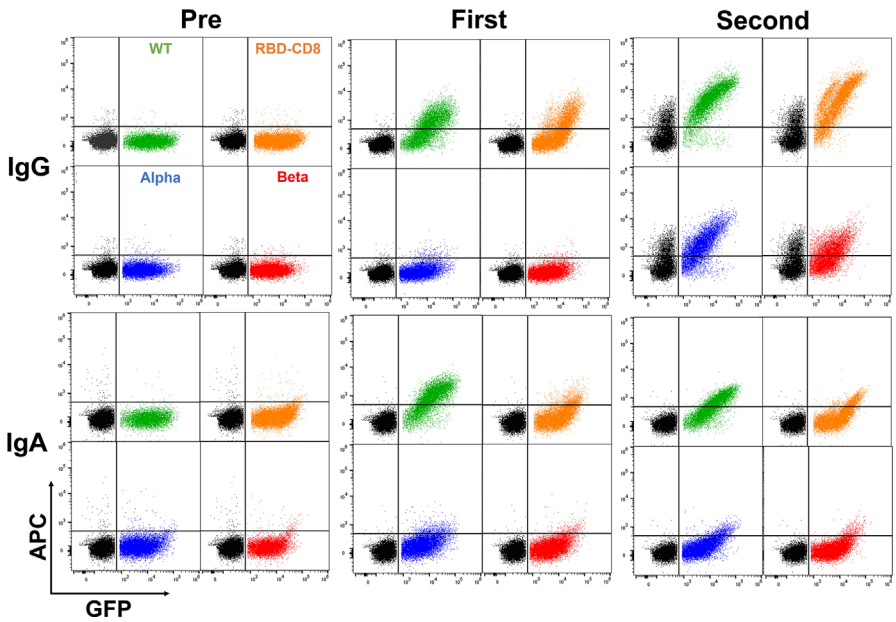

FIGURE 4 | BSFA study of the serum of a vaccinated (BioNTech/Pfizer) 47-year-old female (V7) for anti-S protein IgG (upper panels) and IgA class (lower panels) antibodies. Serum was collected 1 day before (pre) or 12 days after the first vaccination and 10 days after the second vaccination.

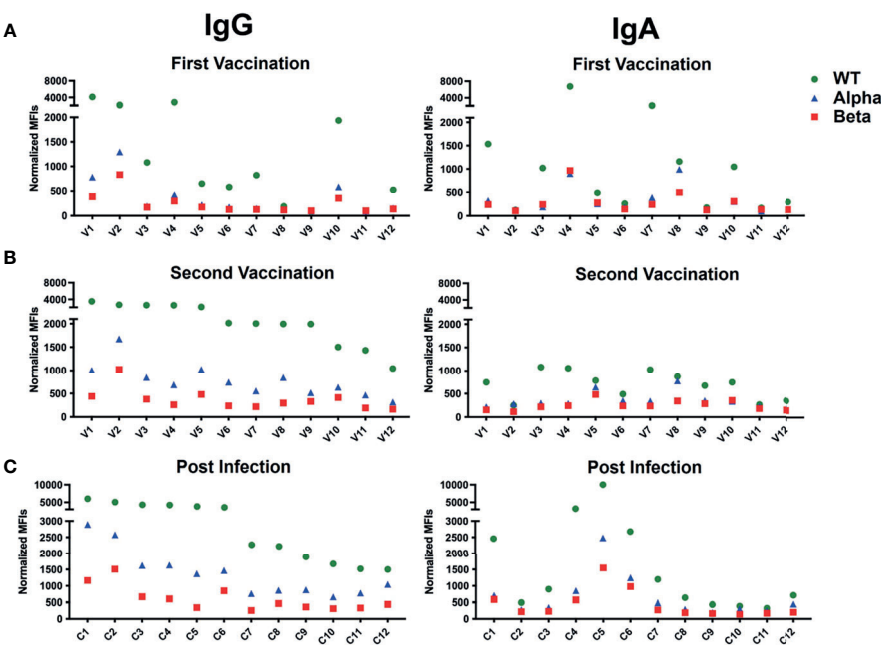

FIGURE 5 | BSFA study of the sera of 12 persons vaccinated with the BioNTech/Pfizer mRNA vaccine after the primary **(A)** and secondary **(B)** vaccine doses and of 12 patients with severe COVID-19 disease **(C)**. Summary of the production of S protein-specific IgG (left panel) or IgA (right panel) antibodies. The sera were diluted 1:100 and analyzed by flow cytometry for antibodies binding to Ramos cells expressing either the WT (green), the alpha variant (blue) or the beta variant (red) S protein. Shown are normalized mean fluorescence intensity (MFI).

TABLE 2 | Demographic data of vaccinated patients.

Vaccinated Cohort	PV (days)	SC V1 (days)	SC V2 (days)	Sex	Age
V1	0	14	10	M	28
V2	4	10	10	M	31
V3	2	12	10	F	57
V4	0	10	10	F	52
V5	4	10	10	F	34
V6	5	12	15	F	73
V7	-1	12	10	F	47
V8	4	10	10	M	36
V9	-1	11	11	F	43
V10	5	12	15	M	79
V11	2	10	10	M	56
V12	0	11	13	M	39

Median Age: 45 +/- 16,19 years; M, male; F, female; PV, Prevaccination; V1, First Vaccination; V2, Second Vaccination; SC, Sample Collection.
V8 had SARS-CoV-2 infection before vaccination.

spike on plastic *versus* full-length spike on the plasma membrane by the anti-SARS-CoV-2 antibodies. Nonetheless, there is an overall good correlation between the ELISA and the BSFA which strengthens the validity of the flow cytometric assay.

We next analyzed the blood of 12 COVID-19 patients (C1-C12) (**Table 2**). These sera were taken 1-12 weeks after the SARS-CoV-2 infection and were analyzed by BSFA for S-specific IgG or IgA antibodies (**Figure 5C**). All 12 persons developed S-specific IgG class antibodies. The 12 tested persons could be grouped into 6 high and 6 low responders with a normalized MFI of above 5000 and below 3000, respectively. The sera of all infected persons also had IgG antibodies that bound to Ramos cells expressing the alpha and beta variant S proteins, albeit with lower binding intensity. The specific IgG antibodies always bound Ramos cells with the alpha variant better than those carrying the beta variant. This is in line with a study showing that pseudoviruses carrying the S protein of the beta variant are most resistant to neutralization by mAb and covalent plasma antibodies (30). Similar to what we found in the analysis of sera of persons after the second vaccination, the IgA response of infected persons is more variable than the IgG response. Four persons (C1, C4, C5 and C6) belonging to the IgG high responder group also had the most robust IgA antibody response. The IgA class antibodies in the sera of infected persons are always bound more strongly to Ramos cells expressing the WT than to those with a variant S protein, with the beta variant being less well recognized than the alpha variant.

Stability and Immune Recognition of Mutated RBD

We next wanted to learn more about how a single amino acid exchange mutation in the RBD of the S protein influences the expression of the RBD-CD8 chimeric protein as well as its recognition by soluble ACE2-IgG or anti-RBD antibodies. For this, we introduced in the RBD-CD8 construct the N501Y and the E484K point mutations characteristic for the alpha and beta variant, respectively (**Figure 6A**). In addition, we introduced a glycine to isoleucine (G496I) amino acid exchange predicted to

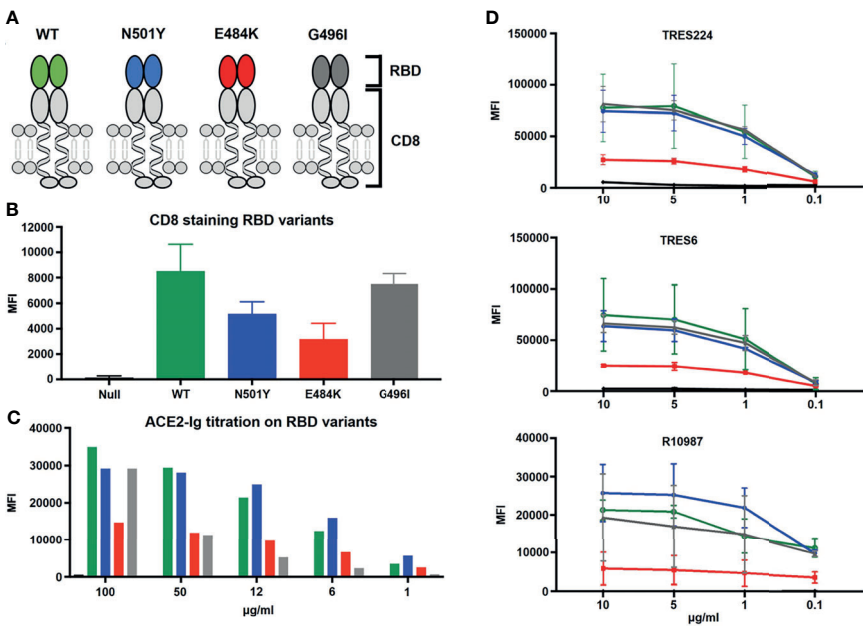

FIGURE 6 | Influence of single amino acid exchange mutation in the RBD of the S protein on the expression and binding activity of the chimeric RBD-CD8 protein. **(A)** Schematic drawing of the RBD-CD8 protein with either an WT (green), or an N501Y (blue), E484K (red) or G496I (grey) mutated RBD sequence. **(B)** Flow cytometric analysis of the expression of the RBD-CD8 protein on Ramos cells stained with anti-mouse CD8 antibodies. **(C)** Titration of the ACE2-Ig binding to the four indicated Ramos cell populations. **(D)** Titration of mAb TRES224, TRES6 and R10987 binding to Ramos cells carrying the indicated RBD-CD8 proteins. As negative control we used non-transfected Ramos cells (black). The mean values of three different experiments are shown.

increase the interaction surface between the RBD and the ACE2 receptor (31). Ramos cells expressing the different RBD-CD8 constructs were barcoded and first tested for the chimeric RBD-CD8 protein expression by using anti-CD8 antibodies (**Figure 6B** and **Supplementary Figure 3**). This experiment showed that the N501Y and E484K mutant RBD-CD8 constructs are less expressed on Ramos cells than the WT or G496I mutated construct. Apparently, the two former mutations introduced some instability into the RBD of SARS-CoV-2 that is recognized by the quality control mechanism in the endoplasmic reticulum of Ramos B cell. We next exposed the four RBD-CD8-expressing Ramos-null cells to different concentrations of ACE2-Ig and analyzed them for receptor binding (**Figure 6C**).

Interestingly, we found that, despite its lower expression, the N501Y mutant RBD-CD8 is bound better by ACE2-Ig than the WT RBD-CD8 construct, whereas Ramos cells expressing the G496I and E484K mutant RBD-CD8 constructs are less well bound by ACE2-Ig. This finding is in line with a biolayer interferometry study of ACE binding to RBD mutants (32). The three RBD-specific mAb (TRES224, TRES6 and R10987) bind to a similar extent to Ramos cells expressing the WT, N501Y, or G496I mutant RBD-CD8 proteins, whereas those cells expressing the E484K mutant RBD-CD8 constructs are poorly bound by these antibodies (**Figure 6D**). This study suggests that E484K is an immune escape mutation of the S protein. This notion is supported by BSFA of the immune sera of the 12 BioNTech/Pfizer vaccinated persons of our study groups (**Figure 7A, B**). RBD-specific IgG produced during the secondary response of the 12 vaccinated persons binds to a similar extent to Ramos cells carrying the WT, N501Y or G496I RBD-CD8 but to a lesser extent to those expressing the E484K mutant RBD-CD8 constructs. The analysis of the immune sera of the 12 infected persons with COVID-19 reveals a similar picture (**Figure 7C**). The RBD-specific IgA response showed a clear difference between the sera from the vaccinated and those of the SARS-CoV-2-infected group. Only 3 of the 12 BioNTech/Pfizer-vaccinated persons developed some RBD-specific IgA antibodies after the boost. In contrast, most infected persons showed an RBD-specific IgA response that was relatively high in three (C1, C5 and C6) of the infected COVID-19 patients (right panel **Figure 7**). However, as most IgA antibodies are present in mucosal tissues it is not clear how accurately blood IgA antibody levels represent the total IgA response.

DISCUSSION

We show here that retrovirally transfected Ramos-null B cells can stably express WT or mutated variants of the S proteins and chimeric proteins carrying only the RBD of the SARS-CoV-2 viruses. In combination with a color-coded barcoding method, this feature allowed us to compare different S-proteins or RBD mutants in their binding to either soluble ACE2-Ig molecule,

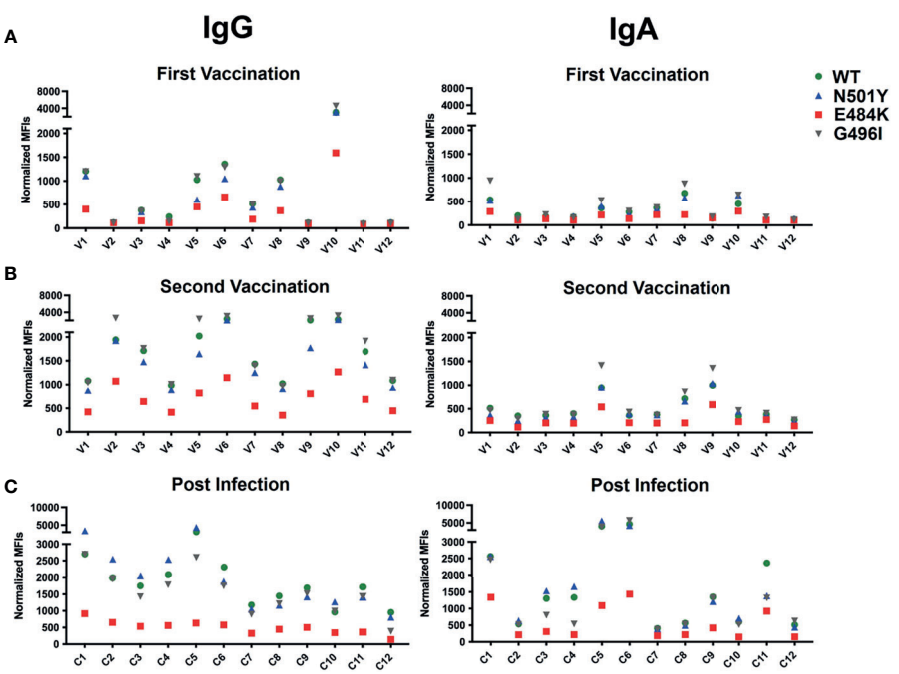

FIGURE 7 | RBD binding activity of the sera of 12 persons vaccinated with the BioNTech/Pfizer mRNA vaccine after the primary **(A)** and secondary **(B)** vaccination doses and of 12 patients with severe COVID-19 disease **(C)**. Shown is the IgG (left panel) and IgA (right panel) antibody response of the sera diluted 1:100 and analyzed for binding to Ramos cells expressing RBD-CD8 protein with either a WT (green), or an N501Y (blue), E484K (red) or G496I (grey) mutated RBD sequence. Shown are normalized MFI values.

specific mAb or antibodies of different classes in the sera of vaccinated or infected persons. Ramos cells are human B cells and are expected to express the trimeric S proteins with a glycosylation pattern and a membrane orientation found on viral particles emerging from human infected cells. The transfected Ramos cells share these features with HEK293T and Jurkat cells currently used in a coronavirus spike flow cytometric assay (16–18). An advantage of our system is that we use a retroviral transfection system to produce the native form of different S proteins on the surface of Ramos cells. In addition, retroviral vectors are efficiently and randomly integrated into many different gene loci of a transfected cell and thus generate a heterogenous population of transgene-expressing cells.

Furthermore, by using an IRES-GFP vector, we can to some extent correlate transgene with GFP expression. In this way, we can monitor the interaction of a specific binding reagent to Ramos cells carrying low, medium or high amounts of native S proteins on their surface. In addition, by using the color-coded barcoding method BSFA, we can combine up to 4 different Ramos cells in one test tube and expose them to the same binding reagent at a given concentration. In this way, we can directly compare the interaction of WT and mutant S proteins with either the soluble ACE2 receptor or specific antibodies. The BSFA can easily be adapted to test humoral immune responses against new SARS-CoV-2 variants and has the potential of high throughput of antibody screening and evaluation in a time-saving fashion.

Like other RNA viruses, SARS-CoV-2 can rapidly generate mutations during its expansion in an infected person (14). Thus, during the corona pandemic, several SARS-CoV-2 variants have emerged that became dominant in different world regions (33). Successful SARS-CoV-2 variants can be classified as either fitness and/or immune escape mutants (6). The former mutants infect and propagate themselves more efficiently in target cells, whereas the human immune system poorly recognizes the latter mutants. Our BSFA study found that Ramos cells expressing the full-length S proteins of the alpha and beta variant of SARS-CoV-2 are better bound by ACE2-Ig and by anti-RBD mAbs. This finding suggests that the variant S proteins are either more stably expressed on the Ramos cell than the WT S protein or resume a conformation with a more accessable RBD. In the case of the alpha variant, we provide direct evidence for a stronger ACE2 binding as the N501Y mutated RBD-CD8 chimera is less well expressed yet better recognized by the ACE2-Ig reagent. This is in line with data from a biolayer interferometry study (32). An unexpected finding of our study was that a single point mutation in the RBD reduces the expression of the RBD-CD8 chimera on transfected Ramos cells. Thus, these mutations seem to have an impact on the stability of the whole domain. In the full-length S protein, the RBD is either in a closed or a more open conformation, with only the open conformation able to bind to the ACE2 target (28). Hereto, the RBD amino acid point mutations selected by the alpha and beta variant may change not only the stability of the RBD but also the close/open equilibrium of the S protein and thus enable the variant virus to attach more readily to and infect its target cell.

With our BSFA approach, we can evaluate the quality of a coronavirus antibody response in terms of its specificity towards WT and variant S proteins and its target, namely epitopes within or outside the RBD structure. As most anti-RBD antibodies block the binding of the virus to the ACE2 entry receptor, they are likely to have neutralizing activity (12). Furthermore, with BSFA, we can analyze different classes of antibodies for these criteria. The evaluation of the humoral anti-SARS-CoV-2 immunity of the BioNTech/Pfizer-vaccinated group clearly showed an improved IgG response directed against the S protein and the RBD after the boost. Thus, two rounds of vaccinations are required for the efficiency of this vaccine. The IgG response of boosted persons was similar to that of patients with severe COVID-19 disease. However, the 50% high responder of the latter group developed more antibodies against the alpha variant. The humoral immunity towards the beta variant of SARS-CoV-2 was always lower in line with the finding that beta is an immune escape variant (30). A striking difference was seen in the IgA response between these groups. The S protein-specific IgA response did not improve after the second vaccination, and only 3 of the 12 vaccinated persons produced some anti-RBD antibodies after the boost. In contrast, 7 of the 12 COVID-19 patients had high IgA class anti-RBD antibodies titers in their serum.

In summary, our data show that our assay is a valuable tool to evaluate the humoral response of different immunoglobulin classes to either the vaccine or a SARS CoV-2 infection with either the wild-type or the mutant form of this virus.

DATA AVAILABILITY STATEMENT

The raw data supporting the conclusions of this article will be made available by the authors, without undue reservation.

ETHICS STATEMENT

The study was approved by the Ethical Committee of the University of Freiburg (EK-Freiburg no 210/20 and 315/10). The patients/participants provided their written informed consent to participate in this study.

AUTHOR CONTRIBUTIONS

NV, cloned the expression vector and conducted the flow cytometric assay. YO, conducted the flow cytometric assay, developed the barcoding protocol and analysed the data. FB-B, helped with the cloning. JY, designed the expression vectors and the barcoding protocol. KR, provided the ACE-Ig construct. MT, provided the pVAX1-SARS2-S plasmid. SS, SF, HE and RV collected the human sera and organized the biobank. H-MJ, generated and provided the anti-S monoclonal antibodies. MR, designed and supervised the study. RV and MR wrote the

manuscript. All authors contributed to the article and approved the submitted version.

FUNDING

This project was funded in part by the German Research Foundation (Deutsche Forschungsgemeinschaft [DFG]) through TRR130 (project2 to MR), part of this work was supported by DFG 394523286, the Helmholtz association to KR, and the GRK1660, "NaFoUniMedCovid19" (FKZ: 01KX2021) - COVIM and the Bayerische Forschungsstiftung and the Kastnerstiftung to H-MJ, and the Bayerisches Staatsministerium für Wissenschaft und Kunst.

ACKNOWLEDGMENTS

We thank Nicole Peter and Rita Rzepka for assistance with biobanking and Lise Leclercq for editing the manuscript.

SUPPLEMENTARY MATERIAL

The Supplementary Material for this article can be found online at: https://www.frontiersin.org/articles/10.3389/fimmu.2021.730766/full#supplementary-material

Supplementary Figure 1 | Serum IgG (left) and IgA (right) response in 12 persons before receiving the fisrt dose of the BioNTech/Pfizer mRNA vaccine. Evaluation of the binding to Ramos cells expressing either the WT (green), the alpha variant (blue) or the beta variant (red) S protein. **(A)** or Ramos cells expressing RBD-CD8 protein with either a WT (green), or an N501Y (blue), E484K (red) or G496I (grey) mutated RBD sequences **(B)**. Shown are normalized mean fluorescence intensity (MFI) values.

Supplementary Figure 2 | ELISA study for IgG-class anti-S1 antibodies in the sera of 12 persons vaccinated with the BioNTech/Pfizer mRNA vaccine and tested before (black), after the first (orange) or the secondary vaccination (green). Shown are the measure values related to the calibrator (measured value/calibrator).

Supplementary Figure 3 | Flow cytometric analysis of the expression of the RBD-CD8 variants on Ramos Null cells stained with anti-mouse CD8 antibodies, mAb TRES224, serum IgG of the individuals C1 and V7.

REFERENCES

1. Hu B, Guo H, Zhou P, Shi Z-L. Characteristics of SARS-CoV-2 and COVID-19. *Nat Rev Microbiol* (2021) 19(3):141–54. doi: 10.1038/s41579-020-00459-7
2. Wang M-Y, Zhao R, Gao L-J, Gao X-F, Wang D-P, Cao J-M. SARS-CoV-2: Structure, Biology, and Structure-Based Therapeutics Development. *Front Cell Infect Microbiol* (2020) 10:587269. doi: 10.3389/fcimb.2020.587269
3. Gorbalenya AE, Baker SC, Baric RS, de Groot RJ, Drosten C, Gulyaeva AA, et al. The Species Severe Acute Respiratory Syndrome-Related Coronavirus: Classifying 2019-Ncov and Naming It SARS-CoV-2. *Nat Microbiol* (2020) 5 (4):536–44. doi: 10.1038/s41564-020-0695-z
4. Chen Y, Guo Y, Pan Y, Zhao ZJ. Structure Analysis of the Receptor Binding of 2019-Ncov. *Biochem Biophys Res Commun* (2020) 525(1):135–40. doi: 10.1016/j.bbrc.2020.02.071
5. Sterlin D, Mathian A, Miyara M, Mohr A, Anna F, Claër L, et al. IgA Dominates the Early Neutralizing Antibody Response to SARS-CoV-2. *Sci Transl Med* (2021) 13(577). doi: 10.1126/scitranslmed.abd2223
6. Harvey WT, Carabelli AM, Jackson B, Gupta RK, Thomson EC, Harrison EM, et al. SARS-CoV-2 Variants, Spike Mutations and Immune Escape. *Nat Rev Microbiol* (2021) 19(7):409–24. doi: 10.1038/s41579-021-00573-0
7. Hoffmann M, Kleine-Weber H, Schroeder S, Krüger N, Herrler T, Erichsen S, et al. SARS-CoV-2 Cell Entry Depends on ACE2 and TMPRSS2 and Is Blocked by a Clinically Proven Protease Inhibitor. *Cell* (2020) 181(2):271–280. doi: 10.1016/j.cell.2020.02.052
8. Duan L, Zheng Q, Zhang H, Niu Y, Lou Y, Wang H. The SARS-CoV-2 Spike Glycoprotein Biosynthesis, Structure, Function, and Antigenicity: Implications for the Design of Spike-Based Vaccine Immunogens. *Front Immunol* (2020) 11:2593. doi: 10.3389/fimmu.2020.576622
9. Barnes CO, Jette CA, Abernathy ME, Dam K-MA, Esswein SR, Gristick HB, et al. SARS-CoV-2 Neutralizing Antibody Structures Inform Therapeutic Strategies. *Nature* (2020) 588(7839):682–7. doi: 10.1038/s41586-020-2852-1
10. Ou X, Liu Y, Lei X, Li P, Mi D, Ren L, et al. Characterization of Spike Glycoprotein of SARS-CoV-2 on Virus Entry and Its Immune Cross-Reactivity With SARS-CoV. *Nat Commun* (2020) 11(1):1620. doi: 10.1038/s41467-020-15562-9
11. Walls AC, Park Y-J, Tortorici MA, Wall A, McGuire AT, Veesler D. Structure, Function, and Antigenicity of the SARS-CoV-2 Spike Glycoprotein. *Cell* (2020) 181(2):281–292.e6. doi: 10.1016/j.cell.2020.02.058
12. Piccoli L, Park Y-J, Tortorici MA, Czudnochowski N, Walls AC, Beltramello M, et al. Mapping Neutralizing and Immunodominant Sites on the SARS-CoV-2 Spike Receptor-Binding Domain by Structure-Guided High-Resolution Serology. *Cell* (2020) 183(4):1024–42.e21. doi: 10.1016/j.cell.2020.09.037
13. *Tracking SARS-CoV-2 Variants* (2021). Available at: https://www.who.int/en/activities/tracking-SARS-CoV-2-variants/ (Accessed cited 2021 June 17).
14. Wang P, Nair MS, Liu L, Iketani S, Luo Y, Guo Y, et al. Increased Resistance of SARS-CoV-2 Variants B.1.351 and B.1.1.7 to Antibody Neutralization. *bioRxiv* (2021). doi: 10.1101/2021.01.25.428137
15. D'Cruz RJ, Currier AW, Sampson VB. Laboratory Testing Methods for Novel Severe Acute Respiratory Syndrome-Coronavirus-2 (SARS-CoV-2). *Front Cell Dev Biol* (2020) 8:468. doi: 10.3389/fcell.2020.00468
16. Goh YS, Chavatte J-M, Lim Jieling A, Lee B, Hor PX, Amrun SN, et al. Sensitive Detection of Total Anti-Spike Antibodies and Isotype Switching in Asymptomatic and Symptomatic Individuals With COVID-19. *Cell Rep Med* (2021) 2(2):100193. doi: 10.1016/j.xcrm.2021.100193
17. Lapuente D, Maier C, Irrgang P, Hübner J, Peter AS, Hoffmann M, et al. Rapid Response Flow Cytometric Assay for the Detection of Antibody Responses to SARS-CoV-2. *Eur J Clin Microbiol Infect Dis* (2021) 40(4):751–9. doi: 10.1007/s10096-020-04072-7
18. Horndler L, Delgado P, Abia D, Balabanov I, Martínez-Fleta P, Cornish G, et al. Flow Cytometry Multiplexed Method for the Detection of Neutralizing Human Antibodies to the Native SARS-CoV-2 Spike Protein. *EMBO Mol Med* (2021) 13(3):e13549. doi: 10.15252/emmm.202013549
19. Cao L, Pauthner M, Andrabi R, Rantalainen K, Berndsen Z, Diedrich JK, et al. Differential Processing of HIV Envelope Glycans on the Virus and Soluble Recombinant Trimer. *Nat Commun* (2018) 9(1):3693. doi: 10.1038/s41467-018-06121-4
20. Song G, He W, Callaghan S, Anzanello F, Huang D, Ricketts J, et al. Cross-Reactive Serum and Memory B-Cell Responses to Spike Protein in SARS-CoV-2 and Endemic Coronavirus Infection. *Nat Commun* (2021) 12(1):2938. doi: 10.1038/s41467-021-23074-3
21. Hörnich BF, Großkopf AK, Schlagowski S, Tenbusch M, Kleine-Weber H, Neipel F, et al. SARS-CoV-2 and SARS-CoV Spike-Mediated Cell-Cell Fusion Differ in Their Requirements for Receptor Expression and Proteolytic Activation. *J Virol* (2021) 95(9):e00002-21. doi: 10.1128/JVI.00002-21
22. Peter AS, Roth E, Schulz SR, Fraedrich K, Steinmetz T, Damm D, et al. A Pair of Non-Competing Neutralizing Human Monoclonal Antibodies Protecting From Disease in a SARS-CoV-2 Infection Model. *bioRxiv* (2021). doi: 10.1101/2021.04.16.440101
23. Kreer C, Zehner M, Weber T, Ercanoglu MS, Gieselmann L, Rohde C, et al. Longitudinal Isolation of Potent Near-Germline SARS-CoV-2-Neutralizing Antibodies From COVID-19 Patients. *Cell* (2020) 182(4):843–854.e12. doi: 10.1016/j.cell.2020.06.044
24. Klein G, Giovanella B, Westman A, Stehlin JS, Mumford D. An EBV-Genome-Negative Cell Line Established From an American Burkitt Lymphoma; Receptor Characteristics. EBV Infectibility and Permanent

Conversion Into EBV-Positive Sublines by *In Vitro* Infection. *Intervirology* (1975) 5(6):319–34. doi: 10.1159/000149930
25. Kläsener K, Jellusova J, Andrieux G, Salzer U, Böhler C, Steiner SN, et al. CD20 as a Gatekeeper of the Resting State of Human B Cells. *Proc Natl Acad Sci USA* (2021) 118(7). doi: 10.1073/pnas.2021342118
26. He X, Kläsener K, Iype JM, Becker M, Maity PC, Cavallari M, et al. Continuous Signaling of CD79b and CD19 Is Required for the Fitness of Burkitt Lymphoma B Cells. *EMBO J* (2018) 37(11). doi: 10.15252/embj.201797980
27. Wang P, Nair MS, Liu L, Iketani S, Luo Y, Guo Y, et al. Antibody Resistance of SARS-CoV-2 Variants B.1.351 and B.1.1.7. *Nature* (2021) 593(7857):130–5. doi: 10.1038/s41586-021-03398-2
28. Wrapp D, Wang N, Corbett KS, Goldsmith JA, Hsieh C-L, Abiona O, et al. Cryo-EM Structure of the 2019-Ncov Spike in the Prefusion Conformation. *Science* (2020) 367(6483):1260–3. doi: 10.1126/science.abb2507
29. Muik A, Wallisch A-K, Sänger B, Swanson KA, Mühl J, Chen W, et al. Neutralization of SARS-CoV-2 Lineage B.1.1.7 Pseudovirus by BNT162b2 Vaccine-Elicited Human Sera. *Science* (2021) 371(6534):1152–3. doi: 10.1126/science.abg6105
30. Wang R, Zhang Q, Ge J, Ren W, Zhang R, Lan J, et al. Analysis of SARS-CoV-2 Variant Mutations Reveals Neutralization Escape Mechanisms and the Ability to Use ACE2 Receptors From Additional Species. *Immunity* (2021) 54(7):1611–21. doi: 10.1016/j.immuni.2021.06.003
31. Smaoui MR, Yahyaoui H. Unraveling the Stability Landscape of Mutations in the SARS-CoV-2 Receptor-Binding Domain. *Sci Rep* (2021) 11(1):9166. doi: 10.1038/s41598-021-88696-5
32. Amanat F, Thapa M, Lei T, Sayed Ahmed SM, Adelsberg DC, Carreno JM, et al. SARS-CoV-2 mRNA Vaccination Induces Functionally Diverse Antibodies to NTD, RBD and S2. *Cell* (2021) 184(15):3936–48. doi: 10.1016/j.cell.2021.06.005
33. Volz E, Mishra S, Chand M, Barrett JC, Johnson R, Geidelberg L, et al. Transmission of SARS-CoV-2 Lineage B.1.1.7 in England: Insights From Linking Epidemiological and Genetic Data. (2021). doi: 10.1101/2020.12.30.20249034

Conflict of Interest: The authors declare that the research was conducted in the absence of any commercial or financial relationships that could be construed as a potential conflict of interest.

Publisher's Note: All claims expressed in this article are solely those of the authors and do not necessarily represent those of their affiliated organizations, or those of the publisher, the editors and the reviewers. Any product that may be evaluated in this article, or claim that may be made by its manufacturer, is not guaranteed or endorsed by the publisher.

frontiers in Immunology

ORIGINAL RESEARCH
published: 18 March 2022
doi: 10.3389/fimmu.2022.770982

Evaluation of Spike Protein Epitopes by Assessing the Dynamics of Humoral Immune Responses in Moderate COVID-19

Lingyun Chen[1,2†], Pengfei Pang[3†], Huan Qi[4†], Keqiang Yan[1,2], Yan Ren[2], Mingliang Ma[4], Ruyin Cao[2], Hua Li[5], Chuansheng Hu[5], Yang Li[4], Jun Xia[1,2], Danyun Lai[4], Yuliang Dong[2], Hewei Jiang[4], Hainan Zhang[4], Hong Shan[3], Shengce Tao[4*] and Siqi Liu[1,2*]*

[1] College of Life Science, University of Chinese Academy of Sciences, Beijing, China, [2] Department of Proteomics, Beijing Genomics Institution, Shenzhen, China, [3] Center for Interventional Medicine, The Fifth Affiliated Hospital of Sun Yat-sen University, Zhuhai, China, [4] Shanghai Center for Systems Biomedicine, Shanghai Jiaotong University, Shanghai, China, [5] State Key laboratory for Oncogenes and Bio-ID Center, School of Biomedical Engineering, Shanghai Jiao Tong University, Shanghai, China

The coronavirus disease 2019 (COVID-19) pandemic is caused by a novel coronavirus called severe acute respiratory syndrome coronavirus 2 (SARS-CoV-2). The spike protein (S) of SARS-CoV-2 is a major target for diagnosis and vaccine development because of its essential role in viral infection and host immunity. Currently, time-dependent responses of humoral immune system against various S protein epitopes are poorly understood. In this study, enzyme-linked immunosorbent assay (ELISA), peptide microarray, and antibody binding epitope mapping (AbMap) techniques were used to systematically analyze the dynamic changes of humoral immune responses against the S protein in a small cohort of moderate COVID-19 patients who were hospitalized for approximately two months after symptom onset. Recombinant truncated S proteins, target S peptides, and random peptides were used as antigens in the analyses. The assays demonstrated the dynamic IgM- and IgG recognition and reactivity against various S protein epitopes with patient-dependent patterns. Comprehensive analysis of epitope distribution along the *spike* gene sequence and spatial structure of the homotrimer S protein demonstrated that most IgM- and IgG-reactive peptides were clustered into similar genomic regions and were located at accessible domains. Seven S peptides were generally recognized by IgG antibodies derived from serum samples of all COVID-19 patients. The dynamic immune recognition signals from these seven S peptides were comparable to those of the entire S protein or truncated S1 protein. This suggested that the humoral immune system recognized few conserved S protein epitopes in most COVID-19 patients during the entire duration of humoral immune response after symptom onset. Furthermore, in this cohort, individual patients demonstrated stable immune recognition to certain S protein epitopes throughout their hospitalization period. Therefore, the dynamic characteristics of humoral immune responses to S protein have provided valuable information for accurate diagnosis and immunotherapy of COVID-19 patients.

Keywords: SARS-CoV-2, COVID-19, S protein, epitope, dynamics, ELISA, microarray, AbMap

OPEN ACCESS

Edited by:
Moncef Zouali, Institut National de la Santé et de la Recherche Médicale (INSERM), France

Reviewed by:
Lázaro Gil, St. Michael's Hospital, Canada
Karina Andrea Gomez, CONICET Instituto de Investigaciones en Ingeniería Genética y Biología Molecular Dr. Héctor N. Torres (INGEBI), Argentina

***Correspondence:**
Siqi Liu
siqiliu@genomics.cn
Shengce Tao
taosc@sjtu.edu.cn
Hong Shan
shanhong@mail.sysu.edu.cn

†These authors have contributed equally to this work and share the first authorship

Specialty section:
This article was submitted to B Cell Biology, a section of the journal Frontiers in Immunology

Received: *05 September 2021*
Accepted: *15 February 2022*
Published: *18 March 2022*

Citation:
Chen L, Pang P, Qi H, Yan K, Ren Y, Ma M, Cao R, Li H, Hu C, Li Y, Xia J, Lai D, Dong Y, Jiang H, Zhang H, Shan H, Tao S and Liu S (2022) Evaluation of Spike Protein Epitopes by Assessing the Dynamics of Humoral Immune Responses in Moderate COVID-19. Front. Immunol. 13:770982. doi: 10.3389/fimmu.2022.770982

INTRODUCTION

The coronavirus disease 2019 (COVID-19) pandemic is caused by a novel and highly contagious and pathogenic coronavirus (CoV) called severe acute respiratory syndrome coronavirus 2 (SARS-CoV-2) (1). To date, seven human CoVs, namely hCoV-NL63, hCoV-229E, hCoV-OC43, hCoV-HKU1, severe acute respiratory syndrome CoV (SARS-CoV), Middle East respiratory syndrome CoV (MERS-CoV), and SARS-CoV-2 have been identified and characterized (2, 3). SARS-CoV, MERS-CoV, and SARS-CoV-2 infections can cause life-threatening diseases with strong pandemic potential (4). Multiple factors, including host immunity against viral infection influence COVID-19 diagnosis and therapy (5–7). Therefore, the characterization of humoral immune responses against SARS-CoV-2 would greatly advance the development of novel diagnostic approaches and effective vaccines.

The innate or adaptive immune responses of the host that are elicited upon encountering SARS-CoV-2, generate detectable SARS-CoV-2-specific antibodies between 10 and 14 days after symptom onset (8–11). The identification of viral antigenic epitopes that induce humoral immune responses is essential for understanding host immunity against SARS-CoV-2. As previously observed with other coronaviruses, SARS-CoV-2 genome-encoded *spike* (*S*) and *nucleocapsid* (*N*) gene expression products are highly immunogenic and major targets of antibodies (12, 13). Hence, both these antigens are relevant for the diagnosis of COVID-19 and form the basis for most immunoassays available in the clinic (14, 15). In contrast to the nucleocapsid (N) protein, the spike (S) protein is not only the main causal factor of immunogenicity, but also plays a central role in viral entry into host cells by binding to angiotensin-converting enzyme 2 (ACE2) (16). Zhou et al. reported that convalescent serum against S protein was both a marker for viral exposure and an indicator of recovery from viral infection (17). Dispinseri et al. claimed a strong correlation between IgG antibodies against the S protein of COVID-19 and viral neutralization (18). Therefore, the S protein is the primary focus of studies related to SARS-CoV-2 vaccines and antibody-based therapeutics.

The immunogenic characteristics of the S protein from SARS-CoV-2 are well known. Poh et al. reported that two linear S epitopes elicited the neutralizing antibodies (19). Shrock et al. showed the IgA and IgG recognition of immunodominant regions in S protein (20). Recently, some studies reported temporal changes in the humoral immune response after symptom onset (21–25). Ravichandran et al. performed a comprehensive longitudinal analysis of the antibody repertoire to S protein in COVID-19 patients during their hospital stay between the second and tenth weeks and demonstrated a correlation between increased antibody affinity maturation to prefusion COVID-19 S protein and disease severity (23).

Effective immunity against viral infection relies on the ability of B cells to generate a diverse repertoire of antibodies to neutralize the virus (26). Activated B cells form germinal centers in the secondary lymphoid tissues (spleen and peripheral lymph nodes) after encountering the virus and undergo iterative cycles of clonal expansion and somatic hypermutations in the variable regions of their immunoglobulin heavy and light chain genes, followed by affinity-based selection of antibodies with high antigen specificity (27). Moreover, recent high-throughput sequencing technologies have shown novel perspectives regarding the generation of B cell receptor (BCR) repertoires in a time- and individual-dependent manner, which orchestrate dynamic humoral immune responses against influenza virus, Zika virus (28), Ebola virus (29), and HIV (30). As for SARS-CoV-2, BCR repertoire sequencing revealed the usage frequency of different *V* and *J* gene segments and B-cell clonal expansion in infected individuals during the period after symptom onset (31–34). Nielsen et al. reported extensive class switching to IgG and IgA subclasses with limited hypermutations during the initial weeks of COVID-19 infection (31).

Several research groups are currently attempting to understand the mechanisms underlying the role of immunoglobulin gene editing or immunoglobulin recognition in the S protein of SARS-CoV-2. Most reports in this research area have relied on data generated from a single technology; therefore, the relevant conclusions have lacked supporting evidence through different technologies. In addition, early studies did not focus on designing and analyzing the general patterns of longitudinal recognition of immunoglobulins to S epitopes, while the scattered reports from different investigators were difficult to integrate for a fundamental understanding of the time-dependent rule of humoral immune responses against SARS-CoV-2. These prompted us to initiate a project, which carried out a systematical survey to the longitudinal changes of humoral immune responses specifically against S epitopes. A total of 123 serum samples from 19 patients with COVID-19 were collected over a period of approximately two months after symptom onset. The time-dependent reactivity of immunoglobulins in patients was assessed using three types of antigens *in vitro*: recombinant truncated S proteins, synthesized S peptides, and random peptides. The experimental design and data analysis are illustrated in **Supplementary Figure 1**.

MATERIALS AND METHODS

Collection of Serum Samples From Moderate COVID-19 Patients

Nineteen COVID-19 patients were recruited, who were admitted to the Fifth Affiliated Hospital of Sun Yat-sen University and were clinically treated according to the Diagnosis and Treatment Protocol for Novel Coronavirus Pneumonia (Trial Version 4 released by the National Health Commission & State Administration of Traditional Chinese Medicine on January 27, 2020). All COVID-19 patients were positive for SARS-CoV-2 according to the RT-PCR results from oropharyngeal swabs and showed moderate COVID-19 disease symptoms. All patients had been hospitalized after symptom onset and blood samples were collected during hospitalization. Considering the common cases of COVID-19 patients and comparable treatments in the hospital, 123 blood specimens were collected in a time-interval mode from these 19 patients during the hospitalization period of approximately two months, starting on February 1st and ending on March 29th (**Supplementary Tables 1**, **2**). The average age of the patients was 51 years (range: 29–71; 9 women and 10 men). As the control group,

the non-COVID-19 sera were donated from 27 healthy donors whose blood samples were collected from the same hospital. Blood specimen collection was approved by the Research Ethics Committee of the Fifth Affiliated Hospital of Sun Yat-sen University, Zhuhai, China (Approval No. K62-1), and signed written informed consent was obtained from all the participants of the study.

Estimation of Humoral Immune Responses Against SARS-CoV-2 by Enzyme Linked Immunosorbent Assay (ELISA)

Serum antibodies were analyzed in COVID-19 patients and healthy subjects using the commercial ELISA kits. Serum IgG activity against purified antigens of inactivated viral lysates was measured using the SARS-CoV-2 Virus IgG Antibody Detection Kit (Beijing BGI-GBI Biotech Co., Ltd., Beijing, China). Serum IgM activity against recombinant S1 and N proteins with IgM μ-chain capture was measured using the SARS-CoV-2 Virus IgM Antibody Detection Kit (Beijing BGI-GBI Biotech Co., Ltd., Beijing, China).

Microarray Analysis of Humoral Immune Responses Against SARS-CoV-2

Microarray Construction

The *S* gene sequence (MN908947.3) of SARS-CoV-2 was downloaded from the GenBank database. The *S* gene fragments corresponding to *S1*, *RBD*, and *S2* were synthesized (Sangon Biotech, Shanghai, China) and cloned into the pGEX-4T-1 vector. The expression vector was transformed into *Escherichia coli* BL21 for the expression of the recombinant S1, S2, and RBD, and the expressed proteins were purified using GST-Sepharose beads (Senhui Microsphere Technology, Suzhou, China (35). The 12-mer linear peptides covering the entire S protein sequence (1–1,273, YP_009724390.1) were designed based on the interval overlap of six residues, and in total of 211 peptides with N-terminal amidated were chemically synthesized (GL Biochem, Ltd., Shanghai, China). These S peptides were conjugated with BSA using Sulfo-SMCC (Thermo Fisher Scientific, MA, USA) according to the instructions of the manufacturer. The S recombinants and synthesized peptides were printed in triplicate onto PATH substrate slides (Grace Bio-Labs, Oregon, USA) using the Super Marathon printer (Arrayjet, Roslin, UK) to generate identical arrays in a 1 × 7 subarray format (36). The microarrays were stored at −80°C until further use. To normalize the fluorescence signals in the microarray, GST, biotin-control, and eGFP were used as negative controls, while human IgG, human IgM, and ACE2-Fc as positive controls.

Microarray-Based Immunoassay

A 14-chamber rubber gasket was mounted on each slide to create individual chambers with 14 identical homemade subarrays. The previously frozen arrays were warmed to room temperature and incubated in the block buffer (3% BSA in 1 × PBS buffer with 0.1% Tween 20) for 3 h. The serum samples were diluted with 1× PBS containing 0.1% Tween 20 (1:200) and incubated with each subarray for 2 h at room temperature. After washing with 1× PBST, the subarrays were incubated with secondary antibodies, namely Cy3-conjugated goat anti-human IgG and Alexa Fluor 647-conjugated donkey anti-human IgM (Jackson ImmunoResearch, PA, USA) at room temperature for 1 h. Subsequently, the subarrays were washed with 1× PBST again, dried at room temperature by centrifugation, and scanned using LuxScan 10 K-A (CapitalBio Corporation, Beijing, China) with the following parameters: 95% laser power/PMT 550 for IgM and 95% laser power/PMT 480 for IgG.

Microarray Data Processing

The fluorescence intensities (FI) from the microarray were extracted using the GenePix Pro 6.0 software (Molecular Devices, CA, USA). For each spot, the FI was obtained by subtracting the FI of the background from that of the foreground. The FI quantification of humoral immune responses to the individual recombinant S proteins or peptides was performed by calculating the average of FI from triplicate spots. The positive peptides were recognized from the COVID-19 sera by using a cut-off value of mean FI + 3 × standard deviation (SD) of healthy subjects. The intensity of the immune reactivity for each peptide was normalized in different patients using the Z-score, which was calculated as follows: $Z\ score = FI_{Ppn} - meanFI_{Pp1\ldots Ppn})/SD_{Pp1\ldots Ppn}$, where *Ppn* is defined as the peptide or protein reactivity at a sampling point from a COVID-19 patient and *Pp1…Ppn* represents cumulative measurements of all sampling points from the same COVID-19 patient (37).

AbMap Analysis of Humoral Immune Responses Against SARS-CoV-2

Purification of Antibodies Against S1 Protein in the Patient Sera

Recombinant S1 protein (Sino Biological, Beijing, China) was biotinylated according to the protocol of the manufacturer (Thermo Fisher Scientific, Rockford, USA). The biotinylated S1 protein was then incubated with Dynabesads™ Myone™ Streptavidin T1 (Thermo Fisher Scientific, Carlsbad, USA) at room temperature for 1 h to immobilize the protein on the surface of the magnetic beads (S1-magnetic beads). Then, the serum samples from COVID-19 patients were incubated with the S1-magnetic beads at 4°C for 4 h. Then, the S1-magnetic beads were washed with PBST to eliminate non-specific binding. The bound antibodies were eluted with 50 mM glycine (pH 2.8) followed by neutralization with 1M Tris buffer (pH 8.0).

AbMap Assay

The antibody binding epitope mapping (AbMap) assay developed in our laboratory was previously performed (38). Briefly, 96-well PCR plates were blocked with PBST containing 3% BSA at 4°C for 16 h. Each well was then loaded with Ph.D.-12 phage display libraries (New England Biolabs, MA, USA) followed by adding the S1 antibody purified above. The mixtures were incubated at 4°C for 16 h. Dynabeads™ Protein G (Thermo Fisher Scientific, Carlsbad, CA, USA) was added into each well to capture the antibody and phage complex at 4°C for 4 h. The magnetic beads in each well were collected and washed. The beads suspended in water were boiled at 98°C for 10 min, and the resulting supernatant was collected for further PCR analysis.

To introduce the adapter sequence and unique barcode or index for each sample, two rounds of PCR were carried out on the phage lysate using Q5 hot-start polymerase. The first round of PCR was performed by using XX-S5XX-23R and XX-N7XX-18 primers (5′-TCGTCGGCAGCGTCAGATGTGTATAAGAG ACAGXXXXXXXXGTGGTACCTTTCTATTCTCACTCT-3′, and 5′-GTCTCGTGGGCTCGGAGATGTGTATAAGAGA CAGXXXXXXXXTTCAACAGTTTCGGCCGAACCT-3′, respectively; where, "XXXXXXXX" denotes an eight-nucleotide barcode sequence; the sequence with the underline represents the specific primer for amplifying the corresponding nucleotides of the displayed peptides from the phage genome; the remaining sequence represents the Illumina index). After electrophoresis, all PCR products were mixed and purified as templates for the second round of PCR. In the second round of PCR, unique indices of Illumina next generation sequencing (NGS) were introduced for each mixture. The products obtained from the second round of PCR were sequenced using Illumina HiSeq 2000 (Illumina Inc. CA, USA).

AbMap Data Processing

The NGS results were split and assigned to each sample based on the index and barcode combinations. For each sample, the NGS data were trimmed further and only sequences of 36 base pairs corresponding to the 12-mer displayed peptides remained. All the remaining sequences were translated into peptides and the translation frequency of each peptide was counted. The enrichment and reverse enrichment factors for each peptide from the samples were calculated and set as cutoff values. The peptides with the enrichment factors above the cutoff were retained for subsequent motif analysis. The remaining peptides were subjected to MEME (Motif-based Sequence Analysis Tools, https://techtransfer.universityofcalifornia.edu/NCD/20911.html) to identify motifs that represent clusters of 12-mer peptides. During this analysis, eight motifs were generated for each sample and a motif with an E value less than 0.01 was considered significant and further matched to the S protein sequence using the MAST (Motif Alignment & Search Tools, https://mccb.umassmed.edu/meme/doc/mast.html).

Dynamic Immune Response Data Analysis

Since the time points of specimen collection varied between different patients in this study, the dynamic data were normalized according to the weeks after symptom onset during hospitalization. For individual patients, dynamic analysis was performed on the immune responses against different S proteins or epitopes that were consistently observed during the hospitalization weeks and normalized by Z-scores. The dynamic analysis included (1) estimating positive frequencies of immune recognition in all patients for individual peptides from the microarray or AbMap, (2) hierarchically clustering the quantified immune responses from the microarray, and (3) assessing the dynamic behaviors of the S proteins or peptides commonly observed in the patient sera by (1) statistical curve fitting of the normalized intensities of immune responses at different time points and (2) generating heatmaps with intensities of immune responses. All statistical analyses were performed using R statistical software.

Spatial Analysis of the S Epitopes

The secondary structures of the potential S epitopes were analyzed by DPSS (Dictionary of Protein Secondary Structure, https://2struc.cryst.bbk.ac.uk/about/). The 3D structure of the S protein from Zhang's laboratory (https://zhanglab.ccmb.med.umich.edu) was taken to analyze the spatial location of the potential epitopes. All the spatial images were processed using the PyMOL software (The PyMOL Molecular Graphics System, Version 2.0, Schrödinger, NY, USA).

RESULTS

Dynamics of Humoral Immune Responses Against S Proteins in the COVID-19 Patients

First, the humoral immune responses to SARS-CoV-2 in COVID-19 patients were estimated by ELISA, and the levels of specific IgM and IgG antibodies were measured using N and recombinant S1 proteins and viral extracts as antigens. The Z-scores of IgM against the N and recombinant S1 protein were significantly high during the first two weeks after symptom onset and then gradually diminished during the remaining period of hospitalization (**Figure 1A**). In contrast, the Z-scores of IgG against the viral extracts remained in a continuously increased mode during the first four weeks and reached a plateau between the fifth and sixth weeks after symptom onset (**Figure 1A**).

Next, the humoral immune responses against SARS-CoV-2 were evaluated by microarray using three recombinant truncated S proteins: S1, S2 and RBD. The serum samples of COVID-19 patients exhibited significantly higher IgG antibody reactivity against all three recombinant S proteins than healthy subjects (**Figure 1B**). Moreover, the strength of serum antibody reactivity varied significantly between individual recombinant S proteins. The recombinant S1 protein showed 10-fold higher serum antibody reactivity than the recombinant S2 and RBD proteins (**Figure 1B**). In the COVID-19 patients, serum IgM reactivity was generally lower than the corresponding serum IgG reactivity against the recombinant S proteins (**Figure 1B**). Furthermore, although IgM reactivity signals against RBD in COVID-19 patients were significantly higher than those in healthy subjects, the signals were relatively low among the COVID-19 patients and did not provide reliable dynamic data. The IgM antibodies in the COVID-19 patients displayed poor reactivity against S2 and the signal was similar to that displayed by healthy subjects (**Figure 1B**). These findings demonstrated much stronger affinity of the patient serum samples against S1 than RBD and S2 recombinant proteins in the microarray assay. In further dynamic analysis of humoral immune responses to S-truncated proteins, S1 was selected as the main immune target but not S2 and RBD. The time-dependent serum IgM and IgG reactivity against S1 in all patients were plotted in **Figure 1C**, in which the trends of immune reactivity were similar to the ELISA

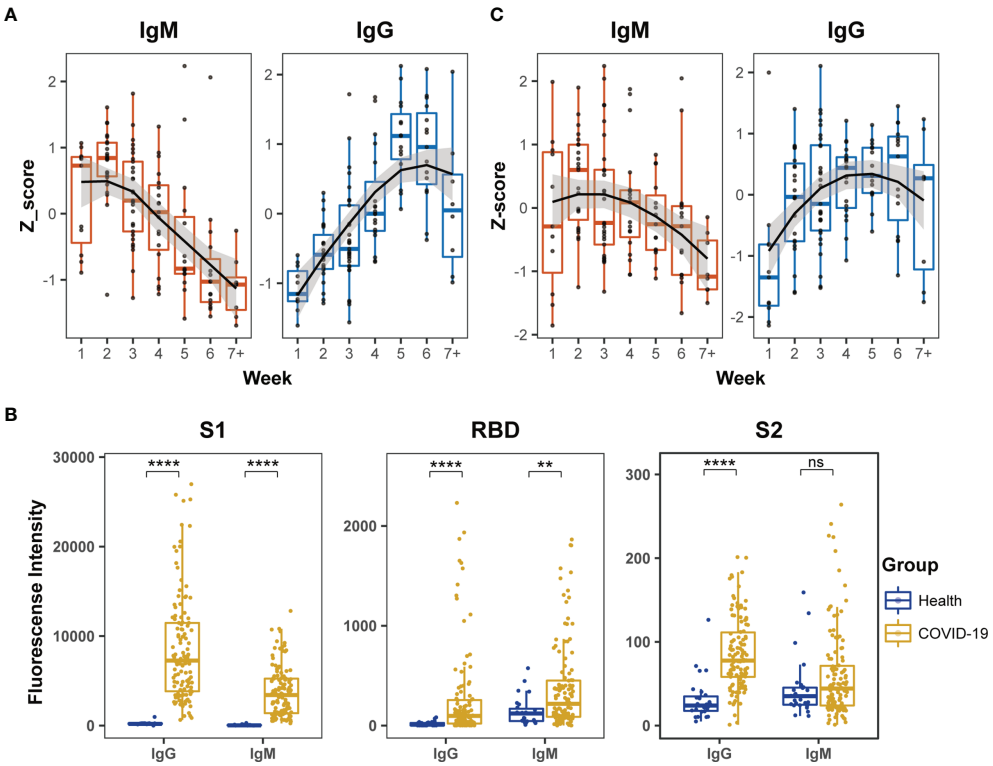

FIGURE 1 | Dynamic behaviors of humoral immune responses against S protein in COVID-19 patients. **(A)** The dynamic changes of IgM against N and recombinant S1 protein and IgG against the extract proteins from virus lysate based on ELISA. The signals of antibody responses in the patient serum samples were normalized by Z-scores and the trends of signal changes were mimicked by curve fitting. **(B)** Comparisons of IgM or IgG immune signals against the truncated S proteins, S1, RBD and S2, between healthy subjects (n = 27) and all COVID-19 (n = 123) serum samples based on the microarray data. Unpaired Student's t-test was used in the statistical analysis. Note: **p < 0.01, ****p < 0.0001, and ns, non-significance. **(C)** The dynamic changes of IgM and IgG against recombinant S1 protein based on microarray.

data illustrated in **Figure 1A**; IgM activity emerged at an early time point and subsided, whereas IgG activity emerged at a later time point and was sustained for longer. As the time-dependent pattern of IgG reactivity to the intact proteins in the extract of virus-infected cells (**Figure 1A**) was similar to the pattern derived from **Figure 1C**, these data suggested that the humoral immune responses of COVID-19 patients mainly targeted the S1 protein compared to other viral antigens.

Evaluation Towards the Epitope Features of S Peptides Recognized by the COVID-19 Sera on Microarray

To further study the dynamic features of humoral immune responses to S epitopes during the period of hospitalization, a peptide microarray comprising 211 peptides derived from the S protein was implemented to assess the immune reactivity between the peptides and the patient sera. Hierarchical clustering analysis illustrated that serum IgM reactivity against the S peptides were similar in COVID-19 patients and healthy individuals, few serum samples from COVID-19 patients gave positive signals (**Figure 2A**). However, serum IgG from COVID-19 patients showed higher reactivity against some S peptides than healthy individuals (**Figure 2A**). Furthermore, the signals from both IgM and IgG antibodies for individual patient samples at multiple time points were clustered together (**Figure 2A**). This suggested generation of highly specific and unique antibodies in individual patients against the S peptides.

After applying strict criteria (mean + 3 SD of the signal in healthy subjects) to remove S peptides with weak immune signals, 124 IgM-reactive S peptides and 165 IgG-reactive S peptides were identified in COVID-19 patients. The number of S peptides recognized by the serum samples was patient-dependent, with 1–45 IgM-reactive peptides and 38–91 IgG-reactive peptides per patient (**Supplementary Figure 2**). The peptides uniquely recognized by individual patients occupied relatively higher ratios: 42.7% (53/124) for IgM and 16.4% (27/165) for IgG. Specifically, none of the S peptides (0/124) were commonly recognized by IgM antibodies in the sera of all 19 patients, whereas 10 (6%; 10/165) S peptides were commonly recognized by IgG antibodies in the serum samples of all 19 COVID-19 patients. These results implied that the S epitopes commonly recognized by patient serum samples were quite limited, even for IgG antibodies. On the other hand, IgM

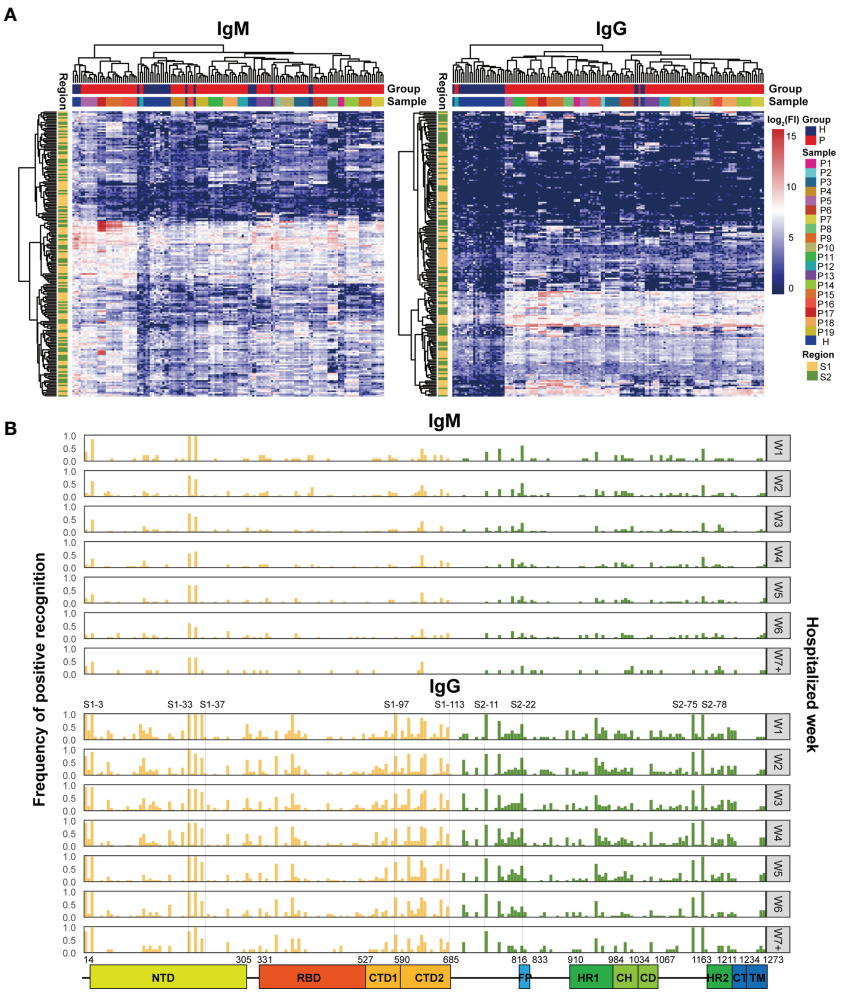

FIGURE 2 | Microarray analysis of the immune recognition features in the S peptide epitopes. **(A)** Hierarchical clustering of signals based on immune reactivity from IgM or IgG of healthy subjects and COVID-19 patients against all the S synthesized peptides measured by microarray. The bars upper: distribution of the healthy (blue) and COVID-19 (red) samples (top) and of all the individual samples (bottom) based on the clustered results. The bars right: the intensity indicator of immune reactivity (left) and the indicator of individual samples (right). The bar left indicates the distribution of S1 (yellow) and S2 (green) based on the cluster results. **(B)** Frequency distribution of the S peptides positively recognized by the patient IgM or IgG during hospitalization. The x axis represents the entire *S* gene sequence; the color bars at the bottom denote functional domains of S protein, namely, N-terminal domain (NTD, 14–305), receptor binding domain (RBD, 331–527), C-terminal domain 1 (CTD1, 528–590), C-terminal domain 2 (CTD2, 591–684), fusion peptide (FP, 816–83), heptad repeat 1 (HR1, 910–984), central helix (CH, 985–1034), connector domain (CD, 1,035–1,067), HR2 (heptad repeat 2, 1,163–1,211), transmembrane domain (TM, 1,212–1,234), and cytoplasmic tail (CT, 1,235–1,273).The y axis (left) represents the frequency of the S peptides that are positively recognized by antibodies, while the gray signs on right mean the hospitalization time (weekly counted). The yellow and green bars indicate S peptides located in the S1 and S2 subunits, respectively.

reactivity against the S peptides was very weak in the patient serum samples, and therefore accounted for greater diversity in the recognition of the S peptides between COVID-19 patient serum samples.

The question was how the S peptides recognized by COVID-19 IgM or IgG antibodies were localized along the viral genomic sequences. The frequencies of S peptide recognition by IgM or IgG antibodies in all patients during the consecutive periods of hospitalization were plotted against the *S* gene regions in the SARS-CoV-2 genome, as shown in **Figure 2B** (Top: IgM; Bottom: IgG). The S peptides reacting with higher frequencies against patient IgG were mainly present in four regions, namely, residues 193–228 in NTD (S1-33 to S1-37), residues 577–684 in CTD (S1-97 to S1-113), 746–829 in S2C1 adjacent FP (S2-11 to S2-22) and 1,130–1,219 in HR2 and TM (S2-75 and S2-88). Although IgM antibodies recognized fewer S peptides with high affinity, those that were highly reactive and frequent were also distributed in the same four regions (**Figure 2B**). The epitopes of the S protein corresponding to those reactions with the IgM and IgG antibodies from different COVID-19 patients were clustered to similar genomic regions, even though the recognition specificity and reactivity varied significantly among the COVID-19 patients. The recognition frequencies of many peptides, including those from the four regions mentioned

above, progressively decreased during the later stages of hospitalization. This suggested that the humoral immune responses to epitopes in a population were further diverse after symptom onset. Overall, the S peptide microarray analysis results demonstrated that the reactivity of the S peptides was significantly weaker for IgM antibodies than for IgG antibodies in all COVID-19 patients. Moreover, some IgM- and IgG-specific S peptides showed similar genomic distributions in the *S* gene. In addition, if the IgG-specific S peptides with 50% frequency in the COVID-19 patients (M50) were introduced (**Supplementary Table 3**), the peptides of M50 were distributed along S1, RBD and S2 as 4.5, 2, and 2.5 M50 peptides per fragment of hundred amino acids, respectively. This evidence supported the conclusion drawn from the microarray with recombinant S antigens, in which the S1 region occupied more antigenicity sites than RBD and S2.

Dynamics of Humoral Immune Responses Against S Peptides in the COVID-19 Patients

The recognition status of humoral immune responses to S peptides was individually scrutinized at multiple time points during hospitalization. Based on the threshold setting (mean + 3 SD of the signal in healthy subjects) for the positive detection of the S peptides on the microarray, the S peptides recognized by patient-specific IgM and IgG antibodies could be classified into continuous and discontinuous groups between the first and seventh weeks. The S peptides in the continuous group were defined as detectable recognition signals at alltime points, whereas those in the discontinuous group were not. Microarray analysis showed that 0–24 and 1–37 S peptides were recognized by IgM, and 5–45 and 14–71 S peptides were recognized by IgG in the continuous and discontinuous groups per patient, respectively (**Supplementary Figure 3**). In two representative COVID-19 patients (P3 and P8), 6 and 12 S peptides were continuously recognized by IgM and 25 and 29 S peptides were continuously recognized by IgG (**Figures 3A, B**). Importantly, in the continuous groups, almost all the S peptides recognized by IgM were enclosed within those that reacted with IgG, whereas in the discontinuous group, the majority of the S peptides recognized by IgM did not show reactivity with IgG and vice-versa. These results revealed that recognition of humoral immune responses to certain S peptides was relatively stable in a COVID-19 patient during the first two months after symptom onset. The observation prompted a deduction that once the B cells are matured in response to SARS-CoV-2 infection in an individual, the recognition affinity of the IgM and IgG antibodies to some epitopes is fixed for a long duration after symptom onset. Moreover, the stability of immune recognition is typically individual-dependent.

To analyze whether the humoral immune responses to COVID-19 infection possessed the common recognition to S peptides in this cohort in a longitudinal manner, the S peptides generally recognized by the patient sera were selected based on a cutoff of signal intensity. Five IgM-specific peptides with 50% positive frequency and seven IgG-specific peptides with 100% were identified. Meanwhile, all IgM-specific S peptides with 50% positive frequency completely overlapped with the 100% IgG-specific S peptides detected. The longitudinal changes of the Z-scores for these selected peptides in the corresponding patients were profiled during the entire period of serum collection (**Figure 3C**). The dynamic behaviors of the five IgM-specific peptides were divided into two types: the Z-scores of four peptides (S1-3, S1-33, S1-35 and S2-78) retained the attenuation trends from the first to seventh week, whereas only one peptide (S1-105) exhibited a bell curve with a peak in the third week. The dynamic responses of the patient IgM antibodies against these selected peptides were basically consistent with the time-dependent changes in S1 protein recognition by IgM, as analyzed by ELISA and microarray (**Figures 1A, C**). As for the immune responses against the seven IgG-specific S peptides selected, all patient sera appeared the lowest intensity of immune reaction during the first week after symptom onset. Then, four of the seven IgG-specific peptides (S1-1, S1-3, S1-33 and S1-35) increased continuously until the sixth week, whereas, the remaining three IgG-specific S peptides (S1-101, S1-105 and S2-78) displayed bell-shaped curves with peaks around the second to fourth week. The dynamic behaviors of IgG-specific S peptides were similar to those of ELISA and microarray data, which showed increased IgG reactivity between the second and sixth week (**Figures 1A, C**). Despite variations in the recognition of S peptides by IgM or IgG antibodies, seven IgG-specific S peptides were likely regarded as the typical S epitopes that are commonly recognized by humoral immune response, and their patterns of dynamics coincided with that of the recombinant S1. As stated earlier, the humoral immune responses to the S2 protein at relatively lower extent, thus the seven epitopes mainly from S1 would represent intact S proteins for the study of COVID-19 related immunology.

Appraisal of the Epitope and Dynamic Features of the Random Peptides Recognized by the COVID-19 Patients Using Abmap

An alternative approach, AbMap, was adopted to further evaluate the dynamic behavior of S epitopes recognized the COVID-19 sera. To acquire antibodies against the S protein from patient sera, the antibodies were individually purified from the patient sera through magnetic beads conjugated with recombinant S1 protein. The purified antibodies were then hybridized with random peptides generated from the phage display peptide pool. DNA sequencing data were used to annotate the coding nucleotides of a peptide, and several annotated peptides with similar structures in their amino acid sequences were termed motifs. Stronger immune interaction between the motif and the corresponding antibody was observed when the peptides were derived from distinct sequences representing a motif. Then, motifs from multiple peptides with similar structures were aligned to the sequences of the S protein and the matched motifs were designated as the S epitope.

Based on motif analysis, 575 motifs were identified from the sera of 19 patients. Among these, 174 motifs matched with the

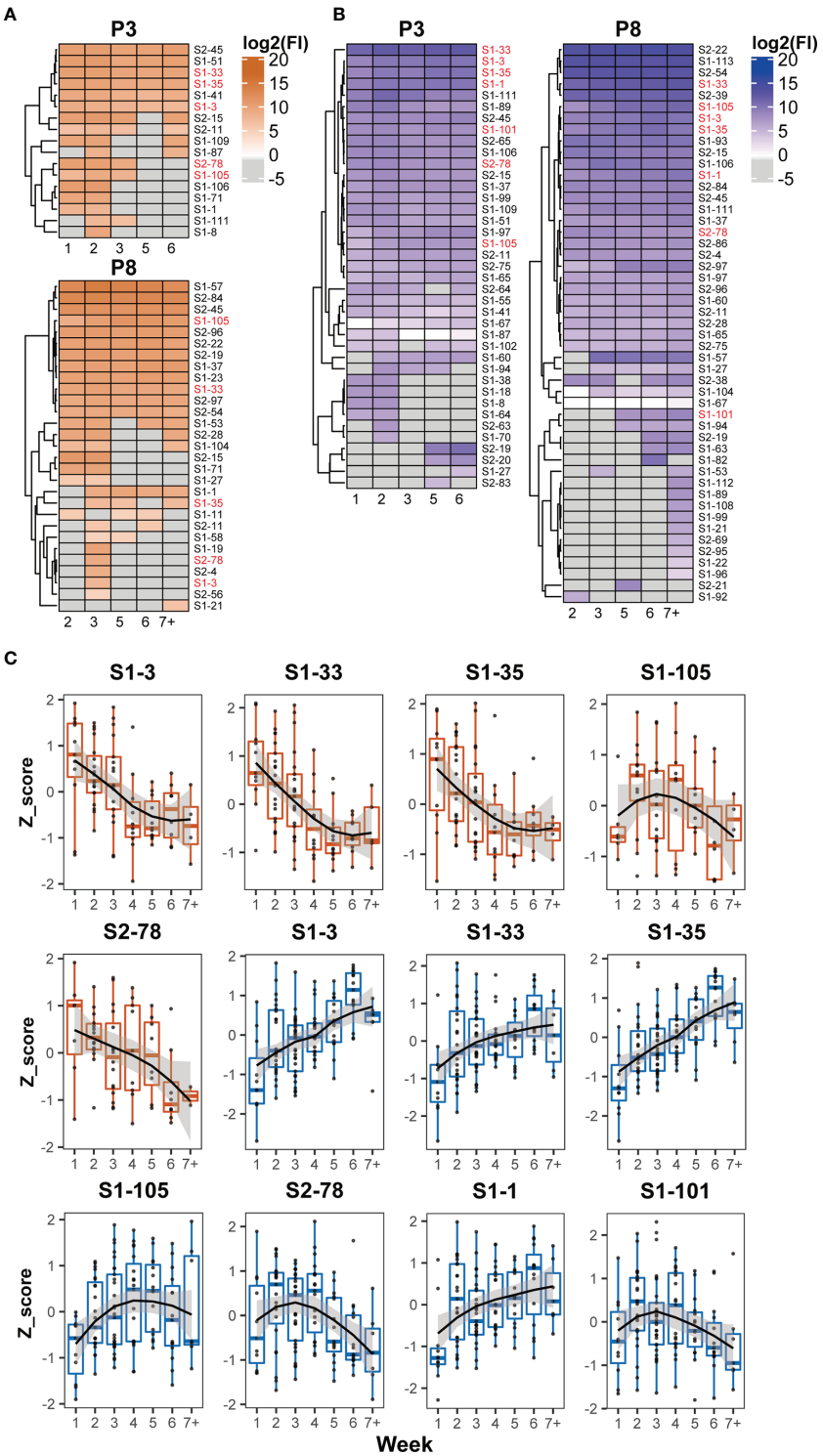

FIGURE 3 | Dynamic patterns of humoral immune responses against reactive S peptides in the COVID-19 patients. Heatmaps of IgM **(A)** and IgG **(B)** against S-reactive peptides during hospitalization in the sera of two COVID-19 patients, P3 and P8. The gray cells on the heatmaps indicate signals with values lower than the cutoffs. The x axis of heatmap indicates the time intervals (week) during the hospitalization after symptom onset. **(C)** The dynamic changes of IgM (boxplot colored in orange) and IgG (boxplot colored in blue) against five IgM-reactive S peptides recognized in at least 50% patients and seven IgG-reactive S peptides recognized in all patients. The signals were normalized by the Z-score and the signal patterns were mimicked by curve fitting.

amino acid sequence of the S protein. The distribution of matched and unmatched motifs in individual patients was shown in **Figure 4A**. The matched motifs from 1 (P13) to 34 (P15) were fitted to the 24 S epitopes and ranged from 2 motifs/epitope to 36 motifs/epitope (**Figure 4B**). In addition, AbMap analysis showed that the antibodies from each patient recognized 1–5 S epitopes (**Supplementary Figure 4**). For instance, epi-5 was recognized in only one patient (P11), whereas four epitopes (epi-1, epi-7, epi-14, and epi-18) were commonly recognized in several patients. The matched motifs were unevenly distributed along the *S* gene regions in the SARS-CoV-2 genome for all samples and mainly covered residues 207–317 (NTD), 348–472

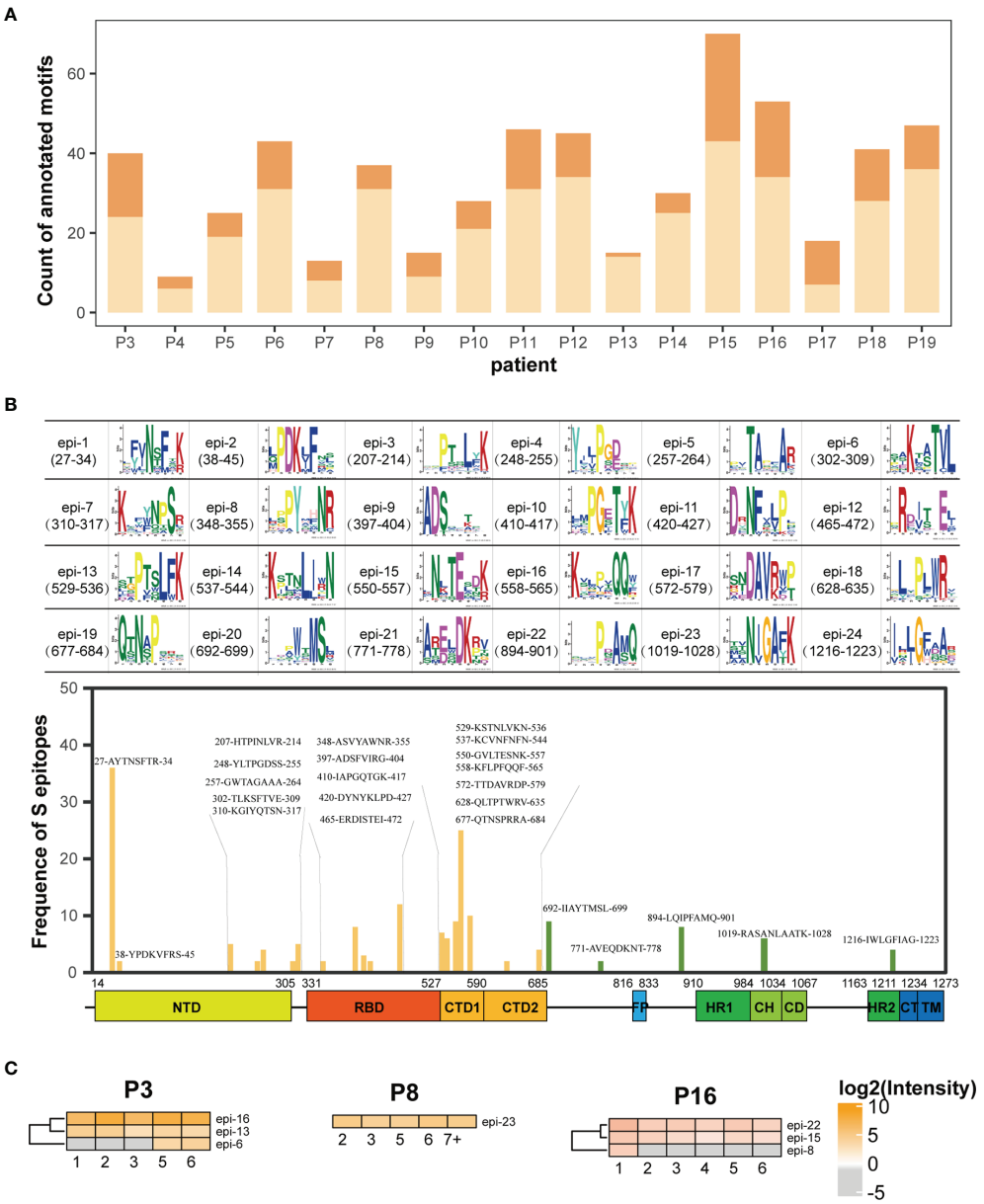

FIGURE 4 | AbMap analysis to identify epitopes with a random peptide library for S1-specific antibodies enriched from the COVID-19 sera. **(A)** Distribution of annotated motifs identified by AbMap in all the COVID-19 patients; motifs matched to the S protein are shown in dark orange and unmatched motifs are shown in light orange. **(B)** Frequency distribution of epitopes recognized by the purified IgG antibodies against the S1 protein in all COVID-19 sera. The upper panel represents 24 structures of matched motifs. The lower panel illustrated frequency distribution of 24 epitopes along the S protein sequence. The x axis represents the entire *S* gene sequence and the color bars at the bottom denote the different domains as indicated in **Figure 2B**. The y axis represents frequency of epitopes detected in the COVID-19 patients. The yellow and green bars indicate epitopes located in the S1 and S2 subunits, respectively. **(C)** Heatmaps of the S epitopes recognized by the purified IgG in the three COVID-19 patients, P3, P8 and P16. The gray cells indicate unmatched S epitopes identified from the corresponding samples. The x axis of heatmap indicates the time intervals (week) during the hospitalization after symptom onset.

(RBD), and 529–579 (CTD) of the S1 protein (**Figure 4B**). The results reached the expectations of the experimental design because the patient IgG would have an affinity binding to the recombinant S1. Moreover, if the number of annotated peptides in an S epitope contributed to a high intensity of immune reactivity, the intensities of all the S epitopes in a patient were clustered during the entire duration of serum collection, thereby allowing the assessment of dynamic humoral immune responses against S epitopes (**Supplementary Figure 4**). As shown in **Figure 4C**, one, three, and four epitopes in P8, P16, and P3 were well-recognized by the patient antibodies, respectively. The dynamic intensities of the immune reactivity against these S epitopes were irregular during hospitalization. Some S epitopes showed continuous positivity, whereas others showed positivity for shorter durations. However, in all 19 patients, at least one S epitope per patient was continuously recognized by the corresponding serum antibodies. The data in **Figure 4C** confirmed the conclusion elicited from **Figures 3A, B** that some recognition specificities of antibodies against the S protein in individual COVID-19 patients were relatively stable after symptom onset in this study.

Assessment of immune recognition against the S epitopes in the COVID-19 patients was implemented using two approaches in parallel: microarray and AbMap. The analysis focused on two aspects: epitope distribution along *S* gene and the dynamic immune reactivity. The number of S epitopes identified through the microarray analysis was higher than those identified through the AbMap analysis; moreover, S epitopes identified by the AbMap analysis overlapped with the microarray data (**Figures 3A, B**, **4C**). Deeply looking at the distribution of the epitopes on the *S* gene, however, there were two S1 epitope regions detected by microarray that overlapped with the same regions on S1 identified by AbMap, whereas the two epitope regions on S2 upon microarray analysis were almost undetected by AbMap (**Figures 2B**, **4B**). This result was expected because we purified the IgGs for AbMap based on their affinity binding to the recombinant S1 protein, which showed poor overlap with S2. Carefully checking the dynamic responses of the S epitopes, the immune recognition of either the commonly shared or individual unique epitopes appeared to be inconsistent. However, the dynamic behavior of some S epitopes on AbMap was in agreement with the microarray observations, recognition specificity, and reaction intensity in an individual consistently lasting for a relatively long period after symptom onset. These results demonstrated that the microarray and AbMap data were reasonably comparable and complementary.

Spatial Characteristics of the S Epitopes Recognized by COVID-19 Serum Antibodies

The secondary structures of the S peptides that were designed for microarray analysis were analyzed using DSSP, and the prediction results were illustrated in **Supplementary Table 3**. Peptides negatively recognized by the COVID-19 sera showed a significantly higher percentage of alpha helical structures and a significantly lower percentage of β-sheet and random coil structures than those that reacted positively with the patient serum samples (alpha-helix: 23.2% vs. 18.7%; β-sheet: 21.4% vs. 23.1% and random coil: 51.4% vs. 58.2%). Furthermore, the alpha helix percentage decreased to 17.7% and the random coil percentage increased to 59.6% in the positive S peptides with 50% frequency in the COVID-19 patients (M50) (**Figure 5A**). The S epitopes corresponding to the matched motifs by AbMap displayed a similar distribution of secondary structures (13.4% alpha helix and 65% random coils; **Figure 5A**). These data suggested that S peptides with higher β-sheets or random coil secondary structures were easily recognized by the humoral immune system. This conclusion agrees with epitope theory that random coils possess a higher potential for antigenicity (39, 40).

The cryo-EM model of the trimeric S protein demonstrated that the four domains of S1, namely NTD, RBD, CTD1, and CTD2, wrap around a threefold axis and cover S2; moreover, the surface-exposed and disordered loop model showed the furin cleavage site at the S1/S2 boundary (41). To overview the spatial structures of the S epitopes, Pymol was applied to map the identified S epitopes onto the molecular model of the S protein in the closed state. The M50 peptides were mainly located in the surface-exposed regions of S1 (25/40; **Figure 5B**). The spatial locations of the S epitopes corresponding to the matched motifs by AbMap were also mapped to the three-dimensional model of S proteins. Approximately 62% of the epitopes were exposed on the S protein surface (**Figure 5B**). Therefore, the immunogenicity of the S protein is well explained by the location of immune-positive peptides in the tertiary structure of the S protein. Moreover, the relatively poorer antigenicity of S2 may be related to its higher percentage of alpha helices (40%) compared to the low percentage of alpha helical structures in S1 in the closed state.

Among the M50 S peptides, five peptides with a higher helical content (>75%) were well-recognized by COVID-19 sera. In the spatial structure of the S protein, three peptides (S2-15, S2-45 and S2-56) were located around the FP region of S2 and shielded by the CTD2 region of S1 in the closed trimer, whereas two peptides (S2-78 and S2-83) were located in the HR2 region of S2, which is close to the viral membrane (**Figure 5C**). Closely checking the status of the three former peptides in response to viral infection, S protein is likely cleaved by furin-like protease followed by cleavage of serine protease; then, the truncated S2 proteins would be expected to be in an exposure status and bring some configuration changes (42), which influence their antigenicity and recognition by the humoral immune system. With regard to the two later peptides, these HR2 peptides are anticipated to be in an exposed location upon the tertiary structure of the S protein. In addition, the S epitopes derived from AbMap also supported the above deduction; epitopes (epi-23: residues 771–778 and epi-25: residues 1,019–1,028) overlapped with S2–15 (residues 770–781) and S2–56 (residues 1016–1,027), respectively.

DISCUSSION

Considering the technology bias of misjudging epitope recognition, in this study, three types of S antigens, recombinant truncated S proteins, S peptides, and random peptides, were used to examine the

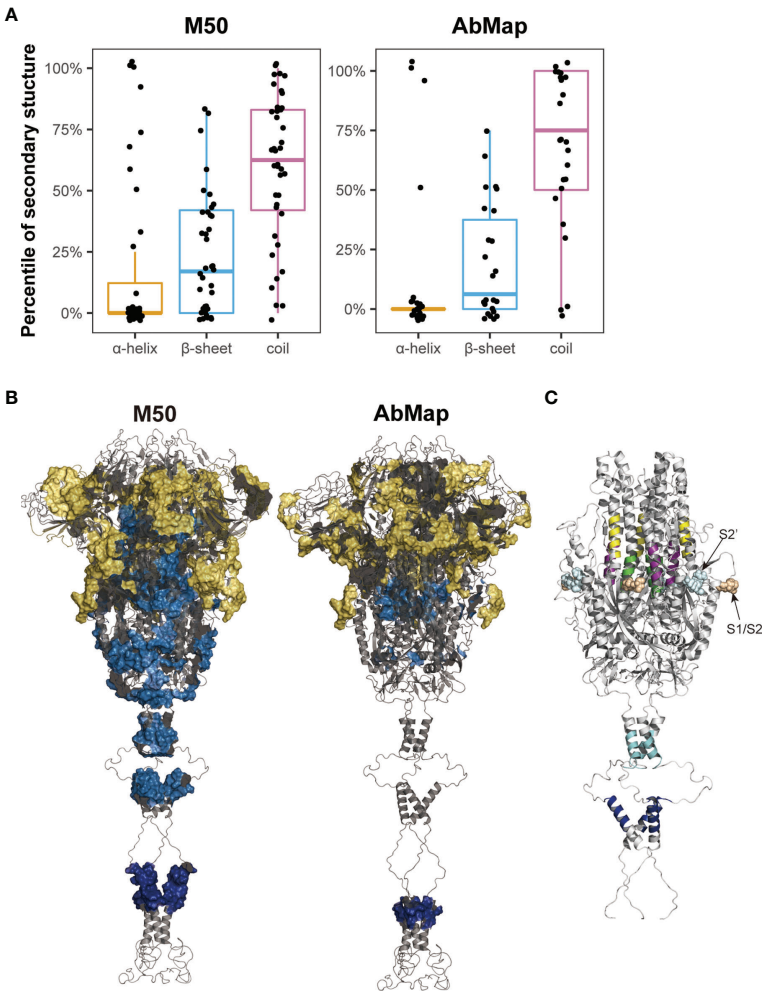

FIGURE 5 | Spatial characteristic of the epitopes on S protein. **(A)** Distribution of secondary structures (α-helix, β-sheet, and random coil) analyzed by DSSP in M50 S peptides based on the microarray and 24 epitopes identified by AbMap. The y axis represents the percentiles of secondary structures in each of the S epitopes. **(B)** Spatial localization of the epitopes identified by the microarray (M50) (left) and AbMap (right) analysis on the trimer model of the S protein (side view). The backbone structure is illustrated in the gray cartoon mode. Each set of epitopes are highlighted on the surface. Epitopes located in the S1, S2, and transmembrane regions are shown in yellow, light blue, and dark blue, respectively. **(C)** Spatial localization of the five S epitopes with α-helical structures on the trimer model of S2 protein. Stalk region of the S2 protein is shown in gray cartoon. The five peptide epitopes, namely, S2-15, S2-45, S2-56, S2-78, and S2-83 are shown in purple, yellow, green, cyan, and blue respectively.

dynamics of humoral immune responses in the sera of COVID-19 patients. The question naturally arises as to how experimental evidence supports the theoretical design. First of all, the patterns of longitudinal reactivity of the patient IgM and IgG against these antigens, intact S protein measured by ELISA, recombinant S1 protein and commonly recognized S peptides detected by microarray, were similar, with the IgM responses rising early and IgG coming later. Secondly, the distribution of the positive S peptides with higher frequencies identified by microarray along the *S* gene was similar to the regions of the S epitopes found by AbMap. Thus, the two approaches to explore the S epitopes recognized by the COVID-19 sera reached an agreed conclusion. Finally, both the S peptides microarray and AbMap results showed that the recognition of the S epitopes by IgG varied among different individuals, but the humoral immune responses against certain the S epitopes were relatively stable in individual COVID-19 patient for a period of two months after symptom onset. Hence, the main conclusions regarding the S epitopes recognized by humoral immune responses were well endorsed by multiple datasets obtained from different approaches.

Several studies have monitored the humoral immune responses to SARS-CoV-2 infection and to identify viral antigens through serological assays (23, 43, 44). In the present study, ELISA demonstrated that the IgM reactivity peak was obtained during the first two weeks after symptom onset, whereas the IgG reactivity peak was observed around the fifth or sixth week after symptom onset in the COVID-19 cohort (**Figure 1A**). These observations are consistent with

those of previous studies (22, 45, 46). The evidence obtained from the microarray with truncated S proteins as antigens supported our previous conclusion that the intensity of immune responses against S1 was significantly higher than that against S2 and RBD domains of the S protein (35). However, the humoral immune responses against viral antigens such as S1, S2, and RBD of the S protein are still contradictory (21, 47–51). Premkumar et al. reported that RBD is immunodominant and a highly specific target for humoral immune system in COVID-19 patients (51). Nguyen et al. compared the antigenicity of S, S1, S2, and RBD by ELISA and reported that S2 and S proteins were preferentially recognized by patient antibodies at two weeks after symptom onset (50). Norman et al. performed an ultra-sensitive single molecular array (Simoa) assay and reported similar binding capacities for IgA, IgM, and IgG antibodies against S1, RBD, and S protein in patients with COVID-19 (48). However, Tian et al. demonstrated that S1 displayed higher sensitivity and specificity than RBD (52). With solid data support from three approaches, the conclusion elicited from this study advocated that the antigenicity of S1 was higher than that of S2 and RBD.

As mentioned above, 124 IgM- and 165 IgG-reactive S peptides were identified through serological assays using the sera of COVID-19 patients. To extract S peptides commonly recognized by individual patients, a new concept M50 was introduced in this study. The epitope distribution along the *S* gene and epitope accessibility of the S protein is well elucidated by the M50 peptides. Recently, several SARS-COV-2 variants have been reported, especially several variants of concern (VOCs). All the M50 S peptides were compared with the varied sequences of S protein in VOCs (CoV-GLUE-Viz), while the comparison revealed 30% (12/40) of M50 S peptides containing the mutated amino acid residues, indicating that the variants of SARS-COV-2 are likely to affect humoral immune responses against the virus (**Supplementary Table 4**). Specifically, for the epitope identified in M50, seven peptides (S1-1, S1-3, S1-33, S1-35, S1-101, S1-105 and S2-78) were generally recognized by IgG of all the patients with COVID-19 in this cohort. In addition, the panel with the seven S peptides showed dynamic patterns similar to those of the S1 protein. The four S peptides in this panel were defined in previous reports as S1-35 (residues 205–216) in NTD (53), S1-101 (residues 601–612) and S1-105 (residues 635–636) in CTD (54), and S2-78 (residues 1,148–1,159) in S2 adjacent to HR2 (54–57). The remaining three peptide epitopes, S1-1 (residues 1–12), S1-3 (residues 13–24) and S1-33 (residues 193–204) were first identified by this study. The clinical value of these general and new epitopes will be verified and explored in future studies.

The human immune system is highly variable between individuals but relatively stable over time within a given person (58). Xiang et al. studied the B-cell immune repertoire of COVID-19 patients and reported that despite significant differences in *V* gene usage among the COVID-19 patients, the frequency of different *V* and *J* gene segment usage remained relatively stable over time in individual COVID-19 patients (34). Niu et al. reported that the IgM and IgG expression in B cells at transcript levels displayed a large diversity at the early SARS-CoV-2 infection within four days, whereas the diversity in the continued clonal expansion of dominant B cells decreased after recovery from infection (32). Nevertheless, details regarding the dynamic nature of epitope recognition during the course of SARS-CoV-2 infection are unclear. Therefore, we systematically assessed the dynamic humoral immune response against the S protein or S peptides. Our results showed that the recognition of S epitopes by IgG and IgM antibodies was highly diverse and patient-specific. However, the pattern of recognizing certain general or individual-specific S epitopes by IgM or IgG antibodies was consistent in each patient with COVID-19 during the hospitalization period (**Figures 3A, B**, **4C**). The observation suggested that B cells undergo a series of transcriptional edits in response to SARS-CoV-2 infection during the early phase of infection, while the specific clones are selected and the IgM and IgG antibodies matured during the period of infection. Thus, after immunoglobins against the viral antigens are mature their recognition affinities to certain S epitopes in a given individual are almost fixed to provide effective humoral immunity for a long duration after symptom onset. The longitudinal characterization of humoral immunity to SARS-COV-2 may contribute novel information on how to consider a proper therapy for COVID-19 patients, especially during the early phase of infection.

DATA AVAILABILITY STATEMENT

The original contributions presented in the study are included in the article/**Supplementary Material**. Further inquiries can be directed to the corresponding author.

ETHICS STATEMENT

The studies involving human participants were reviewed and approved by the Research Ethics Committee in the Fifth Affiliated Hospital of Sun Yat-sen University. The patients/participants provided their written informed consent to participate in this study.

AUTHOR CONTRIBUTIONS

SL, ST, and HS conceived of the study and prepared the manuscript. LC designed the experiments, analyzed the data, and assisted with manuscript preparation. HQ and MM performed epitope mapping of protein-enriched antibodies. YL, HZ HJ, and DL performed microarray experiments. JX, HL, and CH performed NGS and data analysis. KY analyzed the data and prepared the figures. RC and YL provided suggestions for the spatial analysis of the epitopes. PP and YR collected the clinical samples and acquired the data. All authors listed have

made a substantial, direct, and intellectual contribution to the work and approved it for publication.

FUNDING

This study was supported by the National Key Research and Development Program of China (Grant Nos. 2016YFA0500600 and 2018YFC1003100) and the National Natural Science Foundation of China (Grant Nos. 31970130, 31600672, 31900112, 21907065, 32000027, and 81873478).

ACKNOWLEDGMENTS

We thank Huanming Yang for expert technical assistance and the Beijing BGI-GBI Biotech Co., Ltd. for the ELISA kits.

SUPPLEMENTARY MATERIAL

The Supplementary Material for this article can be found online at: https://www.frontiersin.org/articles/10.3389/fimmu.2022.770982/full#supplementary-material

REFERENCES

1. Coronaviridae Study Group of the International Committee on Taxonomy of Viruses. The Species Severe Acute Respiratory Syndrome-Related Coronavirus: Classifying 2019-nCoV and Naming it SARS-CoV-2. *Nat Microbiol* (2020) 5(4):536–44. doi: 10.1038/s41564-020-0695-z
2. Lu G, Wang Q, Gao GF. Bat-To-Human: Spike Features Determining 'Host Jump' of Coronaviruses SARS-CoV, MERS-CoV, and Beyond. *Trends Microbiol* (2015) 23(8):468–78. doi: 10.1016/j.tim.2015.06.003
3. Wevers BA, van der Hoek L. Recently Discovered Human Coronaviruses. *Clin Lab Med* (2009) 29(4):715–24. doi: 10.1016/j.cll.2009.07.007
4. Rabaan AA, Al-Ahmed SH, Haque S, Sah R, Tiwari R, Malik YS, et al. SARS-CoV-2, SARS-CoV, and MERS-COV: A Comparative Overview. *J Infez Med* (2020) 28(2):174–84.
5. Wu JT, Leung K, Bushman M, Kishore N, Niehus R, de Salazar PM, et al. Estimating Clinical Severity of COVID-19 From the Transmission Dynamics in Wuhan, China. *Nat Med* (2020) 26(4):506–10. doi: 10.1038/s41591-020-0822-7
6. McKechnie JL, Blish CA. The Innate Immune System: Fighting on the Front Lines or Fanning the Flames of COVID-19? *Cell Host Microbe* (2020) 27 (6):863–9. doi: 10.1016/j.chom.2020.05.009
7. Ellinghaus D, Degenhardt F, Bujanda L, Buti M, Albillos A, Invernizzi P, et al. Genomewide Association Study of Severe Covid-19 With Respiratory Failure. *N Engl J Med* (2020) 383(16):1522–34. doi: 10.1056/NEJMoa2020283
8. Guo L, Ren L, Yang S, Xiao M, Chang D, Yang F, et al. Profiling Early Humoral Response to Diagnose Novel Coronavirus Disease (COVID-19). *Clin Infect Dis* (2020) 71(15):778–85. doi: 10.1093/cid/ciaa310
9. Jin Y, Wang M, Zuo Z, Fan C, Ye F, Cai Z, et al. Diagnostic Value and Dynamic Variance of Serum Antibody in Coronavirus Disease 2019. *Int J Infect Dis* (2020) 94:49–52. doi: 10.1016/j.ijid.2020.03.065
10. Robbiani DF, Gaebler C, Muecksch F, Lorenzi JCC, Wang Z, Cho A, et al. Convergent Antibody Responses to SARS-CoV-2 in Convalescent Individuals. *Nature* (2020) 584(7821):437–42. doi: 10.1038/s41586-020-2456-9
11. Sun B, Feng Y, Mo X, Zheng P, Wang Q, Li P, et al. Kinetics of SARS-CoV-2 Specific IgM and IgG Responses in COVID-19 Patients. *Emerg Microbes Infect* (2020) 9(1):940–8. doi: 10.1080/22221751.2020.1762515
12. Huang AT, Garcia-Carreras B, Hitchings MDT, Yang B, Katzelnick LC, Rattigan SM, et al. A Systematic Review of Antibody Mediated Immunity to Coronaviruses: Antibody Kinetics, Correlates of Protection, and Association of Antibody Responses With Severity of Disease. *medRxiv* (2020) 11(1):1–16. doi: 10.1101/2020.04.14.20065771
13. Weissleder R, Lee H, Ko J, Pittet M. COVID-19 Diagnostics in Context. *Sci Trans Med* (2020) 12(546):eabc1931. doi: 10.1126/scitranslmed.abc1931
14. Liu W, Liu L, Kou G, Zheng Y, Ding Y, Ni W, et al. Evaluation of Nucleocapsid and Spike Protein-Based Enzyme-Linked Immunosorbent Assays for Detecting Antibodies Against SARS-CoV-2. *J Clin Microbiol* (2020) 58(6):e00461-20. doi: 10.1128/JCM.00461-20
15. Vashist SK. *In Vitro* Diagnostic Assays for COVID-19: Recent Advances and Emerging Trends. *Diagnostics (Basel)* (2020) 10(4):202. doi: 10.3390/diagnostics10040202
16. Lan J, Ge J, Yu J, Shan S, Zhou H, Fan S, et al. Structure of the SARS-CoV-2 Spike Receptor-Binding Domain Bound to the ACE2 Receptor. *Nature* (2020) 581(7807):215–20. doi: 10.1038/s41586-020-2180-5
17. Zhou D, Duyvesteyn HME, Chen CP, Huang CG, Chen TH, Shih SR, et al. Structural Basis for the Neutralization of SARS-CoV-2 by an Antibody From a Convalescent Patient. *Nat Struct Mol Biol* (2020) 27(10):950–8. doi: 10.1038/s41594-020-0480-y
18. Dispinseri S, Secchi M, Pirillo MF, Tolazzi M, Borghi M, Brigatti C, et al. Neutralizing Antibody Responses to SARS-CoV-2 in Symptomatic COVID-19 is Persistent and Critical for Survival. *Nat Commun* (2021) 12(1):2670. doi: 10.1038/s41467-021-22958-8
19. Poh CM, Carissimo G, Wang B, Amrun SN, Lee CY, Chee RS, et al. Two Linear Epitopes on the SARS-CoV-2 Spike Protein That Elicit Neutralising Antibodies in COVID-19 Patients. *Nat Commun* (2020) 11(1):2806. doi: 10.1038/s41467-020-16638-2
20. Shrock E, Fujimura E, Kula T, Timms RT, Lee I-H, Leng Y, et al. Viral Epitope Profiling of COVID-19 Patients Reveals Cross-Reactivity and Correlates of Severity. *Science* (2020) 370(6520):eabd4250. doi: 10.1126/science.abd4250
21. Anand SP, Prevost J, Nayrac M, Beaudoin-Bussieres G, Benlarbi M, Gasser R, et al. Longitudinal Analysis of Humoral Immunity Against SARS-CoV-2 Spike in Convalescent Individuals Up to 8 Months Post-Symptom Onset. *Cell Rep Med* (2021) 2(6):100290. doi: 10.1016/j.xcrm.2021.100290
22. Seow J, Graham C, Merrick B, Acors S, Pickering S, Steel KJA, et al. Longitudinal Observation and Decline of Neutralizing Antibody Responses in the Three Months Following SARS-CoV-2 Infection in Humans. *Nat Microbiol* (2020) 5(12):1598–607. doi: 10.1038/s41564-020-00813-8
23. Ravichandran S, Lee Y, Grubbs G, Coyle EM, Klenow L, Akasaka O, et al. Longitudinal Antibody Repertoire in "Mild" Versus "Severe" COVID-19 Patients Reveals Immune Markers Associated With Disease Severity and Resolution. *Sci Adv* (2021) 7(10):eabf2467. doi: 10.1126/sciadv.abf2467
24. Zheng Y, Zhang Q, Ali A, Li K, Shao N, Zhou X, et al. Sustainability of SARS-CoV-2 Induced Humoral Immune Responses in COVID-19 Patients From Hospitalization to Convalescence Over Six Months. *Virol Sin* (2021) 36 (5):869–78. doi: 10.1007/s12250-021-00360-4
25. Kellam P, Barclay W. The Dynamics of Humoral Immune Responses Following SARS-CoV-2 Infection and the Potential for Reinfection. *J Gen Virol* (2020) 101(8):791–7. doi: 10.1099/jgv.0.001439
26. Dorner T, Radbruch A. Antibodies and B Cell Memory in Viral Immunity. *Immunity* (2007) 27(3):384–92. doi: 10.1016/j.immuni.2007.09.002
27. Hoehn KB, Fowler A, Lunter G, Pybus OG. The Diversity and Molecular Evolution of B-Cell Receptors During Infection. *Mol Biol Evol* (2016) 33 (5):1147–57. doi: 10.1093/molbev/msw015
28. Niu X, Yan Q, Yao Z, Zhang F, Qu L, Wang C, et al. Longitudinal Analysis of the Antibody Repertoire of a Zika Virus-Infected Patient Revealed Dynamic Changes in Antibody Response. *Emerg Microbes Infect* (2020) 9(1):111–23. doi: 10.1080/22221751.2019.1701953
29. Davis CW, Jackson KJL, McElroy AK, Halfmann P, Huang J, Chennareddy C, et al. Longitudinal Analysis of the Human B Cell Response to Ebola Virus Infection. *Cell* (2019) 177(6):1566–82 e17. doi: 10.1016/j.cell.2019.04.036
30. Hoehn KB, Gall A, Bashford-Rogers R, Fidler SJ, Kaye S, Weber JN, et al. Dynamics of Immunoglobulin Sequence Diversity in HIV-1 Infected Individuals. *Philos Trans R Soc Lond B Biol Sci* (2015) 370(1676). doi: 10.1098/rstb.2014.0241
31. Nielsen SCA, Yang F, Jackson KJL, Hoh RA, Roltgen K, Jean GH, et al. Human B Cell Clonal Expansion and Convergent Antibody Responses to SARS-CoV-2. *Cell Host Microbe* (2020) 28(4):516–25 e5. doi: 10.1016/j.chom.2020.09.002

32. Niu X, Li S, Li P, Pan W, Wang Q, Feng Y, et al. Longitudinal Analysis of T and B Cell Receptor Repertoire Transcripts Reveal Dynamic Immune Response in COVID-19 Patients. *Front Immunol* (2020) 11:582010. doi: 10.3389/fimmu.2020.582010
33. Montague Z, Lv H, Otwinowski J, DeWitt WS, Isacchini G, Yip GK, et al. Dynamics of B-Cell Repertoires and Emergence of Cross-Reactive Responses in COVID-19 Patients With Different Disease Severity. *arXiv* (2020) 35 (8):109173. doi: 10.2139/ssrn.3751051
34. Xiang H, Zhao Y, Li X, Liu P, Wang L, Wang M, et al. Landscapes and Dynamic Diversifications of B-Cell Receptor Repertoires in COVID-19 Patients. *Hum Immunol* (2022) 83(2):119–29. doi: 10.1016/j.humimm.2021.10.007
35. Jiang HW, Li Y, Zhang HN, Wang W, Yang X, Qi H, et al. SARS-CoV-2 Proteome Microarray for Global Profiling of COVID-19 Specific IgG and IgM Responses. *Nat Commun* (2020) 11(1):3581. doi: 10.1038/s41467-020-17488-8
36. Li Y, Lai DY, Zhang HN, Jiang HW, Tian X, Ma ML, et al. Linear Epitopes of SARS-CoV-2 Spike Protein Elicit Neutralizing Antibodies in COVID-19 Patients. *Cell Mol Immunol* (2020) 17(10):1095–7. doi: 10.1038/s41423-020-00523-5
37. Cheadle C, Vawter MP, Freed WJ, Becker KG. Analysis of Microarray Data Using Z Score Transformation. *J Mol Diagn* (2003) 5(2):73–81. doi: 10.1016/S1525-1578(10)60455-2
38. Qi H, Ma M, Hu C, Xu ZW, Wu FL, Wang N, et al. Antibody Binding Epitope Mapping (AbMap) of Hundred Antibodies in a Single Run. *Mol Cell Proteomics* (2021) 20:100059. doi: 10.1074/mcp.RA120.002314
39. Ofran Y, Schlessinger A, Rost B. Automated Identification of Complementarity Determining Regions (CDRs) Reveals Peculiar Characteristics of CDRs and B Cell Epitopes. *J Immunol* (2008) 181 (9):6230–5. doi: 10.4049/jimmunol.181.9.6230
40. Rubinstein ND, Mayrose I, Halperin D, Yekutieli D, Gershoni JM, Pupko T. Computational Characterization of B-Cell Epitopes. *Mol Immunol* (2008) 45 (12):3477–89. doi: 10.1016/j.molimm.2007.10.016
41. Cai Y, Zhang J, Xiao T, Peng H, Sterling SM, Walsh RMJr., et al. Distinct Conformational States of SARS-CoV-2 Spike Protein. *Science* (2020) 369 (6511):1586–92. doi: 10.1126/science.abd4251
42. Walls AC, Park YJ, Tortorici MA, Wall A, McGuire AT, Veesler D. Structure, Function, and Antigenicity of the SARS-CoV-2 Spike Glycoprotein. *Cell* (2020) 181(2):281–92 e6. doi: 10.1016/j.cell.2020.02.058
43. Schwarz T, Heiss K, Mahendran Y, Casilag F, Kurth F, Sander LE, et al. SARS-CoV-2 Proteome-Wide Analysis Revealed Significant Epitope Signatures in COVID-19 Patients. *Front Immunol* (2021) 12:629185. doi: 10.3389/fimmu.2021.629185
44. Seow J, Graham C, Merrick B, Acors S, Steel KJA, Hemmings O, et al. Longitudinal Evaluation and Decline of Antibody Responses in SARS-CoV-2 Infection. *Nat Microbiol* (2020) 5(12):1598–607. doi: 10.1101/2020.07.09.20148429
45. Adams ER, Ainsworth M, Anand R, Andersson MI, Auckland K, Baillie JK, et al. Antibody Testing for COVID-19: A Report From the National COVID Scientific Advisory Panel. *Wellcome Open Res* (2020) 5(139):139. doi: 10.12688/wellcomeopenres.15927.1
46. Ibarrondo FJ, Fulcher JA, Goodman-Meza D, Elliott J, Hofmann C, Hausner MA, et al. Rapid Decay of Anti–SARS-CoV-2 Antibodies in Persons With Mild Covid-19. *N Engl J Med* (2020) 383(11):1085–7. doi: 10.1056/NEJMc2025179
47. Chen Y, Tong X, Li Y, Gu B, Yan J, Liu Y, et al. A Comprehensive, Longitudinal Analysis of Humoral Responses Specific to Four Recombinant Antigens of SARS-CoV-2 in Severe and non-Severe COVID-19 Patients. *PloS Pathog* (2020) 16(9):e1008796. doi: 10.1371/journal.ppat.1008796
48. Norman M, Gilboa T, Ogata AF, Maley AM, Cohen L, Busch EL, et al. Ultrasensitive High-Resolution Profiling of Early Seroconversion in Patients With COVID-19. *Nat BioMed Eng* (2020) 4(12):1180–7. doi: 10.1038/s41551-020-00611-x
49. Wang Y, Zhang L, Sang L, Ye F, Ruan S, Zhong B, et al. Kinetics of Viral Load and Antibody Response in Relation to COVID-19 Severity. *J Clin Invest* (2020) 130(10):5235–44. doi: 10.1172/JCI138759
50. Nguyen-Contant P, Embong AK, Kanagaiah P, Chaves FA, Yang H, Branche AR, et al. S Protein-Reactive IgG and Memory B Cell Production After Human SARS-CoV-2 Infection Includes Broad Reactivity to the S2 Subunit. *mBio* (2020) 11(5):e01991–20. doi: 10.1128/mBio.01991-20
51. Premkumar L, Segovia-Chumbez B, Jadi R, Martinez DR, Raut R, Markmann A, et al. The Receptor Binding Domain of the Viral Spike Protein is an Immunodominant and Highly Specific Target of Antibodies in SARS-CoV-2 Patients. *Sci Immunol* (2020) 5(48):eabc8413. doi: 10.1126/sciimmunol.abc8413
52. Tian Y, Lian C, Chen Y, Wei D, Zhang X, Ling Y, et al. Sensitivity and Specificity of SARS-CoV-2 S1 Subunit in COVID-19 Serology Assays. *Cell Discov* (2020) 6:75. doi: 10.1038/s41421-020-00224-3
53. Amrun SN, Lee CY, Lee B, Fong SW, Young BE, Chee RS, et al. Linear B-Cell Epitopes in the Spike and Nucleocapsid Proteins as Markers of SARS-CoV-2 Exposure and Disease Severity. *EBioMedicine* (2020) 58:102911. doi: 10.1016/j.ebiom.2020.102911
54. Mishra N, Huang X, Joshi S, Guo C, Ng J, Thakkar R, et al. Immunoreactive Peptide Maps of SARS-CoV-2. *Commun Biol* (2021) 4(1):225. doi: 10.1038/s42003-021-01743-9
55. Farrera-Soler L, Daguer JP, Barluenga S, Vadas O, Cohen P, Pagano S, et al. Identification of Immunodominant Linear Epitopes From SARS-CoV-2 Patient Plasma. *PloS One* (2020) 15(9):e0238089. doi: 10.1371/journal.pone.0238089
56. Zamecnik CR, Rajan JV, Yamauchi KA, Mann SA, Loudermilk RP, Sowa GM, et al. ReScan, a Multiplex Diagnostic Pipeline, Pans Human Sera for SARS-CoV-2 Antigens. *Cell Rep Med* (2020) 1(7):100123. doi: 10.1016/j.xcrm.2020.100123
57. Holenya P, Lange PJ, Reimer U, Woltersdorf W, Panterodt T, Glas M, et al. Peptide Microarray-Based Analysis of Antibody Responses to SARS-CoV-2 Identifies Unique Epitopes With Potential for Diagnostic Test Development. *Eur J Immunol* (2021) 51(7):1839–49. doi: 10.1002/eji.202049101
58. Brodin P, Davis MM. Human Immune System Variation. *Nat Rev Immunol* (2017) 17(1):21–9. doi: 10.1038/nri.2016.125

Conflict of Interest: Authors LC, KY, YR, RC, YD and SL are employed by Beijing Genomics Institution.

The remaining authors declare that the research was conducted in the absence of any commercial or financial relationships that could be construed as a potential conflict of interest.

Publisher's Note: All claims expressed in this article are solely those of the authors and do not necessarily represent those of their affiliated organizations, or those of the publisher, the editors and the reviewers. Any product that may be evaluated in this article, or claim that may be made by its manufacturer, is not guaranteed or endorsed by the publisher.

frontiers | Frontiers in Immunology

ORIGINAL RESEARCH
published: 03 May 2022
doi: 10.3389/fimmu.2022.807104

Pandemic, Epidemic, Endemic: B Cell Repertoire Analysis Reveals Unique Anti-Viral Responses to SARS-CoV-2, Ebola and Respiratory Syncytial Virus

Alexander Stewart[1†], Emma Sinclair[1†], Joseph Chi-Fung Ng[2†], Joselli Silva O'Hare[1,3], Audrey Page[3], Ilaria Serangeli[4], Christian Margreitter[5], Federica Orsenigo[1,6], Katherine Longman[5], Cecile Frampas[5], Catia Costa[5], Holly-May Lewis[5], Nora Kasar[1], Bryan Wu[3], David Kipling[1], Peter JM Openshaw[7], Christopher Chiu[7], J Kenneth Baillie[8], Janet T. Scott[9], Malcolm G. Semple[10], Melanie J. Bailey[5], Franca Fraternali[2‡] and Deborah K. Dunn-Walters[1*‡]*

[1] School of Biosciences and Medicine, University of Surrey, Guildford, United Kingdom, [2] Randall Centre for Cell & Molecular Biophysics, King's College London, London, United Kingdom, [3] Faculty of Life Sciences and Medicine, King's College London, London, United Kingdom, [4] Dipartimento di Biologia e Biotecnologie Charles Darwin, Sapienza Università di Roma, Rome, Italy, [5] Department of Chemistry, University of Surrey, Guildford, United Kingdom, [6] Department of Biotechnology and Biosciences, Università degli Studi di Milano-Bicocca, Milan, Italy, [7] Faculty of Medicine, Imperial College London, London, United Kingdom, [8] Roslin Institute, University of Edinburgh, Edinburgh, United Kingdom, [9] MRC-University of Glasgow Centre for Virus Research, University of Glasgow, Glasgow, United Kingdom, [10] Faculty of Health & Life Sciences, University of Liverpool, Liverpool, United Kingdom

Immunoglobulin gene heterogeneity reflects the diversity and focus of the humoral immune response towards different infections, enabling inference of B cell development processes. Detailed compositional and lineage analysis of long read IGH repertoire sequencing, combining examples of pandemic, epidemic and endemic viral infections with control and vaccination samples, demonstrates general responses including increased use of *IGHV4-39* in both Zaire Ebolavirus (EBOV) and COVID-19 patient cohorts. We also show unique characteristics absent in Respiratory Syncytial Virus or yellow fever vaccine samples: EBOV survivors show unprecedented high levels of class switching events while COVID-19 repertoires from acute disease appear underdeveloped. Despite the high levels of clonal expansion in COVID-19 IgG1 repertoires there is a striking lack of evidence of germinal centre mutation and selection. Given the differences in COVID-19 morbidity and mortality with age, it is also pertinent that we find significant differences in repertoire characteristics between young and old patients. Our data supports the hypothesis that a primary viral challenge can result in a strong but immature humoral response where failures in selection of the repertoire risk off-target effects.

Keywords: B cell, COVID-19, ebola, RSV (respiratory syncytial virus), immunity, repertoire, class-switch recombination (CSR)

OPEN ACCESS

Edited by:
Moncef Zouali, Institut National de la Santé et de la Recherche Médicale (INSERM), France

Reviewed by:
Victor Greiff, University of Oslo, Norway
Gur Yaari, Bar-Ilan University, Israel

***Correspondence:**
Deborah K. Dunn-Walters
d.dunn-walters@surrey.ac.uk
Alexander Stewart
Alexander.stewart@surrey.ac.uk

[†]*These authors have contributed equally to this work and share first authorship*

[‡]*These authors have contributed equally to this work and share senior authorship*

Specialty section:
This article was submitted to B Cell Biology, a section of the journal Frontiers in Immunology

Received: *01 November 2021*
Accepted: *15 March 2022*
Published: *03 May 2022*

Citation:
Stewart A, Sinclair E, Ng JC-F, O'Hare JS, Page A, Serangeli I, Margreitter C, Orsenigo F, Longman K, Frampas C, Costa C, Lewis H-M, Kasar N, Wu B, Kipling D, Openshaw PJM, Chiu C, Baillie JK, Scott JT, Semple MG, Bailey MJ, Fraternali F and Dunn-Walters DK (2022) Pandemic, Epidemic, Endemic: B Cell Repertoire Analysis Reveals Unique Anti-Viral Responses to SARS-CoV-2, Ebola and Respiratory Syncytial Virus. Front. Immunol. 13:807104. doi: 10.3389/fimmu.2022.807104

INTRODUCTION

The emergence of SARS-CoV-2 in 2019, the ensuing pandemic and evolution of novel variants continues to make COVID-19 a matter of global public health significance. The recent SARS, MERS, Zika and Ebola outbreaks have also highlighted a need to better understand how the human immune system responds to novel infections, develop better treatments and control their emergence and spread. Initial reports from the COVID-19 pandemic, relying heavily on serum antibody titres, saw rapid declines in SARS-CoV-2 specific antibodies (1) that raised concerns over the nature and duration of B cell memory. While total antibody titres decrease the persistent presence of SARS-CoV-2-specific memory responses some months after infection mitigates these concerns (2, 3).

Immunoglobulins (Ig), both as secreted antibodies and as B Cell Receptors (BCRs), mediate immunity against multiple pathogens through their vast variability in antigen binding. This variability is produced by V-D-J recombination (4), where V, D and J genes are recombined from a pool of diverse genes. B cells with Ig genes encoding disease-specific antibodies are expanded upon challenge, causing a skewing of the repertoire towards greater use of antigen-specific genes associated with the challenge in question. Furthermore, the imprecise joining of gene segments, together with the action of terminal deoxynucleotidyl transferase (TdT) creates a highly diverse complementarity determining region (CDR)3, which is important for antigen binding, and can be used to identify "clones" of B cells within a repertoire. These clonal assignments allow us to track lineages and follow the progress of the post-activation diversification events of somatic hypermutation (SHM) and Class Switch Recombination (CSR) as the B cell response develops. Thus, repertoire analyses can help to characterise changes in the memory/effector B cell compartments and identify individual genes of interest for possible antibody therapeutics.

Both SHM and CSR are mediated by the enzyme Activation-Induced cytidine Deaminase (AID) and have traditionally been associated with germinal centre events in secondary lymphoid tissue, involving T cell help (5–7). There is, however, also evidence that CSR may occur outside of the germinal centre environment (8–11) and may not require direct T cell help. The ability of a B cell to mount a directed effector response prior to the formation of a germinal centre allows a more rapid immune response but with lower affinity.

Immune responses are often impaired in older people, which has been of particular concern in COVID-19 patients. The older immune system has shown reduced responses to vaccination, frequently with higher numbers of autoreactive antibodies and inflammatory cytokines (12–14). In B cells we, and others, have shown that particular subsets of B cells are altered with age: IgM memory cells (CD19+CD27+IgD+) are decreased in older people while the Double Negative (CD19+CD27-IgD-) are increased (15, 16). Since IgM memory cells are often associated with a T-independent response, the decrease in IgM memory in older people could have severe consequences in infections where a rapid extrafollicular response is required (17, 18). It has also been shown that the B cell repertoire is skewed towards sequences with longer, more hydrophobic CDR3 regions as we age (16, 19). As an immune response can result in a shift towards lower, less hydrophobic CDR3 regions (14, 20), and higher hydrophobicity has previously been correlated with increased polyspecificity (21–23), the older immune repertoire seems to be disadvantaged in this respect.

In this study we took a long-read repertoire amplification approach that allowed us to track the V-D-J clonal lineages in the context of antibody subclass to better understand, compare and contrast B cell responses to emerging or endemic viruses. Samples were taken from COVID-19 patients during and after infection, Ebola virus disease (EBOV) survivors from West Africa and the UK, volunteers challenged with Respiratory Syncytial Virus and compared with samples from healthy donors. We report the variation of repertoire between disease states in novel virus infection, with a focus on elderly who are known to respond less well to infection, particularly in SARS-CoV-2.

METHODS

Sample Collection

Whole blood samples (RSV, COVID-19, Healthy) were collected into Tempus™ Blood RNA tubes, kept at 4°C, and frozen down to -20°C within 12 hours. Ebola samples were cone filters from plasmapheresis, dissolved in Tri reagent. RNA was extracted using Tempus™ kits according to instructions. Healthy samples taken after SARS-CoV-2 emergence were all confirmed negative for anti-SARS-CoV-2 antibodies by SureScreen lateral flow test and by ELISA (24). Ebola RNA blood samples were collected from convalescent patients with viral RNA negative PCR tests in the 2014-2016 West African outbreak, three patients were Caucasian treated in the UK, and the remaining were convalescent plasma donor participants from a trial in Sierra Leone (25) (consented under the Sierra Leone Ethics and Scientific Review Committee ISRCTN13990511 and PACTR201602001355272 and authorised by Pharmacy Board of Sierra Leone, #PBSL/CTAN/MOHS-CST001). COVID-19 samples were collected from SARS-CoV-2 positive patients at Frimley and Wexham Park hospitals during 2020 (consented under UK London REC 14/LO/1221). Each participant was attributed a "severity score" in relation to their fitness observations at the time of hospital admission using the metadata collected. This score used the "mortality scoring" approach of SR Knight et al. (26) adapted to disregard age, sex at birth and comorbidities, and ranged from 0 to 6; patients scoring 0 to 3 were attributed low severity and patients scoring 4 to 6 were attributed high severity (25). Convalescent COVID-19 patients, from hospital sampling, were contacted for further donations and sample taken 2-3 months post hospital discharge. RSV samples were collected from participants who took part in a human challenge study and were monitored for infection by viral PCR tests (consented under UK London REC 11/LO/1826). Briefly, healthy participants were challenged intranasally with 10^4 plaque-forming units of the M37 strain of RSV and monitored for up to 6 months as previously described (27).

Repertoire Library Generation

Tempus™ tube samples were defrosted at room temperature and RNA was extracted using the Tempus™ RNA extraction kit according to the manufacturer's instructions. RNA samples were template switch reverse transcribed using SMARTScribe™ reverse transcriptase (Clonetech) according to manufacturer's instructions using the SmartNNN TSO Primer (**Supplementary Methods Table 1**) with a minimum of 170 ng of RNA input. The samples were then treated with 0.5 units/µl of Uracil-DNA Glycosylase (NEB) for 60 min at 37°C to reduce UMI interference, then incubated at 95°C for 10 min to inactivate the enzyme. Samples were amplified using Q5 polymerase (NEB) according to manufacturer's instructions with an annealing step of 65°C for 20s and extension step of 72°C for 50 s for 21 cycles. Round one of PCR was performed with forward primer Smart20 and mixed heavy chain (IG[M, G, A]-R1) reverse primers (**Supplementary Methods Table 1**). For PCR1 8 x 20 µl reactions were performed with 1 µl of RNA input per reaction. A semi-nested 2nd PCR was performed with forward primer PID-Step and reverse primers IG[M/G/A]-R2 (**Supplementary Methods Table 1**); 16 reactions of 20µl each was performed for each isotype with the same thermal cycling conditions as PCR1 but with 12 cycles, with 1µl of template. The primers in PCR2 also contain Patient Identifier (PID) sequences to allow multiplexing on PacBio (**Supplementary Methods Table 2**). Samples were run on a bioanalyzer (Agilent 7500), isotypes from patients were pooled at equal concentrations and concentrated using Wizard PCR Clean-up kits (Promega) according to manufacturer's instructions with 30 µl of elute. Each isotype was then purified using a PippinPrep™ with Marker K reagents (Sage Biosciences) used as an external ladder reference (IgM/G/A 600-100bp). The concentration was checked using a DNA quantification kit on the Qubit according to manufacturer's protocol, the different isotype samples were pooled at equal concentrations and purified with SPRIselect beads (Beckman Coulter) at X0.8 sample volume with elution in 30µl of TE buffer. Sequencing was performed on either the PacBio RSII or Sequel platforms (See **Supplementary Methods Table 2**).

Quality control, data cleaning and removal of multiplicated UMIs was carried out as previously published (16, 28). Immunoglobulin V-D-J gene usage and CDRH3 was determined using IMGT/High V-quest. Clonotype clustering was carried out as per (16, 28), in brief: a Levenshtein distance matrix was generated on the CDRH3, hierarchically clustered and branches cut at 0.05 to generate clones. Physicochemical properties were calculated using the R Peptides package (29).

Analysis of Clonal Diversity

We sought for methods to qualitatively (visualising clone size distribution) and quantitatively compare clonal diversity (calculating metrics which summarise clonal diversity). We first noted, as one would expect, that sequencing depth (i.e., number of sequences sampled per repertoire) was a strong predictor of the number of clones (**Supplementary Figure S1**). For all repertoires considered here, a wide range of sequencing depth was observed (number of sequences range from 836 to 105,323, median = 12,040). We therefore adopted the following procedure in this analysis: first, to quantify the extent of clonal diversity we used the Gini coefficient which measures the evenness in the distribution of clone size across clones; application of this metric to quantify BCR clonal diversity has been well documented (30–32). For a given repertoire, clones were ordered by their clone sizes, and the cumulative distributions of clone sizes (in terms of percentage of sequences in repertoire) and its percentile distribution were compared for evenness. As such, the resulting metric was independent from the *absolute* numbers of sequences and clones, thereby allowing fair comparison across repertoires of different sequencing depths. As Gini coefficient is an indicator of evenness, we took (1 – Gini coefficient) as the metric of clonal diversity. To qualitatively compare clonal diversity, we generated visualisation using the following procedure to minimise the impact of sequencing depth differences: we first sampled 12,000 sequences (≈ median sequencing depth; see above) from each repertoire; for repertoires with less than 12,000 unique observations, this number of sequences was sampled with replacement. We then sampled up to 100 clones with probability scaled by clone sizes to generate bubble plots where each bubble represents a clone and bubble sizes are scaled with clone sizes. Genotypic features like V gene usage can be represented as colours. Such plots were included in **Figure 2C**.

Analysis of BCR Clone Lineage Trees

Lineage trees were reconstructed using the maximum parsimony method implemented in the dnapars executable in the phylip package (33). All clones with at least 3 sequences were considered; IMGT-gapped, V-gene nucleotide sequences of all observations in the clone together with the annotated germline V-gene sequence (included to root the tree) were included as input to dnapars. Functionalities implemented in the alakazam R package (34) were used to call dnapars and reformat the output into text-based tree files (newick format) and directed graphs (igraph objects manipulated in R). The directed graphs were further parsed using functions in alakazam and igraph to obtain, for each observed sequence in the given clone, its distance D from the given germline gene g (denoted here as D_g), as estimated by the dnapars-reconstructed lineage tree: the closer this distance is to 0, the closer the sequence is to germline and therefore a lower mutational level.

We sought to summarise, for a given clone, the distribution of D_g; this distribution would indicate the overall mutational level of sequences within the clone (summarised using conventional statistics like the median of D_g) and the evenness of mutational level (i.e. whether the clone consists of expansion of sequences with a similar mutational level, or it comprises sequences with a wide range of mutational levels). This can be visualised as a heatmap (clones [vertical axis] versus D_g [horizontal axis], with colours scaling with density of the distribution; see **Figure 5B**), or as a curve (clones [vertical axis] versus the median of D_g [horizontal axis], See **Figure 5C**). The curve representation allows calculation of area-under-curve (AUC) as a metric which we termed "Germline Likeness", to quantify mutational

levels across clones. This is similar to quantifying sequence similarity to germline, except that here Germline Likeness quantifies the tendency to which all clones from the BCR repertoire of a given individual have high similarity to the germline (and therefore lower mutational levels).

Detecting Class-Switch Recombination Events From Lineage Trees

Since the lineage trees were constructed using only V-gene sequences (see above), in theory antibody sequences of different subclasses could be ordered in the tree in a way that imply class-switch recombination (CSR) events which are mechanistically impossible. We therefore pruned the dnapars-reconstructed tree to remove edges which imply CSR events that violate the physical order of constant region genes in the human IGH locus. This was performed using a Python implementation of the Edmond's algorithm to construct a minimum spanning arborescence tree with the given germline V gene sequence as root. With this arborescence tree the type of CSR (subclass switched from/to) and the distance-from-germline at which the CSR event occurred (estimated as the median distance-from-germline of the two observations relevant to the given event) were obtained.

We noticed that the quantification of CSR events is dependent on the number of sequences sampled in the repertoire. To eliminate this confounding factor, we followed the sampling protocol for the clone size visualisation (**Figure 2C**): briefly, we sampled 12,000 sequences (≈ median sequencing depth across all samples) from each repertoire; for repertoires with less than 12,000 unique observations, sampling was performed with replacement. The analysis presented here (**Figure 6**) is the result after this subsampling analysis, therefore corrected for difference in sequencing depth.

Convergent Network

Productive heavy chain sequences with CDRH3 of length shorter than 30 amino acids were considered in the construction of a convergent network. Sequences were connected if they meet the following criteria (a) same V and J gene usage; (b) from different individuals; (c) same CDRH3 amino acid length, and (d) ≥85% CDRH3 amino acid identity. The same criteria have been applied in published studies investigating convergent clonotypes across SARS-CoV-2 B-cell repertoires (35, 36). To allow interpretation of possible targets of sequences in convergent network clusters, known binders were included in constructing the network. Known binders were taken from the following sources: first experimentally determined antigen-antibody structural complexes deposited in the Protein Data Bank (PDB). PDBe was queried on 19 May 2021 with the search term 'Organism: Severe acute respiratory syndrome coronavirus 2'. The resulting list of PDB entries was overlapped with entries in the SAbDab structural antibody databases (37) to obtain list of PDB complexes of antibodies and SARS-CoV-2 proteins. A total of 215 heavy chains from 186 structures were considered. Second, known binders validated in experiments where antibody variable regions were cloned and assessed for SARS-CoV-2 protein binding were taken from published work (38–43). All known binder sequences were annotated for V/J gene usage using either IMGT/High-VQuest (if DNA sequences were provided) or IMGT/DomainGapAlign (if only amino acid sequences were provided). Information regarding specificity (i.e. SARS-CoV-2 protein targets) was obtained from either **Supplementary Data Files** in the cited publications or by visual inspection (for PDB structures). **Supplementary Table S2** contains all known binder sequences included in this analysis. To construct the network, known binders were connected to one another and to repertoire sequences using the identical criteria mentioned above. In total 809 unique CDRH3 sequences were considered in constructing the convergence network. The resulting network contains 7500 sequences (7370 from repertoire, 130 known binders).

We note that the method of constructing convergent networks is comparable to single-linkage clustering. We compared these results with complete-linkage clustering (applied in R using the command 'hclust(method = "complete")') and found that using the same amino-acid identity cutoff, it produced clusters which are notably smaller (**Supplementary Figure S6A**). Since in the binders list we have SARS-CoV-2 binders for which crystal structures are available, we reason that those antibody structures which bind the antigen in the same way should be grouped together. Manual inspection of these structures found that they are grouped together in our networks, but are separated under complete-linkage clustering (**Supplementary Figure S6A**). We confirm this observation quantitatively, by comparing the antibody-antigen structures by calculating the TM-score (44) between every pair of binder structures, which confirm that our convergent networks group together binders with similar interface at the three-dimensional structural level (**Supplementary Figure S6B**, see figure legend therein). We therefore reason that complete linkage is too stringent, and our networks are likely to group sequences which engage with the antigen in the same way.

Analogous convergent networks were constructed using the EBOV and RSV repertoire data, separately considered with respective known binders and Healthy individuals' repertoire; the majority of clusters were formed mainly of sequences from Healthy donors absent of known binders (45–48), although we were able to identify two convergent clusters of RSV-infected individuals with similar CDRH3 to known binders of the RSV fusion glycoprotein (**Supplementary Figure S7**). To investigate whether clusters shared across disease conditions exist, convergent networks were also constructed considering CV19, RSV and EBOV repertoire and binder sequences altogether (**Supplementary Figure S8**). **Supplementary Table S3** contains all convergent networks constructed, presented as list of pairwise sequences.

Statistical Analysis and Data Visualisation

V-D-J gene usage for each patient was turned into a proportion to normalise for different numbers of sequences and allow for comparison. Gene usage analysis was performed in GraphPad Prism 8.4.3 using a two-way ANOVA with a Dunnett's *post hoc* test. P-values have been corrected using the Benjamini-Hochberg method wherever applicable. All other statistical analyses were performed in the R statistical computing environment (version 4.0.2). Data visualisation was performed using the R ggplot2 package and the following specialised R packages: visNetwork

(forvisualising convergent CDRH3 network clusters) and ggseqlogo (for visualising CDRH3 sequence logos). PDB structures were visualised using PyMOL (version 2.3.0). Histograms of CDRH3 length and hydrophobicity, as measured by Kidera factor 4, were constructed on the Brepertoire website (49).

RESULTS

Patient Cohorts

IGH sequences, of total V-D-J plus ~150-200 bp of C regions, were obtained from pandemic, epidemic and endemic diseases and stages along with 24 healthy controls across multiple age ranges (**Figure 1** and **Table 1**). This included: 16 hospitalised COVID-19 patients (CV19), 5 of these patients had follow-up convalescent samples (CV19-Recovered, hereafter CV19R), 12 Ebola convalescent plasma donors (EBOV), 12 participants challenged with RSV, 6 of whom became infected (RSV-I) and 6 of whom did not (RSV-U). Healthy Samples (Healthy) were a grouping of YFVD0, RSVD0 and samples taken as controls during the (COVID-19) pandemic (n=24). Numbers of sequences varied from 836 to 105,323, median = 12,040 per sample, *IGH* gene usage for each patient was expressed as a proportion of the total in order to normalise for differences in sequence numbers between different samples.

IGH Gene Repertoire Changes in Response to Viral Infection

Although the humoral immune response is varied, with different subclasses of antibody having different effector functions (50), many methods of repertoire analysis have hitherto not distinguished between antibody subclasses. We have used PacBio methods to obtain full V-D-J sequence in the context of subclass usage to investigate class switching events during immune responses to infection. We also distinguish between mutated versus unmutated IgM sequences, as a proxy for identifying IgM memory responses. Comparisons of subclass distribution, in relation to healthy controls, revealed a significant increase in the proportion of IgA1 compared to IgA2 in CV19, and RSV-I and the proportion of IgG1 relative to IgG2 in CV19, EBOV and RSV-I (**Figures 2A, B**). The differences in CV19 IgG and IgA repertoire returned to 'normal' healthy levels by the time of convalescent sampling (CV19-Recovered) 2-3 months later.

Immune challenge is characterised by clonal expansion of B cells that express Ig which reacts with the challenging antigen. We identify members of clones in the repertoire by clustering the CDRH3 regions and looking at the largest clones in each sample we can see evidence of increased clonal expansions in CV19 patients (**Figure 2C**). In the full CV19 repertoire *IGHV4* family genes were expanded (**Figure 2C**), more specifically of *IGHV4-39* (**Supplementary Figure S2**) and some *IGHV3* family; this is particularly noticeable in IgG1 and IgA1. Analysis of clonal diversity of memory B cells using the Gini coefficient, taking all possible clones into account, found that CV19 patients had a less clonally diversified repertoire in all but the IgM mutated, IgG2 and IgG4 partitions (**Figure 2D** and **Supplementary Figure S3**), suggesting pervasive expansions of specific BCR clones. Unusually, we also saw a decrease in diversity of unmutated IgM sequences, indicative of clonal expansion prior to SHM and CSR (**Figure 2D**). These values returned to normal in the CV19R samples. In comparison, *IGHV1* family was expanded in RSV-I IgG1 partition (**Figure 2C**), particularly of *IGHV1-18* (**Supplementary Figure S4**). Active infection with RSV, as well as samples taken 28 days after yellow fever vaccination, showed an increase in diversity of IgA2. Interestingly, EBOV memory B cell populations were more diverse than healthy controls in all the main switched subclasses (IgG1, IgG2, IgA1, IgA2) (**Figure 2D** and **Supplementary Figure S3**).

Large clone sizes can mask whole repertoire changes, so we analysed the frequency of gene use after reducing the data to one representative sequence per clone. We found increased use of *IGHV3-30* in IgM mutated sequences in CV19 patients (**Figure 2E**), and also of IgM-mutated/IgA1/IgG1 in CV19R; this was unique to CV19. An increase in use of *IGHV4-39* was found in CV19 IgA1 sequences and was also found increased across the board in EBOV and RSV-U samples (**Figure 2E**). *IGHV3-23* was found to be reduced in ongoing infection (likely an offset as a result of relative increases in usage of other genes) but exceeded the healthy levels in CV19R. *IGHV1-69*, which has previously been associated with viral infections (51, 52), was increased in RSV-I but not EBOV or CV19. The YF day 28 vaccine samples increased use of *IGHV3-7* in IgM-mutated only (**Figure 2E**; comparisons for other V genes in **Supplementary Figure S4**).

Complementarity Determining Region 3 (CDRH3) Immaturity in COVID-19

Given the importance of CDRH3 in antibody recognition, and the contribution to CDRH3 from the *IGHD* and *IGHJ* genes, we analysed these also. In CV19 samples there was a significant increase in use of *IGHD2-2*, *IGHD3-3* and *IGHJ6* (**Figure 2E**). These genes tend to be more hydrophobic (*IGHJ6* being the exception) and all have among the longest amino acid lengths with only *IGHD3-16* being 2 AA longer. This contribution can be seen in the overall CV19 repertoire which skews towards longer amino acid sequences and increased hydrophobicity, indicative of early response as affinity maturation causes shorter less hydrophobic CDRs (**Supplementary Figure S5**). A clustering analysis of peptide physicochemical properties of CDRH3 regions generally results in a difference between IgM sequences and memory sequences (**Figure 2F**), presumably reflecting biases in antigen selection during post-challenge development. We can see that healthy and CV19 subclass sequences mostly have similar CDRH3 properties to each other, however, in the case of CV19 IgG1 and IgG3 cluster closer to IgM sequences from healthy and EBOV rather than healthy IgG1 and IgG3 sequences implying a more 'naïve', unselected, repertoire.

Convergent Antibody Clusters Reveal Distinct VDJ Preferences

To assess the functional importance of the skewed patterns of V, D and J gene usage in CV19 we created networks connecting sequences observed in our CV19 and control repertoire data

(**Figure 3A**), using criteria previously employed in discovering 'convergent' antibody sequences shared between patients (53). By also including known SARS-CoV-2 binders (see Methods), we determined that this method is superior in comparison with complete-linkage clustering, in grouping together antibody sequences which bind the antigen in similar manner (**Supplementary Figure S6**). We obtain clusters of CDR3 sequences found in both CV19 patients and healthy controls, some of which converge towards known binders of SARS-CoV-2 proteins such as those targeting the receptor binding domain (RBD) of the spike protein (**Figure 3B**). Many of these large convergent clusters did not, however, include a known binder in the network (**Figure 3C**). Interestingly, we observe that some of these convergent clusters also contain sequences from Healthy controls, suggesting that our baseline repertoire contains B cells capable of recognising SARS-CoV-2 proteins, as reported by others (36, 53). Overall, convergent clusters use a diverse set of V genes, but most of our larger convergent clusters contain *IGHV3* or *IGHV4* families and demonstrate increased *IGHJ*6 usage as well as the more commonly used *IGHJ4* (**Figure 3C**). A comparison exclusively of the known binders to date reveals distinct combinations of V and J gene preferences (**Figure 3D**). We do find clusters of sequences using *IGHV3-53* and *IGHV1-58* such as those used in anti-RBD antibodies (e.g. **Figure 3B**). We find that sequences from convergent clusters tend to be found in larger clonal expansions than those without evidence of convergence (**Figure 3E**), possibly implying that specific clonal expansions in response to challenge are shared across patients. We note that half of the larger clusters have substantial contributions from healthy control sequences, so there may be some IGH genes, such as *IGHV3-33*/*IGHJ5* found also in RSV-I and EBOV convergent networks (**Figure 3C** and **Supplementary Figures 6A, B**), which have increased versatility such that they are often seen in response to multiple different challenges.

Similar analyses of RSV and EBOV repertoires were limited by the paucity of information on antibody binders, however it was notable that only RSV-I, and not RSV-U, showed evidence of convergence. *IGHV1-18* appears in a large cluster with a known RSV F-protein binder and although the large *IGHV3-23* cluster does not contain a known binder it forms part of the larger expansion of *IGHV3-23* genes in mutated IgM genes from this cohort (**Figure 2E**, **Supplementary Figure S7B**).

VDJ Selection Differs Between Ages in COVID-19

The disparity in COVID-19 severity and mortality between age groups is striking, so we looked for age-related differences in our B cell repertoire data, grouping by <50 and >60 based on this mortality disparity. The difference in IgA1/IgA2 ratio is less in older people, not reaching statistical significance. (**Figure 4A**). On the other hand, the increase usage of IgG1 in CV19 is robust across age (**Figure 4B**). Considering Ig gene usage, we observe the intriguing case of *IGHV3-30* which is only preferentially used by the over 60s during infection (**Figure 4C**). Conversely, *IGHV3-53*, which appears relatively frequently in known binder data in combination with *IGHJ4/6* but did not appear in our total cohort analysis (**Figure 2E**), is significantly increased in the under 50s IgM-mutated partition (**Figure 4C**). We also found that *IGHV4-39*, *IGHD2-2*, *IGHD3-3* and *IGHJ6*, which we find are expanded in CV19 across multiple B cell partitions, only have significantly increased expression in the under 50s and not the over 60s; *IGHV4-34* appeared increased in both age groups in the IgG1 partition, but did not reach statistical significance (**Figure 4C**).

IgG1 Is Immature in Response to COVID-19

Beyond the scope of gene usage, our BCR repertoire data also enabled reconstruction of individual BCR lineage trees to make inferences about the evolution of a particular clone. Using the annotated germline V allele as the root of the tree, we estimate, for each sequence in the lineage, its distance from the root (**Figure 5A**); this distance being directly proportional to mutational level. We visualise the distribution of this germline distance across all clonotypes observed in each given individual, and observe that the repertoire is dominated by clonotypes with very low mutational levels for a subset of CV19 patients, whilst the predominance of such clones is broadly absent in healthy controls (**Figure 5B, C**). Interestingly, in repertoires from convalescent individuals (both EBOV and CV19), we instead observe dominance of clonotypes with higher mutational levels, although the pattern is less striking than the CV19 patients during hospitalisation (**Figure 5C**). These curves allow for quantification of the Area Under the Curve (AUC), which constitutes a metric we term "Germline Likeness": a higher Germline Likeness corresponds to a lower level of mutation across all clones (**Figure 5D**); this is akin to quantifying sequence similarity to the germline, except that Germline Likeness here quantifies such phenomenon for a given repertoire in general, rather than a specific sequence. Using this metric we confirm that CV19 repertoires were dominated by clones that were largely unmutated, while EBOV samples carried the greatest mutation rate (**Figure 5E**). As might be expected, with time to generate a germinal centre response, Germline Likeness in CV19 faded with time (**Figure 5F**), to the point where the CV19R repertoires have similar level of mutations compared to the EBOV-convalescent and healthy control repertoires. Partitioning the analysis by isotype, RSV and healthy controls demonstrate the expected trend where an increased level of mutations can be found in both IgG and IgA compared to IgM (**Figure 5G**). However, in CV19 only IgA showed a significant change in Germline Likeness from IgM, albeit with a similar level of Germline Likeness to the healthy IgM (**Figure 5G**).

Ongoing Class Switch Recombination (CSR) Is Detectable in PBMCs of COVID-19 and EBOV Patients

Our lineage trees were further analysed for CSR events: respecting the sequential order of CSR in the genome, we identify CSR events where sequences of different antibody classes/subclasses are directly connected in the lineage tree. This enables us to trace the timing of CSR events (distance from the germline), the direction of class switching (e.g. from IgM to IgG1) and frequency of observation. Many clones have

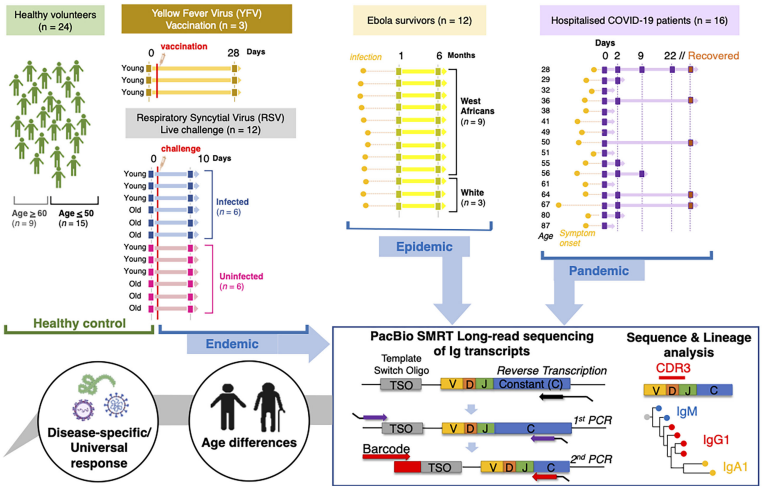

FIGURE 1 | Schematic to illustrate data collection and analysis conducted in this study. Samples were taken from Healthy individuals, recovered Ebola survivors, hospitalised COVID-19 patients, live RSV challenge participants that either became infected or did not and Yellow Fever vaccine recipients before vaccine and 28 days post-inoculation. Extracted sample RNA was subject to a heavy gene specific race 5' and nested PCR amplification process retaining V-D-J and sub-class information.

TABLE 1 | Donor characteristics.

Sample	Age	Gender	Ethnicity	COVID-19 Severity Score (out of 6)	Days since symptom onset
Healthy (n = 24)	Median 29.5 (Range 23 - 76) ≤50 years old: 15/24 (62.5%) ≥60 years old: 9/24 (37.5%)	Female: 7/24 (29.2%) Male: 5/24 (20.8%) Unknown: 12/24 (50%)	White: 12/24 (50%) Unknown: 12/24 (50%)		
COVID-19 (n = 16)	Median 50.5 (Range 28 - 87) ≤50: 8/16 (50%) 50-60: 3/16 (18.75%) ≥60: 5/16 (31.25%)	Female: 7/16 (43.75%) Male: 9/16 (56.25%)	White: 13/16 (81.25%) South East Asian: 1/16 (6.25%) Indian Subcontinent: 2/16 (12.5%)	Median 3 (Range 1 - 5)	Median 8 (Range 1 – 35)
COVID-19 Recovered (n = 5)	Median 50 (Range 28 - 87) ≤50: 3/5 (60%) ≥60: 2/5 (40%)	Female: 3/5 (60%) Male: 2/5 (40%)	White: 4/5 (80%) Indian Subcontinent: 1/5 (20%)		
RSV Infected (n = 6) **RSV Uninfected (n = 6)**	Young: 3/6 (50%) Older: 3/6 (50%) Young: 3/6 (50%) Older: 3/6 (50%)				
Ebola (n = 12)	Young: 3/12 (50%) Unknown: 9/12 (50%)	Female: 1/12 (8.3%) Male: 2/12 (16.7%) Unknown: 9/12 (75%)	White: 3/12 (25%) West African: 9/12 (75%)		
YFV D28 (n = 3)	Median 28 (Range 27 - 28) Young: 3/3 (100%)	Female: 1/3 (33.3%) Male: 2/3 (66.7%)	White: 3/3 (100%)		

*See **Supplementary Table S1** for a detailed summary of metadata per donor.*

evidence of CSR, particularly in EBOV, even after correcting for clone sizes (**Figure 6A**). In particular, CV19 patients were more likely to switch early to IgG1 from IgM, with little mutation (**Figures 6B–D**) and to IgA1 from IgG1 later in the lineage with more mutation (**Figures 6B, D**). This agrees with the lack of CDRH3 "maturity" in IgG1 (**Figure 2F**) and the overall increased use of IgG1 and IgA1 seen in CV19 (**Figures 2A, B**).

The evidence of increased CSR in convalescent EBOV patients is striking and occurs across the board with the exception of IgM switching to IgG1 (**Figure 6D**). We noticed

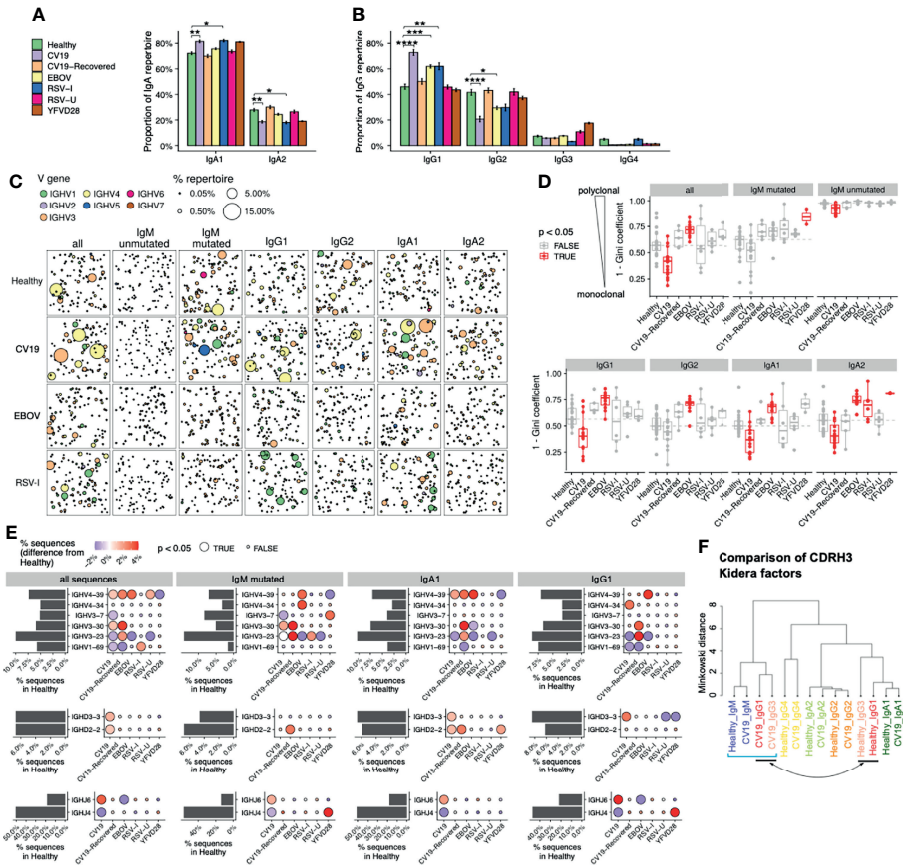

FIGURE 2 | Distinct V-D-J and isotype repertoires in CV19, EBOV and RSV BCR have occasional similarities. **(A, B)** Difference in sub-class use of IgA (panel a) and IgG **(B)** in viral disease and healthy BCR repertoires. **(C)** Clonal expansion of sequences of relevant effector types (as revealed in A) plus unmutated and mutated IgM to identify trends of V gene usage in viral infections. Each bubble sampled to a uniform depth (see Methods), with size proportional to clone size, represents one clone colour-coded by V-family usage. **(D)** Quantification of clonal expansion calculated using the Gini coefficient (see methods), revealed clonally expanded effector populations (more monoclonal/less diverse, closer to 1) or more diverse clones (closer to 0) in viral infections. Sample types with significant differences (false discovery rate [FDR] < 0.05) compared against Healthy were highlighted in red. Dashed line indicates the median diversity in the Healthy cohort. **(E)** Frequency of selected V-D-J gene usage in different cohorts for all sequences and further subdivided by IgM-mutated, IgA1, IgG1. Bar charts depict gene frequency usage in the Healthy cohort. Bubble plots depict the difference in usage (coloured: blue reduced/red increased) compared to healthy repertoires. **(F)** CDRH3 physicochemical characteristics (represented by Kidera factors) were analysed separated by sub-classes and disease status (Healthy/CV19), and compared using Minkowski distance. Note that IgG1 and IgG3 sequences from CV19 cluster together with IgM (square bracket), away from those of the same sub-classes from healthy individuals (indicated by arrow). Statistical significance in panels a, d and e was evaluated using one-way ANOVA and Dunnett *post-hoc* comparison against the Healthy cohort: p-value was corrected using the Benjamini-Hochberg method and expressed as false discovery rate (FDR), indicated either with colour (panel c), bubble size **(E)** or the symbols under the following scheme: *, FDR < 0.05; **, FDR < 0.01, ***, FDR < 0.001, ****, FDR < 0.0001.

that although there is a similar pattern of CSR preferences in White and West Africans individuals, the overall distance from germline is longer before CSR occurs in West Africans (**Figure 6B**). This may suggest that the ethnic bias in existing immunoglobulin sequence databases has resulted in mis-assignment of germline alleles. No CSR differences were seen in the RSV data.

DISCUSSION

We compared immunoglobulin gene sequences from pandemic (SARS-CoV-2), epidemic (Ebola) and endemic (Respiratory Syncytial Virus) patients in order to discover features that might distinguish newly emergent and endemic infections. We notice that although the sequencing depth varies between sample types, metrics related to gene usage and mutational levels are typically highly stable at different sequencing depths (**Supplementary Note**), allowing us to perform robust comparisons across different immune challenges. The ability of B cells to generate a highly diverse immunoglobulin repertoire that might bind any antigen, and the diverse functionality of the antibodies produced, is critical for an effective immune response. Repertoire studies aim to identify specific antibodies by looking for biased usage of particular Ig genes, and have been useful in the past (16, 28). However, not all expanded genes encode

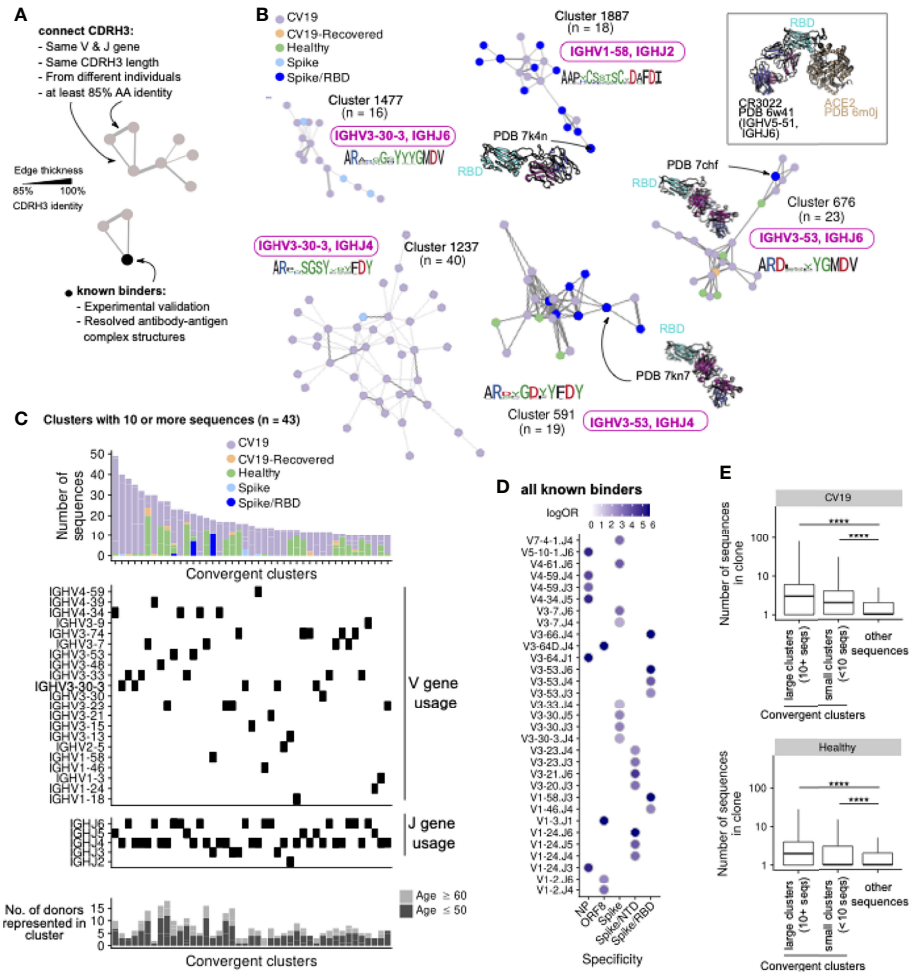

FIGURE 3 | CDR3 regions from different CV19 patient repertoires converge, some with known SARS-CoV-2 binders. **(A)** CDR3 known binder networks were created using same V, J and CDR3 length with at least 85% amino acid (AA) identity. **(B)** Convergent clusters from healthy and CV19 repertoire with known PDB structures. *IGHV* and *IGHJ* use and the CDR3 AA sequence were noted. **(C)** Clusters containing at least 10 sequences were visualized, with breakdown of repertoire origin (stacked bar plots), and the *IGHV* and *IGHJ* gene usage of each cluster aligned beneath. The number of donors with sequences in each depicted cluster are shown as bar graphs (bottom panel, **C**), broken down into subsets with age ≤50 (light grey) and ≥60 (dark grey). **(D)** All known binders were analysed for similarity of *IGHV*/J gene use to specific SAR-CoV-2 antibody targets. Dots coloured by enrichment (log-odds ratio, logOR). For each V/J combination only the target with the top logOR metric was shown. **(E)** Comparison of clonal expansion of convergent (split by clone size; ≥10 or <10 sequences) and non-convergent clusters in healthy and CV19 repertoires. Statistical significance evaluated using a Wilcoxon rank-sum test, ****: FDR < 0.0001. See **Supplementary Figure S7** for analogous analyses on RSV and EBOV repertoires.

specific binders (49) and we need to consider the possibility that expansions found in the midst of an acute response may be a side effect of the disease involving inappropriate expansion of B cells carrying antibodies with off-target effects rather than a specific targeting to the challenge. Repertoire selection is normally a delicate balance between tolerance versus immune response to a pathogen and the inflammatory state of acute disease can upset the balance. Serological studies have shown an increase in autoreactive antibodies, particularly to interferons, during acute COVID-19 for example (54, 55).

Looking across different viral diseases, we found a general increase of *IGHV4-39* use in the repertoire of two different viral diseases (COVID-19 and Ebola). Despite this, only one of our convergent clusters, dominated by COVID-19 sequences, uses *IGHV4-39* (**Figure 3C**); it is possible that there are unannotated *IGHV4-39* SAR-CoV-2 binders. One single cluster does not, however, explain the larger expansion in *IGHV4-39* use across the COVID-19 or Ebola repertoire. *IGHV4-39* may therefore be involved in the pathogenesis of the disease by promiscuous binding to self-proteins. Alternatively, *IGHV4-39* may simply support a wide range of specific binding properties, supported by the lack of convergence and given it has also been dominant in cancer, bacterial infection, influenza and HIV responses (56–59). Such promiscuous binders would have networks contributed to by more than 1 cohort with 52 networks matching this description in our data. It is also significant across all 64 large clusters 14 were

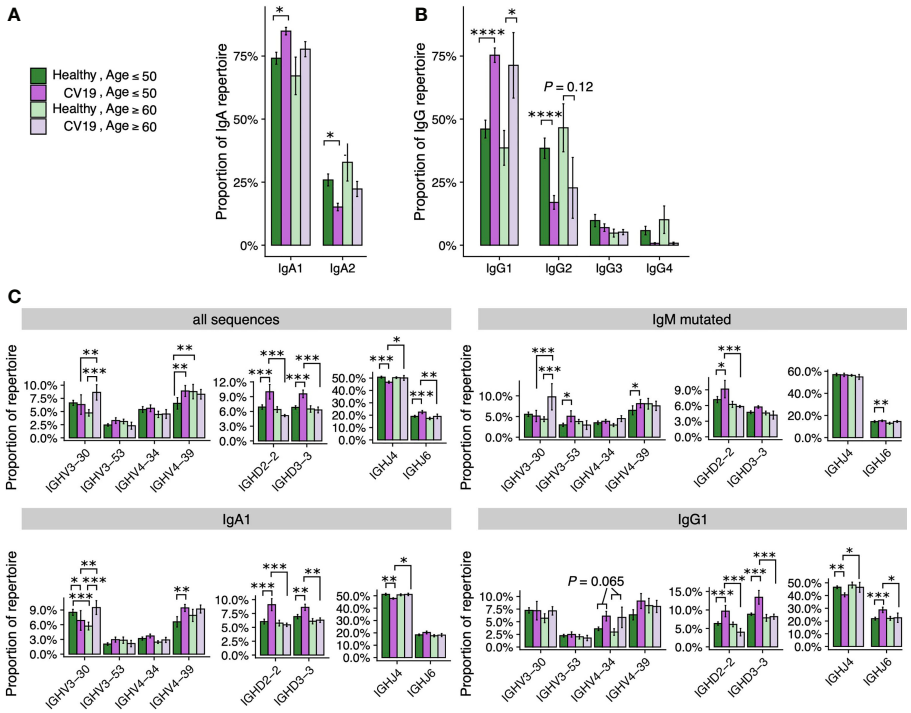

FIGURE 4 | V-D-J and isotype usage repertoire differences between healthy and CV19 are not as apparent in older ages. CV19 and healthy patients were split by over 60s and under 50s and were compared for IgA **(A)**, IgG **(B)** usage and selected V-D-J gene usage **(C)**. Statistical significance evaluated using two-way ANOVA and Tukey's *post-hoc* test: *, false discovery rate (FDR, corrected using the Benjamini-Hochberg method) < 0.05; **, FDR < 0.01, ***, FDR < 0.001, ****, FDR < 0.0001.

dominated by CV19/CV19-R sequences, yet only 5 matched known binders, suggesting previously unknown SARS-CoV-2 specific binders. As more studies on both naturally infected and vaccinated individuals identify and validate new SARS-CoV-2 binders, we expect more experimental validation to ascertain the relevance of these clonotypes in the immune response. Further data integration exercise incorporating more repertoires (from both healthy and infected/vaccinated individuals) will discover more convergent clusters which richer annotations.

In addition to expansion of gene use as an indicator of activation, we can infer biological information from assessment of the AID-mediated activities of CSR and SHM. These have long been associated with germinal centre formation (60, 61). However, there is mounting evidence that CSR can occur prior to the germinal centre formation (8–11, 36, 53). T-independent activation has been shown to be driven by CD40-independent TLR/TACI activation (62). Our data indicates an early switching to IgG1 without extensive hypermutation. This data is consistent with Woodruff et al. (63) who also found high germline similarity in IgA1, and (42) where COVID-19 samples were found to have more naïve-like characteristics. Our COVID-19 IgA1 sequences also indicate a lower level of hypermutation than the control group, albeit higher than the COVID-19 IgG1, likely reflecting their distance along the CSR hierarchy. Uniquely, our diversity analyses also indicate expansion of unmutated IgM clones. Alongside these data we see that CDRH3 region maturation of IgG1 and IgG3 genes in the COVID-19 patients is less removed from the IgM state than healthy IgG1 and IgG3, or any other class switched repertoires. Together with the lineage analysis of CSR timing, the whole picture in COVID-19 is of an early immature response of IgM, switching to IgG1 but without much SHM such as might occur in the absence of T cell help in a GC reaction, and then to IgA1. Whether these responses are unique to a live infection or because the virus is so novel is difficult to ascertain, with future vaccine and comparative studies likely to shed further light on this phenomenon. IgG1 is known for its antiviral properties (50, 64) so is expected in this data. The majority of rapid immunological protection assays for COVID-19 focus on IgM or IgG (65–68). Since switching to IgA1 is notable in our data it would be useful for future serology assays to include IgA. Euroimmun's IgA on LFA had one of the highest sensitivities at 87.8% compared to IgM and IgG from other assays (range 43.8-93%, mean 72.5%, median 76%) (67, 69).

It is known that healthy older people generally have more antibodies capable of binding self-proteins (70). The balance between antibodies with positive versus negative/bystander activity may be changed in older patients. We cannot tell this from our data except that we see a higher frequency of known spike binders clustering with COVID-19 repertoires in the younger cohort. Significant age-related differences occur in the dominant IGH COVID-19 genes: the increased use of *IGHV3-30* is only seen in older COVID-19 patients and that of *IGHV4-39*

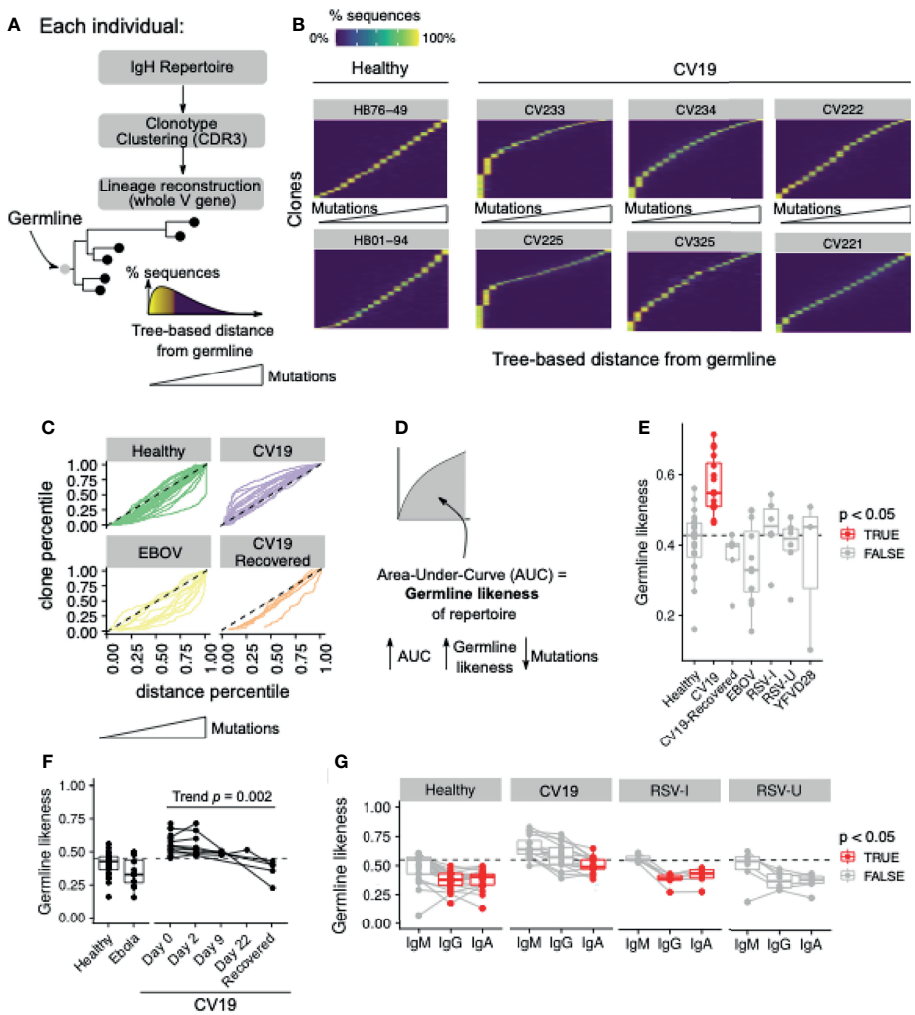

FIGURE 5 | Mutational levels in BCR lineages indicate lower somatic hypermutation in CV19. **(A)** Lineage trees were constructed by clonotyping the IgH CDR3 and the lineages reconstructed using the whole V gene rooting on the predicted germline, allowing the distance from germline to be estimated for each sequence. This allows ordering of sequences based on this distance from germline: depicted as a histogram [**(A)** bottom right]. **(B)** Clones in the repertoire, for selected donors, were ordered (vertical axis) using median distance from germline (horizontal axis), and the distribution of such distance for each clone was plotted with heatmap colours being the percentage of sequences within the clone containing the a given level of mutation. **(C)** Distance from germline distributions for every donor, split by condition, represented as curves. Dotted line represents the theoretical expectation of mutational level. **(D)** From each of these curves (in **c**) the area under the curve (AUC) was calculated giving a statistic of 'Germline Likeness', a higher AUC resembling more the germline and a lower AUC indicating more mutations. **(E)** Comparison of Germline Likeness between conditions: sample types with significant (Benjamini-Hochberg-corrected false discovery rate [FDR] < 0.05) differences compared to Healthy (Wilcoxon rank-sum test) are highlighted in red with the dotted line being the healthy median. **(F)** The Germline Likeness across timepoints for CV19 patients with Healthy and Ebola data are reproduced here for comparison: trend was evaluated using the Jonckheere-Terpstra test. **(G)** Comparison of germline distance split by immunoglobulin isotype was performed split by cohort: significant (FDR < 0.05) differences compared to IgM (Wilcoxon rank-sum test) are highlighted in red.

only in the younger group. We also see selection for *IGHD2-2*, *IGHD3-3* and *IGHJ6* only in the young, with *IGHJ6* occurring frequently in known binder networks, given the importance of *IGHD* and *IGHJ* genes to the CDRH3 region it is striking that the differences seen here are solely in the younger age group. We note that by separating samples by age group the small sample size limits the potential to discover more gene usage differences with strong statistical significance. In the future integration with other repertoire datasets, including those in response to SARS-CoV-2 vaccination, would yield more insights into age-related differences in the humoral response against this virus.

In comparison to our CV19 data our EBOV data paints an unusual picture where, even 2-3 months post-recovery with viral negative PCR tests, there are abnormally high proportions of class switched clones with little or no direction towards a particular sub-class. Given CSR is largely understudied, as far as we can tell such high rates of class switching, particularly so long after recovery, are entirely unique to this infection. Another unusual observation was that EBOV

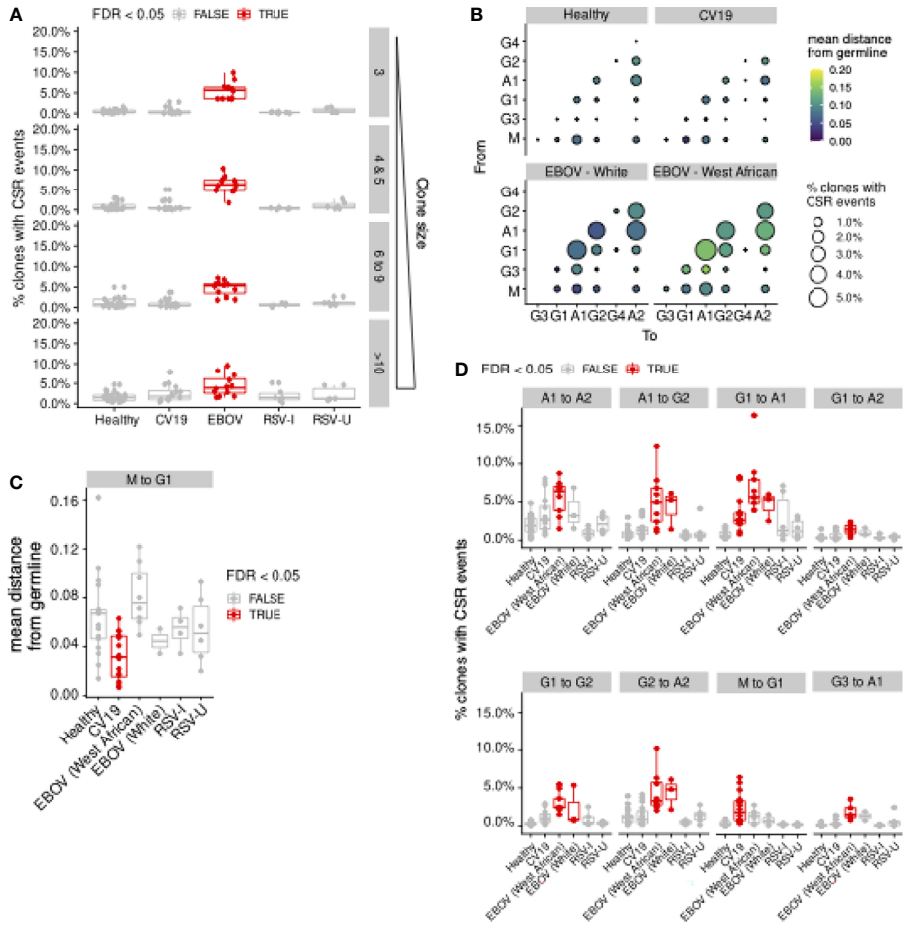

FIGURE 6 | Evidence of Class-switch recombination is increased in EBOV and in large CV19 expansions. Repertoires from each donor were sampled to uniform depth (12,000, approximately the median sequence counts over all donors across all sample types). **(A)** Lineage clones (see Figure 5) were assessed for prevalence of CSR events in terms of the proportion of clones and plotted by clone size and split by condition. **(B)** Bubble plot depicting the frequency and distance-from-germline of CSR events, separated by the CSR start ('From', vertical axis) and end ('To', horizontal axis) isotypes. Quantification was performed separately for different sample types. Bubble sizes are proportional to the frequency of CSR and colour is scaled by distance from germline at which CSR occurs, as estimated from the reconstructed lineage trees. **(C)** Statistical comparison of the median distance from germline at which CSR events occurred across sample types. Each donor was considered separately for every switch possibility. **(D)** Comparison of CSR frequency (percentage of clones with evidence of CSR) for each condition was also assessed for each donor (median, **D**). Statistical significance was evaluated using one-way ANOVA and Dunnett *post-hoc* comparison against Healthy with Benjamini-Hochberg-corrected false discovery rate (FDR) < 0.05 highlighted in red **(C, D)**. For **(D)**, **Supplementary Figure S9** contain analogous plots for all CSR combinations with significant (FDR < 0.05) differences compared against Healthy.

survivors' memory B cell populations were more diverse than healthy controls suggesting stimulation with more diverse antigens, or a less structured and directed immune response. A 'decay-stimulation-decay' pattern resulting in the peak of antibody response being some 200 days after infection has previously been reported (71) and cytokine storms during infection may also be contributing to this phenomenon (72, 73). It was not possible to collect blood samples from unrecovered patients, so we do not know if these observations were a requirement of patient recovery or a phenomenon unique to Ebola infection in general. In comparison to other sample types, our EBOV samples were only sequenced to modest depth (median number of sequences for EBOV = 5,346; CV19 = 38020.5; Healthy = 12,486.5). We note that the detection of CSR events within lineages is dependent upon sequencing depth (**Supplementary Note**); it is possible that the estimates of CSR frequencies for EBOV in **Figure 6** only represent the lower bound, further highlighting the importance of CSR in the response against EBOV.

By comparing examples of pandemic, epidemic and endemic viral disease responses our results show that while aspects of B cell responses are unique to particular infections, the human immunoglobulin gene repertoire can show similarities of response across two very different diseases. There are many questions to be answered about the balance of beneficial versus bystander responses in acute inflammatory diseases, where the initial class switched responses seem to be immature (COVID-19) and possibly unregulated (EBOV infection). Coupled with the finding of genes such as *IGHV4-39* appearing in two

completely different diseases, these data add weight to the hypothesis that an emergency humoral immune response to primary challenge can bypass normal stringent regulation and thus allow the production of autoimmune antibodies.

CODE AVAILABILITY

Functions implemented to generate and analyse lineage trees were included in a R package BrepPhylo, which is available at https://github.com/Fraternalilab/BrepPhylo. All other code snippets used in analysing data presented in this work are available as R markdown files available at https://github.com/Fraternalilab/BrepPhyloAnalysis.

DATA AVAILABILITY STATEMENT

IMGT/High-VQuest-annotated immunoglobulin sequence data file is available at Zenodo (https://dx.doi.org/10.5281/zenodo.5146019).

ETHICS STATEMENT

The studies involving human participants were reviewed and approved by UK London REC 14/LO/1221 for COVID-19 samples, UK London REC 11/LO/1826 for RSV samples, and Sierra Leone Ethics and Scientific Review Committee ISRCTN13990511 and PACTR201602001355272 and authorised by Pharmacy Board of Sierra Leone, #PBSL/CTAN/MOHS-CST001 for Ebola samples. The patients/participants provided their written informed consent to participate in this study.

AUTHOR CONTRIBUTIONS

DD-W, AS, JSO'H, and MB designed study and protocols to collected and analyse COVID-19 and YFV samples under REC 14/LO/1221. AS, MB, NK, ES, KL, CF, CCo, HL and FO acquired and biobanked COVID-19 samples. CCh and PO provided RSV samples. MS, JS, and JB provided Ebola samples. ES, AS, IS, JSO'H, AP, and BW devised repertoire protocol and performed repertoire data generation. JN, AS, ES, DK, CM, DD-W, and FF performed bioinformatic analysis and data interpretation. All authors contributed to the article and approved the submitted version.

FUNDING

This work was funded by the MRC (MR/L01257X/1 and MC_PC_15068), BBSRC (BB/T002212/1 and BB/V011456/1), EPSRC (EP/R031118/1) and UK National Core Studies (NCSi4P programme) funding. The study "Convalescent plasma for early Ebola virus disease in Sierra Leone" (ISRCTN13990511 and PACTR201602001355272) was supported by the Wellcome Trust (Award 106491) and Bill and Melinda Gates Foundation; Public Health England Ebola Emergency Response; and the Blood Safety Programme, National Health Service Blood and Transplant. MGS was supported by the UK National Institute for Health Research Health Protection Research Unit in Emerging and Zoonotic Infections. J.T.S. is supported by the Wellcome Trust (204820/Z/16/Z). M.G.S. is supported by the UK National Institute for Health Research Health Protection Research Unit in Emerging and Zoonotic Infections. JTS and MGS were awarded a grant from the Enhancing Research Activity in Epidemic Situations (ERAES) program funded by the Wellcome Trust to support further research into the sequelae of Ebola virus disease. We acknowledge the support of the Medical Research Council (G0902266), the Wellcome Trust (087805/Z/08/Z), and Medical Research Council (MRC) EMINENT Network (MR/R502121/1) which is co-funded by GSK. PO is supported by a Senior Investigator award from the National Institute for Health Research (NIHR201385) and RSV Consortium in Europe (RESCEU) Horizon 2020 Framework Grant 116019. PO and CC are supported by the Biomedical Research Centre award to Imperial College Healthcare NHS Trust, Imperial's Health Protection Research Unit in Respiratory Infections (NIHR HPRU RI), the Comprehensive Local Research Networks (CLRNs), and the MRC HIC-Vac network (MR/R005982/1). Infrastructure support was provided by the NIHR Imperial Biomedical Research Centre and the NIHR Imperial Clinical Research Facility. The funders had no role in the collection and analysis of the samples, in the interpretation of data, in writing the report, nor in the decision to submit the paper for publication.

ACKNOWLEDGMENTS

We acknowledge the contribution of the Sierra Leone Association of Ebola Survivors and Ebola CP Consortium Investigators. Ebola samples were kindly donated by Prof Alain Townsend (Oxford). Thanks also to the Surrey COVID-19 Collaboration and all volunteers for sample collection and to Gill Wallace and Vasiliki Tsioligka for technical support.

SUPPLEMENTARY MATERIAL

The Supplementary Material for this article can be found online at: https://www.frontiersin.org/articles/10.3389/fimmu.2022.807104/full#supplementary-material

REFERENCES

1. Seow J, Graham C, Merrick B, Acors S, Steel K, Hemmings O, et al. Longitudinal Evaluation and Decline of Antibody Responses in SARS-CoV-2 Infection. *Nat Microbiol* (2020) 5:2020.07.09.20148429. doi: 10.1101/2020.07.09.20148429
2. Siggins MK, Thwaites RS, Openshaw PJM. Durability of Immunity to SARS-CoV-2 and Other Respiratory Viruses. *Trends Microbiol* (2021) 29:648–62. doi: 10.1016/J.TIM.2021.03.016
3. Gudbjartsson DF, Norddahl GL, Melsted P, Gunnarsdottir K, Holm H, Eythorsson E, et al. Humoral Immune Response to SARS-CoV-2 in Iceland. *N Eng J Med* (2020) 383:1724–34. doi: 10.1056/NEJMOA2026116

4. Chi X, Li Y, Qiu X. V(D)J Recombination, Somatic Hypermutation and Class Switch Recombination of Immunoglobulins: Mechanism and Regulation. *Immunology* (2020) 160:233–47. doi: 10.1111/imm.13176
5. Xu Z, Zan H, Pone EJ, Mai T, Casali P. Immunoglobulin Class-Switch DNA Recombination: Induction, Targeting and Beyond. *Nat Rev Immunol* (2012) 12:517–31. doi: 10.1038/nri3216
6. Stavnezer J, Guikema JEJ, Schrader CE. Mechanism and Regulation of Class Switch Recombination. *Annu Rev Immunol* (2008) 26:261–92. doi: 10.1146/annurev.immunol.26.021607.090248
7. Pham P, Bransteitter R, Petruska J, Goodman MF. Processive AID-Catalysed Cytosine Deamination on Single-Stranded DNA Simulates Somatic Hypermutation. *Nature* (2003) 424:103–7. doi: 10.1038/nature01760
8. Roco JA, Mesin L, Binder SC, Nefzger C, Gonzalez-Figueroa P, Canete PF, et al. Class-Switch Recombination Occurs Infrequently in Germinal Centers. *Immunity* (2019) 51:337–50.e7. doi: 10.1016/j.immuni.2019.07.001
9. Pape KA, Kouskoff V, Nemazee D, Tang HL, Cyster JG, Tze LE, et al. Visualization of the Genesis and Fate of Isotype-Switched B Cells During a Primary Immune Response. *J Exp Med* (2003) 197:1677–87. doi: 10.1084/jem.20012065
10. Toellner KM, Gulbranson-Judge A, Taylor DR, Sze DMY, MacLennan IC. Immunoglobulin Switch Transcript Production *In Vivo* Related to the Site and Time of Antigen-Specific B Cell Activation. *J Exp Med* (1996) 183:2303–12. doi: 10.1084/jem.183.5.2303
11. King HW, Orban N, Riches JC, Clear AJ, Warnes G, Teichmann SA, et al. Single-Cell Analysis of Human B Cell Maturation Predicts How Antibody Class Switching Shapes Selection Dynamics. *Sci Immunol* (2021) 6:eabe6291. doi: 10.1126/sciimmunol.abe6291
12. Dunn-Walters DK, Stewart AT, Sinclair EL, Serangeli I. Age-Related Changes in B Cells Relevant to Vaccine Responses. *Interdiscip Topics Gerontol Geriatr* (2020) 43:56–72. doi: 10.1159/000504479
13. Lord JM. The Effect of Aging of the Immune System on Vaccination Responses. *Hum Vaccines Immunother* (2013) 9:1364–7. doi: 10.4161/hv.24696
14. Ademokun A, Wu Y-C, Martin V, Mitra R, Sack U, Baxendale H, et al. Vaccination-Induced Changes in Human B-Cell Repertoire and Pneumococcal IgM and IgA Antibody at Different Ages. *Aging Cell* (2011) 10:922–30. doi: 10.1111/j.1474-9726.2011.00732.x
15. Colonna-Romano G, Bulati M, Aquino A, Pellicanò M, Vitello S, Lio D, et al. A Double-Negative (IgD-CD27-) B Cell Population Is Increased in the Peripheral Blood of Elderly People. *Mech Ageing Dev* (2009) 130:681–90. doi: 10.1016/j.mad.2009.08.003
16. Wu YC, Kipling D, Leong HS, Martin V, Ademokun AA, Dunn-Walters DK. High-Throughput Immunoglobulin Repertoire Analysis Distinguishes Between Human IgM Memory and Switched Memory B-Cell Populations. *Blood* (2010) 116:1070–8. doi: 10.1182/blood-2010-03-275859
17. Taylor JJ, Pape KA, Jenkins MK. A Germinal Center-Independent Pathway Generates Unswitched Memory B Cells Early in the Primary Response. *J Exp Med* (2012) 209:597–606. doi: 10.1084/jem.20111696
18. Allman D, Wilmore JR, Gaudette BT. The Continuing Story of T-Cell Independent Antibodies. *Immunol Rev* (2019) 288:128–35. doi: 10.1111/imr.12754
19. Bryan Wu YC, Kipling D, Dunn-Walters DK. Age-Related Changes in Human Peripheral Blood IGH Repertoire Following Vaccination. *Front Immunol* (2012) 3:193. doi: 10.3389/fimmu.2012.00193
20. Townsend CL, Laffy JMJ, Wu YCB, O'Hare JS, Martin V, Kipling D, et al. Significant Differences in Physicochemical Properties of Human Immunoglobulin Kappa and Lambda CDR3 Regions. *Front Immunol* (2016) 7:388. doi: 10.3389/fimmu.2016.00388
21. Dunn-Walters D, Townsend C, Sinclair E, Stewart A. Immunoglobulin Gene Analysis as a Tool for Investigating Human Immune Responses. *Immunol Rev* (2018) 284:132–47. doi: 10.1111/imr.12659
22. Perchiacca JM, Ladiwala ARA, Bhattacharya M, Tessier PM. Aggregation-Resistant Domain Antibodies Engineered With Charged Mutations Near the Edges of the Complementarity-Determining Regions. *Protein Engineering Design Selection* (2012) 25:591–601. doi: 10.1093/protein/gzs042
23. Laffy J, Dodev T, Macpherson J, Townsend C, Lu H, Dunn-Walters D, et al. Promiscuous Antibodies Characterised by Their Physico-Chemical Properties: From Sequence to Structure and Back. *Prog Biophys Mol Biol* (2017) 128:47–56. doi: 10.1016/J.PBIOMOLBIO.2016.09.002
24. Stadlbauer D, Amanat F, Chromikova V, Jiang K, Strohmeier S, Arunkumar GA, et al. SARS-CoV-2 Seroconversion in Humans: A Detailed Protocol for a Serological Assay, Antigen Production, and Test Setup. *Curr Protoc Microbiol* (2020) 57:e100. doi: 10.1002/cpmc.100
25. Tedder RS, Samuel D, Dicks S, Scott JT, Ijaz S, Smith CC, et al. Detection, Characterization, and Enrollment of Donors of Ebola Convalescent Plasma in Sierra Leone. *Transfusion* (2018) 58:1289–98. doi: 10.1111/TRF.14580
26. Knight SR, Ho A, Pius R, Buchan I, Carson G, Drake TM, et al. Risk Stratification of Patients Admitted to Hospital With Covid-19 Using the ISARIC WHO Clinical Characterisation Protocol: Development and Validation of the 4C Mortality Score. *BMJ* (2020) 370:m3339. doi: 10.1136/bmj.m3339
27. Habibi MS, Jozwik A, Makris S, Dunning J, Paras A, DeVincenzo JP, et al. Impaired Antibody-Mediated Protection and Defective Iga B-Cell Memory in Experimental Infection of Adults With Respiratory Syncytial Virus. *Am J Respir Crit Care Med* (2015) 191:1040–9. doi: 10.1164/rccm.201412-2256OC
28. Martin V, Wu YC, Kipling D, Dunn-Walters DK. Age-Related Aspects of Human IgM+ B Cell Heterogeneity. *Ann New York Acad Sci* (2015) 1362:153–63. doi: 10.1111/nyas.12823
29. Osorio D, Rondón-Villarreal P, Torres R. Peptides: A Package for Data Mining of Antimicrobial Peptides. *R J* (2015) 7:4–14. doi: 10.32614/RJ-2015-001
30. Bashford-Rogers R, Bergamaschi L, McKinney E, Pombal D, Mescia F, Lee J, et al. B Cell Receptor Repertoire Analysis in Six Immune-Mediated Diseases. *Nature* (2019) 574:122. doi: 10.1038/S41586-019-1595-3
31. Stephenson E, Reynolds G, Botting RA, Calero-Nieto FJ, Morgan MD, Tuong ZK, et al. Single-Cell Multi-Omics Analysis of the Immune Response in COVID-19. *Nat Med* (2021) 27:904–16. doi: 10.1038/s41591-021-01329-2
32. Bashford-Rogers RJM, Palser AL, Huntly BJ, Rance R, Vassiliou GS, Follows GA, et al. Network Properties Derived From Deep Sequencing of Human B-Cell Receptor Repertoires Delineate B-Cell Populations. *Genome Res* (2013) 23:1874. doi: 10.1101/GR.154815.113
33. Felsenstein J. PHYLIP - Phylogeny Inference Package (Version 3.2). *Cladistics* (1989) 5:164–6.
34. Stern JNH, Yaari G, Vander HJA, Church G, Donahue WF, Hintzen RQ, et al. B Cells Populating the Multiple Sclerosis Brain Mature in the Draining Cervical Lymph Nodes. *Sci Trans Med* (2014) 6:248ra107–248ra107. doi: 10.1126/SCITRANSLMED.3008879
35. Unterman A, Sumida TS, Nouri N, Yan X, Zhao AY, Gasque V, et al. Single-Cell Multi-Omics Reveals Dyssynchrony of the Innate and Adaptive Immune System in Progressive COVID-19. *Nat Commun* (2022) 13:1–23. doi: 10.1038/s41467-021-27716-4
36. Feldman J, Bals J, Altomare CG, Denis KS, Lam EC, Hauser BM, et al. Naive Human B Cells Engage the Receptor Binding Domain of SARS-CoV-2, Variants of Concern, and Related Sarbecoviruses. *Sci Immunol* (2021) 6:5842. doi: 10.1126/SCIIMMUNOL.ABL5842/SUPPL_FILE/SCIIMMUNOL.ABL5842_DATA_FILE_S1.ZIP
37. Dunbar J, Krawczyk K, Leem J, Baker T, Fuchs A, Georges G, et al. SAbDab: The Structural Antibody Database. *Nucleic Acids Res* (2014) 42:D1140–6. doi: 10.1093/NAR/GKT1043
38. Zost SJ, Gilchuk P, Chen RE, Case JB, Reidy JX, Trivette A, et al. Rapid Isolation and Profiling of a Diverse Panel of Human Monoclonal Antibodies Targeting the SARS-CoV-2 Spike Protein. *Nat Med* (2020) 26:1422–7. doi: 10.1038/s41591-020-0998-x
39. Robbiani DF, Gaebler C, Muecksch F, Lorenzi JCC, Wang Z, Cho A, et al. Convergent Antibody Responses to SARS-CoV-2 in Convalescent Individuals. *Nature* (2020) 584:437–42. doi: 10.1038/s41586-020-2456-9
40. Kreer C, Zehner M, Weber T, Ercanoglu MS, Gieselmann L, Rohde C, et al. Longitudinal Isolation of Potent Near-Germline SARS-CoV-2-Neutralizing Antibodies From COVID-19 Patients. *Cell* (2020) 182:843–854.e12. doi: 10.1016/j.cell.2020.06.044
41. Gaebler C, Wang Z, Lorenzi JCC, Muecksch F, Finkin S, Tokuyama M, et al. Evolution of Antibody Immunity to SARS-CoV-2. *Nature* (2021) 591:639–44. doi: 10.1038/s41586-021-03207-w
42. Dugan HL, Stamper CT, Li L, Changrob S, Asby NW, Halfmann PJ, et al. Profiling B Cell Immunodominance After SARS-CoV-2 Infection Reveals Antibody Evolution to Non-Neutralizing Viral Targets. *Immunity* (2021) 54:1290–303.e7. doi: 10.1016/j.immuni.2021.05.001

43. Brouwer PJM, Caniels TG, van der Straten K, Snitselaar JL, Aldon Y, Bangaru S, et al. Potent Neutralizing Antibodies From COVID-19 Patients Define Multiple Targets of Vulnerability. *Science* (2020) 369:643–50. doi: 10.1126/science.abc5902
44. Zhang Y, Skolnick J. Scoring Function for Automated Assessment of Protein Structure Template Quality. *Proteins: Struct Function Bioinf* (2004) 57:702–10. doi: 10.1002/PROT.20264
45. Cortjens B, Yasuda E, Yu X, Wagner K, Claassen Y, Bakker A, et al. Broadly Reactive Anti-Respiratory Syncytial Virus G Antibodies From Exposed Individuals Effectively Inhibit Infection of Primary Airway Epithelial Cells. *J Virol* (2017) 91:e02357-16. doi: 10.1128/JVI.02357-16
46. Goodwin E, Gilman M, Wrapp D, Chen M, Ngwuta J, Moin S, et al. Infants Infected With Respiratory Syncytial Virus Generate Potent Neutralizing Antibodies That Lack Somatic Hypermutation. *Immunity* (2018) 48:339–49.e5. doi: 10.1016/J.IMMUNI.2018.01.005
47. Gilman MSA, Castellanos CA, Chen M, Ngwuta JO, Goodwin E, Moin SM, et al. Rapid Profiling of RSV Antibody Repertoires From the Memory B Cells of Naturally Infected Adult Donors. *Sci Immunol* (2016) 1:eaaj1879. doi: 10.1126/SCIIMMUNOL.AAJ1879
48. Davis C, Jackson K, McElroy A, Halfmann P, Huang J, Chennareddy C, et al. Longitudinal Analysis of the Human B Cell Response to Ebola Virus Infection. *Cell* (2019) 177:1566–82.e17. doi: 10.1016/J.CELL.2019.04.036
49. Margreitter C, Lu H-C, Townsend C, Stewart A, Dunn-Walters DK, Fraternali F. BRepertoire: A User-Friendly Web Server for Analysing Antibody Repertoire Data. *Nucleic Acids Res* (2018) 46:W264–70. doi: 10.1093/NAR/GKY276
50. Vidarsson G, Dekkers G, Rispens T. IgG Subclasses and Allotypes: From Structure to Effector Functions. *Front Immunol* (2014) 5:520. doi: 10.3389/fimmu.2014.00520
51. Smith SA, Burton SL, Kilembe W, Lakhi S, Karita E, Price M, et al. VH1-69 Utilizing Antibodies Are Capable of Mediating Non-Neutralizing Fc-Mediated Effector Functions Against the Transmitted/Founder Gp120. *Front Immunol* (2019) 0:3163. doi: 10.3389/FIMMU.2018.03163
52. Avnir Y, Watson C, Glanville J, Peterson E, Tallarico A, Bennett A, et al. IGHV1-69 Polymorphism Modulates Anti-Influenza Antibody Repertoires, Correlates With IGHV Utilization Shifts and Varies by Ethnicity. *Sci Rep* (2016) 6:1-13. doi: 10.1038/SREP20842
53. Nielsen SCA, Yang F, Jackson KJL, Hoh RA, Röltgen K, Jean GH, et al. Human B Cell Clonal Expansion and Convergent Antibody Responses to SARS-CoV-2. *Cell Host Microbe* (2020) 28:516–25.e5. doi: 10.1016/J.CHOM.2020.09.002
54. Richter AG, Shields AM, Karim A, Birch D, Faustini SE, Steadman L, et al. Establishing the Prevalence of Common Tissue-Specific Autoantibodies Following Severe Acute Respiratory Syndrome Coronavirus 2 Infection. *Clin Exp Immunol* (2021) 205:99–105. doi: 10.1111/CEI.13623
55. Bastard P, Rosen LB, Zhang Q, Michailidis E, Hoffmann H-H, Zhang Y, et al. Autoantibodies Against Type I IFNs in Patients With Life-Threatening COVID-19. *Science* (2020) 370:eabd4585. doi: 10.1126/SCIENCE.ABD4585
56. Rossi D, Spina V, Bomben R, Rasi S, Dal-Bo M, Bruscaggin A, et al. Association Between Molecular Lesions and Specific B-Cell Receptor Subsets in Chronic Lymphocytic Leukemia. *Blood* (2013) 121:4902–5. doi: 10.1182/blood-2013-02-486209
57. Yamayoshi S, Yasuhara A, Ito M, Uraki R, Kawaoka Y. Differences in the Ease With Which Mutant Viruses Escape From Human Monoclonal Antibodies Against the HA Stem of Influenza A Virus. *J Clin Virol* (2018) 108:105–11. doi: 10.1016/j.jcv.2018.09.016
58. Morris Abdool Karim L, Moore PL, Travers SA, Garrett N, Abdool Karim Q, Dshanta Naicker SS, et al. Germline Ig Gene Repertoire HIV-1 Antibodies Is Not Restricted by the Ability To Develop Broadly Neutralizing. *J Immunol* (2021) 194:4371–8. doi: 10.4049/jimmunol.1500118
59. Yeung YA, Foletti D, Deng X, Abdiche Y, Strop P, Glanville J, et al. Germline-Encoded Neutralization of a Staphylococcus Aureus Virulence Factor by the Human Antibody Repertoire. *Nat Commun* (2016) 7:1–14. doi: 10.1038/ncomms13376
60. Muramatsu M, Kinoshita K, Fagarasan S, Yamada S, Shinkai Y, Honjo T. Class Switch Recombination and Hypermutation Require Activation-Induced Cytidine Deaminase (AID), a Potential RNA Editing Enzyme. *Cell* (2000) 102:553–63. doi: 10.1016/S0092-8674(00)00078-7
61. Muramatsu M, Sankaranand VS, Anant S, Sugai M, Kinoshita K, Davidson NO, et al. Specific Expression of Activation-Induced Cytidine Deaminase (AID), a Novel Member of the RNA-Editing Deaminase Family in Germinal Center B Cells. *J Biol Chem* (1999) 274:18470–6. doi: 10.1074/jbc.274.26.18470
62. Pone EJ, Zhang J, Mai T, White CA, Li G, Sakakura JK, et al. BCR-Signalling Synergizes With TLR-Signalling for Induction of AID and Immunoglobulin Class-Switching Through the Non-Canonical NF-κb Pathway. *Nat Commun* (2012) 3:1–12. doi: 10.1038/ncomms1769
63. Woodruff MC, Ramonell RP, Nguyen DC, Cashman KS, Saini AS, Haddad NS, et al. Extrafollicular B Cell Responses Correlate With Neutralizing Antibodies and Morbidity in COVID-19. *Nat Immunol* (2020) 21:1506–16. doi: 10.1038/s41590-020-00814-z
64. Ferrante A, Beard LJ, Feldman RG. IgG Subclass Distribution of Antibodies to Bacterial and Viral Antigens. *Pediatr Infect Dis J* (1990) 9:S16–24. doi: 10.1097/00006454-199008001-00004
65. Higgins RL, Rawlings SA, Case J, Lee FY, Chan CW, Barrick B, et al. Longitudinal SARS-CoV-2 Antibody Study Using the Easy Check COVID-19 IgM/IgG^{TM} Lateral Flow Assay. *PloS One* (2021) 16:e0247797. doi: 10.1371/journal.pone.0247797
66. Wu JL, Tseng WP, Lin CH, Lee TF, Chung MY, Huang CH, et al. Four Point-of-Care Lateral Flow Immunoassays for Diagnosis of COVID-19 and for Assessing Dynamics of Antibody Responses to SARS-CoV-2. *J Infect* (2020) 81:435–42. doi: 10.1016/j.jinf.2020.06.023
67. Flower B, Brown JC, Simmons B, Moshe M, Frise R, Penn R, et al. Clinical and Laboratory Evaluation of SARS-CoV-2 Lateral Flow Assays for Use in a National COVID-19 Seroprevalence Survey. *Thorax* (2020) 75:1082–8. doi: 10.1136/thoraxjnl-2020-215732
68. Whitman JD, Hiatt J, Mowery CT, Shy BR, Yu R, Yamamoto TN, et al. Evaluation of SARS-CoV-2 Serology Assays Reveals a Range of Test Performance. *Nat Biotechnol* (2020) 38:1174–83. doi: 10.1038/s41587-020-0659-0
69. Jääskeläinen AJ, Kuivanen S, Kekäläinen E, Ahava MJ, Loginov R, Kallio-Kokko H, et al. Performance of Six SARS-CoV-2 Immunoassays in Comparison With Microneutralisation. *J Clin Virol* (2020) 129:104512. doi: 10.1016/j.jcv.2020.104512
70. Dunn-Walters DK. The Ageing Human B Cell Repertoire: A Failure of Selection? *Clin Exp Immunol* (2016) 183:50–6. doi: 10.1111/CEI.12700
71. Adaken C, Scott JT, Sharma R, Gopal R, Dicks S, Niazi S, et al. Ebola Virus Antibody Decay–Stimulation in a High Proportion of Survivors. *Nature* (2021) 590:468–72. doi: 10.1038/s41586-020-03146-y
72. Zampieri CA, Sullivan NJ, Nabel GJ. Immunopathology of Highly Virulent Pathogens: Insights From Ebola Virus. *Nat Immunol* (2007) 8:1159–64. doi: 10.1038/ni1519
73. Kennedy JR. Phosphatidylserine's Role in Ebola's Inflammatory Cytokine Storm and Hemorrhagic Consumptive Coagulopathy and the Therapeutic Potential of Annexin V. *Med Hypotheses* (2020) 135:109462. doi: 10.1016/j.mehy.2019.109462

Conflict of Interest: The authors declare that the research was conducted in the absence of any commercial or financial relationships that could be construed as a potential conflict of interest.

frontiers | Frontiers in Immunology

ORIGINAL RESEARCH
published: 09 May 2022
doi: 10.3389/fimmu.2022.876306

Rapid Hypermutation B Cell Trajectory Recruits Previously Primed B Cells Upon Third SARS-Cov-2 mRNA Vaccination

*Lisa Paschold[1], Bianca Klee[2], Cornelia Gottschick[2], Edith Willscher[1], Sophie Diexer[2], Christoph Schultheiß[1], Donjete Simnica[1], Daniel Sedding[3], Matthias Girndt[4], Michael Gekle[5], Rafael Mikolajczyk[2] and Mascha Binder[1]**

[1] Department of Internal Medicine IV, Oncology/Hematology, Martin-Luther-University Halle-Wittenberg, Halle (Saale), Germany, [2] Institute for Medical Epidemiology, Biometrics and Informatics (IMEBI), Interdisciplinary Center for Health Sciences, Medical School of the Martin-Luther University Halle-Wittenberg, Halle (Saale), Germany, [3] Mid-German Heart Center, Department of Cardiology and Intensive Care Medicine, University Hospital, Martin-Luther-University Halle-Wittenberg, Halle (Saale), Germany, [4] Department of Internal Medicine II, Martin-Luther-University Halle-Wittenberg, Halle (Saale), Germany, [5] Julius Bernstein-Institute of Physiology, Faculty of Medicine, Martin-Luther-University Halle-Wittenberg, Halle (Saale), Germany

OPEN ACCESS

Edited by:
Marko Radic,
University of Tennessee College of Medicine, United States

Reviewed by:
Mats Bemark,
University of Gothenburg, Sweden
Matthew H. Collins,
Emory University, United States

***Correspondence:**
Mascha Binder
Mascha.Binder@uk-halle.de

Specialty section:
This article was submitted to B Cell Biology, a section of the journal Frontiers in Immunology

Received: 15 February 2022
Accepted: 14 April 2022
Published: 09 May 2022

Citation:
Paschold L, Klee B, Gottschick C, Willscher E, Diexer S, Schultheiß C, Simnica D, Sedding D, Girndt M, Gekle M, Mikolajczyk R and Binder M (2022) Rapid Hypermutation B Cell Trajectory Recruits Previously Primed B Cells Upon Third SARS-Cov-2 mRNA Vaccination. Front. Immunol. 13:876306. doi: 10.3389/fimmu.2022.876306

The COVID-19 pandemic shows that vaccination strategies building on an ancestral viral strain need to be optimized for the control of potentially emerging viral variants. Therefore, aiming at strong B cell somatic hypermutation to increase antibody affinity to the ancestral strain - not only at high antibody titers - is a priority when utilizing vaccines that are not targeted at individual variants since high affinity may offer some flexibility to compensate for strain-individual mutations. Here, we developed a next-generation sequencing based SARS-CoV-2 B cell tracking protocol to rapidly determine the level of immunoglobulin somatic hypermutation at distinct points during the immunization period. The percentage of somatically hypermutated B cells in the SARS-CoV-2 specific repertoire was low after the primary vaccination series, evolved further over months and increased steeply after boosting. The third vaccination mobilized not only naïve, but also antigen-experienced B cell clones into further rapid somatic hypermutation trajectories indicating increased affinity. Together, the strongly mutated post-booster repertoires and antibodies deriving from this may explain why the third, but not the primary vaccination series, offers some protection against immune-escape variants such as Omicron B.1.1.529.

Keywords: SARS-CoV-2, COVID-19, delta, B cell maturation, omicron variant, booster vaccination

INTRODUCTION

Until February 2022, the World Health Organization (WHO) counted 400 million severe acute coronavirus disease 2019 (COVID-19) infections caused by respiratory syndrome coronavirus 2 (SARS-CoV-2). By then, the number of deaths had totaled almost 6 million individuals globally. While mRNA-based and adenovirus-vectored vaccines have been developed at unprecedented

speed, global vaccination strategies remain challenging and new SARS-CoV-2 variants with varying potential to evade adaptive immunity and/or to enhance transmissibility constantly emerge. Since memory B cell populations play a decisive role in severity reduction of COVID-19 and early antibody-mediated virus neutralization may even prevent infections, understanding infection- and vaccine-induced SARS-CoV-2 specific B cell immunity is critical (1–3).

As recently reviewed by Laidlaw et al. (4), COVID-19 generates both germinal center and extrafollicular B cell responses in unvaccinated individuals – depending on the severity of infection - that converge on B cells expressing antigen receptors with preferential immunoglobulin heavy chain variable-joining gene (IGHV-J) usage (1, 5–12). Interestingly, even B cells with low or absent IGHV affinity maturation can generate antibodies that specifically recognize and neutralize the ancestral strain of SARS-CoV-2 (6, 11, 13–15). Yet, a continued evolution of the humoral response appears to take place over at least six months after infection – even without re-infection – as demonstrated by sustained acquisition of IGHV somatic hypermutation despite waning antibody titers (16–21). There is emerging evidence that these rather prolonged B cell maturation dynamics may also be characteristic for vaccine-induced anti-SARS-CoV-2 immune responses (22, 23).

With the advent of SARS-CoV-2 variants of concern, affinity to the ancestral strain's S protein (currently used in all licensed vaccines) does not necessarily predict antibody neutralization potency. Immune escape can affect clones with high affinity against the ancestral strain but, depending on the targeted epitope, some clones also retain their neutralizing potency against variants of concern (24). This is in clear contrast to clones that have been induced by the ancestral strain and show only low affinity to this strain. Such clones constantly fail to neutralize variants (24). This finding suggests that high affinity binding to the ancestral strain may provide some flexibility in compensating the effect of individual immune escape mutations (24). Therefore, in times of emerging viral variants an optimal vaccination strategy should aim at inducing the highest possible level of affinity maturation through somatic hypermutation, even if the available vaccines are targeted at the ancestral strain.

In the study presented here, we used two cohorts of not previously infected patients to compare antibody levels and somatic hypermutation trajectories across a primary series of two standard vaccinations with those induced by a third "booster" vaccination using immune repertoire sequencing. We show that B lineage evolution is low after the priming vaccinations. In contrast, the maturation trajectories induced by the third vaccination is compatible with selective mobilization and germinal center recruitment of naïve but also previously matured memory B cell lineages to undergo fast and extensive somatic hypermutation. This considerable affinity maturation and the resulting high antibody titers may explain the increased protection of the third "booster" vaccination against variants such as the Omicron variant B.1.1.529.

METHODS

Non-Interventional Study Design and Biobanking of NIS635

This study was registered as non-interventional study (NIS) at the Paul-Ehrlich-Institute (NIS635). It consisted of data and biological samples collected in the DigiHero and HACO cohorts.

DigiHero is a population-based cohort study for digital health research in Germany conducted in the city of Halle (Saale) which registered 8,077 participants until November 2021. The recruitment was conducted in different waves and included mailed invitation to all 129,733 households in Halle as well as promotion *via* media. The study was approved by the institutional review board (approval number 2020-076). Its digital design allowed targeted invitation of participants to modules that included different surveys and blood biobanking subprojects. The COVID-19 module of DigiHero recruited participants with prior positive SARS-CoV-2 testing in their households. Until December 2021, 514 individuals had completed the survey on their COVID-19 history as well as on their vaccination status and had donated blood for this module at this data cut. These samples were used for antibody analyzes. The SARS-CoV-2 booster vaccination module of DigiHero recruited participants willing to respond to a survey on the third SARS-CoV-2 booster vaccination. Until December 2021, 4,670 participants had completed the survey. Fifteen randomly chosen participants without prior COVID-19 infection donated blood prior to and on day 14 (d14) after booster vaccination at this data cut. These samples were used for antibody and B cell repertoire next-generation sequencing analyzes.

As a reference within NIS635, 40 samples from 20 uninfected control cases completing their primary vaccination series with the BioNTech/Pfizer vaccine were recovered from the biobank of the Halle COVID-19 cohort (HACO). These 20 control cases had donated blood prior to and at d28 of their primary vaccination series (d7 after the second vaccination). Informed written consent was obtained and the study was approved by the institutional review board (approval number 2020-039). These samples were used for antibody and B cell repertoire next-generation sequencing analyzes.

Table 1 summarizes all relevant participant numbers, their basic characteristics and biological samples used in NIS635. The study was conducted in accordance with the ethical principles stated by the Declaration of Helsinki. Informed written consent was obtained from all participants or legal representatives.

Sample Collection

The collected plasma samples were isolated by centrifugation of whole blood for 15 min at 2,000xg, followed by centrifugation at 12,000xg for 10 min and stored at - 80°C. Peripheral mononuclear cells (PBMC) were isolated by standard Ficoll gradient centrifugation. Genomic DNA was extracted from PBMCs using the GenElute Mammalian Genomic DNA Miniprep Kit (Sigma-Aldrich, St. Louis, USA).

TABLE 1 | Characteristics of participants in the DigiHero COVID-19 and SARS-CoV-2 booster vaccination modules and the HACO subcohort used for NIS635.

	DigiHero COVID-19 module	DigiHero SARS-CoV-2 booster vaccination module	Control cases from HACO cohort
Nb of participants	514	4670	20
Sex			
Female	307 (59.7%)	2825 (60.5%)	12 (60%)
Male	207 (40.3%)	1721 (36.9%)	8 (40%)
Other	0 (0%)	7 (0.15%)	0 (0%)
NA	0 (0%)	117 (2.5%)	0 (0%)
Age (years)			
Median age	47	50	40
Range	14-86	18-87	29-58
Prior confirmed COVID-19 infection			
Yes	436 (84.8%)	428 (9.2%)	0 (0%)
No	78 (15.2%)	4242 (90.8%)	20/20 (100%)
Prior SARS-COV-2 vaccination			
Yes	417 (81.1%)	4670 (100%)	0 (0%)
No	97 (18.9%)	0 (0%)	20/20 (100%)
Prior SARS-COV-2 booster vaccination			
Yes	0 (0%)	893 (19.1%)	
No	514 (100%)	3768 (80.7%)	
NA	0 (0%)	9 (0.2%)	
Biobanking			
Prior COVID-19	Total 436		
No SARS-CoV-2 vaccination	85		
SARS-CoV-2 vaccination	351		
No prior COVID-19	Total 78		
No SARS-CoV-2 vaccination	10		20 (d0 and d28)
1st SARS-CoV-2 vaccination	8		
2nd SARS-CoV-2 vaccination	60	15 (d0 and d14)	20 (d0 and d28)
3rd SARS-CoV-2 booster vaccination		15 (d0 and d14)	
Sequenced			
No prior COVID-19			
No SARS-CoV-2 vaccination			20 (pre-vacc1+2)
1st SARS-CoV-2 vaccination			
2nd SARS-CoV-2 vaccination		15 (pre-vacc3)	20 (post-vacc1+2)
3rd SARS-CoV-2 vaccination ("booster")		15 (post-vacc3)	

SARS-CoV-2 Antibody Profiling

Antibodies against the S1 domain of the spike (S) protein and the nucleocapsid protein (NCP) of SARS-CoV-2 were determined by Anti-SARS-CoV-2-ELISA IgA/IgG and Anti-SARS-CoV-2-NCP-ELISA kits from Euroimmun (Lübeck, Germany). Readouts were performed at 450 nm using a Tecan Spectrophotometer SpectraFluor Plus (Tecan Group Ltd., Männedorf, Switzerland).

Next-Generation Sequencing of B Cell Immune Repertoires

Immunosequencing of B cell repertoires was performed as described in (25). In brief, V(D)J rearranged IGH loci were amplified from 500 ng of genomic DNA using a multiplex PCR, pooled at 4 nM and quality-assessed on a 2100 Bioanalyzer (Agilent Technologies). Sequencing was performed on an Illumina MiSeq (paired-end, 2 x 301-cycles, v3 chemistry). Rearranged IGH loci were annotated using MiXCR v3.0.13 (26) and the IMGT 202011-3.sv6 IGH library as reference. Non-productive reads and sequences with less than 2 counts were discarded. All repertoires were normalized to 30,000 reads. Each unique complementarity-determining region 3 (CDR3) nucleotide sequence was considered a clone. Broad repertoire metrics (clonality, diversity, richness) were analyzed as previously described (27). IGHV genes were regarded as somatically hypermutated if they showed < 98% identity to the germline sequence and B cell clones with hypermutated IGHV gene were considered antigen-experienced.

B Cell Clonotype Search Algorithm

We searched our IGH repertoires for validated SARS-CoV-2 antibody rearrangements with identical or highly similar CDR3 amino acid sequence (Levenshtein distance of ≤ 2) and identical IGHV-J gene usage as described in (13). The validated SARS-CoV-2 antibody sequences were derived from CoV-AbDab accessed at 17th December 2021 (28) and classified into 3,195 total SARS-CoV-2 binding sequences and 1,147 SARS-CoV-2 neutralizing sequences. A list of the target sequences is provided in **Supplementary Table 1**.

B Cell Network Analysis

To calculate network connectivity in BCR repertoires, we used the Levenshtein distance of all unique CDR3 amino acid (aa) sequences per repertoire using the imnet tool (https://github.

com/rokroskar/imnet). Sequences with Levenshtein distance ≤ 3 were connected. For visualization as petri dish plots we used R package igraph and the fruchterman-reingold layout (29). Each dot represents a different unique CDR3aa sequence, which is termed a 'clone'. The number of identical CDR3aa sequences (= frequency of the clone in the repertoire) is not reflected in this kind of graphical presentation. CDR3aa sequences with a Levenshtein distance of ≤ 3 are connected. Data analysis and plotting was performed using R version (v4.1.2).

Identification of B Cell Lineages

We identified overlapping B cell lineages in the pre- and post-vaccination time point per patient. A B cell lineage was defined as a group of B cell clonotypes that share a common V and J gene and a CDR3 sequence differing only in up to 10% of its amino acid positions (30). Lineages and their evolution were visualised as stream plots with function plot.stacked from (https://www.r-bloggers.com/2013/12/data-mountains-and-streams-stacked-area-plots-in-r/). Data analysis and plotting was performed using R version (v4.1.2).

Statistics

Differences between the four groups were analyzed by ordinary one-way ANOVA and post-ANOVA analyses between individual columns were performed using Tukey's multiple comparisons test. Differences between two groups were studied by unpaired, two-tailed student's t-test or in the case of paired samples by paired, two-tailed student's t-test. All statistical analyses were performed using R version 4.1.2 and GraphPad Prism 8.3.1 (GraphPad Software, La Jolla, CA, USA).

Study Approval

This study was registered as non-interventional study (NIS) at the Paul-Ehrlich-Institute (NIS635). DigiHero and HACO were approved by the institutional review board (approval numbers 2020-076 and 2020-039). Written informed consent was received prior to participation.

RESULTS

Surveys, Data Collection and Biobanking in NIS635

For NIS635, we used a classical biobanking study (HACO) and a digital cohort study (DigiHero) with flexible recruitment of participants into different survey modules to obtain COVID-19 and vaccination data in a large cohort and to acquire relevant biological samples from subgroups of interest. In DigiHero, 514 participants donated blood and completed the survey of the COVID-19 module until December 2021. 4,670 participants completed the survey on the third SARS-CoV-2 "booster" vaccination until the same data cut. In HACO, data and sample collection had been completed in January 2021. Using this data, complete COVID-19 and vaccination histories could be deduced for all participants of NIS635. Details for all subcohorts are given in **Table 1**.

In the DigiHero SARS-CoV-2 „booster" vaccination survey, the majority of participants indicated to have already received their third vaccination or to be planning to receive it shortly (**Figure 1A**). The time between completion of the primary vaccination series and the third booster vaccination is shown

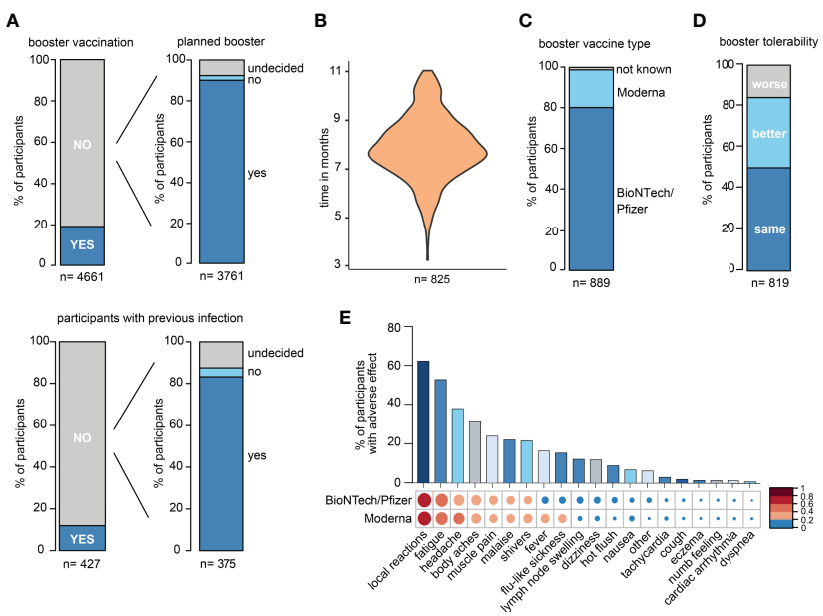

FIGURE 1 | Survey data from the DigiHero SARS-CoV-2 booster vaccination module. **(A)** Statistics of participants with prior or planned third SARS-CoV-2 vaccination (booster). **(B)** Time between completion of the primary vaccination series and third vaccination in months. **(C)** SARS-CoV-2 third vaccination type. **(D)** Tolerability of the third vaccination compared to previous SARS-CoV-2 vaccinations. **(E)** Adverse events upon third vaccination.

in **Figure 1B**. The majority of participants received BioNTech/Pfizer as their third vaccine (**Figure 1C**). The tolerability of the "booster" was roughly comparable to that of first and second SARS-CoV-2 vaccinations (**Figure 1D**). Most frequent side effects were local reactions, fatigue, and headache with comparable tolerability of both mRNA vaccines (**Figure 1E**).

Based on this survey, 15 participants without prior COVID-19 infection that planned a third vaccination within the next four weeks were randomly chosen and invited to donate blood before and after their third vaccination for antibody and B cell repertoire NGS analyzes.

SARS-CoV-2 Antibodies After Infection, Priming Vaccinations, Third Vaccination and Hybrid Immunity

All biobanked samples indicated in **Table 1** were tested for S1 and NCP antibodies by ELISA. **Figure 2A** shows the distribution of antibody levels for the different subgroups. Participants vaccinated after infection (hybrid immunity) and participants after their third "booster" vaccination achieved the highest S1 antibody levels followed by previously uninfected participants that had only completed their primary vaccination series (**Figure 2A**). Only few individuals showed elevated NCP antibody levels despite having indicated no prior COVID-19 potentially pointing at unrecognized previous infection. All other participants showed antibody levels compatible with their infection/vaccination status. In all participants with matched pre- and post-vaccination samples, clear increases in S1 antibodies were noted with highest levels after the third vaccination, while NCP antibodies remained negative (**Figure 2B**).

Next, we compared antibody levels in participants with hybrid immunity to those after three vaccinations. Given the over-time decay in antibody titers both after infection and vaccination (16, 17, 20, 31–34), we included only participants in this analysis who donated blood in a standard interval of 2-4 weeks after the last vaccination dose. This analysis showed that antibody levels were similarly high in both subsets indicating that the third "booster" dose may mimic the hybrid-like response observed in individuals after infection and vaccination (**Figure 2C**).

Global B Cell Immune Metrics After Priming and Third Vaccinations

Matched blood samples of two cohorts were subjected to next-generation sequencing of the B cell receptor repertoire. Cohort

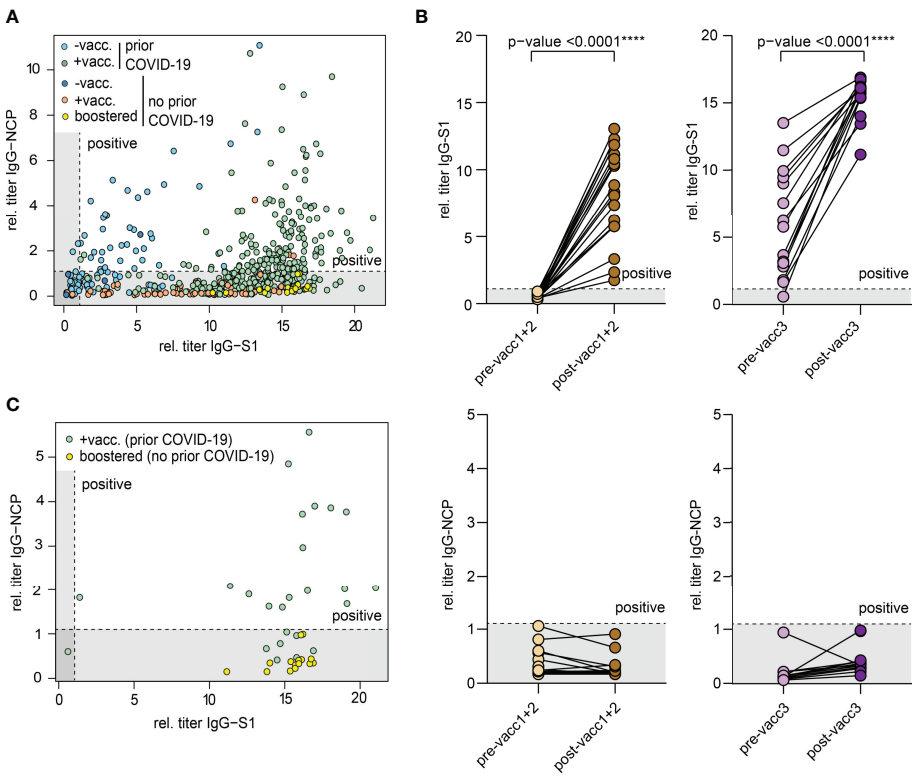

FIGURE 2 | Antibodies against the S1 domain of the spike (S) protein and the nucleocapsid protein (NCP) of SARS-CoV-2. **(A)** Comparison of IgG-NCP and IgG-S1 antibodies in vaccinated individuals with or without prior COVID-19 infection. **(B)** Matched IgG-S1 and IgG-NCP antibody titers of previously uninfected individuals prior to and after the primary vaccination series (pre-/post-vacc1+2) and the third vaccination (pre-/post-vacc3). Statistical test: Two-tailed paired t-test. p-value cut-offs: <0.0001 extremely significant (****). **(C)** Comparison of IgG-NCP and IgG-S1 antibodies between previously infected participants that received a subsequent vaccination (green) and previously uninfected participants with three vaccinations (yellow). Both types of blood samples were collected at a maximum of 4 weeks from last vaccination. Cut-off values are presented as hatched lines.

'vacc1+2' consists of 20 individuals who donated blood before their first SARS-CoV-2 vaccination (pre-vacc1+2) and after their second vaccination (post-vacc1+2). Cohort 'vacc3' consists of 15 different individuals -not overlapping with individuals from cohort vacc1+2- who donated blood before (pre-vacc3) and after (post-vacc3) their third vaccination. The time points of blood collection are shown in **Figure 3A**. All of the sequenced samples included in this manuscript were derived from participants without a prior SARS-CoV-2 infection which was confirmed by negative levels of NCP antibodies (**Figure 2B**).

All patients included in this analysis had received mRNA vaccines; 8 of 15 participants received the BionTech/Pfizer

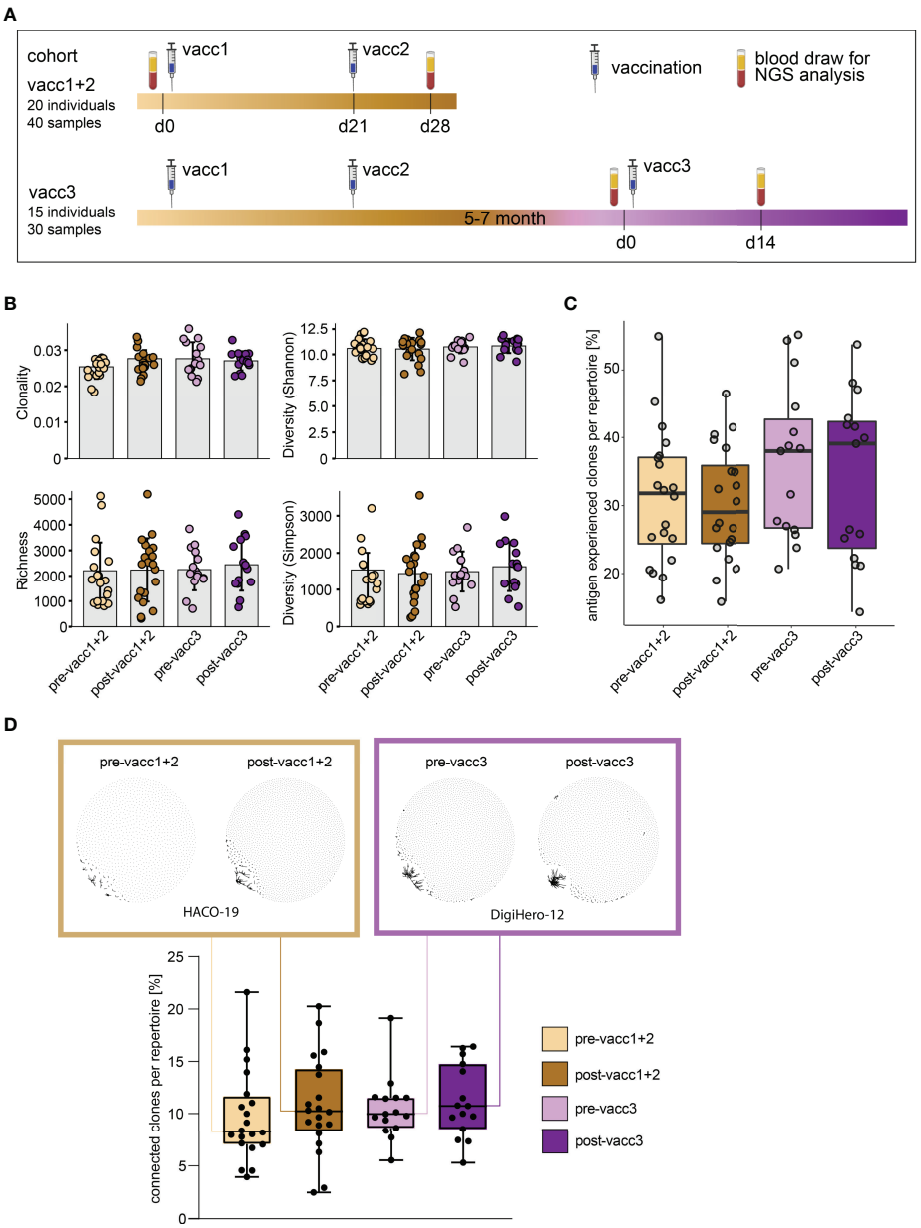

FIGURE 3 | Matched pre- and post-SARS-CoV-2 vaccination blood sampling and global B cell repertoire analysis. **(A)** Vaccination and blood sampling scheme. **(B)** Broad B cell repertoire metrics. Bars indicate mean ± standard deviation. **(C)** Percentage of antigen experienced clones with somatic hypermutation (<98% identity to germline) per B cell repertoire. Box and whiskers plot are shown in the style of Tukey. **(D)** Quantitative connectivity analysis of B cell clones per repertoire. A clone is defined as a unique CDR3aa sequence. Clones are connected if they have a Levenshtein distance of ≤ 3 are connected. Boxes outline 25th to 75th percentile with a line at the median and whiskers from minimum to maximum. Petri dish plots of two representative pre-/post vaccination B cell repertoires are shown in brown and violet boxes on top (patients HACO-19 and DigiHero-12). Each dot in the petri dish plot represents one clone.

vaccine as third vaccination. There were no global differences in immune repertoire metrics such as diversity, richness or clonality across groups (**Figure 3B**). In addition, B cell repertoire somatic hypermutation rates of IGHV genes that reflect antigen-mediated affinity maturation were roughly identical on the global immune repertoire level (**Figure 3C**). There were, however, trends in repertoire connectivity: Pre-vaccination B cell repertoires showed lowest connectivity between B cell clonotypes while samples taken after the third vaccination showed highest connectivity (**Figure 3D**, lower part). B cell connectivity plots of two patients with representative connectivity levels are shown in the upper part of **Figure 3D**.

SARS-CoV-2 Specific B Cell Clonotypes Prior to and After First/Second Versus Third Vaccination

While global B cell repertoire metrics were rather stable across the studied subgroups, we hypothesized that the subrepertoire of B cells with known SARS-CoV-2 specificity may provide more insight into affinity maturation in response to vaccination. We, therefore, searched our set of immune repertoires for 3,195 known SARS-CoV-2 antibody sequences (28) to determine blood circulation of B cells carrying SARS-CoV-2 reactive B cell receptors. 1,147 thereof derived from neutralizing SARS-CoV-2 antibodies. Interestingly, blood-circulation of such B cells appeared to be increased shortly after the first two vaccinations (**Figures 4A, B**). After the third vaccination, we also noted increases as compared to the matched time point before the third vaccination (**Figures 4A, B**). Yet, in absolute numbers, the increase in blood circulation of these clones was lower than after the primary vaccination series.

In a next step, we determined somatic hypermutation rates of SARS-CoV-2 specific clones from matched pre- and post-vaccination samples. We reasoned that the rate of somatically hypermutated clones should increase with the number of applied vaccinations. Indeed, we found a continuous increase in the fraction of somatically hypermutated B cell clones within the SARS-CoV-2 specific repertoire from pre-vaccination samples to samples acquired after the third vaccination (**Figure 4C**). Interestingly, the rate of somatically hypermutated SARS-CoV-2 specific clones was lower after completion of the primary vaccination series than prior to the third vaccination. This suggests that even „short-lived" mRNA vaccines trigger affinity maturation of B cells over months in line with recent data (22). Although the somatic hypermutation load per SARS-CoV-2 specific sequence numerically increased in primed participants, it was dramatically boosted by the third vaccination (**Figure 4D**). This was especially observed for BCR sequences encoded by the IGHV3-21, IGHV3-23, IGHV3-53 and IGHV3-30-3 genes (**Figure 4E**) which have been already linked to S-reactive antibodies with exceptional neutralizing potency (12, 35–39). However, IGHV3-23 is generally mutated more often in unselected B cells of vaccinated and unvaccinated controls (**Supplementary Figure 1**). The amount of hypermutation did not correlate with age (**Figure 4F**).

Maturation Trajectories in the Primary Vaccination Series and Upon Third Vaccination

To be able to analyze individual maturation trajectories of B cells in the primary vaccination series versus upon third vaccination, we set out to identify developmental B lineages in all individual participants and to track them across the vaccination period. A B cell lineage is a group of clonotype-defined B cells that share a common V and J gene and a CDR3 sequence differing only in up to 10% of its amino acid positions (30). While we did not detect expanding B cell lineages in a substantial proportion of participants receiving their primary vaccination series, we found expanding lineages in the majority of patients receiving their third vaccination (**Figure 5A**). The repertoire space taken up by these vaccine-induced expanding B cell lineages was substantially higher after the third vaccination than after completion of the primary vaccination series (**Figure 5B**). The stream plots in **Figure 5C** and **Supplementary Figure 2** show the development of B cell lineages from the pre- to the post-vaccination time point in all investigated cases. All overlapping, expanding lineages are shown as individual colored stream mapping its frequency within the pre- and post-vaccination repertoire. Detailed analysis of these maturation trajectories showed that the precursors of highly mutated post-booster clones were either naive or antigen-experienced cells that were mobilized into a secondary round of somatic hypermutation, most likely through a second recruitment to a germinal center. We found evidence for different scenarios: Further mutation of highly mutant clones and of clones with low numbers of mutations. Exemplary mutational trajectories induced by the third vaccination starting from naive or antigen-experienced clones are shown in **Figure 5D**. Finally, we looked at the IGHV gene usage of expanding lineages during the primary vaccination series and the third vaccination and found an overrepresentation of IGHV3-23 and IGHV3-53 in somatically hypermutated clones in both cohorts (**Supplementary Figure 3**).

DISCUSSION

Dissection of infection-, but especially vaccine-induced B cell immunity to SARS-CoV-2 has become even more a priority in light of the advent of SARS-CoV-2 variants of concern that differ from the ancestral strain in transmissibility and immune evasion. In the second half of 2021, when the majority of blood samples for this analysis were collected, Delta (B.1.617.2) was the dominant SARS-CoV-2 variant worldwide. The Omicron variant B.1.1.529 has been first reported to WHO on the 24th of November 2021 and thereafter spread across the globe at unprecedented rate. In January 2022, Omicron replaced Delta as the dominant variant accompanied by a record of 15 million new COVID-19 cases worldwide in a single week. Both Delta and Omicron variants cause concerns also in fully vaccinated populations since the current vaccines are targeted at the ancestral SARS-CoV-2 strain (40–47). In addition, it was also

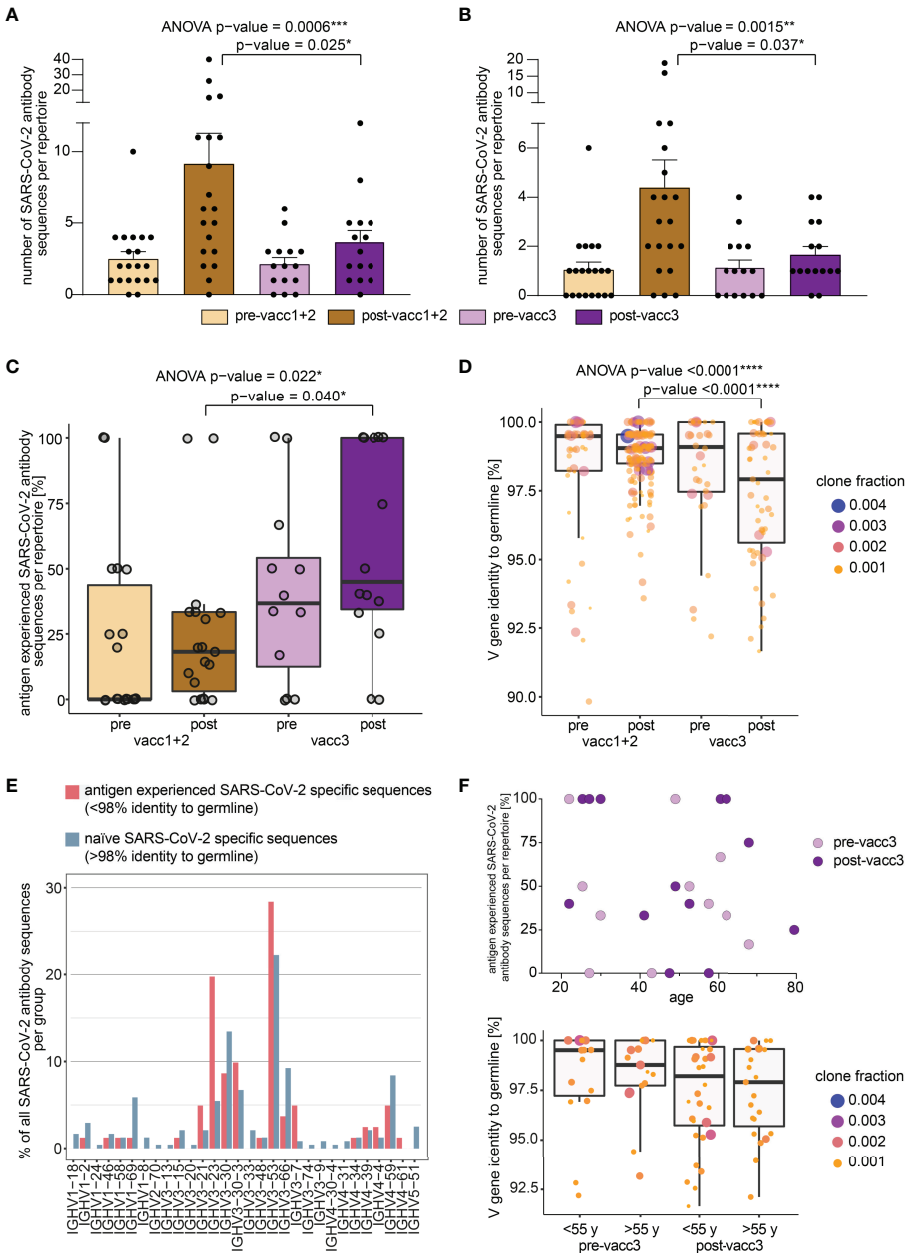

FIGURE 4 | Search of SARS-CoV-2 directed B cell clonotypes in matched pre- and post-vaccination blood samples. Search of 3,195 total **(A)** and 1,147 neutralizing **(B)** antibody sequences in all immune repertoires. Bars indicate mean ± s.e.m. **(C)** Somatic hypermutation analysis of SARS-CoV-2 directed antibody sequences. The percentage of antigen experienced clones within the SARS-CoV-2 specific subrepertoires per patient is shown. A clone was considered antigen-experienced if the IGHV gene showed < 98% identity to the germline nucleotide sequence. **(D)** Somatic hypermutation load per SARS-CoV-2 directed antibody sequence is shown. Respective clone fractions are coded by color/size. Box and whiskers plot are shown in the style of Tukey. Ordinary one-way ANOVA was performed as statistical test and post-ANOVA analyses between individual columns were performed using Tukey's multiple comparisons test. p-value cut-offs: <0.05 significant (*), <0.01 very significant (**), <0.001 extremely significant (***), <0.0001 extremely significant (****). **(E)** IGHV gene usage in naïve versus antigen-experienced SARS-CoV-2 directed antibody sequences. **(F)** Somatic hypermutation analysis of SARS-CoV-2 directed antibody sequences before and after the third vaccination (pre-/post-vacc3) in correlation to participant's age. The percentage of antigen experienced clones within the SARS-CoV-2 specific subrepertoires per patient is shown in the upper panel. Somatic hypermutation load per SARS-CoV-2 directed antibody sequence is shown before and after the third vaccination (pre-/post-vacc3) subdivided into age groups of </> 55 years (y) in the lower panel. Respective clone fractions are coded by color/size. Box and whiskers plot are shown in the style of Tukey.

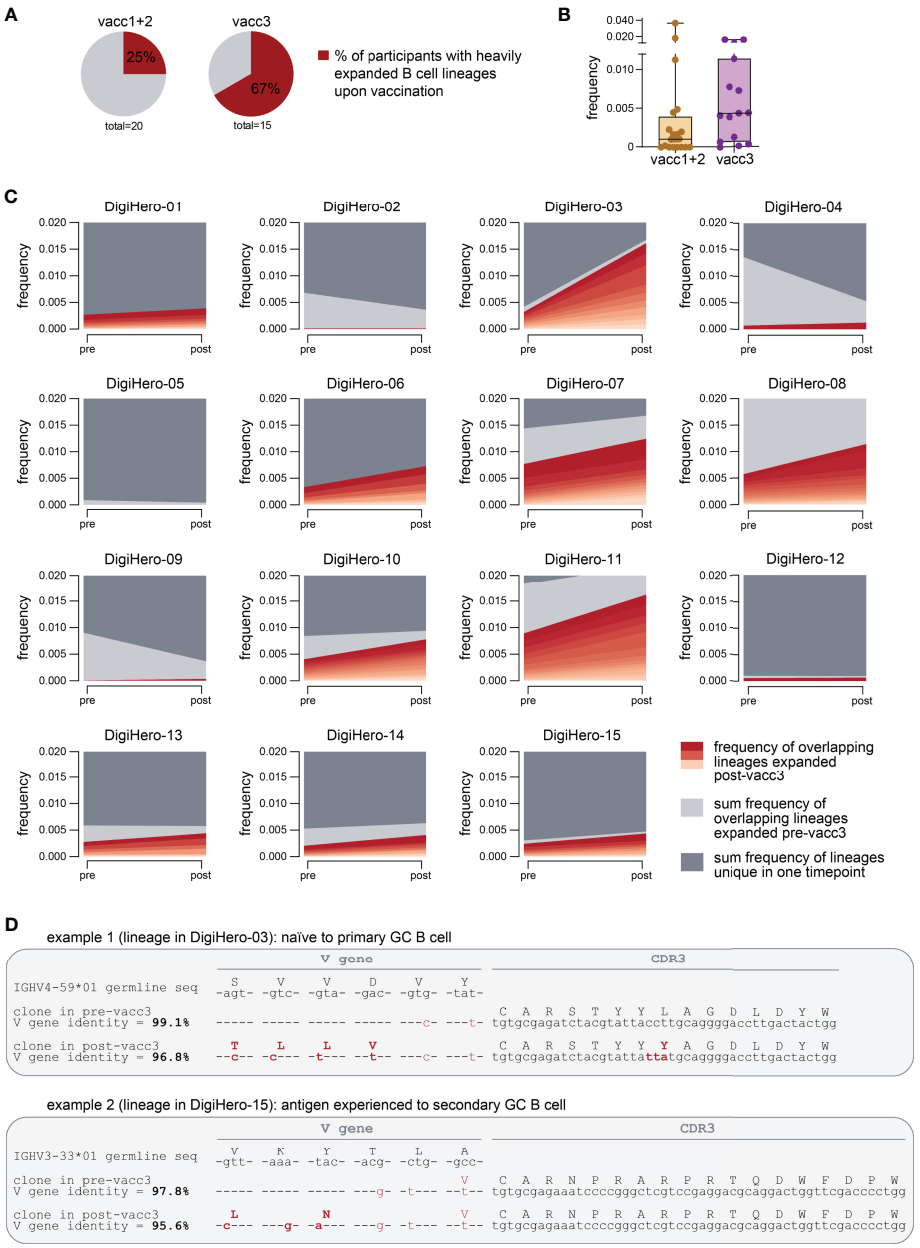

FIGURE 5 | Expanding B cell lineages upon vaccination. B cell lineages in individual patients pre- and post-vaccination were constructed based on V and J gene identity as well as CDR3 sequence homology. **(A)** The percentage of participants with heavily expanded B cell lineages (more than 0.3% frequency within the post-vaccination repertoire taken up by overlapping expanded lineages) after the first/second (vacc1+2) or third vaccination (vacc3) are shown as pie charts. **(B)** Repertoire frequency of expanding B cell lineages at the post-vaccination time point. **(C)** Stream plots showing expanding B cell lineages in patients receiving their third SARS-CoV-2 vaccination (vacc3). **(D)** Exemplary detailed somatic hypermutation analysis of two antibody sequences. GC = germinal center. Seq = sequence.

reported that the type and/or sequence of different exposures triggers SARS-CoV-2-directed immune responses varying in specificity and neutralizing potency (48). It is therefore crucial to understand the biology of SARS-CoV-2 vaccination in detail to design better vaccination protocols and eventually vaccine updates providing sufficient protection against emerging variants.

In the study presented here, we show complex B cell maturation trajectories induced by the third "booster" vaccination that by far exceeded the level of somatic hypermutation measurable directly after completion of the primary vaccination series. Interestingly, the strong mutational activity was essentially restricted to few lineages that were present and mutated already before the third vaccination and

therefore likely involved in previously induced memory B cells that were once again recruited to the lymph node's germinal center for further refinement. Notably, we observed high mutational rates especially in IGHV3-21, IGHV3-23, IGHV3-53 and IGHV3-30-3 genes that were linked to antibodies isolated from elite neutralizers that have previously shown neutralizing potency against variants of concern after infection with the ancestral strain (12, 35–39). Interestingly, we did not observe any age-restriction for this maturation process indication that also older people benefit from a third vaccination although this needs further validation due to the limited size of the analyzed cohort. Since somatic hypermutation reflects affinity maturation, our data is not only well compatible with the strong increase in neutralization potential towards the ancestral strain induced by the third vaccination (49), it also may explain why individuals after a recent third vaccination are usually protected from infection with the Delta variant that shows only few immune-evasive S protein mutations (50–52). This postulated increase in affinity may also explain why the third vaccination but not the primary vaccination series produces some level of protection against infection with the Omicron strain that harbors a large number of immune-evasive mutations within the S protein (53, 54).

We found a gap between the fraction of somatically hypermutated SARS-CoV-2 directed B cell clones after completion of priming and directly before boosting. This suggested that SARS-CoV-2 vaccines might trigger long-term maturation and affinity selection in the B cell compartment over months even with mRNA vaccines that consist in short-lived injected molecules. This data is well compatible with recent findings from Sokal et al. (24) that show continuous maturation of B cells over months after vaccination by flow cytometry. From a translational perspective, this data may suggest that the shortening of the interval between priming and boosting may come at a price of lower booster efficacy if the time span for ongoing B cell maturation and affinity selection is too short. Increasing the time interval between the first and the second dose has been shown to promote effectiveness in the AstraZeneca vector vaccine trial for the first two vaccinations (55). At the same time, this needs to be balanced against the current risk associated with the inability of a primary vaccination series to protect against the current Omicron variant.

The third vaccination rapidly generated a considerable somatic hypermutation load in SARS-CoV-2 specific B cell receptor clonotypes given that the time interval between the pre- and post-booster vaccination sampling was only 14 days. To achieve a somatic hypermutation rate of the IGHV gene between 2 and 10% (typical for the antigen-experienced B cells seen in our study), between 6 and 30 nucleotide exchanges are required per clone. Given the increased somatic hypermutation rate of immunoglobulin genes of approximately 10(-3) mutations per base pair per cell division (56), more than three cell divisions are necessary to statistically exchange one nucleotide per IGHV gene. This very rough calculation may show the high proliferative stimulus of the third booster vaccination. The clinical correlate thereof may be the rather high rate of ipsilateral axillary lymph node swelling compared to other cohorts (57) observed by almost 10% of our DigiHero participants after the third vaccination.

The major limitation of our work is the purely computational approach. To derive firm conclusions regarding variant specificity of vaccination-induced B cell clones, functional validation of binding properties are clearly needed and part of many ongoing studies worldwide. Another limitation of the study design consists in a comparison of two vaccinations (the primary series) with just one third vaccination. Furthermore, it is noteworthy that our sequencing approach does not distinguish between memory B cells and plasmablasts, which may show different frequencies in both cohorts. This needs to be taken into account when comparing the primary vaccination series with the third vaccination.

Taken together, our data show that the primary vaccination series quickly generates antibodies from B cells that have only undergone low-level affinity maturation and may therefore not be protective for immune-escape viral variants such as Omicron B.1.1.529. Our analyzes confirm the role of the third SARS-CoV-2 "booster" to generate affinity-matured clones and mobilize them for antibody production.

DATA AVAILABILITY STATEMENT

The datasets presented in this study can be found in online repositories. The names of the repository/repositories and accession number(s) can be found below:

https://www.ebi.ac.uk/ena, PRJEB50803.

ETHICS STATEMENT

This study was registered as non-interventional study (NIS) at the Paul-Ehrlich-Institute (NIS635). DigiHero and HACO were approved by the institutional review board (approval numbers 2020-076 and 2020-039). Written informed consent was received prior to participation. The patients/participants provided their written informed consent to participate in this study.

AUTHOR CONTRIBUTIONS

Idea and design of research project: MB, LP, RM, CG. Supply of critical material (e.g. patient material, cohorts): RM, DSe, MB, MGe, MGi, SD, BK; Establishment of Methods: LP, CS, EW; Experimental work: LP, CS, DSi; Data analysis and interpretation: MB, LP, CS; Drafting of manuscript: MB, LP.

FUNDING

This project was partially funded by the CRC 841 of the German Research Foundation (to MB) as well as by the Martin-Luther-University Halle (Saale).

ACKNOWLEDGMENTS

We thank the participants of our DigiHero and HACO cohorts for their great support. Moreover, we thank Christoph Wosiek, Aline Patzschke, Jenny Wehde and Katrin Nerger for excellent technical assistance.

SUPPLEMENTARY MATERIAL

The Supplementary Material for this article can be found online at: https://www.frontiersin.org/articles/10.3389/fimmu.2022.876306/full#supplementary-material

REFERENCES

1. Robbiani DF, Gaebler C, Muecksch F, Lorenzi JCC, Wang Z, Cho A, et al. Convergent Antibody Responses to Sars-Cov-2 in Convalescent Individuals. *Nature* (2020) 584:437–42. doi: 10.1038/s41586-020-2456-9
2. Schafer A, Muecksch F, Lorenzi JCC, Leist SR, Cipolla M, Bournazos S, et al. Antibody Potency, Effector Function, and Combinations in Protection and Therapy for Sars-Cov-2 Infection in Vivo. *J Exp Med* (2021) 218(3): e20201993. doi: 10.1084/jem.20201993
3. Israelow B, Mao T, Klein J, Song E, Menasche B, Omer SB, et al. Adaptive Immune Determinants of Viral Clearance and Protection in Mouse Models of Sars-Cov-2. *Sci Immunol* (2021) 6(64):eabl4509. doi: 10.1126/sciimmunol.abl4509
4. Laidlaw BJ, Ellebedy AH. The Germinal Centre B Cell Response to Sars-Cov-2. *Nat Rev Immunol* (2022) 22(1):7–18. doi: 10.1038/s41577-021-00657-1
5. Schultheiss C, Paschold L, Simnica D, Mohme M, Willscher E, von Wenserski L, et al. Next-Generation Sequencing of T and B Cell Receptor Repertoires From Covid-19 Patients Showed Signatures Associated With Severity of Disease. *Immunity* (2020) 53(2):442–55.e4. doi: 10.1016/j.immuni.2020.06.024
6. Seydoux E, Homad LJ, MacCamy AJ, Parks KR, Hurlburt NK, Jennewein MF, et al. Analysis of a Sars-Cov-2-Infected Individual Reveals Development of Potent Neutralizing Antibodies With Limited Somatic Mutation. *Immunity* (2020) 53(1):98–105.e5. doi: 10.1016/j.immuni.2020.06.001
7. Barnes CO, West AP Jr, Huey-Tubman KE, Hoffmann MAG, Sharaf NG, Hoffman PR, et al. Structures of Human Antibodies Bound to Sars-Cov-2 Spike Reveal Common Epitopes and Recurrent Features of Antibodies. *Cell* (2020) 182(4):828–42.e16. doi: 10.1016/j.cell.2020.06.025
8. Nielsen SCA, Yang F, Jackson KJL, Hoh RA, Roltgen K, Jean GH, et al. Human B Cell Clonal Expansion and Convergent Antibody Responses to Sars-Cov-2. *Cell Host Microbe* (2020) 28(4):516–25.e5. doi: 10.1016/j.chom.2020.09.002
9. Dejnirattisai W, Zhou D, Ginn HM, Duyvesteyn HME, Supasa P, Case JB, et al. The Antigenic Anatomy of Sars-Cov-2 Receptor Binding Domain. *Cell* (2021) 184(8):2183–200.e22. doi: 10.1016/j.cell.2021.02.032
10. Kreer C, Zehner M, Weber T, Ercanoglu MS, Gieselmann L, Rohde C, et al. Longitudinal Isolation of Potent Near-Germline Sars-Cov-2-Neutralizing Antibodies From Covid-19 Patients. *Cell* (2020) 182(4):843–54.e12. doi: 10.1016/j.cell.2020.06.044
11. Galson JD, Schaetzle S, Bashford-Rogers RJM, Raybould MIJ, Kovaltsuk A, Kilpatrick GJ, et al. Deep Sequencing of B Cell Receptor Repertoires From Covid-19 Patients Reveals Strong Convergent Immune Signatures. *Front Immunol* (2020) 11:605170. doi: 10.3389/fimmu.2020.605170
12. Yuan M, Liu H, Wu NC, Lee CD, Zhu X, Zhao F, et al. Structural Basis of a Shared Antibody Response to Sars-Cov-2. *Science* (2020) 369(6507):1119–23. doi: 10.1126/science.abd2321
13. Paschold L, Simnica D, Willscher E, Vehreschild MJ, Dutzmann J, Sedding DG, et al. Sars-Cov-2-Specific Antibody Rearrangements in Prepandemic Immune Repertoires of Risk Cohorts and Patients With Covid-19. *J Clin Invest* (2021) 131(1):e142966. doi: 10.1172/JCI142966
14. Zost SJ, Gilchuk P, Chen RE, Case JB, Reidy JX, Trivette A, et al. Rapid Isolation and Profiling of a Diverse Panel of Human Monoclonal Antibodies Targeting the Sars-Cov-2 Spike Protein. *Nat Med* (2020) 26(9):1422–7. doi: 10.1038/s41591-020-0998-x
15. Andreano E, Nicastri E, Paciello I, Pileri P, Manganaro N, Piccini G, et al. Extremely Potent Human Monoclonal Antibodies From Covid-19 Convalescent Patients. *Cell* (2021) 184(7):1821–35 e16. doi: 10.1016/j.cell.2021.02.035
16. Gaebler C, Wang Z, Lorenzi JCC, Muecksch F, Finkin S, Tokuyama M, et al. Evolution of Antibody Immunity to Sars-Cov-2. *Nature* (2021) 591 (7851):639–44. doi: 10.1038/s41586-021-03207-w
17. Sokal A, Chappert P, Barba-Spaeth G, Roeser A, Fourati S, Azzaoui I, et al. Maturation and Persistence of the Anti-Sars-Cov-2 Memory B Cell Response. *Cell* (2021) 184(5):1201–13 e14. doi: 10.1016/j.cell.2021.01.050
18. Sakharkar M, Rappazzo CG, Wieland-Alter WF, Hsieh CL, Wrapp D, Esterman ES, et al. Prolonged Evolution of the Human B Cell Response to Sars-Cov-2 Infection. *Sci Immunol* (2021) 6(56):eabg6916. doi: 10.1126/sciimmunol.abg6916
19. Rodda LB, Netland J, Shehata L, Pruner KB, Morawski PA, Thouvenel CD, et al. Functional Sars-Cov-2-Specific Immune Memory Persists After Mild Covid-19. *Cell* (2021) 184(1):169–83.e17. doi: 10.1016/j.cell.2020.11.029
20. Dan JM, Mateus J, Kato Y, Hastie KM, Yu ED, Faliti CE, et al. Immunological Memory to Sars-Cov-2 Assessed for Up to 8 Months After Infection. *Science* (2021) 371(6529):eabf4063. doi: 10.1126/science.abf4063
21. Schultheiss C, Paschold L, Willscher E, Simnica D, Wostemeier A, Muscate F, et al. Maturation Trajectories and Transcriptional Landscape of Plasmablasts and Autoreactive B Cells in Covid-19. *iScience* (2021) 24(11):103325. doi: 10.1016/j.isci.2021.103325
22. Kim W, Zhou JQ, Sturtz AJ, Horvath SC, Schmitz AJ, Lei T, et al. Germinal Centre-Driven Maturation of B Cell Response to Sars-Cov-2 Vaccination. *Nature* (2022) 604:141–5. doi: 10.1038/s41586-022-04527-1
23. Pape KA, Dileepan T, Kabage AJ, Kozysa D, Batres R, Evert C, et al. High-Affinity Memory B Cells Induced by Sars-Cov-2 Infection Produce More Plasmablasts and Atypical Memory B Cells Than Those Primed by Mrna Vaccines. *Cell Rep* (2021) 37(2):109823. doi: 10.1016/j.celrep.2021.109823
24. Sokal A, Barba-Spaeth G, Fernandez I, Broketa M, Azzaoui I, de la Selle A, et al. Mrna Vaccination of Naive and Covid-19-Recovered Individuals Elicits Potent Memory B Cells That Recognize Sars-Cov-2 Variants. *Immunity* (2021) 54(12):2893–907.e5. doi: 10.1016/j.immuni.2021.09.011
25. Schultheiss C, Simnica D, Willscher E, Oberle A, Fanchi L, Bonzanni N, et al. Next-Generation Immunosequencing Reveals Pathological T-Cell Architecture in Autoimmune Hepatitis. *Hepatology* (2021) 73(4):1436–48. doi: 10.1002/hep.31473
26. Bolotin DA, Poslavsky S, Mitrophanov I, Shugay M, Mamedov IZ, Putintseva EV, et al. Mixcr: Software for Comprehensive Adaptive Immunity Profiling. *Nat Methods* (2015) 12(5):380–1. doi: 10.1038/nmeth.3364
27. Simnica D, Akyuz N, Schliffke S, Mohme M, VW L, Mahrle T, et al. T Cell Receptor Next-Generation Sequencing Reveals Cancer-Associated Repertoire Metrics and Reconstitution After Chemotherapy in Patients With Hematological and Solid Tumors. *Oncoimmunology* (2019) 8(11):e1644110. doi: 10.1080/2162402X.2019.1644110
28. Raybould MIJ, Kovaltsuk A, Marks C, Deane CM. Cov-Abdab: The Coronavirus Antibody Database. *Bioinformatics* (2021) 37(5):734–5. doi: 10.1093/bioinformatics/btaa739
29. Gabor C, Tamas N. The Igraph Software Package for Complex Network Research. *InterJournal Complex Syst* (2006) 1695(5):1–9.
30. Xiang H, Zhao Y, Li X, Liu P, Wang L, Wang M, et al. Landscapes and Dynamic Diversifications of B-Cell Receptor Repertoires in Covid-19 Patients. *Hum Immunol* (2022) 83(2):119–29. doi: 10.1016/j.humimm.2021.10.007
31. Kim N, Shin S, Minn D, Park S, An D, Park JH, et al. Sars-Cov-2 Infectivity and Antibody Titer Reduction for 6 Months After Second Dose of Bnt162b2 Mrna Vaccine in Healthcare Workers: A Prospective Cohort Study. *J Infect Dis* (2022) jiac035. doi: 10.1093/infdis/jiac035
32. Koerber N, Priller A, Yazici S, Bauer T, Cheng CC, Mijocevic H, et al. Dynamics of Spike-And Nucleocapsid Specific Immunity During Long-Term Follow-Up and Vaccination of Sars-Cov-2 Convalescents. *Nat Commun* (2022) 13(1):153. doi: 10.1038/s41467-021-27649-y
33. Seow J, Graham C, Merrick B, Acors S, Pickering S, Steel KJA, et al. Longitudinal Observation and Decline of Neutralizing Antibody Responses in the Three Months Following Sars-Cov-2 Infection in Humans. *Nat Microbiol* (2020) 5(12):1598–607. doi: 10.1038/s41564-020-00813-8

34. Iyer AS, Jones FK, Nodoushani A, Kelly M, Becker M, Slater D, et al. Persistence and Decay of Human Antibody Responses to the Receptor Binding Domain of Sars-Cov-2 Spike Protein in Covid-19 Patients. *Sci Immunol* (2020) 5(52):eabe0367. doi: 10.1126/sciimmunol.abe0367
35. Vanshylla K, Fan C, Wunsch M, Poopalasingam N, Meijers M, Kreer C, et al. Discovery of Ultrapotent Broadly Neutralizing Antibodies From Sars-Cov-2 Elite Neutralizers. *Cell Host Microbe* (2022) 30(1):69–82.e10. doi: 10.1016/j.chom.2021.12.010
36. Tong P, Gautam A, Windsor IW, Travers M, Chen Y, Garcia N, et al. Memory B Cell Repertoire for Recognition of Evolving Sars-Cov-2 Spike. *Cell* (2021) 184(19):4969–80 e15. doi: 10.1016/j.cell.2021.07.025
37. He B, Liu S, Wang Y, Xu M, Cai W, Liu J, et al. Rapid Isolation and Immune Profiling of Sars-Cov-2 Specific Memory B Cell in Convalescent Covid-19 Patients *Via* Libra-Seq. *Signal Transduct Target Ther* (2021) 6(1):195. doi: 10.1038/s41392-021-00610-7
38. Zhang Q, Ju B, Ge J, Chan JF, Cheng L, Wang R, et al. Potent and Protective Ighv3-53/3-66 Public Antibodies and Their Shared Escape Mutant on the Spike of Sars-Cov-2. *Nat Commun* (2021) 12(1):4210. doi: 10.1038/s41467-021-24514-w
39. Zou J, Li L, Zheng P, Liang W, Hu S, Zhou S, et al. Ultrapotent Neutralizing Antibodies Against Sars-Cov-2 With a High Degree of Mutation Resistance. *J Clin Invest* (2022) 132(4):e154987. doi: 10.1172/JCI154987
40. Hirabara SM, Serdan TDA, Gorjao R, Masi LN, Pithon-Curi TC, Covas DT, et al. Sars-Cov-2 Variants: Differences and Potential of Immune Evasion. *Front Cell Infect Microbiol* (2021) 11:781429. doi: 10.3389/fcimb.2021.781429
41. Hoffmann M, Kruger N, Schulz S, Cossmann A, Rocha C, Kempf A, et al. The Omicron Variant Is Highly Resistant Against Antibody-Mediated Neutralization: Implications for Control of the Covid-19 Pandemic. *Cell* (2022) 185(3):447–56.e11. doi: 10.1016/j.cell.2021.12.032
42. Dejnirattisai W, Huo J, Zhou D, Zahradnik J, Supasa P, Liu C, et al. Sars-Cov-2 Omicron-B.1.1.529 Leads to Widespread Escape From Neutralizing Antibody Responses. *Cell* (2022) 185(3):467–84.e15. doi: 10.1016/j.cell.2021.12.046
43. Thorne LG, Bouhaddou M, Reuschl AK, Zuliani-Alvarez L, Polacco B, Pelin A, et al. Evolution of Enhanced Innate Immune Evasion by Sars-Cov-2. *Nature* (2021) 602:487–95. doi: 10.1038/s41586-021-04352-y
44. Zhang J, Xiao T, Cai Y, Lavine CL, Peng H, Zhu H, et al. Membrane Fusion and Immune Evasion by the Spike Protein of Sars-Cov-2 Delta Variant. *Science* (2021) 374(6573):1353–60. doi: 10.1126/science.abl9463
45. Planas D, Veyer D, Baidaliuk A, Staropoli I, Guivel-Benhassine F, Rajah MM, et al. Reduced Sensitivity of Sars-Cov-2 Variant Delta to Antibody Neutralization. *Nature* (2021) 596(7871):276–80. doi: 10.1038/s41586-021-03777-9
46. McCallum M, Walls AC, Sprouse KR, Bowen JE, Rosen LE, Dang HV, et al. Molecular Basis of Immune Evasion by the Delta and Kappa Sars-Cov-2 Variants. *Science* (2021) 374(6575):1621–6. doi: 10.1126/science.abl8506
47. Mlcochova P, Kemp SA, Dhar MS, Papa G, Meng B, Ferreira I, et al. Sars-Cov-2 B.1.617.2 Delta Variant Replication and Immune Evasion. *Nature* (2021) 599(7883):114–9. doi: 10.1038/s41586-021-03944-y
48. Greaney AJ, Loes AN, Gentles LE, Crawford KHD, Starr TN, Malone KD, et al. Antibodies Elicited by Mrna-1273 Vaccination Bind More Broadly to the Receptor Binding Domain Than Do Those From Sars-Cov-2 Infection. *Sci Transl Med* (2021) 13(600):eabi9915. doi: 10.1126/scitranslmed.abi9915
49. Garcia-Beltran WF, St Denis KJ, Hoelzemer A, Lam EC, Nitido AD, Sheehan ML, et al. Mrna-Based Covid-19 Vaccine Boosters Induce Neutralizing Immunity Against Sars-Cov-2 Omicron Variant. *Cell* (2022) 185(3):457–66.e4. doi: 10.1016/j.cell.2021.12.033
50. Perez-Then E, Lucas C, Monteiro VS, Miric M, Brache V, Cochon L, et al. Neutralizing Antibodies Against the Sars-Cov-2 Delta and Omicron Variants Following Heterologous Coronavac Plus Bnt162b2 Booster Vaccination. *Nat Med* (2022) 28:481–5. doi: 10.1038/s41591-022-01705-6
51. Gross R, Zanoni M, Seidel A, Conzelmann C, Gilg A, Krnavek D, et al. Heterologous Chadox1 Ncov-19 and Bnt162b2 Prime-Boost Vaccination Elicits Potent Neutralizing Antibody Responses and T Cell Reactivity Against Prevalent Sars-Cov-2 Variants. *EBioMedicine* (2022) 75:103761. doi: 10.1016/j.ebiom.2021.103761
52. Levine-Tiefenbrun M, Yelin I, Alapi H, Katz R, Herzel E, Kuint J, et al. Viral Loads of Delta-Variant Sars-Cov-2 Breakthrough Infections After Vaccination and Booster With Bnt162b2. *Nat Med* (2021) 27(12):2108–10. doi: 10.1038/s41591-021-01575-4
53. van Gils MJ, van Willigen HDG, Wynberg E, Han AX, van der Straten K, Burger JA, et al. A Single Mrna Vaccine Dose in Covid-19 Patients Boosts Neutralizing Antibodies Against Sars-Cov-2 and Variants of Concern. *Cell Rep Med* (2022) 3(1):100486. doi: 10.1016/j.xcrm.2021.100486
54. Wang K, Jia Z, Bao L, Wang L, Cao L, Chi H, et al. Memory B Cell Repertoire From Triple Vaccinees Against Diverse Sars-Cov-2 Variants. *Nature* (2022) 603:919–25. doi: 10.1038/s41586-022-04466-x
55. Voysey M, Clemens SAC, Madhi SA, Weckx LY, Folegatti PM, Aley PK, et al. Safety and Efficacy of the Chadox1 Ncov-19 Vaccine (Azd1222) Against Sars-Cov-2: An Interim Analysis of Four Randomised Controlled Trials in Brazil, South Africa, and the UK. *Lancet* (2021) 397(10269):99–111. doi: 10.1016/S0140-6736(20)32661-1
56. Odegard VH, Schatz DG. Targeting of Somatic Hypermutation. *Nat Rev Immunol* (2006) 6(8):573–83. doi: 10.1038/nri1896
57. Barda N, Dagan N, Ben-Shlomo Y, Kepten E, Waxman J, Ohana R, et al. Safety of the Bnt162b2 Mrna Covid-19 Vaccine in a Nationwide Setting. *N Engl J Med* (2021) 385(12):1078–90. doi: 10.1056/NEJMoa2110475

Conflict of Interest: The authors declare that the research was conducted in the absence of any commercial or financial relationships that could be construed as a potential conflict of interest.

frontiers | Frontiers in Immunology

REVIEW
published: 30 June 2022
doi: 10.3389/fimmu.2022.889876

Role of IgM Memory B Cells and Spleen Function in COVID-19

Carlo Maria Rossi, Marco Vincenzo Lenti, Stefania Merli and Antonio Di Sabatino *

University of Pavia, First Department of Internal Medicine, IRCCS San Matteo Hospital Foundation, Pavia, Italy

IgM memory B cells, are a peculiar subset of memory B cells, which probably originates in the spleen and outside germinal centers and provide a rapid line of defence against mucosal infections. Their role in counteracting COVID-19 is still elusive but, recent evidence, mainly boosted by studies on spleen function/involvement in COVID-19, seems to support the notion that this subset of memory B cells could exert a protective role against this virus, along with other coronaviruses, particularly in the acute setting of the infection, as outlined by worst clinical outcomes observed in unvaccinated patients with impaired IgM B memory response and spleen function. Herein we critically summarise the current landscape of studies on IgM memory B cells, focusing on the clinical impact of their depletion, by comparing the COVID-19-related splenic dysfunction with other hypo- and asplenic conditions and by adding recent data on follow-up studies and postulate a mechanistic explanation for their reduced numbers. The early detection of an impaired IgM memory B cell response in patients with COVID-19 may contribute to their improved care through different strategies, such as through tailored vaccine strategies, prompt hospital admission and/or administration of anti-infective treatments, thus resulting in an better prognosis, although at present management algorithms are still unavailable. Moreover, further studies with longer follow-up are needed to assess the evolution of COVID-19-associated/exacerbated immune deficit.

Keywords: plasma cells, hyposplenism, SARS-CoV-2, B cell, IgM memory B cell

OPEN ACCESS

Edited by:
Moncef Zouali, Institut National de la Santé et de la Recherche Médicale (INSERM), France

Reviewed by:
Peter Bergman, Karolinska Institutet (KI), Sweden
Leire de Campos Mata, Karolinska Institutet (KI), Sweden

***Correspondence:**
Antonio Di Sabatino
a.disabatino@smatteo.pv.it

Specialty section:
This article was submitted to B Cell Biology, a section of the journal Frontiers in Immunology

Received: *04 March 2022*
Accepted: *27 May 2022*
Published: *30 June 2022*

Citation:
Rossi CM, Lenti MV, Merli S and Di Sabatino A (2022) Role of IgM Memory B Cells and Spleen Function in COVID-19. Front. Immunol. 13:889876. doi: 10.3389/fimmu.2022.889876

INTRODUCTION

Severe acute respiratory syndrome coronavirus 2 (SARS-CoV-2) is the cause of coronavirus disease 2019 (COVID-19) pandemic, which has dramatically impacted our globalized society, with more than 500 million reported infections and more than6million deaths worldwide as of April 2022 (1). SARS-CoV-2 has been shown to elicit a strong immune activation mirrored by the so-called "cytokine storm" and the complex interaction between the virus and immune system contributes shaping the heterogenous landscape of COVID-19-related pathology, including lung, liver, skin and spleen or other lymphoid organ damage, among others, and of clinical manifestations (2, 3).

Clinical presentation and outcomes of COVID-19 are highly variable, including asymptomatic, mild and severe cases with lung and/or multiorgan failure, the so-called viral sepsis, and complete resolution without sequelae or death (2). Symptoms related to COVID-19 may also be persisting, defining the so-called long COVID syndrome (4). Yet immunological correlates underpinning these

disease states have been recently outlined. To control the pandemic, it is vital to characterize the immune response against the virus, and possibly manipulate it, through immunological therapeutical strategies, including among others, vaccines and monoclonal antibodies (5, 6).

An effective antiviral immune response usually requires the coordinated and dynamic interplay of both humoral and cellular effectors, with the participation of both the innate and adaptive arm of immunity, to arrest the spreading of a virus, minimize disease severity and prevent reinfection with the same virus strains and, possibly, its variants (7).

Although the precise protective mechanisms against SARS-CoV-2 are still elusive, several features of the immune responses against SARS-CoV-2 have been identified. More precisely, the role of innate immunity and of T cell, both CD4 and CD8, has been recognized as important, particularly for primary infection (8). B cells and antibody-mediated immunity have also been shown to play a prominent role against SARS-CoV-2, since a rapid appearance of virus-specific antibodies is observed in most individuals, and a high titre of neutralizing antibodies to the spike protein and its receptor binding domain (RBD) have been found to confer protection both in humans and animal models (9). Moreover, other antiviral activities of antibodies, including fraction constant (Fc)-effector related-functions, such as antigen-dependent cell-mediated cytotoxicity (ADCC), are thought to play a role (3). In parallel, a compromised humoral development with attenuated IgG responses has been found to be associated with worse outcomes in acute patients with moderate-to-severe disease (5). In addition, B cell deficiency states, including X-linked agammaglobulinemia (XLA), Good's syndrome, and common variable immunodeficiency (CVID), at least in some patients, or following monoclonal antibody therapy, seem to be associated with a worse prognosis according to some studies (9). Moreover, the possible beneficial effect in the acute setting of the convalescent plasma therapy, as shown by systematic reviews and meta-analyses, in terms of reduced mortality, increased virus clearance and clinical improvements, may point at a possible role of the antibody response in counteracting the infection, at least in more severe cases (6, 10).

However, the role of antibody-immunity remains a matter of debate, principally due to some inconsistencies (11). In some studies, patients with CVID, CVID-like disorders or other primary antibody deficiencies were not found to be at increased risk for severe outcomes, or the increased risk only applied to specific subsets of patients, such as those with chronic lung involvement of CVID (12, 13). Moreover, the benefit of convalescent plasma was negligible in non-severe cases and the evidence to recommend its use in severely-ill patients is still, overall, inadequate according to the WHO (14).

Moreover, virus specific antibody titre to the spike, the RBD and the nucleocapsid has been shown to be very heterogenous and to decline over time (15, 16). In spite of waning virus specific antibody titre, antigen-specific memory B cell responses appear to be stable (17).

Given the relatively slow course of the disease in severe and even fatal cases of COVID-19, which have a median disease duration of 22.2 ± 3.6 days (16) the role of the memory compartment, which requires some weeks to assure recall cellular and antibody responses, is deemed particularly relevant. Moreover, to guarantee a long-lasting protective effect, to the same virus strain or different variants, memory compartments exert a pivotal role, as derived from the evidence regarding the immune response to SARS-CoV-2 related viruses, SARS-CoV, and Middle East respiratory syndrome coronavirus (MERS-CoV) (18, 19).

Initially overlooked, memory B cell responses to SARS-CoV-2 have been recently intensively studied, as attested by the rapidly increasing number of published papers, including more than 300 entries as of April 2022, aimed at characterizing their functional landscape during the disease and/or after anti-SARS-CoV-2 vaccines.

Reasons accounting for this renewed interest in memory B cells are tightly linked to the studies on the spleen involvement in COVID-19. Earlier in the epidemic, asplenia was found to confer a mortality risk comparable to other recognised risk factors, such as cardiovascular ones (20). SARS-CoV-2, like other coronaviruses, was shown to display a particular tropism for the spleen, particularly the white pulp, possibly mediated by the angiotensin converting enzyme (ACE)-2 receptor. Moreover, in autopsy studies, white pulp atrophy with reduction/absence of lymphoid follicles was revealed (21). Spleen functional alterations were thus thought to contribute, along with other mechanisms, to the B and T cell lymphopenia which is a typical feature of COVID-19. In addition, given that the spleen marginal zone is the specific site where IgM memory B cells are produced and stored and which exert important protective functions against disseminated infection sustained by encapsulated bacterial and viral infections (such as influenza and HIV), a compromised spleen function was thought to contribute to impaired memory B cell responses.

Concomitantly, it is of importance to identify predisposing conditions associated with impaired generation of memory B cell responses, among them splenic hypofunction state, since this subset of patients may be susceptible to more severe manifestations and/or adverse outcomes and hence may benefit from therapeutical strategies aimed at modifying the immune response against the virus.

We herein summarize in a narrative fashion the existing evidence on the role of IgM B memory cell populations and spleen immune function in COVID-19 and their relationship with disease severity and outcomes, especially in the acute setting. We will also consider the COVID-19-induced spleen dysfunction and draw a parallelism with other hypo- and asplenic states, namely, CVID and splenectomy.

THE GERMINAL CENTRE AND EXTRAFOLLICULAR MEMORY B CELL RESPONSES TO SARS-COV-2

Within the B cell follicle, mainly in lymph nodes and the spleen, but also in mucosal tissues, antigen-activated B cells with T cell help may determine the germinal centre (GC) reaction, which is

vital for the development of affinity-matured plasma cells and long-lived memory B cells that are collectively responsible for a long term and broad protective immunity (22). Within the GC antibodies with enhanced neutralizing activity and breadth resulting from somatic hypermutations arise through a continuous process of clonal evolution of B cells.

However, besides GC reactions, extrafollicular and/or T cell-independent responses may arise. Their aim is to elicit rapid responses, through the generation of memory B cells and short-lived plasma cells with the production of antibodies with a low level of specificity and thus broad reactivity to different bacteria and viruses. These responses take part in early inflammatory responses and have a role in life-threatening, rapid-developing infections.

Interestingly, the severity of COVID-19 seems to have an influence on the quality of the B cell response, with severe disease being associated with extrafollicular responses and defective GC reactions, correlating with high levels of pro-inflammatory cytokines and reduced T follicular helper numbers (19, 23). Memory B cells in this instance display a low level of somatic hypermutation. Whereas in mild disease, both GC- and extrafollicular reactions arise, in which naïve and seasonal coronavirus-specific memory B cells differentiate into activated B cells and short-live plasma cells (24).

As compared to switched memory B cells, which are generated in GC reactions, IgM^+ $IgD^{+/-}$ $CD27^+$ B lymphocytes, also known as IgM memory B cells, seem to arise from a different lineage and develop through GC- and T- independent reactions **Figure 1** (25, 26). IgM memory B cells, which are also known as innate IgM memory B cells, natural memory, or marginal zone B cells, are found in the spleen and peripheral blood, respond to bacterial polysaccharide antigens, and display functional similarities with mouse B-1a cells, the major source of secretory (natural) IgA antibodies (sIgA) lining the intestinal epithelium. Toll-like receptor 9 stimulation has been shown to induce the *in vitro* generation of human IgM memory B cells from transitional B cells (27). Moreover, it has been recently observed that this subset may differentiate *in vitro*, with a T cell-independent mechanism, into IgA secreting plasma cells in the lamina propria and the lymphoid tissue in the gut (25). SIgA exert an important protective function and constitute one of the most relevant components of the mucosal barrier, binding a vast array of antigens and thus preventing the dissemination of bacteria and the entry of allergens and viruses through the formation of immune complexes with cognate Fc receptors.

Moreover, in immunocompetent patients, who were splenectomised for traumatic causes, a depletion of IgM memory B cells has been observed, together with a marked reduction of intestinal IgA^+ plasma cells and a long-lasting defect in the IgA lining, as assessed up to 15 years after splenectomy. This deficit was thus not compensated by GC dependent mechanisms in lymph nodes and in the mucosa-associated lymphoid tissue of the gut by naïve or transitional B cells (25). Parallelly, in the mouse model, B-1a cells and sIgA are not detectable in the gut of asplenic mice (28). Moreover, in the subset of CVID patients with a IgM memory B cell deficiency the IgA layer in the gut is absent (25).

This clinical and experimental evidence has led the researchers to hypothesise the existence of a functional spleen-gut axis, which is characterised by the trafficking of IgM memory B cells from the spleen to the gut mucosa, where they undergo class-switch to IgA and coordinate mucosal immune responses (25). Interestingly, this immune response seems to be evolutionary conserved, being present also in fish species, which are devoid of bone marrow, lymph nodes and GCs. In fish, dimeric immunoglobulin, IgT, resembling IgA, are generated in the spleen and transported to the gut (29).

These findings may have relevant clinical implications since SARS-Cov-2 like among other viruses associated with pandemics, such as influenza virus, show a mucosal tropism and elicit mucosal inflammation. Mucosal memory B cell responses could contribute to viral clearance during reinfection through a rapid and local increase in IgA antibody levels and to sterilizing immunity at mucosal surface, thus limiting the spread of variants (13, 30).

Taken together, these observations constitute the rationale for assessing the role of IgM memory B cells in COVID-19, particularly in the primary infection and, possibly, also in reinfections and in asymptomatic carriers.

THE ROLE OF IGM MEMORY B CELLS IN COVID-19

Few studies have primarily addressed the role of IgM memory B cells in COVID-19 (**Table 1**).

They vary in terms of the studied population -paediatric or adult-, the setting of disease, -acute leading to hospitalisation or not- or convalescent, and to various memory B cell subsets, together with different times of evaluation. Almost all studies refer to unvaccinated patients. One limitation of most of these studies refers to the age of the heathy controls used for comparison. These are usually much younger than the hospitalised patients, with multimorbidity. This may constitute a bias since memory B cell numbers are known to be reduced with aging (38).

In a US study evaluating memory B cell subsets, in recovered non-hospitalized patients with COVID-19, a negative correlation between the duration of symptoms and frequency of memory B cells, including the IgM subset, was found (15). The likelihood that this result was due to a sample time bias was ruled out by the relatively stable number of memory B cells. Of note, a correlation between total B memory cells with RBD antibodies, both IgG1 and IgM, was found. Interestingly, by analysing memory B cell subsets, this correlation was only present in the IgM^+ one. To explain this paradoxical finding, since IgM memory B cells do not usually produce switched immunoglobulins, the Authors postulate that a subset of IgM memory B cells could have undergone class switching to IgG with or without entering a germinal center, possibly following a related-coronavirus infection or have originated from T-cell independent pathways, possibly from circulating marginal zone- like cells, given their low CD38 expression.

TABLE 1 | Studies primarily evaluating the role of IgM memory B cells in COVID-19.

Author (year)	Country	Type of study	Population	SARS-Cov-2 vaccination	Subset of MBC	Time of evaluation of IgM MBC	Comments
Tian X et al. (31) (2022)	China	Observational	31 convalescent children (0-14 years) with mild COVID-19	NA	-IgM -IgG -IgA	At baseline and at 6-8 months	Higher proportion of recovering patients with IgM^+ B cells than IgG^+ IgG+ memory response increases with age as opposed to IgM^+ and IgA^+
Newell K et al. (15) (2021)	U.S.	Observational	40 COVID-19 non-hospitalized patients at baseline 15 also sampled at 3 months 24 healthy subjects	NA	-$CD27^+$, IgD^+, -$CD27^+$ switched memory -$CD24^-$	-69 days after symptoms onset -3 months	IgM memory B cells correlate with virus specific antibodies (IgG1 and IgM) and are stable at 3 months
Mazzoni A et al. (32) (2021)	Italy	Experimental	22 individuals; of which 11 with previous infection	mRNA (II doses)	-$CD27^+$ IgM^+ memory -$CD27^+$ IgA -$CD27^+$ IgG	7, 14, 21, 28 days	IgM^+ increase only after II dose in COVID-19-naïve individuals, while they increase after I dose in those who had COVID-19
Anand S et al. (33) (2021)	Canada	Observational	32 convalescent individuals sampled up to 31 weeks (n=13)	NA	-IgM	6,11,21,31 weeks	IgM^+ decrease over time while IgG^+ are stable
Yang J et al. (34) (2021)	China	Observational	55 recovered patients, 55 healthy donors	NA	-IgM^+ -IgM^-	On average 42.2 days after discharge	Lower frequency of IgM isotype-switched memory B cells in recovered patients as compared to heathly donors
Piepenbrink M et al. (35) (2021)	U.S.	Experimental	Hamsters	NA	IgM MBC	Acute infection	Intraperitoneal/aerosol delivery of a human mAb derived from a COVID19 RBP specific IgM memory B cell reduces respiratory tract viral burden/pathology
Lenti MV et al. (36) (2020)	Italy	Observational	63 patients, 3 splenectomised patients excluded	NA	IgM^+ IgD^+, CD27+	Acute infection, median 25 days	IgM MBC depletion in 87% of patients
De Biasi S et al. (37) (2020)	Italy	Observational	14 hospitalized patients with pneumonia 11 healthy subjects as controls	NA	-IgM MBC -switched -unswitched	Acute infection, 2-4 days following admission	Decreased number of MBC

MAb, monoclonal antibody; MBC, memory B cell, NA, not assessed.

In a study from our centre located in Northern Italy, close to the first COVID-19 outbreak, and enrolling 66 patients admitted to an Internal Medicine ward, 87.3% of them were found to have IgM memory B cell depletion (defined as absolute counts of IgM^+ IgD^+ $CD27^+$ <26/microliter) as compared to 25 healthy volunteers. Splenectomy was an exclusion criterium for enrolment. Around 28% of patients died during the hospitalisation. Of note, all patients with adverse outcome were IgM memory B cell deficient and had an intervening infection. Interestingly, IgM memory B cell depletion had an independent prognostic effect on mortality, in the absence of other statistically associated prognostic factors, such as male sex, age, multimorbidity, and total peripheral lymphocyte depletion (36). Additionally, in a Chinese study enrolling hospitalised paediatric patients with mild COVID-19, a strong virus-specific IgM memory B cell response was observed regardless of age (31).

Taken together, these observations seem to associate IgM memory B cell changes with different COVID-19 severity states and outcomes. More precisely, a reduction of this subset correlates with more severe presentations and unfavourable outcomes, whereas a robust IgM memory B cell response is present in patients with a milder or more rapidly resolving forms of the disease.

To corroborate these clinical findings, the IgM memory B cell-mediated response has found to be beneficial in a hamster model of COVID-19. More precisely, 1212C2, a functional antibody derived from a IgM memory B cell line derived from a COVID-19 patient, was shown to exert a protective and preventive effect when administered intraperitoneally and through aerosolization (35).

Surprisingly, the analysis of RBD-specific IgA in COVID-19 patients has reserved little attention despite their likely protective role in the early phases of the viral infection. The following observations have been made in this regard. A cross-reactive human antibody against SARS-CoV and SARS-CoV-2 was found to have neutralizing properties against SARS-CoV-2 when converted to sIgA (39). Also, virus-specific IgA have been found at low titers in convalescent sera and are stable during an 8-month study follow-up (24). Finally, neutralizing IgA antibodies have also been detected for long periods in the saliva of previously infected patients (40). However, to the best of our knowledge, no study has ever evaluated whether IgM memory B cell-deficiency correlated with the depletion of virus-specific IgA at a mucosal level. All these findings may potentially have a clinical implication for stratifying the risk of severe and

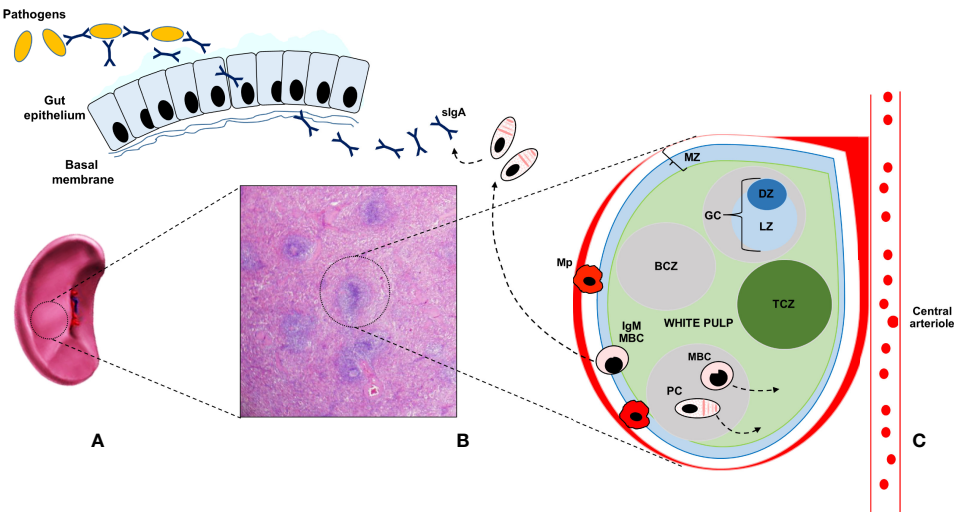

FIGURE 1 | The human splenic is depicted in **(A)**; whereas its histologic appearance is shown in **(B)** The main part of the splenic tissue is the red pulp, whereas the white pulp represents less than 25 percent of the volume. Antigens reach the spleen only through the blood stream, *via* the splenic artery (not depicted for clarity), since the spleen lacks lymphatic vessels. The white pulp is made up of multiple lymph node-like regions, which are embedded in the red pulp, without a capsule. In **(C)** the ultrastructure of the white pulp is represented. The white pulp is surrounded by a layer of innate cells, like specialized macrophages subsets (Mp), making up the marginal zone (MZ) in mice and the perifollicular zone in humans. Bridges channels connecting the red and white pulp are not shown for clarity. Within the white pulp, different compartments can be identified, such as the B cell zone (BCZ) and the T cell zone (TCZ), which in humans is also called periarteriolar lymphoid sheath (PALS). In the BCL, germinal centers (GC) are found. They comprise a dark zone (DZ) and a light zone (LZ). In the DZ, B cells undergo cell division and somatic hypermutation; in the LZ, B cells with productive rearrangements in their B cell receptor, present antigens to T cells and differentiate into memory B cells (MBC) and plasma cells (PC), during germinal center reactions. MBC display migratory features to the extrafollicular areas of the spleen, as suggested by the arrow, and reach lymph nodes *via* the blood. After antigen encounter, MBC give rise to antibody-secreting PC. MBC can also re-enter the GC to acquire increased affinity for the antigen. PC preferentially migrate to the bone marrow, where they constitutively secrete antibodies with a precise specificity. GC- and T- cell independent reactions are also depicted. IgM memory cells (IgM-MBC) arise outside GC, mainly in the MZ. In humans, IgM-MBC are migratory; their trafficking to the gut epithelium is suggested by means of a dashed arrow. In the gut, IgM MBC give rise to IgA-secreting PC, which mediate mucosal immune responses against bacteria and viruses, through the production and delivery up to the intestinal lumen of secretory IgA (sIgA).

disseminated COVID-19, even though the translational application in humans still need to be ascertained (2).

The knowledge of the natural evolution of the IgM memory B cell response in COVID-19 is still elusive. According to one study, virus specific IgM memory B cell counts appear stable at 3 months (15), whereas at week 31 their numbers are reduced according to another study (33). Additional prospective studies with longer follow-up are warranted to study the kinetic of the alteration in the IgM memory population and its clinical effects.

Moreover, the exact mechanisms underlying this deficit require further research. In addition to the COVID-19-mediated splenic hypofunction, other mechanisms may be implicated. In the acute setting, TNF, IL6 and other mediators of the cytokine storm, have been shown to influence B cell differentiation, activation and survival, leading to a complex B cell compartment alteration, with recruitment of more immature cells, such as transitional cells, as a consequence of mature B cell exhaustion (37).

Interestingly, a significant reduction (both relative and absolute) of $CD27^{dull}$ memory B cells, has been observed in individuals aged 60 and above (41). This population of memory B cells is largely of IgM isotype, arise in a GC- and T cell independent fashion, displays a reduced mutational status and is necessary for the production mucosal sIgA. This population bears great resemblance to the IgM memory B cells subset (25).

Advanced age is one the main recognized factors accounting for the increased mortality rate in hospitalized patients with COVID-19 which may be related to $CD27^{dull}$ memory B cell depletion in this subset of patients. COVID-19 may thus syndemically interact with pre-existing risk factors, such as age-related immune dysfunction, accounting for unfavourable outcomes (42, 43).

Taken together, these observations put forward the possibilities that the reduced IgM memory B cell pool in COVID-19 patients may be related to the COVID-19-related spleen damage and/or to the age-related B memory cell dysfunction, that may be already present in older patients suffering with COVID-19.

ASSESSING SPLEEN IMMUNE FUNCTION IN COVID-19

Spleen filtering function can be assessed by counting pitted red cells (PRC), i.e., erythrocytes with membrane alterations, the so-

called "pits", which are detectable under interference phase microscopy on peripheral blood samples (44, 45). A functional impairment is present when more than 4% PRC -out of 1000 counted red cells- are detected (46). This is often the case of disorders such as untreated or refractory celiac disease and other gastrointestinal immune-mediated disorders, such as inflammatory bowel disease, which are frequently characterised by functional hyposplenism (47). Given the association between the filtering and immune spleen function, the evaluation of the haemocatheretic ability of the spleen constitute a surrogate for the analysis of the immune function of the spleen (46).

In the aforementioned study comparing the median counts of IgM memory B cells and of PRC in acute COVID-19 patients, as opposed to hyposplenic and asplenic ones, no inverse correlation despite a reduction of memory B cells was found (36). This finding can be explained by the fact that in patients with acute COVID-19 the haemocateretic function of the spleen seems to be preserved and consequently no PRC increase is usually observed as opposed to its immune function, which appears to be precociously impaired, due to the selective virus-induced damage of the white-pulp and marginal zone as attested by the autoptic exam carried out in a subgroup of patient of our cohort (48). Consequently, the quantification of IgM memory B cells in patients with COVID-19 in the acute phase is the sole method for measuring the spleen immune function. At the same time, the long-term effects of COVID-19 on the IgM memory B compartment are not known at present.

CLINICAL AND THERAPEUTICAL IMPLICATIONS OF A DYSFUNCTIONAL IGM MEMORY B CELL RESPONSE

An intact IgM memory B cell response and spleen immune function seems to exert a relevant role in the acute setting of COVID-19 acting, as a first and broadly reactive defence system against SARS-CoV-2, possibly arising from previous contacts with related coronaviruses. At present, it is not known which is the optimal management for patients displaying a derangement in the IgM memory B cell response during or following COVID-19, particularly in terms of vaccination for encapsulated bacteria (49). Accordingly, it can be presumed that their care should be like that of splenectomised patients, but further studies are needed to assess the persistence of the immune deficit in the long run and the infectious risk of these patients. Therefore, prompt hospital admission and/or administration of anti-infective treatments should be advised in case of acute infections. Parallelly, in this subset of patients, vaccinal measures for SARS-CoV-2 appear vital, despite the fact that their efficacy of remains to be ascertained and that tailoring as to the type of vaccines, the timing of administration and the number of booster doses, is probably needed.

The only study available addressing the response to SARS-CoV-2 vaccines in asplenic patients is a cross-sectional study evaluating humoral titers to SARS-Cov-2 spike protein in patients with thalassemia mayor, also including splenectomized patients. Interestingly, splenectomized patients were found to have high titers of antibodies, comparable to healthy individuals. None of the patients was infected by COVID-19 during the 6-month follow-up (50).

OUTLOOK

Further studies on larger populations and registries are therefore awaited to develop diagnostic and management guidelines for patients with IgM B memory depletion and spleen dysfunction, this latter either associated with COVID-19 or pre-existent. More in depth, it is still undefined how to manage patients with a pre-existing spleen hypofunction, such as patients with CVID and other primary immunodeficiencies or immune-mediated or autoimmune gastrointestinal disorders, namely celiac disease and inflammatory bowel disease (28). It is in fact well known that these patients may be predisposed to the development of severe and invasive infections, such as invasive pneumococcal disease. Nonetheless, real-world evidence on COVID-19 in patients with coeliac disease or inflammatory bowel disease does not seem to point at a more severe viral infection compared to the general population (48, 51). To note, these patients were not stratified according to the presence or absence -and the quantification- of hyposplenism and IgM memory B cell depletion. All these issues should be the focus of future studies.

AUTHOR CONTRIBUTIONS

All authors significantly participated in the drafting of the manuscript or critical revision of the manuscript for important intellectual content and provided approval of the final submitted version. Individual contributions are as follows: CR wrote the manuscript, ML and SM reviewed the manuscript. AS reviewed the paper and made final critical revision for important intellectual contents.

FUNDING

Italian Ministry of Health. Grant number: Rete Aging-Project PROMISING, RCR-2021-23671216. PI of the project: ML.

ACKNOWLEDGMENTS

We thank Rete Aging-Italian Ministry of Health for supporting the study.

REFERENCES

1. Available at: https://covid19.who.int/.
2. Li H, Liu L, Zhang D, Xu J, Dai H, Tang N, et al. SARS-CoV-2 and Viral Sepsis: Observations and Hypotheses. *Lancet (London England)* (2020) 395:1517–20. doi: 10.1016/S0140-6736(20)30920-X
3. Hagemann K, Riecken K, Jung JM, Hildebrandt H, Menzel S, Bunders MJ, et al. Natural Killer Cell-Mediated ADCC in SARS-CoV-2-Infected Individuals and Vaccine Recipients. *Eur J Immunol* (2022) 2022:10.1002/eji.202149470. doi: 10.1002/EJI.202149470
4. Charfeddine S, Ibn Hadj Amor H, Jdidi J, Torjmen S, Kraiem S, Hammami R, et al. Long COVID 19 Syndrome: Is It Related to Microcirculation and Endothelial Dysfunction? Insights From TUN-EndCOV Study. *Front Cardiovasc Med* (2021) 0:745758. doi: 10.3389/FCVM.2021.745758
5. Zohar T, Loos C, Fischinger S, Atyeo C, Wang C, Slein MD, et al. Compromised Humoral Functional Evolution Tracks With SARS-CoV-2 Mortality. *Cell* (2020) 183:1508. doi: 10.1016/J.CELL.2020.10.052
6. Wang Y, Huo P, Dai R, Lv X, Yuan S, Zhang Y, et al. Convalescent Plasma may be a Possible Treatment for COVID-19: A Systematic Review. *Int Immunopharmacol* (2021) 91:107262. doi: 10.1016/J.INTIMP.2020.107262
7. Rouse BT, Sehrawat S. Immunity and Immunopathology to Viruses: What Decides the Outcome? *Nat Rev Immunol* (2010) 10:514–26. doi: 10.1038/nri2802
8. Nielsen SS, Vibholm LK, Monrad I, Olesen R, Frattari GS, Pahus MH, et al. SARS-CoV-2 Elicits Robust Adaptive Immune Responses Regardless of Disease Severity. *EBioMedicine* (2021) 68:103410. doi: 10.1016/J.EBIOM.2021.103410/ATTACHMENT/3DCD8421-E278-4FFB-856E-9EE5620A5E44/MMC3.DOCX
9. Khoury DS, Cromer D, Reynaldi A, Schlub TE, Wheatley AK, Juno JA, et al. Neutralizing Antibody Levels are Highly Predictive of Immune Protection From Symptomatic SARS-CoV-2 Infection. *Nat Med* (2021) 27:1205–11. doi: 10.1038/s41591-021-01377-8
10. Perotti C, Baldanti F, Bruno R, Del Fante C, Seminari E, Casari S. Mortality Reduction in 46 Severe Covid-19 Patients Treated With Hyperimmune Plasma. a Proof of Concept Single Arm Multicenter Trial. *Haematologica* (2020) 105(12):2834–40. doi: 10.3324/haematol.2020.261784
11. Ameratunga R, Longhurst H, Steele R, Lehnert K, Leung E, Brooks AES, et al. Common Variable Immunodeficiency Disorders, T-Cell Responses to SARS-CoV-2 Vaccines, and the Risk of Chronic COVID-19. *J Allergy Clin Immunol Pract* (2021) 9:3575. doi: 10.1016/J.JAIP.2021.06.019
12. Drabe CH, Hansen ABE, Rasmussen LD, Larsen OD, Møller A, Mogensen TH, et al. Low Morbidity in Danish Patients With Common Variable Immunodeficiency Disorder Infected With Severe Acute Respiratory Syndrome Coronavirus 2. *Infect Dis (London England)* (2021) 53:953–8. doi: 10.1080/23744235.2021.1957144
13. Allie SR, Bradley JE, Mudunuru U, Schultz MD, Graf BA, Lund FE, et al. The Establishment of Resident Memory B Cells in the Lung Requires Local Antigen Encounter. *Nat Immunol* (2019) 20:97–108. doi: 10.1038/S41590-018-0260-6
14. Available at: https://www.who.int/publications/i/item/WHO-2019-nCoV-therapeutics-2021.4.
15. Newell KL, Clemmer DC, Cox JB, Kayode YI, Zoccoli-Rodriguez V, Taylor HE, et al. Switched and Unswitched Memory B Cells Detected During SARS-CoV-2 Convalescence Correlate With Limited Symptom Duration. *PLoS One* (2021) 16):e0244855. doi: 10.1371/JOURNAL.PONE.0244855
16. Gaebler C, Wang Z, Lorenzi JCC, Muecksch F, Finkin S, Tokuyama M, et al. Evolution of Antibody Immunity to SARS-CoV-2. *Nature* (2021) 591 (7851):639–44. doi: 10.1038/s41586-021-03207-w
17. Wheatley AK, Juno JA, Wang JJ, Selva KJ, Reynaldi A, Tan HX, et al. Evolution of Immune Responses to SARS-CoV-2 in Mild-Moderate COVID-19. *Nat Commun* (2021) 12(1):1162. doi: 10.1038/S41467-021-21444-5
18. Li CK, Wu H, Yan H, Ma S, Wang L, Zhang M, et al. T Cell Responses to Whole SARS Coronavirus in Humans. *J Immunol* (2008) 181:5490–500. doi: 10.4049/JIMMUNOL.181.8.5490
19. Zhao J, Alshukairi AN, Baharoon SA, Ahmed WA, Bokhari AA, Nehdi AM, et al. Recovery From the Middle East Respiratory Syndrome Is Associated With Antibody and T-Cell Responses. *Sci Immunol* (2017) 2(14):eaan5393. doi: 10.1126/sciimmunol.aan5393
20. Williamson EJ, Walker AJ, Bhaskaran K, Bacon S, Bates C, Morton CE, et al. Factors Associated With COVID-19-Related Death Using OpenSAFELY. *Nature* (2020) 584:430–6. doi: 10.1038/S41586-020-2521-4
21. Duarte-Neto AN, Monteiro RAA, da Silva LFF, Malheiros DMAC, de Oliveira EP, Theodoro-Filho J, et al. Pulmonary and Systemic Involvement in COVID-19 Patients Assessed With Ultrasound-Guided Minimally Invasive Autopsy. *Histopathology* (2020) 77:186–97. doi: 10.1111/HIS.14160
22. Laidlaw BJ, Ellebedy AH. The Germinal Centre B Cell Response to SARS-CoV-2. *Nat Rev Immunol* (2022) 22:7–18. doi: 10.1038/S41577-021-00657-1
23. Woodruff MC, Ramonell RP, Nguyen DC, Cashman KS, Saini AS, Haddad NS, et al. Extrafollicular B Cell Responses Correlate With Neutralizingantibodies and Morbidity in COVID-19. *Nat Immunol* (2020) 21:1506. doi: 10.1038/S41590-020-00814-Z
24. Dan JM, Mateus J, Kato Y, Hastie KM, Yu ED, Faliti CE, et al. Immunological Memory to SARS-CoV-2 Assessed for Up to 8 Months After Infection. *Science* (2021) 371(6529):eabf4063. doi: 10.1126/SCIENCE.ABF4063
25. Carsetti R, Di Sabatino A, Rosado MM, Cascioli S, Piano Mortari E, Milito C, et al. Lack of Gut Secretory Immunoglobulin A in Memory B-Cell Dysfunction-Associated Disorders: A Possible Gut-Spleen Axis. *Front Immunol* (2020) 10:2937. doi: 10.3389/FIMMU.2019.02937
26. Rosado MM, Scarsella M, Pandolfi E, Cascioli S, Giorda E, Chionne P, et al. Switched Memory B Cells Maintain Specific Memory Independently of Serum Antibodies: The Hepatitis B Example. *Eur J Immunol* (2011) 41:1800–8. doi: 10.1002/EJI.201041187
27. Capolunghi F, Cascioli S, Giorda E, Rosado MM, Plebani A, Auriti C, et al. CpG Drives Human Transitional B Cells to Terminal Differentiation and Production of Natural Antibodies. *J Immunol* (2008) 180:800–8. doi: 10.4049/JIMMUNOL.180.2.800
28. Di Sabatino A, Carsetti R, Corazza GR. Post-Splenectomy and Hyposplenic States. *Lancet (London England)* (2011) 378:86–97. doi: 10.1016/S0140-6736(10)61493-6
29. Zhang YA, Salinas I, Li J, Parra D, Bjork S, Xu Z, et al. IgT, a Primitive Immunoglobulin Class Specialized in Mucosal Immunity. *Nat Immunol* (2010) 11:827–35. doi: 10.1038/NI.1913
30. Russell MW, Moldoveanu Z, Ogra PL, Mestecky J. Mucosal Immunity in COVID-19: A Neglected but Critical Aspect of SARS-CoV-2 Infection. *Front Immunol* (2020) 11:611337. doi: 10.3389/fimmu.2020.611337
31. Tian X, Bai Z, Cao Y, Liu H, Liu D, Liu W, et al. Evaluation of Clinical and Immune Responses in Recovered Children With Mild COVID-19. *Viruses* (2022) 14:85. doi: 10.3390/V14010085
32. Mazzoni A, Di Lauria N, Maggi L, Salvati L, Vanni A, Capone M, et al. First-Dose mRNA Vaccination is Sufficient to Reactivate Immunological Memory to SARS-CoV-2 in Subjects Who Have Recovered From COVID-19. *J Clin Invest* (2021) 131(12):e149150. doi: 10.1172/JCI149150
33. Anand SP, Prévost J, Nayrac M, Beaudoin-Bussières G, Benlarbi M, Gasser R, et al. Longitudinal Analysis of Humoral Immunity Against SARS-CoV-2 Spike in Convalescent Individuals Up to 8 Months Post-Symptom Onset. *Cell Rep Med* (2021) 2(6):100290. doi: 10.1016/J.XCRM.2021.100290
34. Yang J, Zhong M, Zhang E, Hong K, Yang Q, Zhou D, et al. Broad Phenotypic Alterations and Potential Dysfunction of Lymphocytes in Individuals Clinically Recovered From COVID-19. *J Mol Cell Biol* (2021) 13:197. doi: 10.1093/JMCB/MJAB014
35. Piepenbrink MS, Park JG, Oladunni FS, Deshpande A, Basu M, Sarkar S, et al. Therapeutic Activity of an Inhaled Potent SARS-CoV-2 Neutralizing Human Monoclonal Antibody in Hamsters. *Cell Rep Med* (2021) 2(3):100218. doi: 10.1016/J.XCRM.2021.100218
36. Lenti MV, Aronico N, Pellegrino I, Boveri E, Giuffrida P, Borrelli de Andreis F, et al. Depletion of Circulating IgM Memory B Cells Predicts Unfavourable Outcome in COVID-19. *Sci Rep* (2020) 10:20836. doi: 10.1038/S41598-020-77945-8
37. De Biasi S, Lo Tartaro D, Meschiari M, Gibellini L, Bellinazzi C, Borella R, et al. Expansion of Plasmablasts and Loss of Memory B Cells in Peripheral Blood From COVID-19 Patients With Pneumonia. *Eur J Immunol* (2020) 50:1283–94. doi: 10.1002/EJI.202048838
38. Martin V, Wu YC, Kipling D, Dunn-Walters DK. Age-Related Aspects of Human IgM(+) B Cell Heterogeneity. *Ann N Y Acad Sci* (2015) 1362:153–63. doi: 10.1111/NYAS.12823

39. Ejemel M, Li Q, Hou S, Schiller ZA, Tree JA, Wallace A, et al. A Cross-Reactive Human IgA Monoclonal Antibody Blocks SARS-CoV-2 Spike-ACE2 Interaction. *Nat Commun* (2020) 11(1):4198. doi: 10.1038/S41467-020-18058-8
40. Burgess S, Ponsford MJ, Gill D. Are We Underestimating Seroprevalence of SARS-CoV-2? *BMJ* (2020) 370:m3364. doi: 10.1136/BMJ.M3364
41. Ciocca M, Zaffina S, Fernandez Salinas A, Bocci C, Palomba P, Conti MG, et al. Evolution of Human Memory B Cells From Childhood to Old Age. *Front Immunol* (2021) 12:690534/BIBTEX. doi: 10.3389/FIMMU.2021.690534/BIBTEX
42. Corradini E, Ventura P, Ageno W, Cogliati CB, Muiesan ML, Girelli D, et al. Clinical Factors Associated With Death in 3044 COVID-19 Patients Managed in Internal Medicine Wards in Italy: Results From the SIMI-COVID-19 Study of the Italian Society of Internal Medicine (SIMI). *Intern Emerg Med* (2021) 16:1005–15. doi: 10.1007/S11739-021-02742-8
43. Zheng Y, Liu X, Le W, Xie L, Li H, Wen W, et al. A Human Circulating Immune Cell Landscape in Aging and COVID-19. *Protein Cell* (2020) 11:740. doi: 10.1007/S13238-020-00762-2
44. De Porto APNA, Lammers AJJ, Bennink RJ, Ten Berge IJM, Speelman P, Hoekstra JBL. Assessment of Splenic Function. *Eur J Clin Microbiol Infect Dis* (2010) 29:1465–73. doi: 10.1007/S10096-010-1049-1
45. Nardo-Marino A, Braunstein TH, Petersen J, Brewin JN, Mottelson MN, Williams TN, et al. Automating Pitted Red Blood Cell Counts Using Deep Neural Network Analysis: A New Method for Measuring Splenic Function in Sickle Cell Anaemia. *Front Physiol* (2022) 13:859906. doi: 10.3389/FPHYS.2022.859906
46. Riva MA, Ferraina F, Paleari A, Lenti MV, Di Sabatino A. From Sadness to Stiffness: The Spleen's Progress. *Intern Emerg Med* (2019) 14:739–43. doi: 10.1007/S11739-019-02115-2
47. Giuffrida P, Aronico N, Rosselli M, Lenti MV, Cococcia S, Roccarina D, et al. Defective Spleen Function in Autoimmune Gastrointestinal Disorders. *Intern Emerg Med* (2020) 15:225–9. doi: 10.1007/S11739-019-02129-W
48. Santacroce G, Lenti MV, Aronico N, Miceli E, Lovati E, Lucotti PC, et al. Impact of COVID-19 in Immunosuppressive Drug-Naïve Autoimmune Disorders: Autoimmune Gastritis, Celiac Disease, Type 1 Diabetes, and Autoimmune Thyroid Disease. *Pediatr Allergy Immunol* (2022) 33:105–7. doi: 10.1111/PAI.13646
49. Available at: https://www.cdc.gov/vaccines/schedules/hcp/imz/adult-conditions.html.
50. Anastasi E, Marziali M, Preziosi A, Berardelli E, Losardo AA, Ribersani M, et al. Humoral Immune Response to Comirnaty (BNT162b2) SARS-Cov2 mRNA Vaccine in Thalassemia Major Patients. *Microbes Infect* (2022) 104976. doi: 10.1016/J.MICINF.2022.104976
51. Bezzio C, Saibeni S, Variola A, Allocca M, Massari A, Gerardi V, et al. Outcomes of COVID-19 in 79 Patients With IBD in Italy: An IG-IBD Study. *Gut* (2020) 69:1213–7. doi: 10.1136/GUTJNL-2020-321411

Conflict of Interest: The authors declare that the research was conducted in the absence of any commercial or financial relationships that could be construed as a potential conflict of interest.

frontiers | Frontiers in Immunology

TYPE Original Research
PUBLISHED 10 August 2022
DOI 10.3389/fimmu.2022.943476

OPEN ACCESS

EDITED BY
Moncef Zouali,
Institut National de la Santéet de la Recherche Médicale (INSERM), France

REVIEWED BY
Alexander Filatov,
National Research Center Institute of Immunology, Federal Medical &Biological Agency of Russia, Russia
Fabio Fiorino,
University of Siena, Italy
Gabiria Pastore,
University of Siena, Italy

*CORRESPONDENCE
Ana-Luisa Stefanski
ana-luisa.stefanski@charite.de

SPECIALTY SECTION
This article was submitted to B Cell Biology, a section of the journal Frontiers in Immunology

RECEIVED 13 May 2022
ACCEPTED 08 July 2022
PUBLISHED 10 August 2022

CITATION
Stefanski A-L, Rincon-Arevalo H, Schrezenmeier E, Karberg K, Szelinski F, Ritter J, Chen Y, Meisel C, Jahrsdörfer B, Ludwig C, Schrezenmeier H, Lino AC and Dörner T (2022) Persistent but atypical germinal center reaction among 3rd SARS-CoV-2 vaccination after rituximab exposure.
Front. Immunol. 13:943476.
doi: 10.3389/fimmu.2022.943476

Persistent but atypical germinal center reaction among 3rd SARS-CoV-2 vaccination after rituximab exposure

Ana-Luisa Stefanski[1,2]*, Hector Rincon-Arevalo[1,2,3,4], Eva Schrezenmeier[2,3,5], Kirsten Karberg[6], Franziska Szelinski[1,2], Jacob Ritter[1,5], Yidan Chen[1,2], Christian Meisel[7], Bernd Jahrsdörfer[8,9], Carolin Ludwig[8,9], Hubert Schrezenmeier[8,9], Andreia C. Lino[2] and Thomas Dörner[1,2]

[1]Department of Rheumatology and Clinical Immunology, Charité Universitätsmedizin Berlin, Berlin, Germany, [2]Deutsches Rheumaforschungszentrum (DRFZ), Berlin, Germany, [3]Department of Nephrology and Medical Intensive Care, Charité Universitätsmedizin Berlin, Berlin, Germany, [4]Grupo de Inmunología Celular e Inmunogenética, Facultad de Medicina, Instituto de Investigaciones Médicas, Universidad de Antioquia (UdeA), Medellín, Colombia, [5]Berlin Institute of Health Charité Universitätsmedizin Berlin, Berlin Institute of Health (BIH) Academy, Berlin, Germany, [6]Rheumatology Outpatient Office RheumaPraxis Steglitz, Berlin, Germany, [7]Department of Medical Immunology, Charité University Medicine and Labor Berlin-Charité Vivantes, Berlin, Germany, [8]Institute of Transfusion Medicine, Ulm University, Ulm, Germany, [9]Institute for Clinical Transfusion Medicine and Immunogenetics, German Red Cross Blood Transfusion Service Baden-Württemberg – Hessen and University Hospital Ulm, Ulm, Germany

Background: Durable vaccine-mediated immunity relies on the generation of long-lived plasma cells and memory B cells (MBCs), differentiating upon germinal center (GC) reactions. SARS-CoV-2 mRNA vaccination induces a strong GC response in healthy volunteers (HC), but limited data is available about response longevity upon rituximab treatment.

Methods: We evaluated humoral and cellular responses upon 3rd vaccination in seven patients with rheumatoid arthritis (RA) who initially mounted anti-spike SARS-CoV-2 IgG antibodies after primary 2x vaccination and got re-exposed to rituximab (RTX) 1-2 months after the second vaccination. Ten patients with RA on other therapies and ten HC represented the control groups. As control for known long-lived induced immunity, we analyzed humoral and cellular tetanus toxoid (TT) immune responses in steady-state.

Results: After 3rd vaccination, 5/7 seroconverted RTX patients revealed lower anti-SARS-CoV-2 IgG levels but similar neutralizing capacity compared with HC. Antibody levels after 3rd vaccination correlated with values after 2nd vaccination. Despite significant reduction of circulating total and antigen-specific B cells in RTX re-exposed patients, we observed the induction of IgG+ MBCs upon 3rd vaccination. Notably, only RTX treated patients revealed a high amount of IgA+ MBCs before and IgA+ plasmablasts after 3rd vaccination. IgA+ B cells were not part of the steady state TT+ B cell pool. TNF-secretion

and generation of effector memory CD4 spike-specific T cells were significantly boosted upon 3rd vaccination.

Summary: On the basis of pre-existing affinity matured MBCs within primary immunisation, RTX re-exposed patients revealed a persistent but atypical GC immune response accompanied by boosted spike-specific memory CD4 T cells upon SARS-CoV-2 recall vaccination.

KEYWORDS

rituximab (RTX), SARS-CoV-2, vaccination, memory B cell (MBC), germinal center (GC)

Introduction

Durable humoral immune responses to vaccination require generation of long-lived memory B cells (MBCs) and bone marrow plasma cells (BMPCs), commonly differentiating upon germinal center (GC) reactions (1). If circulating antibodies fail to confer protection to exposure, MBCs drive the recall response by forming new antibody secreting plasma cells or reentering germinal centers for additional rounds of somatic hypermutation (SHM) (2). SARS-CoV-2 mRNA 2x vaccination induces a strong GC response in healthy volunteers (3), but circulating antibodies are waning over time (4), emphasizing the role of persisting long-lived MBCs in combating breakthrough infections and preventing severe courses of the disease (5).

Rheumatologists are faced with several questions regarding the effectiveness and durability of SARS-CoV-2 vaccination responses particularly in patients receiving anti-CD20 therapy with rituximab (RTX). These patients are at higher risk for poor COVID-19 associated outcomes (6, 7) as well as substantially diminished SARS-CoV-2 vaccination responses (8–10) and a higher incidence of severe breakthrough infections after vaccination (11, 12). It is known that waning immunogenicity upon primary vaccination can be successfully boosted by a 3rd homologous or heterologous mRNA vaccination associated with better COVID-19 outcomes in patients with autoimmune diseases (13, 14). However, longevity of immune responses in the context of RTX re-exposure still need to be delineated.

In this study we addressed the question about durability of vaccination-induced SARS-CoV-2 immune responses and induction of a secondary immune response in the context of restricted B cell availability upon rituximab re-exposure. Therefore, we assessed humoral as well as B and T cellular vaccination responses upon 3rd vaccination in RTX treated patients who initially mounted anti-spike SARS-CoV-2 IgG antibodies upon primary 2x vaccination (15) and got re-exposed to RTX 1-2 months after the second vaccination. As control for known long-lived induced immunity, we analyzed steady-state humoral and cellular tetanus toxoid (TT) immune responses.

Materials and methods

Study participants

RTX treated outpatients, who participated at our initial vaccination study (15) were screened for RTX treatment after the second vaccination. We identified 7 patients with rheumatoid arthritis [RA, according 2010 ACR Rheumatoid Arthritis Classification Criteria (16)], who received another course of RTX (1-2mg) treatment 1-2 months after the second SARS-CoV-2 vaccination. The patients were scheduled for a 3rd vaccination with BNT162b2, 6 months after 2nd vaccination according to federal state recommendations. We collected peripheral blood samples (EDTA anti-coagulated or serum-tubes, BD Vacutainersystem, BD Diagnostics, Franklin Lakes, NJ, USA) at 6 months (before 3rd vaccination) and at d21 boost (3-4 weeks after the 3rd vaccination). Ten RA patients receiving other therapies (RA group) and ten healthy controls (HC group) served as controls. TT antibody titers and antigen-specific B and T cells served as steady state control (last TT vaccination occurred 2-10 years before blood drawing). All participants gave written informed consent according to the approval of the ethics committee at the Charité University Hospital Berlin (EA2/010/21, EA4/188/20). Humoral vaccine response at d28 and d42 (Figures 2A, C), cellular data at d0 and d28 for total B cells, (Figure 3A), antigen specific (RBD+) B cells (Figures 3D, E) and at d28 for antigen specific T cells Figures 5A, C, D) have been partially previously published (15, 17).

Enzyme-linked immunosorbent assay for SARS-CoV-2 and TT as well as surrogate SARS-CoV-2 neutralization test (GenScript)

The Euroimmun anti-SARS-CoV-2 assay is a classical enzyme-linked immunosorbent assay (ELISA) for the detection of IgG to the S1 domain of the SARS-CoV-2 spike (S) protein and IgG to the SARS-CoV-2 nucleocapsid (NCP) protein. The assay was performed according to the manufacturer´s instructions, as described (15). Briefly, serum samples were diluted at 1:100 in sample buffer and pipetted onto single wells of a 96-well microtiter plate, precoated with recombinant SARS-CoV-2 spike or nucleocapsid proteins. A calibrator, a positive control and a negative control were carried out on each plate. After incubation for 60 minutes at 37°C, wells were washed 3 times and the peroxidase-labelled anti-IgG antibody solution was added, followed by a second incubation step of 30 min. After three additional washing steps, substrate solution was added and the samples were incubated for 15 - 30 minutes in the dark. After adding the stop solution, optical density (OD) values were measured on a POLARstar Omega plate reader (BMG Labtech, Ortenberg, Germany) at 450 nm and at 620 nm. Finally, OD ratios were calculated based on the sample and calibrator OD values. An OD-ratio of ≥ 1.1 was considered to be positive for all analytes. IgG OD-ratio of ≥ 1.1 defines humoral seroconversion. Dilutions of 1:10 were prepared when values were close to the saturation point of the respective ELISA.

The Immunoassay for determination of TT (VaccZyme Tetanus-Toxoid IgG kit; The Binding Site) vaccine titer in serum was performed according to the manufacturers' instructions. A level > 0.1 IU/ml is considered protective.

The blocking ELISA GenScript qualitatively detects anti-SARS-CoV-2 antibodies suppressing the interaction between the receptor binding domain (RBD) of the viral spike glycoprotein (S) and the angiotensin-converting enzyme 2 (ACE2) protein on the surface of cells, as described (17). Scores < 30% were considered negative, scores ≥ 30% were considered positive (linear quantitative range).

Isolation of peripheral blood mononuclear cells and staining

PBMCs were prepared by density gradient centrifugation using Ficoll-Paque PLUS (GE Healthcare Bio-Sciences, Chicago, IL, USA). PBMCs before and after 3rd vaccination were cryopreserved at -80°. Cells were thawed, washed twice in pre-warmed RPMI1640 medium [containing 0.3 mg/ml glutamine, 100 U/ml penicillin, 0.1 mg/ml streptomycin, 10% FCS and 25 U/ml DNase I (Roche International)] and stained as described (15). To identify RBD-specific and TT-specific B cells, respectively, recombinant purified RBD (DAGC149, Creative Diagnostics, New York, USA) and TT (peptides & elephants GmbH, Hennigsdorf, Germany) were labeled with either AF647 or AF488. Double positive cells were considered antigen-specific as reported. A blocking experiment using unlabeled RBD or TT respectively in 100-fold concentration was used to ensure specificity of detection as reported (15, 18). For intracellular staining after T cell stimulation cells were first stained for 30 min with 1:1000 BUV395 Life/Dead (Invitrogen) in PBS, followed by 5 min 2.5 µl Fc Block (Milteny Biotech) in 50 µl resuspended cells. Cells were fixed in LyseFix (Becton Dickinson), permeabilized with FACS Perm II Solution (Becton Dickinson) and intracellularly stained.

Peptide stimulation for antigen specific T cells

2x10^6 frozen PMBC from 8 HC, 8 RA control and 7 RTX were used per stimulation condition. Cells were thawed, washed twice in pre-warmed RPMI1640 medium (containing 0.3 mg/ml glutamine, 100 U/ml penicillin, 0.1 mg/ml streptomycin, 10% FCS and 25 U/ml DNase I (Roche International), rested for 1 h in culture medium (RPMI1640 with glutamine, antibiotics and 10% FCS) and stimulated with SARS-CoV2 spike ("PepMix" SARS-CoV-2 (S B.1.1.7), JPT, Berlin, Germany) or with TT peptide pool (peptides&elephants, Henningsdorf, Germany) or 50ng/ml PMA (SigmaAldrich) with 1µg/ml Ionomycin (SigmaAldrich) for 16 h. Brefeldin A (10 µg/ml, SigmaAldrich) was added after 2 h. Due to cell number limitations, T cell PMA/Ionomycin stimulation was not carried out for all participants. As previously shown, CD4 T cells co-expressing CD154 and CD137 were considered antigen-specific (15, 19). Spike-specific CD8 T cells were identified based on activation-dependent co-expression of CD137 and IFNγ. We defined responders as those with at least a twofold increase in frequency after stimulation compared with unstimulated controls.

Flow cytometry analysis

All flow cytometric analyses were performed using a BD FACS Fortessa (BD Biosciences, Franklin Lakes, NJ, USA). To ensure comparable mean fluorescence intensities (MFIs) over time of the analyses, Cytometer Setup and Tracking beads (CST beads, BD Biosciences, Franklin Lakes, NJ, USA) and Rainbow Calibration Particles (BD Biosciences, Franklin Lakes, NJ, USA) were used. For flow cytometric analysis, the following fluorochrome-labeled antibodies were used: BUV737 anti-CD11c (BD, clone B-ly6), BUV395 anti-CD14 (BD, clone M5E2), BUV395 anti-CD3 (BD, clone UCHT1), BV786 anti-CD27 (BD, clone L128), BV711 anti-CD19 (BD, clone SJ25C1),

BV605 anti-CD24 (BD, clone ML5), BV510 anti-CD10 (BD, clone HI10A), BV421 anti-CXCR5 (BD, clone RF8B2), PE-CF594 anti-IgD (Biolegend, San Diego, CA, USA, clone IA6-2), APC-Cy7 anti-CD38 (Biolegend, clone HIT2), PE-Cy7 anti-IgG (BD, clone G18-145), anti-IgA-Biotin (BD, clone G20-359), BV650 anti-IgM (BD, clone MHM-88), FITC anti-TNFα (Biolegend, clone Mab11), BV650 anti-IFNγ (BD, clone 4S.B3), BV786 anti-CD40L (Biolegend, clone 24-31), PE-CF594 anti-CD137 (Biolegend, clone 4B4-1). Numbers of absolute B and T cells were measured with Trucount (BD) and samples were processed according to the manufacturer's instruction.

Data analysis

All samples included in the final analyses had at least 1×10^6 events with a minimum threshold for CD19+ cells of 5,000 events apart from RTX patients (minimal recorded CD19+ events in the RTX group were 24 and 30 events respectively, out of > 1 Mio total recorded events. Flow cytometric data were analyzed by FlowJo software 10.7.1 (TreeStar, Ashland, OR, USA). For UMAP analysis of antigen-specific CD19+ B cells flow cytometry data of all study participants was pre-gated on RBD+ and TT+ CD19+ B cells respectively, concatenated and clustered by CD27, IgD, CD38, CD24, IgM, IgG, IgA. As settings we selected the Euclidean distance function, nearest neighbor value of 15 and a minimum distance of 0.5.

Statistics

GraphPad Prism Version 5 (GraphPad software, San Diego, CA, USA) was used for statistical analysis. Statistical analysis was conducted as indicated in respective figure legends. For longitudinal analysis Friedman test with Dunn´s post-test was applied. For group comparison Kruskal-Wallis with Dunn´s post-test was used. Wilcoxon matched-pairs signed rank test was applied for paired analysis. Correlation was evaluated using the Spearman test. P-values < 0.05 were considered significant.

Results

Cohorts and patient characteristics

We included 7 RTX treated RA patients, who received rituximab between 2nd and 3rd vaccination (RTX group), 10 RA patients on other therapies (RA group) and 10 healthy controls (HC group) in this study. In addition to the collected data before 3rd vaccination (6 months) and 3 weeks after 3rd vaccination (d21 boost), we also show data of a prior study (15) including d0 (before 1st vaccination), d7 (7 days after 1st vaccination), d28 (7 days after 2nd vaccination) and d42 (3 weeks after 2nd vaccination). The complete study design is summarized in Figure 1. The majority of study participants (22/27, 81,5%) were 3x-vaccinated with the mRNA vaccine BNT162b2. HC were younger (median 55 years old) than the patient groups (RA median 75 years old, RTX median 67 years old) and the majority of patients were female (HC 50%, RA 70% and RTX 100%, respectively). At the time of 3rd vaccination, RTX patients had received B cell depleting therapy on average for 6.5 years and median time since the last RTX treatment was 5 months. Notably, 5/7 RTX treated patients did not have any treatment combination with disease-modifying antirheumatic drugs (DMARDs). Demographics and co-medication of all study participants are summarized in Table 1 (detailed in Supplementary Table S1). To identify previously SARS-CoV-2 infected individuals or post-vaccination breakthrough infections, we measured antibodies against the nucleocapsid protein (NCP). Here 2 RTX patients were identified with positive anti-NCP IgG before first vaccination (Supplementary Figure S1A and as indicated in red in the manuscript figures), No breakthrough infections were recorded throughout the study in all groups (Supplementary Figure S1A).

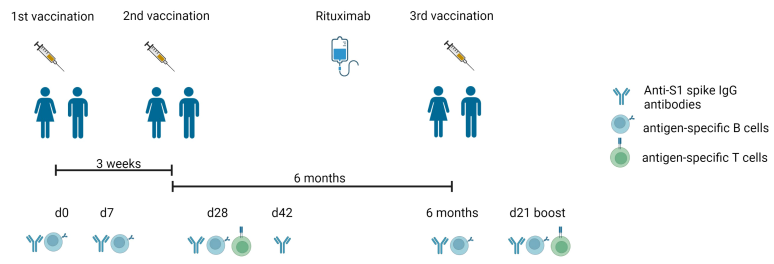

FIGURE 1
Experimental design of the vaccination study. Timeline describing the three-dose vaccination schedule of BNT162b2 mRNA vaccine, blood drawing (d0, d7, d28, d42, 6 months, d21 boost), and RTX treatment between 2nd and 3rd vaccination. Anti-S1 spike IgG antibodies, antigen-specific T and B cells were measured as mentioned. Created with BioRender.com.

TABLE 1 Patient characteristics.

	HC n = 10	RA n = 10	RTX n = 7
Age			
Median [IQR]	55 [41.25 – 61.5]	75 [65 – 79.5]	67 [63 – 73.5]
Under 40	3	1	0
Between 40-69	6	3	4
> 70	1	6	3
Gender			
Female	5	7	7
Male	5	3	0
Vaccines (n)			
3x BNT162b2	8	9	5
2x mRNA-1273, 1x BNT162b2	0	0	1
2x ChAdOx1, 1x BNT162b2	0	1	1
1x ChAdOx1, 2x BNT162b2	2	0	0
Immunosuppression (n)			
MTX		7	1
Leflunomid		1	0
Sulfasalazin		0	1
JAKI		2	0
TNFI		1	0
Abatacept		1	0
Prednisolone		1 (4mg/d)	1 (7.5mg/d)
Months since last RTX			
Median [IQR]			5 [5 – 6]
Years on RTX			
Median [IQR]			6.5 [2.75 – 6.5]

Antibody levels after 2nd vaccination predict humoral response upon 3rd vaccination

Mean trajectory values of antibody responses and their surrogate neutralizing capacity to SARS-CoV-2 vaccines were assessed in the RTX group (after excluding the two pre-infected patients) and compared with HC and RA group (Figures 2A, B). Individual values of all RTX patients (including the two pre-infected patients), RA and HC groups are shown in Supplementary Figures S1B-D. All patients showed neutralizing IgG seroconversion 3 weeks after 2nd vaccination (d42). 6 months after 2nd vaccination there was a clear decline of antibody levels and surrogate neutralisation capacity in all cohorts. However, 6 months after 2nd vaccination and d21 after 3rd vaccination, RTX treated patients revealed the lowest surrogate neutralisation capacity compared with HC and RA group (Figure 2B). Other than in the RTX group, IgG levels and neutralizing capacity of HC and RA patients on other therapies were significantly boosted upon 3rd vaccination (Figures 2A, B). On individual level, 6 months after 2nd vaccination only 3/7 RTX treated patients (including the two previously SARS-CoV-2 infected patients) still revealed neutralizing IgG titres, while two more patients seroconverted upon 3rd vaccination (Supplementary Figure S2B). Upon 3rd vaccination we observed significant lower titres while no difference regarding neutralizing capacity among seroconverted RTX patients compared to HC (Figure 2C). With regard to steady state control antibodies, anti-TT antibody titers revealed no differences between the groups (Figure 2D). In all groups there was a direct correlation between the level of anti-S1 IgG antibodies after 3rd with the one after 2nd vaccination (Figure 2E), suggesting that pre-existing memory predicts subsequently humoral response after boost independently upon RTX treatment.

Diminished circulating total and antigen-specific B cells upon RTX treatment

Total B cell numbers were assessed at different time points in RTX treated patients (Figure 3A) and compared with HC and RA after 2nd and 3rd vaccination (Figure 3B). As expected, subsequent treatment with rituximab led to a significant decrease of B cell counts compared with the control groups RA and HC (Figures 3A, B). Before the 3rd vaccination, naïve B cells had still the highest frequencies of circulating B cells in RTX treated patients. However, we observed an increased frequency of CD27+IgD- switch-memory B cells compared with d0 (Figure 3C, gating strategy in Supplementary Figure S2A).

Next, we studied SARS-CoV-2 specific B cells over time using flow cytometry to quantify receptor-binding domain (RBD) and as internal control, circulating steady state TT specific B cells (gating strategy in Supplementary Figure S2A). In the RTX group the highest RBD+ B cell induction was found at d28 (7 days after 2nd vaccination) compared to lower levels upon RTX treatment and B cell depletion (Figure 3D). Other than in RTX group and similar to anti-spike IgG trajectory, RA patients showed a significant enhancement of antigen-specific B cells upon boost vaccination (Figure 3E). The number of circulating antigen-specific TT+ B cells was also significantly lower after RTX treatment compared with HC and RA at d21 after boost (Figure 3F).

Induction of IgG+ memory B cells upon 3rd vaccination despite peripheral B cell depletion

To identify subsets and specific immunoglobulin characteristics of RBD+ B cells, we implemented a high-dimensional flow cytometry analysis of circulating RBD+ B cell subpopulations before and after 3rd vaccination (and as control TT+ B cells at steady state) using Uniform Manifold Approximation and Projection (UMAP). Clusters corresponding

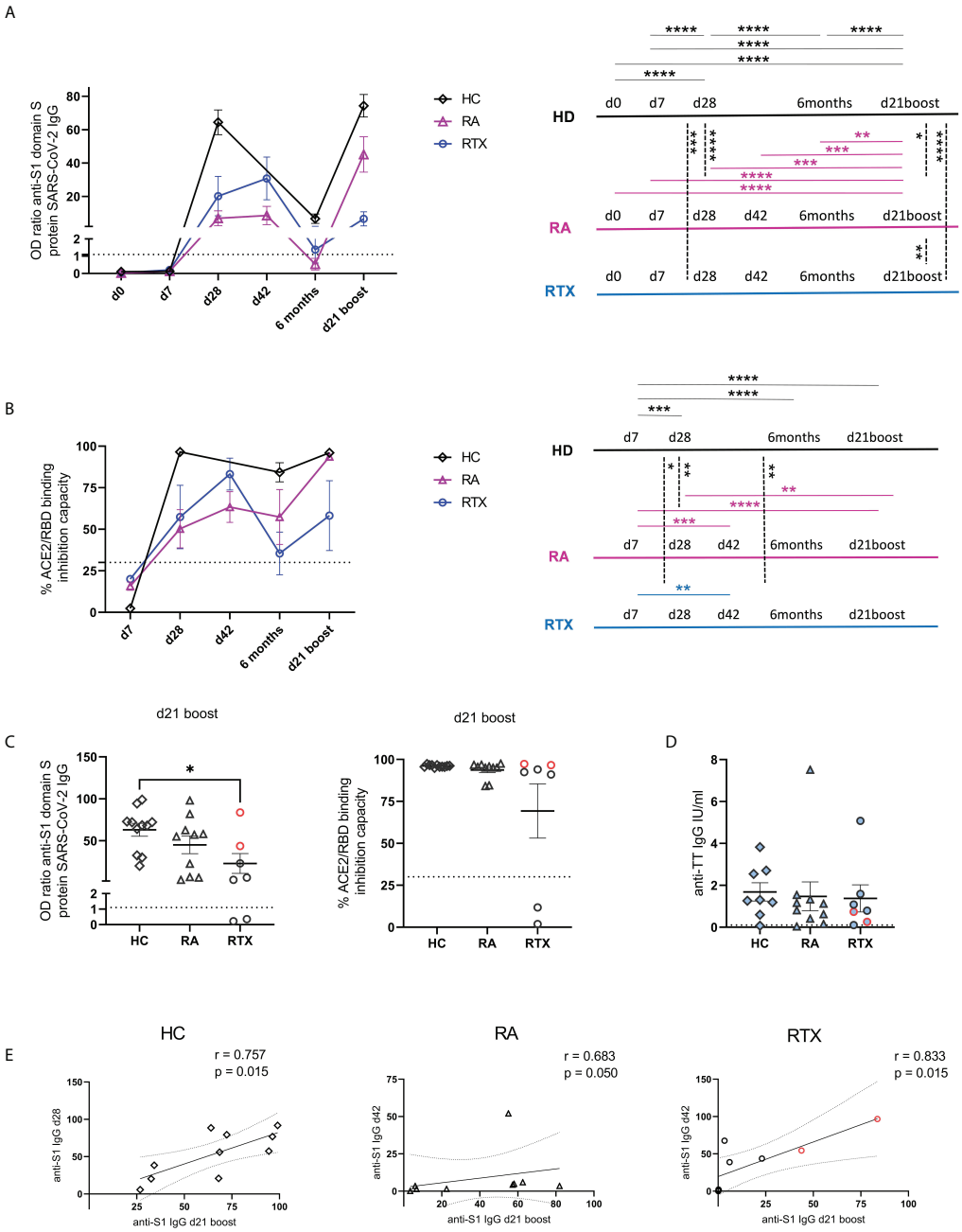

FIGURE 2
Trajectory of humoral response upon anti-SARS-CoV-2 vaccination. Humoral immune response against SARS-CoV-2 for spike protein S1 IgG **(A)** and surrogate neutralization **(B)** over time in HC (n=10), RA group (n=10) and RTX treated patients (n=5, the two pre-infected patients are excluded). Threshold for positive test is indicated by dotted lines. The results of the statistical tests are depicted on the right. Humoral immune response against SARS-CoV-2 for spike protein S1 IgG, surrogate neutralization **(C)** and anti-TT IgG titers **(D)** at d21 boost in HC (n=10), RA (n=10) and RTX (n=7). Correlation between anti-spike S1 IgG at d28 (HD)/d42 (RA and RTX) with anti-S1 levels at d21 boost **(E)**. Mean with SEM **(A-D)**. Two way ANOVA with Šidák's post-test **(A, B)**. Kruskal-Wallis with Dunn´s post-test **(C, D)**. Spearman test **(E)**. *p < 0.05, **p < 0.01, ***p < 0.001, ****p < 0.0001. Color code: previously infected individuals are indicated in red; control TT results are indicated by blue filled circles.

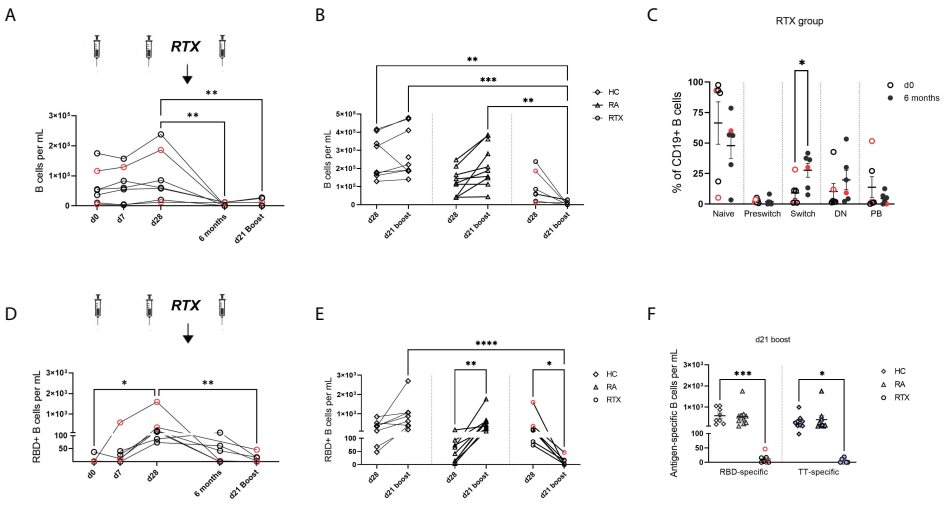

FIGURE 3
Trajectory of total B cells and antigen-specific B cells upon SARS-CoV-2 vaccination in RTX treated patients. **(A)** Total B cell counts over time in the RTX group (n=7). **(B)** Comparison of total B cell numbers between HC (n=10), RA (n=10) and RTX (n=7) at d28 and d21 boost. **(C)** B cell subset distribution at d0 and 6 months (before 3rd vaccination) in the RTX group (n=7). **(D)** Absolute numbers of RBD+ B cells over time in the RTX group (n=7). **(E)** Absolute numbers of RBD+ cells at d28 compared with d21 boost in HC (n=10), RA (n=10) and RTX (n=7). **(F)** Absolute numbers of RBD+ B cells at d21 boost compared with TT+ B cells in HC, RA and RTX. Friedman test with Dunn´s post-test. **(A, D)**. Kruskal-Wallis with Dunn´s post-test **(B, E, F)**. Mann Whitney test for each subset performed **(C)**. *p < 0.05, **p < 0.01, ***p < 0.001, ****p < 0.0001. Color code: previously infected individuals are indicated in red; control TT results are indicated by blue filled circles. DN, "double negative" CD27+IgD- B cells; PB, plasmablasts.

to distinct subsets of CD19+ B cells (Figure 4A) were defined as: naïve (CD27-IgD+), pre-switch memory (CD27+IgD+), switch memory (CD27+IgD-) and plasmablasts (PB, CD27+CD38+, distribution of key markers shown in Supplementary Figure 2B). Switch-memory B cells and PBs clustered according to immunoglobulin specificities IgA, IgM and IgG, respectively. Data of clusters gated in each donor group are shown in Figure 4B (individual distribution in Supplementary Figure S2C, mean values in Supplementary Figure S2D). In HC, RBD+ B cells 6 months after 2nd vaccination and TT+ B cells during steady state showed a similar subset distribution. Pre-switch and switch-memory B cells accounted for more than half of all antigen-specific B cells, followed in frequencies by naïve B cells, while PBs made up less than 2% of circulating antigen-specific B cells. Upon 3rd vaccination there was an enhanced differentiation of RBD+ B cells into IgG+ memory B cells and PBs.

Other than in HC, the majority of RBD+ B cells in RA before 3rd vaccination consisted of naïve cells and RA patients had a higher frequency of circulating TT+ PBs. After 3rd vaccination there was a relevant enhancement of IgG+ switch memory B cells and PBs in RA. However, and distinct to HC, the RA patients showed also a substantial increase in IgM+ PB and switch memory RBD+ B cells, suggesting a delayed immune response in immunosuppressed RA patients (Figure 4B).

Relevant differences were found among the RTX patients, although the number of antigen-specific B cells was limited. The predominant subset consisted of plasmablasts: TT+ and RBD+ PBs before vaccination were mostly IgG specific, followed by IgM in TT+ and IgA in RBD+ B cells. Upon 3rd vaccination we observed a relevant increase in IgG+ class-switched memory B cells to the detriment of naïve B cells, but no obvious difference in the magnitude of plasmablasts compared to RBD+ before vaccination and steady state TT+ cells. Of note, only RTX treated patients revealed a high amount of IgA+ memory B cells before 3rd vaccination with induction of IgA+ plasmablasts upon boost, suggesting a persistent but atypical germinal center activity (Figure 4B).

Memory formation and cytokine production of spike-specific T cells is boosted by 3rd vaccination in RTX patients

Next, we addressed the question if T cell reactivity can be boosted in B cell depleted patients upon 3rd vaccination. Therefore, we assessed induction, memory formation and cytokine production of spike-specific CD4 and CD8 T cells upon 2nd and 3rd vaccination in RTX treated patients. As previously described, antigen-reactive CD4+ T cells were identified based on co-expression of CD154 and CD137, and antigen-reactive CD8+ T cells by co-expression of CD137 and IFNγ ((15, 19), gating strategy Supplementary Figures 3A, B). In a first step, assessment of CD4+, CD8+ and TfH-like

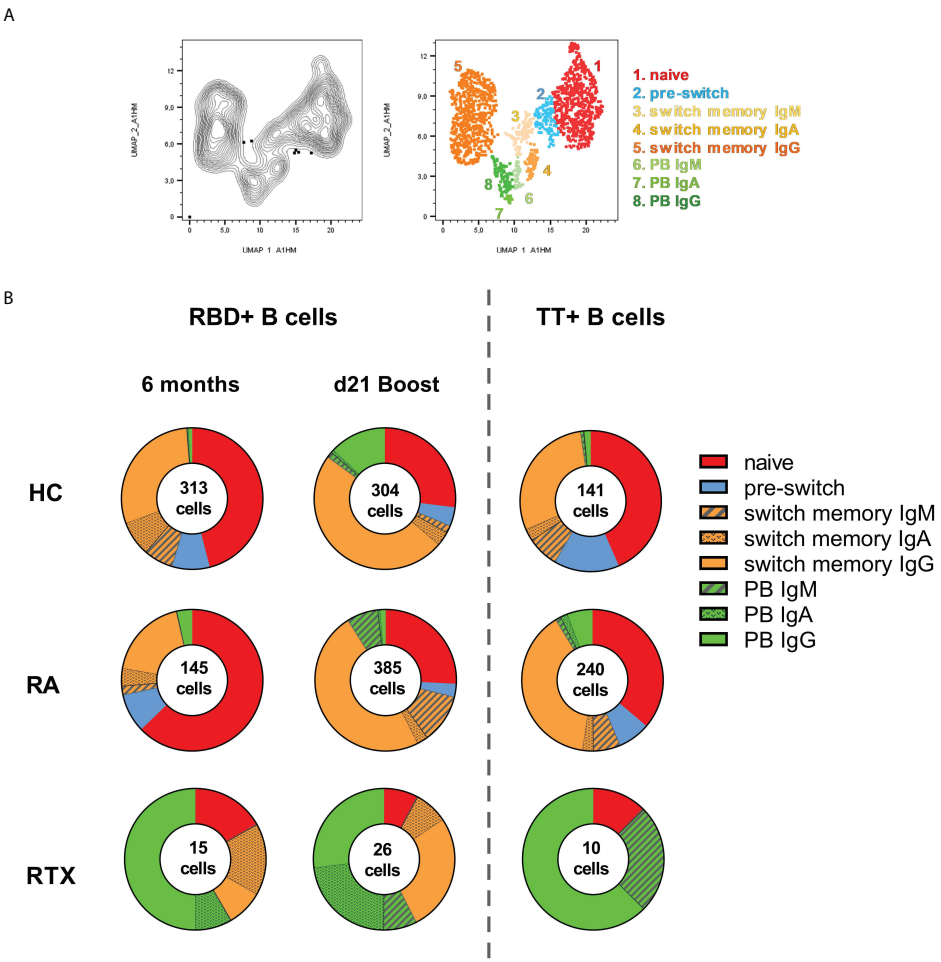

FIGURE 4
Distinct B cell subsets before and after 3rd SARS-CoV-2 vaccination. UMAP (Uniform manifold approximation and projection for dimension reduction) clustering was performed on a concatenated file of pre-gated antigen specific (RBD+ together with TT+) CD19+ B cells composed of total 1579 events. **(A)** Cluster overlay of B cells of all groups for subset identification. **(B)** Distribution of clusters before and after 3rd vaccination, as well as for TT+ B cells in HD, RA and RTX.

(CXCR5+PD1+) total cell numbers did not show any differences between the cohorts (Supplementary Figure S3C). While there was also no significant difference regarding total cell counts (Figure 5A) and proliferation (Figure 5B) of CD4+ antigen-specific T cells between 2nd and 3rd vaccination, we observed a significant increase in TNFα secretion (Figure 5C) accompanied by the tendency for higher IFNγ production (Figure 5D) of spike-specific CD4 T cells upon boost. Notably, spike-specific effector memory CD4 T cells (TEM, CD27-CD45RA-) were significantly increased upon 3rd vaccination, followed by a concomitant decrease in naïve (CD27+CD45RA+) and terminal differentiated TEMRA (CD27-CD45RA+) CD4 T cell frequencies (Figure 5E). When we looked also into the subset distribution upon TNFα and IFNγ secreting spike-specific CD4 T cells, we saw a similar pattern, with highest frequencies upon the TEM subpopulation (Supplementary Figure S3D). Analyzing spike-specific CD8+ T cells, we did not observe any difference regarding total numbers, proliferation and subset distribution of antigen-specific CD8+ T cells between 2nd and 3rd vaccination (Supplementary Figures 3E, F).

Regarding TT+ T cells, total numbers (Figure 5A) and proliferation (Figure 5B) of TT+ CD4 cells were significantly lower in RTX patients compared with HC, but similar when compared with RA group, suggesting rather a disease than a therapy specific effect. TNFα-secretion was significantly higher after 3rd SARS-CoV-2 vaccination in HC and RTX groups than upon TT stimulation at steady state (Figure 5C), likely related to the more recent vaccine challenge by SARS-CoV-2. Spike-specific and TT-specific CD8+ responses showed similar pattern in all groups.

Discussion

In the current study we could show that patients re-exposed to RTX after successfully seroconversion upon 2x SARS-CoV-2 vaccination, reveal a persistent but atypical germinal center activity within recall vaccination. Germinal centers are lymphoid structures in which B cells acquire affinity-enhancing somatic hypermutations, differentiating into memory B cells and long-lived bone marrow plasma cells (BMPCs) and providing durable protective immunity upon infection or vaccination (1)). Extrafollicular activation does not seem to play a significant role upon SARS-CoV-2 mRNA vaccination in healthy, but may be part of the dysfunctional immune response upon vaccination in immunocompromised patients (20). With respect to primary 2x anti-SARS-CoV-2 vaccination, we have previously shown that RTX treated patients carrying a minimum of peripheral B cell repopulation, are able to mount antigen-specific MBCs and plasmablasts comparable with HC, suggesting GC formation and possible generation of long-lived MBCs (15). In line with this, recently published data report similar durability of IgG anti-spike antibodies 6 months after primary immunization in seroconverted patients with anti-CD20 treatments compared with healthy volunteers (21). In our RTX cohort we saw persistent antibody titers for TT at steady state and in some patients also for SARS-CoV-2 at 6 months, suggesting the continued presence of long-lived antigen-specific antibody-secreting cells in the bone marrow regardless of peripheral B cell depletion (21–24).

Interestingly, despite lower SARS-CoV-2 antibody level upon 3rd vaccination, neutralization capacity was similar between seroconverted RTX patients and HC. This fine-tuning of high-affinity antibodies appears to be a direct result of somatic hypermutation (25), which seems functional also in RTX treated patients and may be effected either by still available newly

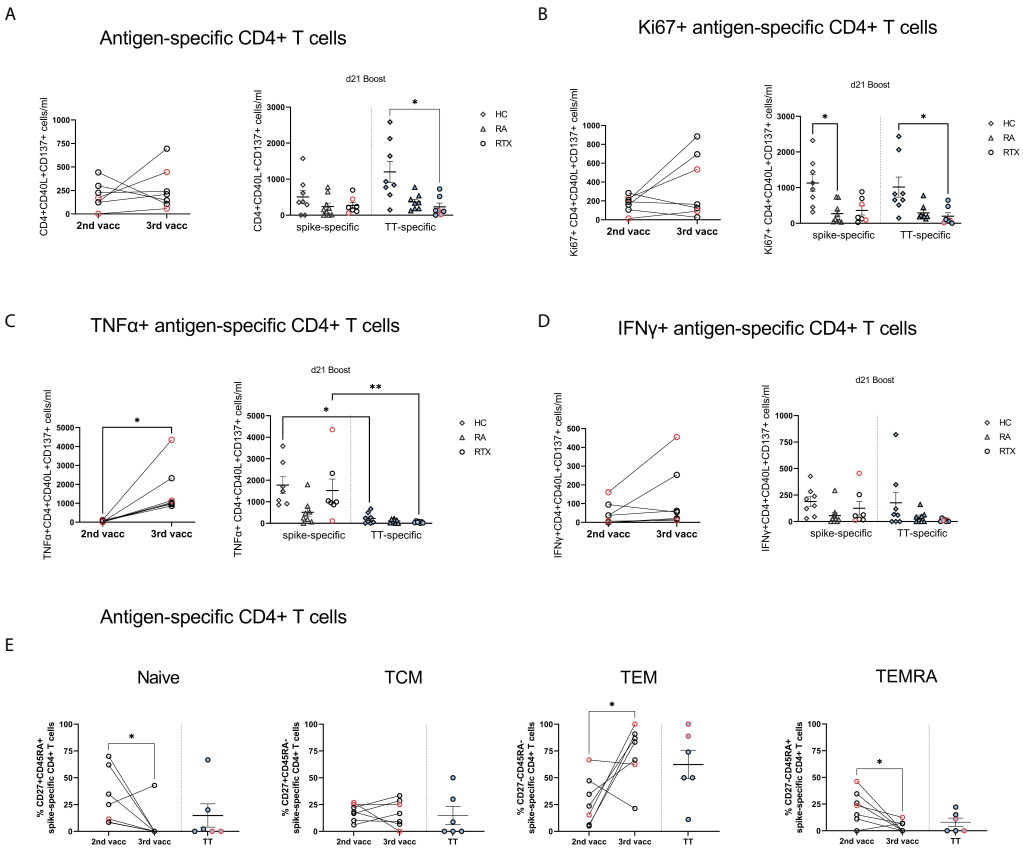

FIGURE 5
Antigen-specific T cells upon 2nd compared with 3rd SARS-CoV-2 vaccination in RTX treated patients. **(A)** Absolute counts **(A)**, Ki67 expression **(B)**, TNFα expression **(C)**, IFNγ expression **(D)** and subset distribution **(E)** of spike-specific CD4+ T cells after 2nd compared with 3rd vaccination in RTX treated patients (n=7). Comparison of spike-specific and TT-specific responses in HC (n=8), RA (n=8) and RTX (n=7) at d21 boost. Mann Whitney test performed for comparisons between 2nd and 3rd vaccination data **(A-E)**. Kruskal-Wallis with Dunn´s post-test for comparisons between the groups **(A-D)**. *p < 0.05, **p < 0.01. Color code: previously infected individuals are indicated in red; control TT results are indicated by blue filled circles. TCM, central memory T cells; TEM, effector memory T cells; TEMRA, terminally differentiated memory T cells.

recruited peripheral B cells or by preformed MBCs reentering germinal centers. Moreover, we observed a direct correlation between anti-spike SARS-CoV-2 antibody values after 2nd with the ones after 3rd vaccination, suggesting that also upon RTX re-exposure, induction strength of the immune response within recall vaccination, is largely related to pre-existing memory formation. In support of this notion, the highest antibody responses occurred in the two previously infected patients, who may have also mounted stronger germinal centre activation with consecutively long-lived memory.

In line with this, persistent antigen-specific MBCs 6 months after primary immunization could be recorded in the circulation despite RTX treatment, moreover, we observed also an expansion of IgG+ memory B cells upon 3rd vaccination. However, the majority of RBD+ and TT+ B cells in RTX treated patients consisted of IgG+ plasmablasts, which may have escaped depletion due to low CD20 expression or have been recently induced in lymphoid tissues without detectable precursors. Notably, only RTX treated patients revealed a high amount of IgA+ memory B cells before 3rd vaccination with induction of IgA+ plasmablasts upon boost. A subset of circulating IgA+ plasmablasts and plasma cells with mucosal characteristics has been previously described to be resistant to B cell depletion upon RTX treatment (22). Moreover, in healthy volunteers, transient IgA-dominant plasmablast response to the BNT162b2 mRNA vaccine is recently reported predominantly after the first vaccination dose and is consistent with a cross-reactive recall response of mucosal MBCs (26). The induction of IgA+ plasmablasts upon boost observed only in the context of limited peripheral B cell availability suggests atypical B cell mobilization from either tissue resident cross-reactive MBCs and/or within naïve mucosal lymphoid follicles/extrafollicular resident B cells. This disturbed GC reaction seems independent upon T cell functions, since in RTX patients we observed significant boosted cytokine secretion and differentiation to effector memory spike-specific CD4 T cells as well as TfH cell counts comparable with HC within 3rd vaccination.

Our data provide also interesting insights about the delayed GC immune response in RA patients on therapies other than RTX. 6 months after the second vaccination the majority of RBD+ B cells in RA consisted of naïve cells, suggesting an insufficient GC activation after the first two injections lacking long-term memory. Upon 3rd vaccination, RA showed a significant boost of antibody levels and circulating RBD+ B cells in parallel with induction of IgG+ RBD+ memory B cells and plasmablast differentiation comparable with the HC group. Nevertheless, other than in HC, RBD+ memory B cells and plasmablasts of RA patients showed also a substantial increase in IgM+ expression upon boost, reflecting a delayed isotype switching in this immunosuppressed population.

The main limitation of the study is the low patient number and limited B cell counts in the RTX cohort included into the analysis. Two of the RTX patients got previously infected and may have mounted stronger long-lived immune responses, which may be a confounder in the analysis. However, we provide a comprehensive data set regarding trajectories of humoral and cellular B and T cell responses over time including steady state findings of TT. Noteworthy, 5/7 of the RTX treated patients did not have other additional immunosuppressive drugs, which excludes co-medication as confounding factor.

Herein, we describe for the first time humoral and cellular responses upon 3rd SARS-CoV-2 injection in patients re-exposed to RTX after initially seroconversion upon primary vaccination. While functional aspects of spike-specific CD4 T cells are boosted upon 3rd vaccination, we report a persistent but atypical germinal center activity, possibly supported by (semi-primary and/or) additional extrafollicular responses in patients re-exposed to RTX as potential compensatory mechanisms employed in such medically induced B cell impairment.

Data availability statement

The raw data supporting the conclusions of this article will be made available by the authors, without undue reservation.

Ethics statement

The studies involving human participants were reviewed and approved by the ethics committee at the Charité University Hospital Berlin (EA2/010/21, EA4/188/20). The patients/participants provided their written informed consent to participate in this study.

Author contributions

The concept of the study was developed by A-LS, ACL, and TD. Patient's samples were collected by KK, A-LS and JR. Data were obtained by A-LS, HR-A, FS, JR, YC, BJ, HS and CL. Data were analyzed by A-LS, HR-A and ACL. The theoretical framework was developed by TD, ES, A-LS and ACL. The work was supervised by ACL and TD. All authors developed, read, and approved the current manuscript.

Funding

A-LS is funded by a grant from the German Society of Rheumatology. HR-A holds a scholarship of the COLCIENCIAS scholarship No. 727, 2015. ES received a grant from the Federal Ministry of Education and Research (BMBF) (BCOVIT, 01KI20161). ES is participant in the BIH-Charité Clinician Scientist Program funded by the Charité Universitätsmedizin

Berlin and the Berlin Institute of Health. JR is supported by a MD scholarship from the Berlin Institute of Health (BIH). HS received funding from the Ministry for Science, Research and Arts of Baden-Württemberg, Germany (CORE-Project) and the European Commission (HORIZON2020 Project SUPPORT-E, no. 101015756). YC is supported by a state scholarship fund organized by China Scholarship Council. TD received funding by the German Research Foundation (DFG) by projects TRR 130/project 24, Do491/7-5, Do 491/10-1.

Conflict of interest

The authors declare that the research was conducted in the absence of any commercial or financial relationships that could be construed as a potential conflict of interest.

Publisher's note

Supplementary material

The Supplementary Material for this article can be found online at: https://www.frontiersin.org/articles/10.3389/fimmu.2022.943476/full#supplementary-material

References

1. Tarlinton D, Radbruch A, Hiepe F, Dörner T. Plasma cell differentiation and survival. *Curr Opin Immunol* (2008) 20(2):162–9. doi: 10.1016/j.coi.2008.03.016

2. Mesin L, Schiepers A, Ersching J, Barbulescu A, Cavazzoni CB, Angelini A, et al. Restricted clonality and limited germinal center reentry characterize memory b cell reactivation by boosting. *Cell* (2020) 180(1):92–106.e11. doi: 10.1016/j.cell.2019.11.032

3. Kim W, Zhou JQ, Horvath SC, Schmitz AJ, Sturtz AJ, Lei T, et al. Germinal centre-driven maturation of b cell response to mRNA vaccination. *Nature* (2022) 604(7904):141–5. doi: 10.1038/s41586-022-04527-1

4. Goldberg Y, Mandel M, Bar-On YM, Bodenheimer O, Freedman L, Haas EJ, et al. Waning immunity after the BNT162b2 vaccine in Israel. *N Engl J Med* (2021) 385(24):e85. doi: 10.1056/NEJMoa2114228

5. Terreri S, Piano Mortari E, Vinci MR, Russo C, Alteri C, Albano C, et al. Persistent b cell memory after SARS-CoV-2 vaccination is functional during breakthrough infections. *Cell Host Microbe* (2022) 30(3):400–8.e4. doi: 10.1016/j.chom.2022.01.003

6. Strangfeld A, Schäfer M, Gianfrancesco MA, Lawson-Tovey S, Liew JW, Ljung L, et al. Factors associated with COVID-19-related death in people with rheumatic diseases: Results from the COVID-19 global rheumatology alliance physician-reported registry. *Ann Rheum Dis* (2021) 80(7):930–42. doi: 10.1136/annrheumdis-2020-219498

7. Jones JM, Faruqi AJ, Sullivan JK, Calabrese C, Calabrese LH. COVID-19 outcomes in patients undergoing b cell depletion therapy and those with humoral immunodeficiency states: A scoping review. *Pathog Immun* (2021) 6(1):76–103. doi: 10.20411/pai.v6i1.435

8. Schietzel S, Anderegg M, Limacher A, Born A, Horn MP, Maurer B, et al. Humoral and cellular immune responses on SARS-CoV-2 vaccines in patients with anti-CD20 therapies: A systematic review and meta-analysis of 1342 patients. *RMD Open* (2022) 8(1):e002036. doi: 10.1136/rmdopen-2021-002036

9. Felten R, Gallais F, Schleiss C, Chatelus E, Javier RM, Pijnenburg L, et al. Cellular and humoral immunity after the third dose of SARS-CoV-2 vaccine in patients treated with rituximab. *Lancet Rheumatol* (2022) 4(1):e13–e6. doi: 10.1016/S2665-9913(21)00351-9

10. Jyssum I, Kared H, Tran TT, Tveter AT, Provan SA, Sexton J, et al. Humoral and cellular immune responses to two and three doses of SARS-CoV-2 vaccines in rituximab-treated patients with rheumatoid arthritis: A prospective, cohort study. *Lancet Rheumatol* (2022) 4(3):e177–e87. doi: 10.1016/S2665-9913(21)00394-5

11. Lawson-Tovey S, Hyrich KL, Gossec L, Strangfeld A, Carmona L, Raffeiner B, et al. SARS-CoV-2 infection after vaccination in patients with inflammatory rheumatic and musculoskeletal diseases. *Ann Rheum Dis* (2022) 81(1):145–50. doi: 10.1136/annrheumdis-2021-221217

12. Cook C, Patel NJ, D'Silva KM, Hsu TY-T, DiIorio M, Prisco L, et al. Clinical characteristics and outcomes of COVID-19 breakthrough infections among vaccinated patients with systemic autoimmune rheumatic diseases. *Ann Rheum Dis* (2022) 81(2):289–91. doi: 10.1136/annrheumdis-2021-221326

13. Bieber A, Sagy I, Novack L, Brikman S, Abuhasira R, Ayalon S, et al. BNT162b2 mRNA COVID-19 vaccine and booster in patients with autoimmune rheumatic diseases: A national cohort study. *Ann Rheum Dis* (2022) 81(7):1028–35. doi: 10.1136/annrheumdis-2021-221824

14. Wieske L, van Dam KPJ, Steenhuis M, Stalman EW, Kummer LYL, van Kempen ZLE, et al. Humoral responses after second and third SARS-CoV-2 vaccination in patients with immune-mediated inflammatory disorders on immunosuppressants: A cohort study. *Lancet Rheumatol* (2022) 4(5):e338–e50. doi: 10.1016/S2665-9913(22)00034-0

15. Stefanski AL, Rincon-Arevalo H, Schrezenmeier E, Karberg K, Szelinski F, Ritter J, et al. B cell numbers predict humoral and cellular response upon SARS-CoV-2 vaccination among patients treated with rituximab. *Arthritis Rheumatol* (2022) 74(6):934–47. doi: 10.1002/art.42060

16. Aletaha D, Neogi T, Silman AJ, Funovits J, Felson DT, Bingham CO3rd, et al. 2010 Rheumatoid arthritis classification criteria: An American college of Rheumatology/European league against rheumatism collaborative initiative. *Arthritis Rheum* (2010) 62(9):2569–81. doi: 10.1002/art.27584

17. Stefanski A-L, Rincon-Arevalo H, Schrezenmeier E, Karberg K, Szelinski F, Ritter J, et al. B cell characteristics at baseline predict vaccination response in RTX treated patients. *Front Immunol* (2022) 13. doi: 10.3389/fimmu.2022.822885

18. Rincon-Arevalo H, Choi M, Stefanski A-L, Halleck F, Weber U, Szelinski F, et al. Impaired humoral immunity to SARS-CoV-2 BNT162b2 vaccine in kidney transplant recipients and dialysis patients. *Sci Immunol* (2021) 6(60):eabj1031. doi: 10.1126/sciimmunol.abj1031

19. Sattler A, Angermair S, Stockmann H, Heim KM, Khadzhynov D, Treskatsch S, et al. SARS–CoV-2–specific T cell responses and correlations with COVID-19 patient predisposition. *J Clin Invest* (2020) 130(12):6477–89. doi: 10.1172/JCI140965

20. Lederer K, Bettini E, Parvathaneni K, Painter MM, Agarwal D, Lundgreen KA, et al. Germinal center responses to SARS-CoV-2 mRNA vaccines in healthy and immunocompromised individuals. *Cell* (2022) 185(6):1008–24.e15. doi: 10.1016/j.cell.2022.01.027

21. Sidler D, Born A, Schietzel S, Horn MP, Aeberli D, Amsler J, et al. Trajectories of humoral and cellular immunity and responses to a third dose of mRNA vaccines against SARS-CoV-2 in patients with a history of anti-CD20 therapy. *RMD Open* (2022) 8(1):e002166. doi: 10.1136/rmdopen-2021-002166

22. Mei HE, Frölich D, Giesecke C, Loddenkemper C, Reiter K, Schmidt S, et al. Steady-state generation of mucosal IgA+ plasmablasts is not abrogated by b-cell depletion therapy with rituximab. *Blood* (2010) 116(24):5181–90. doi: 10.1182/blood-2010-01-266536

23. Ramwadhdoebe TH, van Baarsen LGM, Boumans MJH, Bruijnen STG, Safy M, Berger FH, et al. Effect of rituximab treatment on T and b cell subsets in lymph node biopsies of patients with rheumatoid arthritis. *Rheumatol (Oxford)* (2019) 58 (6):1075–85. doi: 10.1093/rheumatology/key428

24. St Clair EW. Good and bad memories following rituximab therapy. *Arthritis Rheumatol* (2010) 62(1):1–5. doi: 10.1002/art.25039

25. Victora GD, Nussenzweig MC. Germinal centers. *Annu Rev Immunol* (2012) 30:429–57. doi: 10.1146/annurev-immunol-020711-075032

26. Brewer RC, Ramadoss NS, Lahey LJ, Jahanbani S, Robinson WH, Lanz TV. BNT162b2 vaccine induces divergent b cell responses to SARS-CoV-2 S1 and S2. *Nat Immunol* (2022) 23(1):33–9. doi: 10.1038/s41590-021-01088-9

frontiers | Frontiers in Immunology

TYPE Original Research
PUBLISHED 11 August 2022
DOI 10.3389/fimmu.2022.945021

OPEN ACCESS

EDITED BY
Marko Radic,
University of Tennessee College of Medicine, United States

REVIEWED BY
Valentina Gentili,
University of Ferrara, Italy
Jeroen den Dunnen,
Academic Medical Center, Netherlands

*CORRESPONDENCE
Magdalena Plebanski
magdalena.plebanski@rmit.edu.au

†These authors have contributed equally to this work

SPECIALTY SECTION
This article was submitted to B Cell Biology, a section of the journal Frontiers in Immunology

RECEIVED 16 May 2022
ACCEPTED 20 July 2022
PUBLISHED 11 August 2022

CITATION
Moody R, Sonda S, Johnston FH, Smith KJ, Stephens N, McPherson M, Flanagan KL and Plebanski M (2022) Antibodies against Spike protein correlate with broad autoantigen recognition 8 months post SARS-CoV-2 exposure, and anti-calprotectin autoantibodies associated with better clinical outcomes.
Front. Immunol. 13:945021.
doi: 10.3389/fimmu.2022.945021

Antibodies against Spike protein correlate with broad autoantigen recognition 8 months post SARS-CoV-2 exposure, and anti-calprotectin autoantibodies associated with better clinical outcomes

Rhiane Moody[1], Sabrina Sonda[2,3], Fay H. Johnston[4,5], Kylie J. Smith[4,5], Nicola Stephens[6], Michelle McPherson[6], Katie L. Flanagan[1,2,3†] and Magdalena Plebanski[1*†]

[1]School of Health and Biomedical Science, STEM College, RMIT University, Bundoora, VIC, Australia, [2]Tasmanian Vaccine Trial Centre, Clifford Craig Foundation, Launceston General Hospital, Launceston, TAS, Australia, [3]School of Health Sciences and School of Medicine, University of Tasmania, Launceston, TAS, Australia, [4]Public Health Services, Department of Health, Tasmania, TAS, Australia, [5]Menzies Institute for Medical Research, University of Tasmania, Hobart, TAS, Australia, [6]Tasmanian School of Medicine, University of Tasmania, Hobart, TAS, Australia

Autoantibodies to multiple targets are found during acute COVID-19. Whether all, or some, persist after 6 months, and their correlation with sustained anti-SARS-CoV-2 immunity, is still controversial. Herein, we measured antibodies to multiple SARS-CoV-2 antigens (Wuhan-Hu-1 nucleoprotein (NP), whole spike (S), spike subunits (S1, S2 and receptor binding domain (RBD)) and Omicron spike) and 102 human proteins with known autoimmune associations, in plasma from healthcare workers 8 months post-exposure to SARS-CoV-2 (n=31 with confirmed COVID-19 disease and n=21 uninfected controls (PCR and anti-SARS-CoV-2 negative) at baseline). IgG antibody responses to SARS-CoV-2 antigens were significantly higher in the convalescent cohort than the healthy cohort, highlighting lasting antibody responses up to 8 months post-infection. These were also shown to be cross-reactive to the Omicron variant spike protein at a similar level to lasting anti-RBD antibodies (correlation r=0.89). Individuals post COVID-19 infection recognised a common set of autoantigens, specific to this group in comparison to the healthy controls. Moreover, the long-term level of anti-Spike IgG was associated with the breadth of autoreactivity post-COVID-19. There were further moderate positive correlations between anti-SARS-CoV-2 responses and 11 specific autoantigens. The most commonly recognised autoantigens were found in the COVID-19 convalescent cohort. Although there was no overall correlation in self-reported symptom severity and anti-SARS-CoV-2 antibody levels, anti-calprotectin antibodies were associated with return to healthy normal life 8 months post infection. Calprotectin was also the most common target for

autoantibodies, recognized by 22.6% of the overall convalescent cohort. Future studies may address whether, counter-intuitively, such autoantibodies may play a protective role in the pathology of long-COVID-19.

KEYWORDS

SARS-CoV-2, COVID-19, antibodies, autoimmunity, autoantibodies

1 Introduction

Coronavirus Disease-19 (COVID-19), caused by severe acute respiratory syndrome coronavirus-2 (SARS-CoV-2) can result in a range of clinical outcomes and manifestations (1–3). Although rare, an aspect of these manifestations includes various autoimmune and autoimmune-like diseases, such as Guillain-Barré syndrome, multisystem inflammatory syndrome and systemic lupus erythematosus (SLE) [reviewed in (4)]. In addition to these autoimmune-like diseases, there is a growing number of people with long-COVID or post-COVID-19 syndrome, which emerging studies suggest have immune and autoimmune factors in aetiology (5–8).

Antibody responses to the Spike, S1, RBD and Nucleoprotein of SARS-CoV-2 have been shown to last up to a year post disease (9–12). In the initial months post infection, studies report the antibody responses to multiple SARS-CoV-2 antigens (13, 14), however, less is known about the pattern of persistence to multiple antigens, within the same individuals, post 6 months. During the acute phase of infection, the level of antibody responses has been reported to be associated with disease severity, where those with more severe disease had greater antibody levels (13, 15). Contradictory evidence exists on their persistence, with this association reported by some (16–18), but not all (19, 20) studies to continue post-disease. Additionally, reports on the level of the long-term anti-SARS-CoV-2 responses and associations to clinical outcomes are few, although current studies suggest they have no impact on long-COVID (8, 16, 21). With multiple variants emerging since the beginning of the pandemic, understanding cross-reactive immune responses based on prior infection is important for understanding protection against newer variants. Prior infection with Wuhan variant can result in cross-reactive antibodies to the Beta, Delta and Gamma variants (22), and neutralising antibody responses of different variants occur based on shared spike mutations (23). Of latest concern is the Omicron variant and subvariants. The initial Omicron variant (B.1.1.529) was found to escape neutralisation from pre-exposed serum, as well as recipients of 2 mRNA vaccine doses, and instead required a third vaccine dose (23). However, antibodies to the Omicron spike protein have been reported in response to vaccinations (24). To our knowledge, persistence of cross-reactive antibodies, irrespective of neutralisation, between an earlier Wuhan infection and Omicron, without intervening vaccination, has not been investigated.

The presence of autoantibodies to various autoantigens has been described in COVID-19 patients (25–27). There are reports of severe COVID-19 cases with autoantibodies to SSA/Ro (25), cardiolipin (26), beta 1 glycoprotein I (β1GP1) (26) as well as positive antinuclear antibodies (ANAs) (25, 26). Bastard et al. additionally reported autoantibodies to type I interferons (IFNs) in COVID-19 patients, which were associated with acute severe but not mild disease (27). Protein microarrays have additionally been used to identify autoantibody responses on a larger scale, to antigens both with and without known autoimmune associations (28–30). Emerging studies have assessed large-scale autoantibody responses up to six (29) or eight (5) months post-infection. However, to our knowledge, there are no studies comparing the broad range of autoantibodies present in healthy individuals compared to individuals with persistent sequelae following a single natural challenge event; or the association of reactivity or autoreactivity to multiple SARS-CoV-2 antigens, 8 months post exposure with different clinical outcomes.

In the present study, microarray chips consisting of 102 known autoantigens and 6 SARS-CoV-2 antigens were used to measure the IgG antibody responses in plasma samples from COVID-19 convalescent individuals and uninfected controls. Collected 8 months after a single exposure event with the original Wuhan-Hu-1 variant, we sought to further explore lasting anti-SARS-CoV-2 antibody responses and the potential long-term association of autoreactive immunity with COVID-19 responses.

2 Materials and methods

2.1 Clinical cohort

Between 20th March and 13th April 2020, a COVID-19 outbreak occurred at two co-located hospitals and associated health care services in Tasmania, Australia (31). By the end of

the outbreak there were 138 cases including 80 healthcare workers. Healthcare workers (n=1,779), including clinical and non-clinical staff, who worked at the two hospitals during the outbreak were invited to complete an online survey. The survey collected a variety of information including demographic details, if they had COVID-19, and symptoms experienced during the outbreak period of 20th March to 10th May 2020 which includes the 14 days after completion of the compulsory quarantine period.

During December 2020, approximately eight months after the outbreak, 88 participants attended a study clinic, where they gave a blood sample and completed another questionnaire, again reporting on symptoms experienced during 20th March to 10th May 2020, the severity of their symptoms during the outbreak and if they were feeling back to normal. The symptoms data from this survey was used only if the symptom question was not answered in the earlier online survey. Plasma from the whole blood samples collected was isolated using standardised Ficoll-gradient separation and stored at -80 degrees Celsius prior to use. Following the control of this outbreak, no community transmission of COVID-19 occurred in Tasmania until December 2021 (32). Based on PCR data available, the present study used plasma from 31 PCR confirmed positives and corresponding 30 PCR confirmed negatives for SARS-CoV-2 infection.

This study was conducted according to the guidelines of the Declaration of Helsinki and approved by Tasmanian Health and Medical Human Research Ethics Committee (HREC, #21786) and all participants provided prior written informed consent.

2.2 Autoantibody profiling

Antibody responses were analysed using the OmicsArray™ Antigen Microarray Profiling Services by GeneCopoeia (Rockville, Md). IgG specific responses to antigen targets on the Human Coronavirus-associated Autoimmunity (PA012) array were measured. Experimental protocol and data processing were provided by GeneCopoeia and were as follows:

2.2.1 Experimental protocol

Array slides were blocked (room temperature (RT), 30 minutes) and washed 2x with phosphate buffered saline solution-Tween-20 (PBST, 5 minutes). Plasma samples diluted in PBST were added to wells of the slide (RT, 1 hour). After sample incubation arrays were washed with PBST, followed by blocking buffer, then PBST once more for 5 minutes each. After washing, anti-human IgG (Cy3-conjugated) antibodies (1:1000 in PBST) were added and incubated at RT for 1 hour. After incubation, arrays were washed with PBST (3x), PBS (2x) and finally nuclease-free water (2x), for 5 minutes per wash, before being spun down. From the addition of plasma samples, all incubation steps were performed on a shaker.

2.2.2 Array image capture and data processing

Fluorescent signals were acquired using the GenePix 4000B microarray scanner, using 532nm channel to scan Cy3 fluorescence. To obtain the raw data, including foreground and background signals, and the signal to noise ratio (SNR), fluorescent signal was analysed using the GenePix™Pro v7.0 software. The net fluorescence intensity (NFI), representing the foreground median minus the background median, was calculated and the SNR and flags used to filter data. The net fluorescent value was calculated by subtracting the value of the PBS control. Robust linear model (RLM) normalization was performed to normalize the NFI of each sample (represented as NSI-Nor).

2.3 Statistical analysis

Antibody responses were considered positive if the NSI-Nor value was greater than the average plus three standard deviations of the negatives. Initial screening identified 9 uninfected control donors who were positive to at least one SARS-CoV-2 antigen. These were excluded from further analysis and were not included in the results section (final uninfected control cohort, n=21). Statistical significance was assessed using GraphPad Prism (v9.3.1). Where indicated in figure legends, NSI-Nor values were log transformed and normality distribution tested by the Anderson-Darling test, prior to assessing significance. For correlation analysis, Pearson's correlation analysis was performed on log transformed NSI-Nor values and Spearman's correlation on NSI-Nor values, where indicated. A heatmap was created in R Studio (2022.02.01), using the pretty heatmaps ('pheatmap') package.

3 Results

3.1 Clinical characteristics of cohort

In the present study, plasma samples were collected from healthcare workers, who were either previously SARS-CoV-2 PCR negative (n=21) or PCR positive (n=31), 8 months post an outbreak (Table 1). The COVID-19 convalescent cohort consisted of 25 females (80.6%) and 6 males (19.4%) with a median age of 48 years (range: 28-66 years). Additional clinical information such as co-morbidities for COVID-19 and other medical conditions were available for 26 individuals. Amongst these, 10 (38.5%) recorded at least one co-morbidity, including one with diabetes. Additionally, 3 (11.5%) individuals reported other medical conditions. Within the PCR negative cohort, 16

10.3389/fimmu.2022.945021

TABLE 1 Clinical characteristics of study cohort.

	COVID-19 Convalescent (n=31)	Negatives (n=21)
Gender	F (25, 80.6%) M (6, 19.4%)	F (16, 76.2%) M (5, 23.8%)
Age Median (range)	48 (28-66)	50 (31-65)
Co-morbidities	38.5% (10/26)	41.2% (7/17)
Asthma	3.85 (1/26)	5.9% (1/17)
Chronic respiratory disease (excluding asthma)	0	0
Heart disease (excluding high blood pressure)	3.85 (1/26)	5.9% (1/17)
High blood pressure	0	5.9% (1/17)
Immunosuppressive condition/therapy	3.85 (1/26)	0
Diabetes	3.85 (1/26)	5.9% (1/17)
Obesity (BMI >30 kg/m^2)	23.1% (6/26)	17.6% (3/17)
Liver disease	0	0
Kidney disease	0	0
Neurological disorder	0	5.9% (1/17)
Pregnant during the period 20th March to 13th April 2020	0	5.9% (1/17)
Other medical conditions	11.5% (3/26)	23.5% (4/17)

individuals (76.2%) were female, and the median age was 50 years (range: 31-65 years). COVID-19 co-morbidities and other medical conditions were available for 17 individuals, seven of whom, reported the presence of a COVID-19 co-morbidity, including one with diabetes. Four people additionally recorded other medical conditions.

Where information was available, those who tested positive for COVID-19 also self-reported the degree of their symptom severity and the symptoms they had during the outbreak period, where symptom severity was defined as mild (able to perform usual daily activities), moderate (decreased ability to conduct usual activities) or severe (unable to conduct usual daily activities and/or admitted to hospital for care) (Table 2). Additionally, they indicated whether they felt back to normal or not since their infection. Most of the present cohort had either mild (40%) or moderate (43.3%) symptom severity, covering a range of symptoms. The most common symptom was a headache (73.3%), followed by altered sense of taste or smell (56.7%). 16 individuals within the cohort (55.2%) noted that they felt back normal post their infection period.

3.2 Anti-spike and anti-nucleoprotein IgG responses remain high up to eight months post initial exposure

IgG antibody responses to five SARS-CoV-2 antigens, Nucleoprotein (NP), whole Spike (S), Spike S1 (S1), Receptor Binding Domain (RBD) and Spike S2 (S2), were measured and compared between the COVID-19 negative and convalescent cohorts (Figure 1A). Confirming previous reports of lasting antibody responses up to 12 months post infection (9, 10), a significant increase of antibody levels to the NP, S and S subunits was found in the COVID-19 convalescent cohort in comparison to uninfected individuals. We then compared the responses to each of the SARS-CoV-2 targets within the convalescent group (Figure 1B). A greater spread of responses was observed to NP, S1 and RBD, suggesting a potential decrease over time, in comparison to anti-S and -S2 responses, which remained high. Pearson R correlation analysis was performed to identify how the responses were related to each of the antigens (Figure 1C). Strong positive correlations were identified between the anti-S and S subunits. The strongest correlation was between S and S2 (r=0.95), indicating that the lasting antibody responses to the spike protein are most likely to be targeting the S2 region. Similarly, the anti-S1 and anti-RBD regions were strongly correlated (r=0.94) indicating the RBD region as the key targeting region within the S1 segment of S.

To investigate whether clinical characteristics impacted lasting antibody levels to SARS-CoV-2, we divided the COVID-19 convalescent group based on the i) severity of their symptoms, ii) the number of symptoms experienced during the outbreak period and iii) whether they reported to feel 'normal' again post infection (Figure 2). To all five targets (NP, S, S1, RBD and S2) there were no differences in antibody responses among those experiencing mild, moderate or severe symptoms (Figure 2A). In comparison, higher titres of antibodies to SARS-CoV-2 antigens were found among those who self-reported a greater number of symptoms (8+) to those who reported less (0-7), with a significant increase to the S (p=0.029), S1 (p=0.012) and RBD (p=0.049) antigens (Figure 2B). As with symptom severity, no differences were found between those who reported feeling normal, or not, post infection (Figure 2C).

TABLE 2 Characteristics of COVID-19 severity, symptoms, and recovery in COVID-19 convalescent cohort.

Degree of symptom severity	Number (n=30)	%
Mild	12	40.0
Moderate	13	43.3
Severe	5	16.7
Symptoms	Number (n=30)	%
Headache	22	73.3
Altered sense of taste or smell	17	56.7
Muscular Pain	15	50.0
Shortness of breath	15	50.0
Sore throat	15	50.0
Runny nose	14	46.7
Cough	13	43.3
Joint Pain	13	43.3
Fever	12	40.0
Diarrhoea	9	30.0
Chest pain	8	26.7
Irritability/confusion	8	26.7
Nausea/vomiting	8	26.7
Abdominal Pain	5	16.7
Other	2	6.7
No symptoms	0	0
Feel 'normal' post-infection	Number (n=29)	%
Yes	16	55.2
No/Unsure	13	44.8

3.3 Individuals infected with earlier variants of the SARS-CoV-2 virus have low levels of responses to the Omicron variant spike protein

Omicron (B.1.1.529) is the latest variant of concern, already consisting of multiple sub-lineages (33). IgG responses to the Omicron spike protein were measured and found to be significantly increased in the COVID-19 convalescent samples, suggesting cross-reactivity between infection with an earlier variant and the Omicron variant (Figure 3A). To identify how the level of anti-Omicron spike responses compared to the level of the anti-Wuhan-Hu-1 sequence targets, Pearson R correlation analysis was performed (Figure 3B). A low level of positive correlation was found between the anti-S Omicron response and anti-NP responses, r=0.3561 and R^2 = 0.1275. In comparison, a strong positive correlation was observed between the IgG responses to Omicron spike and each of the Wuhan-Hu-1 spike targets, with the strongest correlation being to the RBD region (r=0.8861, R^2 = 0.7852). Given anti-RBD responses are lower than the anti-S, -S1 and -S2 responses, this suggests a low level of cross-reactivity occurring.

With the presence of cross-reactivity to the Omicron spike protein, we investigated whether patient clinical characteristics impacted the level of cross-reactive responses. While no differences were found between symptom severity and feeling 'normal' post infection, the anti-Omicron Spike responses were significantly higher in those who experienced more symptoms (Figure 4).

3.4 Autoantibodies post COVID-19

Autoantibodies towards a variety of antigens have been shown in severe COVID-19 patients in early stages of infection (28, 30) and in convalescent samples (5, 29). IgG specific autoantibodies to 102 known autoantigens were measured in the COVID-19 negative and convalescent cohorts to identify whether COVID-19 results in a potential increase in long-term autoreactivity (Figure 5). A range of reactivities was found to each of the antigens amongst both the COVID-19 convalescent and negative groups. Using the applied average of negatives plus three standard deviations cut-off, the number of positive reactivities in individuals was identified (Figure 6). 26/31 (83.9%) convalescent COVID-19 individuals had a positive reactivity to at least one autoantigen, covering 63/102 (61.8%) autoantigens (Supplementary Table 1). Although negative for SARS-CoV-2 responses, it was also found that 15/21 (71%) COVID-19 negative individuals were positive for at least one autoantigen (majority between 0-4 reactivities). One COVID-19 negative individual had positive autoreactivities to nine targets,

10.3389/fimmu.2022.945021

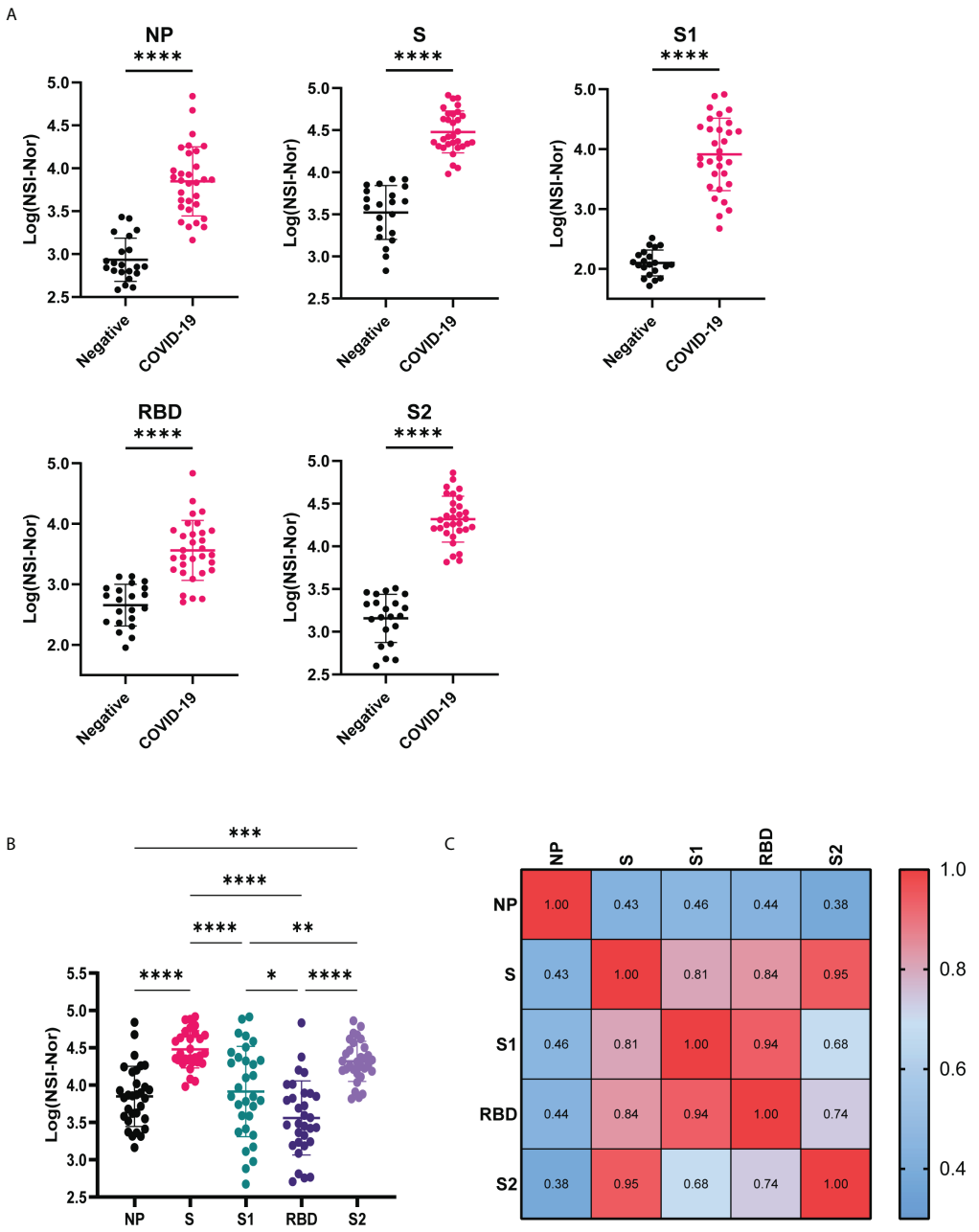

FIGURE 1
Anti-SARS-CoV-2 IgG responses to Nucleoprotein, Spike and Spike subunits. **(A)** Comparison of IgG-specific antibody responses against the SARS-CoV-2 Nucleoprotein (NP), Spike (S) and spike subunits S1, S2 and Receptor Binding Domain (RBD) between COVID-19 negative and convalescent plasma samples. **(B)** Comparison of IgG antibody responses to the different SARS-CoV-2 antigens within the convalescent group. **(C)** Pearson R correlation of anti-SARS-CoV-2 responses. Data shown as log transformed NSI-Nor values with mean ± standard deviation, and statistical significance assessed with unpaired T test **(A)** and Tukey's multiple comparisons test **(B)**, where * p <0.05, ** p <0.01, *** p <0.0005, **** p <0.0001.

which could be a normal state or indicate a break in immune tolerance and some underlying cause of immune dysfunction. Amongst the negative cohort, positive reactivities were identified to 37/102 (36.2%) autoantigens. Almost all autoantigens were positive in only one individual, except for Asparaginyl-tRNA Synthetase (KS), found to be positive in two individuals. When comparing the number of reactivities between the COVID-19 convalescent and negative groups, those who had been infected with SARS-CoV-2 showed a greater range of the number of positive autoantibody reactivities (Figure 4). On average, the

10.3389/fimmu.2022.945021

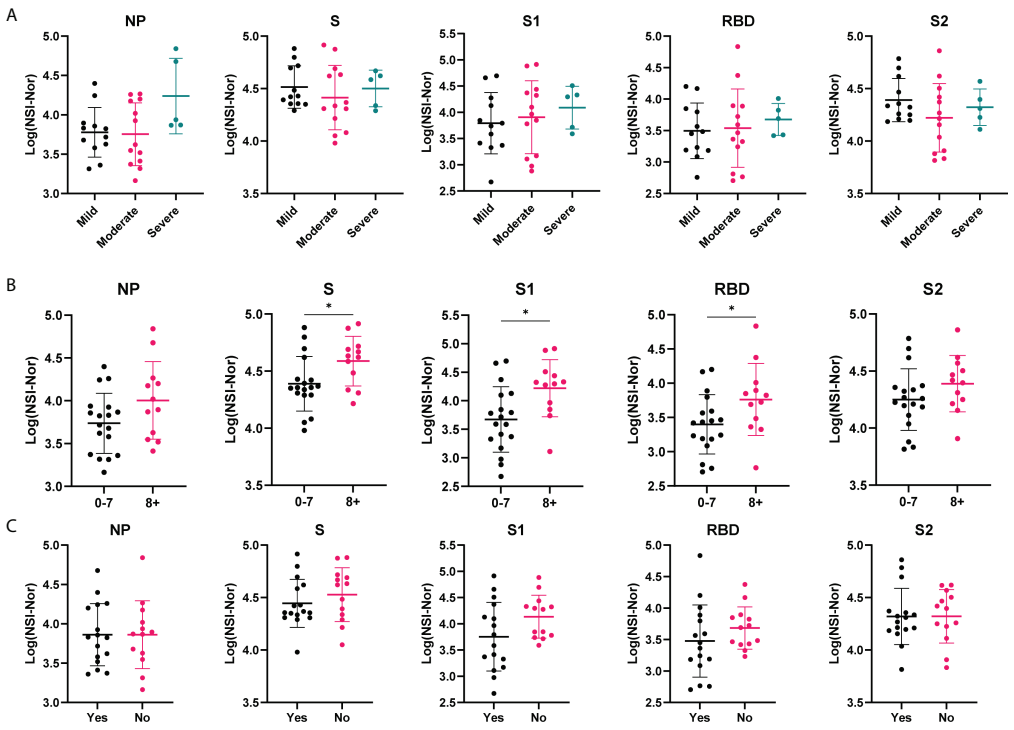

FIGURE 2
Antibody responses to SARS-CoV-2 antigens according to clinical characteristics. Anti-SARS-CoV-2 antibody responses to Nucleoprotein (NP), Spike (S) and spike subunits S1, S2 and Receptor Binding Domain (RBD), in the COVID-19 cohort based on self-reported categories. **(A)** Symptom severity as mild (n=12), moderate (n=13) or severe (n=5). **(B)** Number of symptoms experienced, 0-7 (n= 18) or 8+ (n=12). **(C)** whether 'Yes' they reported to feel normal post-infection (n=16) or 'No' they did not (n=13). Data shown as log transformed NSI-Nor values, with the mean ± standard deviation. Significance (*p<0.05) was assessed with the Kruskal-Wallis test **(A)**, unpaired T test **(B)** and Mann-Whiney test **(C)**.

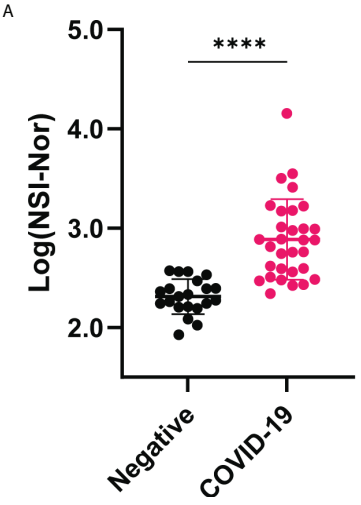

B

Target	r	R^2
Nucleoprotein	0.3571	0.1275
Spike	0.8466	0.7168
Spike-S1	0.7997	0.6395
Spike-RBD	0.8861	0.7852
Spike-S2	0.7817	0.6110

FIGURE 3
IgG antibody responses to Omicron variant spike protein and correlation with Wuhan-Hu-1 antigens **(A)** Comparison of antibody responses to Omicron spike protein between COVID-19 convalescent and negative groups. Data shown as log transformed NSI-Nor values and unpaired T tested performed, **** p <0.0001 **(B)** Pearson R correlation results between anti-Omicron spike antibody response and anti-original Wuhan-specific targets.

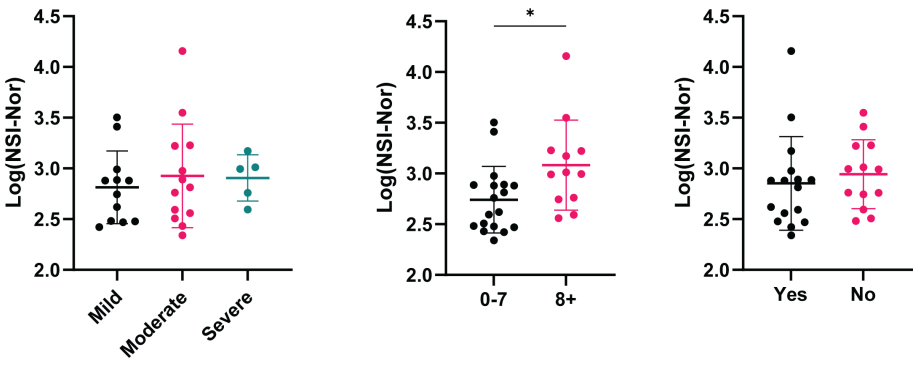

FIGURE 4
Cross-reactive antibody responses to Omicron spike according to clinical characteristics. IgG antibody responses to Omicron spike protein based on self-reported categories (Left) Symptom severity as mild (n=12), moderate (n=13) or severe (n=5). (Middle) Number of symptoms experienced, 0-7 (n=18) or 8+ (n=12), p=0.015. (Right) Whether 'Yes' (n=16) or 'No' (n=13) they reported to feel back to normal, or not, post infection. Data shown as log transformed NSI-Nor values, with the mean ± standard deviation. Significance (*p < 0.05) was assessed with the Kruskal-Wallis test and Mann-Whitney test, respectively.

COVID-19 convalescent group had 5.1 positive reactivities in comparison to the negative cohort's 1.8, highlighting a 2.9-fold increase of the number of autoreactive antibodies post COVID-19.

Due to the range of positive autoantibody responses identified in the COVID-19 convalescent cohort, we were interested in whether the number of positive reactivities was associated with the clinical severity or outcomes (Figure 7). While no significant differences were observed based on disease severity (Figure 7A), those who reported to experience more symptoms during the outbreak period were found to have more positive autoantibody reactivities in comparison to those with less symptoms (Figure 7B). No differences in the number of positive autoantibodies were found between those who reported to feel normal post infection and those who did not (Figure 7C).

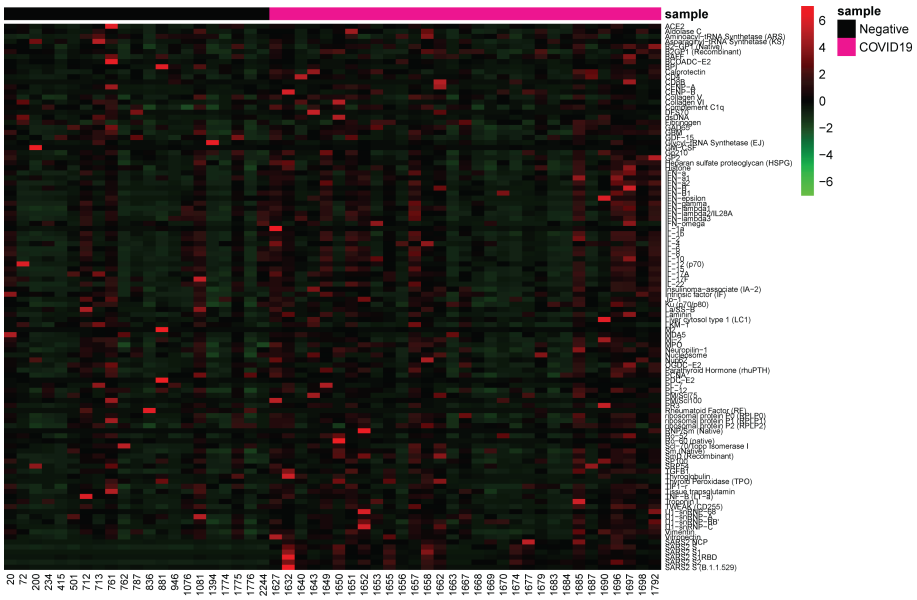

FIGURE 5
Antibody responses to SARS-CoV-2 antigens and autoantigens. Heatmap depicting NSI-Nor values of IgG antibodies to SARS-CoV-2 antigens (n=6) and autoantigens (n=102). COVID-19 negative (n=21) and COVID-19 convalescent (n=31) individuals grouped along the x-axis. Autoantigens listed alphabetically along y-axis, and SARS-CoV-2 antigens at the bottom.

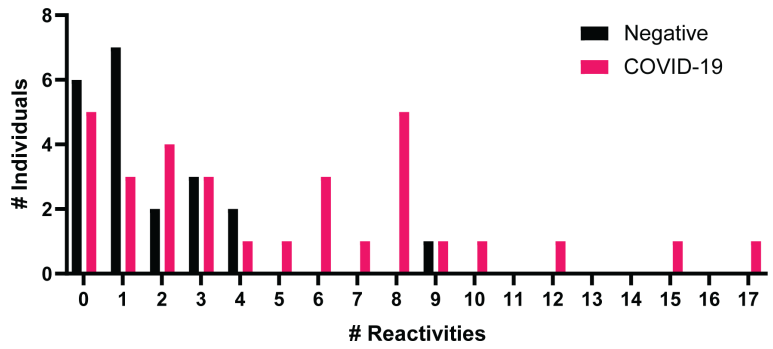

FIGURE 6
Number of positive autoantibody reactivities in COVID-19 negative and convalescent individuals. The number of positive autoantibodies reactivities in COVID-19 negative and convalescent individuals. Positive considered as NSI-Nor values at or above the average plus three standard deviations of the COVID-19 negative cohort.

3.5 Identification of some of the top autoantigen targets in the COVID-19 convalescent cohort

In addition to exploring the number of autoantibody reactivities in an individual, we further explored whether there were common autoantigen targets in convalescent COVID-19 individuals. Of the 63 autoantigens recognised within the cohort, 13 of these were found in 4 individuals or more (Table 3). The most common were autoantibodies to calprotectin, identified in 7 individuals (22.58%).

Using these top antigens based on the number of 'positive' reactivities as potential autoantigens of interest, we compared the antibody responses between the COVID-19 convalescent and negative cohorts (Figure 8). None of the 13 antigens identified in Table 1 were amongst the 37 antigens with a positive reactivity in the negative cohort, suggesting that these targets may be specific to post COVID-19. Of these autoantigens, 9/13 showed a significant difference between the groups, highlighting a potential association of autoantibodies to these autoantigens and COVID-19 infection. No significant difference was observed between the groups for Recombinant β2GP1, RNP/Sm (Native), PM/SCL75 and Histone, highlighting the variation of autoantigens targeted within individuals with COVID-19, as reported previously (30).

Given acute clinical severity has been associated with the presence of autoantibodies, such as type I interferons (27), we furthered investigated whether each of the 13 identified autoantigens (Table 3/Figure 8), specific to the COVID-19 convalescent cohort, had an association with the self-reported clinical symptoms and recovery (Supplementary Figures 1–3). No differences of responses to each of the autoantigens was found based on symptom severity (Supplementary Figure 1). Comparisons based on the number of symptoms experienced or

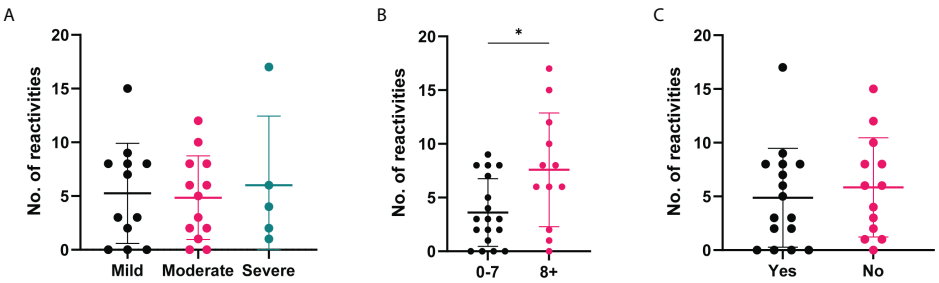

FIGURE 7
Number of positive autoantibody reactivities in COVID-19 convalescent cases based on self-reported symptoms and recovery. The number of positive autoantibodies according to self-reported categories. **(A)** Symptom severity reported as mild (n=12), moderate (n=13) or severe (n=5). **(B)** Number of symptoms experienced, 0-7 (n=18) or 8+ (n=12), p=0.045. **(C)** Whether 'Yes' they felt normal post-infection (n=16) or 'No' they did not (n=13). Data shown as log transformed NSI-Nor values, with the mean ± standard deviation. Significance (*p < 0.05) was assessed with the Kruskal-Wallis test, Mann-Whitney and Unpaired T test, respectively.

TABLE 3 Autoantigens with the highest positive reactivities in COVID-19 convalescent individuals.

Antigen	Number of Individuals	% Positive
Calprotectin	7	22.58
CD4	6	19.35
B2GP1 (Recombinant)	6	19.35
IFN-α2	6	19.35
RNP/Sm (Native)	6	19.35
CENP-B	5	16.13
U1-snRNP-68	5	16.13
IFN-α	4	12.90
PM/Scl75	4	12.90
Vitronectin	4	12.90
Histone	4	12.90
IFN-β1	4	12.90
SmD (Recombinant)	4	12.90

whether individuals reported to feel 'normal' or not post infection both identified one autoantigen with a difference between the groups compared (Figure 9). Autoantibodies to IFN-α were found to be significantly higher in individuals who reported a greater number of symptoms experienced during the initial outbreak (Figure 9A), whereas higher anti-calprotectin antibodies were identified in those who reported to feel normal again (Figure 9B).

3.6 Level of anti-Spike antibodies is associated with the number of autoantibody reactivities

To explore whether there was a correlation between the anti-SARS-CoV-2 responses and autoantigen responses, Spearman R correlation was performed between all targets on the arrays (Supplementary Table 2). The strongest positive correlations were found between the autoantibody responses, particularly within the anti-cytokine antibodies. Using 0.5 as a cut-off for moderate positive correlation, antibody responses to 11 autoantigens were found to correlate with the antibody responses to at least one SARS-CoV-2 antigen (Table 4). The antibody responses to NP did not correlate with autoantibodies. In contrast, it was found that anti-Omicron spike responses had a moderate correlation with the most autoantibodies (10/11). Amongst the 11 autoantigens, two targets, SmD (recombinant) and Thyroglobulin had positive correlations with all SARS-CoV-2 spike targets.

As a range of the number of positive reactivities could be found within the COVID-19 convalescent group (0-17, Figure 6), we explored whether there was an association between the anti-SARS-CoV-2 responses and the number of positive reactivities. Using the median as a cut-off, the convalescent cohort was divided into high and low anti-SARS-CoV-2 responders and the number of reactivities per individual split accordingly (Supplementary Figure 4). In doing so, a significant difference was identified between the number of reactivities in high and low anti-S responders (Figure 10). This suggests an association between the levels of anti-S antibodies and the presence of autoantibodies.

4 Discussion

Viral infections have known associations to autoimmunity [reviewed by Smatti et al. (34)] and autoantibodies have been reported in COVID-19 patients (25–30). Using microarrays consisting of SARS-CoV-2 antigens and 102 autoantigens, we sought to explore the presence of anti-SARS-CoV-2 antibodies, including cross-reactivity to Omicron, and autoantibodies eight months after infection. Antibody responses to the SARS-CoV-2 NP, S and S subunits S1, S2 and RBD remained high in most convalescent samples, in comparison to the uninfected control group. Correlation analysis showed lasting antibody responses to the whole spike protein are specifically to the S2 subunit, whereas within the S1 subunit, it is the RBD region which is highly antigenic. Antibody cross-reactivity was additionally found to the Omicron variant in individuals infected with the Wuhan-Hu-1 variant. A range of autoantibodies were found in both COVID-19 convalescent and uninfected individuals, with a greater spread of the number of positive reactivities found in the convalescent cohort. Higher titres of anti-SARS-CoV-2 responses, positive autoantibody reactivities, and autoantibodies to IFN-α were found to be associated with those who experienced more symptoms during the initial outbreak period. While anti-SARS-CoV-2 responses and autoantibody positivity was not associated with feeling 'back to normal' eight months post infection, we identified one autoantigen of interest, calprotectin, which was found to have higher autoantibody responses among those who reported feeling back to normal. Finally, we found an association between the number of positive autoantibody reactivities and the level of anti-S antibodies.

Antibodies play an important role in the anti-viral response, particularly in neutralisation and immune memory. Given this, understanding their persistence is important in the context of responses following re-exposure and/or vaccination. Studies have reported that antibodies to the SARS-CoV-2 spike protein and nucleoprotein can persist for over 11 months post infection (12, 35). In the present study, antibody responses were measured to five SARS-CoV-2 antigens within the NP and S proteins and while responses to NP, S1 and RBD were lower in some individuals, anti-S and -S2 were consistently high. This trend is consistent with other studies, which report the similar lower or sustained responses, within 2-12 months post COVID-

10.3389/fimmu.2022.945021

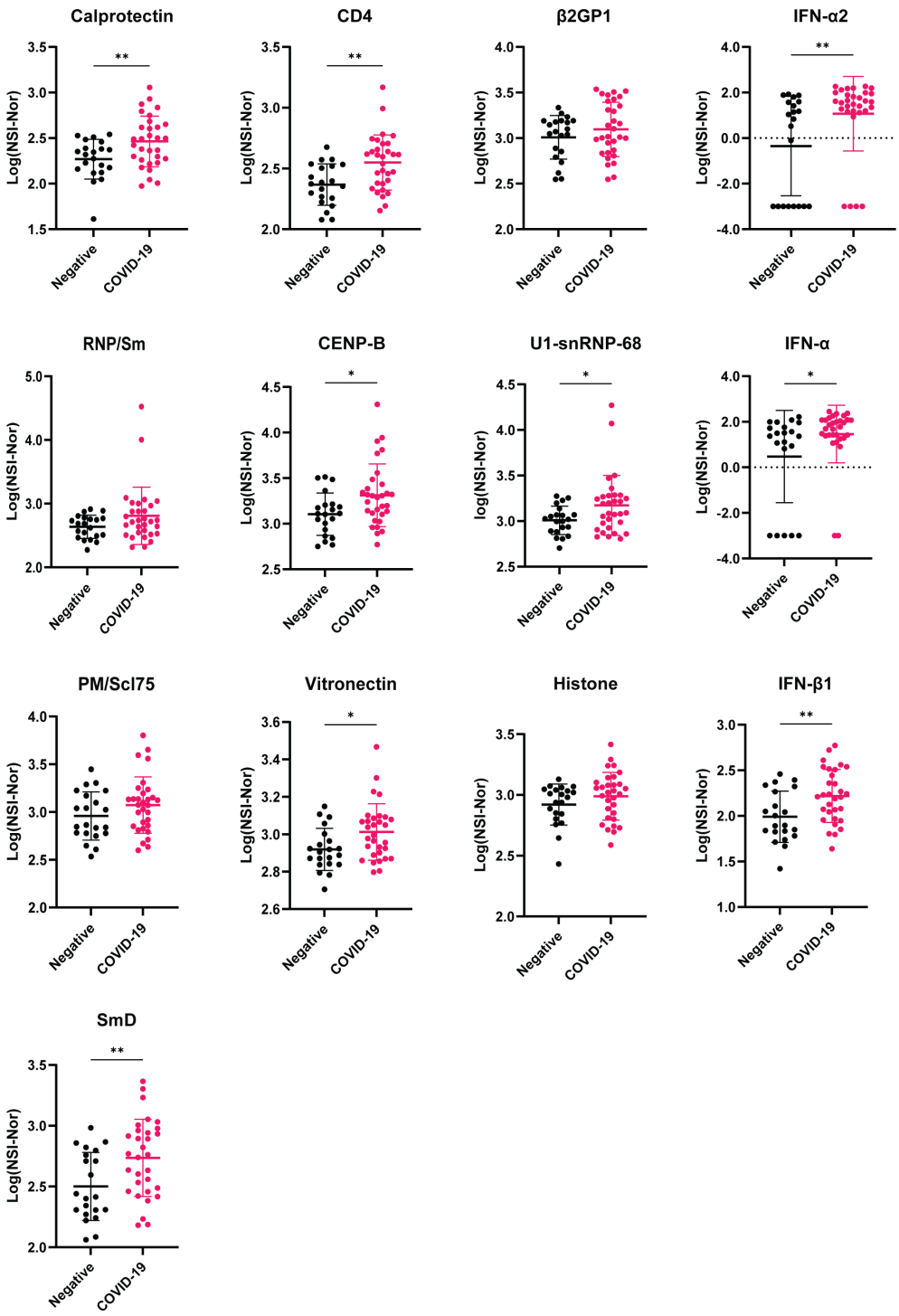

FIGURE 8
Comparison of antibody responses between COVID-19 negative and convalescent individuals for targets with highest number of positive reactivities. Plots of the 13 autoantigens with the highest number of positive COVID-19 convalescent individuals. Following transformation, normality was tested by the Anderson-Darling test prior assessing significance using either unpaired T-test or Mann-Whitney, for normal and non-normal distributed data, respectively. *p<0.05, ** p< 0.01. Data shown as log transformed NSI-Nor values with mean ± standard deviation.

10.3389/fimmu.2022.945021

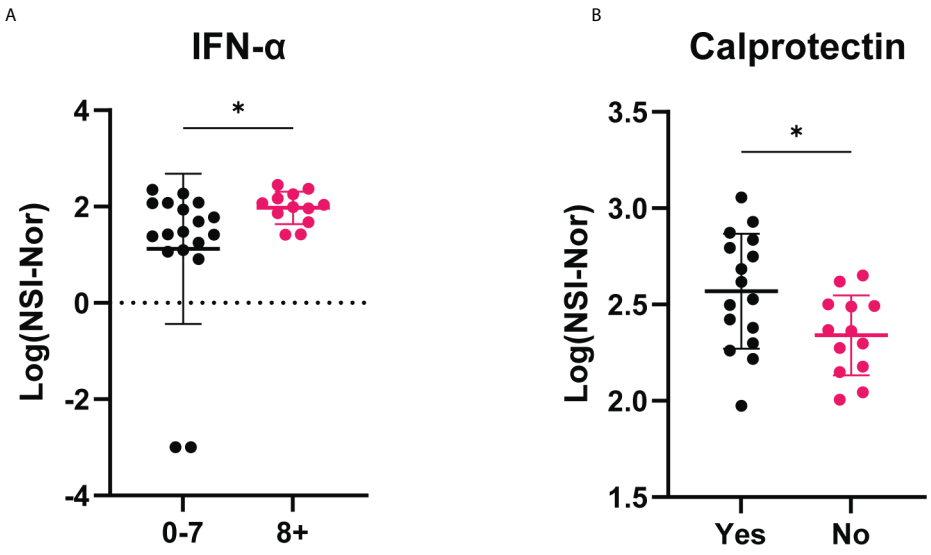

FIGURE 9
IgG antibody responses to IFN-α and calprotectin among COVID-19 convalescent individuals based on self-reported clinical characteristics. **(A)** Anti-IFN-α autoantibody responses compared between those who experienced less (0-7, n=18) or more (8+, n=12) symptoms during the initial outbreak period. **(B)** Anti-calprotectin autoantibodies according to self-reported 'Yes' they felt normal (n=16) or 'No' they did not feel normal (n=13) eight months post infection period. Data shown as log transformed NSI-Nor values with the mean ± standard deviation. Following normality test, significance (*p < 0.05) assessed using **(A)** Mann-Whitney test, p=0.030, and **(B)** unpaired T test, p=0.027.

19 (9, 14, 35, 36). Correlation analysis between the anti-SARS-CoV-2 responses indicated the similarity between responses to S and S2 and between S1 and RBD. To our knowledge, similar correlations between the anti-SARS-CoV-2 antigens responses has not been done, however anti-S1 responses have been shown to correlate with neutralisation (12, 36) indicating the RBD region is the main antigenic target of S1, as observed here. The association between disease severity and lasting anti-SARS-CoV-2 responses post infection is inconsistent, with some studies reporting a correlation with disease severity (37) and higher responses in severe cases (17, 18), and others reporting no differences (19, 20). In the present study, we found anti-SARS-CoV-2 responses did not differ according to the self-reported symptom severity. However, this may be due to low sample numbers within each group, especially the 'severe' group, or because a different measure for severe disease was used, in which participants were unable to conduct usual daily activities and/or admitted to hospital for care. Additionally, anti-SARS-CoV-2 responses did not differ based on returning to 'normal' or not. This is consistent with other studies comparing anti-SARS-CoV-2 responses in individuals with or without long-COVID at four (21), six (16) and 12 (8) months. Indeed, rather than disease

TABLE 4 Moderate correlation between anti-SARS-CoV-2 responses and autoantibody responses.

	NP	S	S1	RBD	S2	Omicron S
CENP-A	-	–	–	–	–	0.52
PDC-E2	-	–	–	–	–	0.50
PR3	-	–	–	–	–	0.50
Ribosomal protein P1 (RPLP1)	-	–	–	–	–	0.57
Ro-52	-	–	–	0.50	–	–
SmD (Recombinant)	-	0.55	0.50	0.57	0.51	0.69
TGFβ1	-	–	–	0.54	–	0.62
Thyroglobulin	-	0.56	0.59	0.59	0.51	0.70
Thyroid Peroxidase (TPO)	-	0.51	–	0.53	–	0.52
LTA (TNF-β)	-	–	–	0.56	–	0.61
Vitronectin	-	–	–	–	–	0.55
# correlated	0	3	2	6	2	10

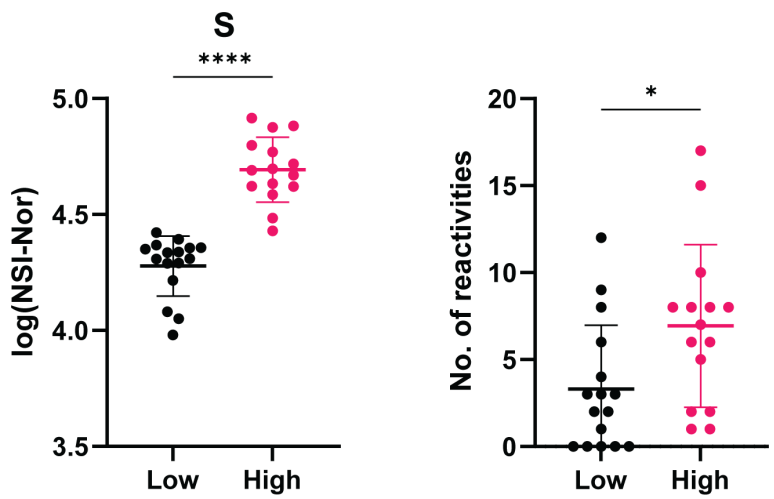

FIGURE 10
Association between level of anti-Spike antibody responses and the number of positive autoantibody reactivities. COVID-19 convalescent individuals (n=31) divided into high and low anti-S using the median of responses as the dividing point. The number of autoantibody reactivities within the individuals split into the corresponding high or low group. Normality tested using the Anderson-Darling test prior assessing significance using the Mann-Whitney test. *p<0.05, **** p< 0.0001. Data shown as mean ± standard deviation.

severity, it was found that individuals who reported a greater number of symptoms, experienced during the initial outbreak period, had significantly higher anti-S, -S1 and -RBD antibody levels, indicating an association between symptoms and antibody responses.

In the present study, COVID-19 convalescent individuals, exposed during the first SARS-CoV-2 (Wuhan-hu-1) outbreak in Tasmania, Australia, in 2020, prior to vaccine development, were found to have antibody responses to the Omicron spike protein, indicating immune cross-reactivity. As a highly vaccinated society, with over 12 billion doses administered worldwide (as of 25th July, 2022) (38), several studies have reported that vaccination-induced protection against Omicron requires three doses for neutralising protection (23, 39). Pre-exposure to other variants alone has shown inability to neutralise the Omicron variant (23). However, some neutralisation of Omicron was found in individuals who had pre-exposure to either D614G variant or Epsilon (B.1.429) then two mRNA vaccine doses. While we did not measure neutralisation, the presence of cross-reactive antibodies, from infection alone, indicates pre-immunity from the prior exposure which can be boosted by vaccination to offer protection against Omicron and possibly future emerging variants.

Autoantibodies have been reported in acute COVID-19 (25–27, 30) and some post-COVID-19 cohorts (5, 29). Here, autoantibodies to a range of antigens in COVID-19 individuals, eight months post infection, and in uninfected individuals were found. Autoimmune responses can be found in healthy individuals and could explain autoantibodies in the uninfected group, given only one individual reported a known autoimmune history (40, 41). Indeed, a recent study investigated the "autoantibodyome" amongst healthy and disease cohorts and identified 77 common autoantibodies within the healthy individuals (42). Amongst the thousands of human proteins measured against, none of the 102 disease specific autoantigens measured in this study were among the 77 common targets. Rather, given high levels of autoantibodies have been reported in COVID-19, in comparison to healthy controls, through identifying the number of positive reactivities, we found that antigen targets in the negative group were recognised by single individuals, whereas there were common antigens amongst the COVID-19 convalescent cohort.

To our knowledge, three antigens that were found to be autoantigens in multiple COVID-19 convalescent individuals, namely calprotectin, CD4 and vitronectin, have not been reported as autoantigens of interest either during acute or post-COVID-19. Of these, calprotectin was recognised by the highest number of individuals in our cohort (7/31, 22.58%) and was the only autoantigen to show an association with clinical recovery, specifically it was higher in those reporting feeling 'normal' post-infection. Calprotectin is a calcium binding protein produced by activated monocytes and neutrophils (43). Increased levels have been found in inflammatory bowel disease (44), rheumatic diseases (45) and myasthenia gravis (46). In COVID-19, calprotectin has been reported in several studies to be increased and associated with severe disease (47, 48). This suggests the autoantibodies could be induced by increased antigen presence and given anti-calprotectin was significantly

higher in individuals reporting being back to normal post-infection, future studies may address whether these autoantibodies may provide functional protection. Interestingly, to our knowledge, IgG specific autoantibodies to calprotectin have only been reported in one other study (5). In that study, using a less stringent positive cut off than in the present study, 3% (3/100) of a long-COVID cohort were anti-calprotectin positive. Given this low positive rate in a long-COVID cohort, it supports a hypothesis that the presence of anti-calprotectin may indeed be protective. However, further studies with larger cohorts comparing individuals with and without long-COVID will provide further insights into the role of these autoantibodies.

Studies using microarrays have reported the presence of autoantibodies in acute COVID-19 individuals who are either hospitalised (30) or exhibit a range of clinical severity (28). While different targets were highlighted within each study, both note a high prevalence of anti-cytokine autoantibodies including to those of type 1 IFNs. Within our COVID-19 convalescent cohort, we found positive reactivities to IFN-α2, IFN-α and IFN-β1 in 19.35%, 12.90% and 12.90% respectively. Interestingly, while anti-IFN's have been reported to be associated with acute severe disease (27), we identified increased titres to IFN-α in those who reported a greater number of symptoms experienced during the outbreak. Also found in our top reactivities were β-2 glycoprotein I (β2GP1) and CENP-B. β2GP1, positive in 19.35% of the present cohort, has previously been reported in acute COVID-19 (26, 30). In contrast, CENP-B, found in 16.13% of the present COVID-19 convalescent cohort, and higher than the COVID-19 negative cohort, has previously been reported to be infrequent in early hospitalisation (30). Given these autoantibody reactivities were identified in convalescent samples, it suggests that autoantibodies raised during acute infection, can last up to 8 months post initial exposure. However, without earlier time points to track changes, this cannot be confirmed. Another study has highlighted that autoantibodies post-COVID-19 can last up to 6 months in a sex-dependent manner, no matter the initial disease severity (29). Lasting autoantibodies may be relevant and open questions about their role in post-COVID-19 syndrome/long-COVID. Indeed, reports of ANAs (8) and functional autoantibodies to G-protein coupled receptors (7) have been reported in those with long-COVID as well as recently emerging literature highlighting persistent autoimmunity (6) and a range of autoreactivities (5). However, except for anti-calprotectin, we found no differences in levels of antibody responses to our top 13 autoantigens between those who reported to feel normal or not post-infection. Therefore, further studies, in larger cohorts, are required to understand autoimmunity, and autoantigens, both during and post COVID-19 to give further insights into the aetiology of long-COVID and potential treatments.

The magnitude of antibody responses to SARS-CoV-2 have been shown to correlate with COVID-19 disease severity, where higher antibody responses develop during acute disease in more severe cases (13, 15). Here, we correlated the anti-SARS-CoV-2 responses with the autoantigen responses and identified a range of degrees of correlation, with the majority showing weak to moderate positive correlations. Similar anti-SARS-CoV-2 and autoantibody correlations have been shown in other study cohorts with anti-NP (29) and -S, -S1, -RBD and -S2 (5). Correlations between anti-NP and autoantibodies were reported to be non-significant (29) or few (5), consistent with our findings of no positive correlation using the 0.5 cut-off. Interestingly, where anti-NP and autoantibody unadjusted correlation was performed, thyroid peroxidase (TPO) was one of nine targets reported to correlate (29). TPO was found to correlate with anti-S, -RBD and -S Omicron in our cohort but with anti-S, -S1, -RBD and -S2 in a third cohort of long-COVID individuals (5). Furthermore, similar correlation patterns were found between our cohort and the cohort of long-COVID individuals with positive correlations between anti-S/S subunits and thyroglobulin and TGF-β1 (5). In the long-COVID cohort, antibodies to these two targets also showed correlation with anti-NP. While amongst our top correlation antigens, CENP-A and LTA (TNF-β) were identified to correlate with anti-S Omicron, which consistent with the long-COVID cohort, there was no correlation with the original Wuhan-Hu-1 antigens. In contrast, antibody responses to SmD and LTA were found to correlate with responses to all Wuhan-Hu-1 and RBD antigens, respectively, but not to any target in the long-COVID cohort. In addition to these correlations, we found individuals with higher antibody responses to the spike protein, had an overall greater number of autoantibody reactivities, further indicating a connection between anti-SARS-CoV-2 responses and the presence of autoantibodies.

In the present study, antibody responses to SARS-CoV-2 antigens and a range of known autoantigens were measured in plasma samples from a cohort of healthcare workers exposed to Wuhan-Hu-1, in a single exposure event, eight months prior to blood collection. A range of autoantibody responses were identified, and a greater number of positive reactivities found within COVID-19 convalescent samples and more-so in those with higher anti-S responses. However, without analysing acute disease samples, or having pre-infection samples, conclusions about the rise and persistence of autoantibodies cannot be made. The identification of anti-calprotectin autoantibodies as potentially protective indicates a need to not only explore the induction of autoimmunity but to understand specific targets that may be involved in pathology or protection. Future analysis investigating the longitudinal autoantibody responses to antigens identified in this study and their correlation with disease severity and outcomes, may give insights into the roles of autoantibodies in long-COVID.

Data availability statement

The original contributions presented in the study are included in the article/Supplementary Material. Further inquiries can be directed to the corresponding author.

Ethics statement

The studies involving human participants were reviewed and approved by Tasmanian Health and Medical Human Research Ethics Committee. The patients/participants provided their written informed consent to participate in this study.

Author contributions

Conceptualization, RM and MP; Participant recruitment and sample collection, FHJ, KLF, KJS, MM, NS, and SS; Methodology, RM, and MP; Investigation, RM; Resources, FJ, NS, KS, KLF and MP; Writing—original draft, review and editing, RM, SS, FHJ, KJS, NS, MM, KLF and MP; Supervision, MP. All authors have read and agreed to the published version of the manuscript

Funding

MP is an NHMRC Research Fellow. MP and KLF receive NHMRC funding; KLF, MP and SS received funding from the Clifford Craig Foundation; RM is a recipient of an Australian Government Research Training Program Scholarship. This study was also supported by a philanthropic donation from Mrs Rebecca Round.

Acknowledgments

The authors thank all the healthcare workers who consented to be part of the study. We also acknowledge the nurses who collected the bloods, Prof Lizzie Shires who supported the logistics of setting up the blood collection clinics and Dr Louise Parry who assisted with blood collections and recruitment.

Conflict of interest

The authors declare that the research was conducted in the absence of any commercial or financial relationships that could be construed as a potential conflict of interest.

Publisher's note

All claims expressed in this article are solely those of the authors and do not necessarily represent those of their affiliated organizations, or those of the publisher, the editors and the reviewers. Any product that may be evaluated in this article, or claim that may be made by its manufacturer, is not guaranteed or endorsed by the publisher.

Supplementary material

The Supplementary Material for this article can be found online at: https://www.frontiersin.org/articles/10.3389/fimmu.2022.945021/full#supplementary-material

References

1. Huang C, Wang Y, Li X, Ren L, Zhao J, Hu Y, et al. Clinical features of patients infected with 2019 novel coronavirus in wuhan, China. *Lancet* (2020) 395 (10223):497–. doi: 10.1016/S0140-6736(20)30183-5

2. Han H, Xie L, Liu R, Yang J, Liu F, Wu K, et al. Analysis of heart injury laboratory parameters in 273 covid-19 patients in one hospital in wuhan, China. *J Med Virol* (2020) 92(7):819–23. doi: 10.1002/jmv.25809

3. Nalleballe K, Reddy Onteddu S, Sharma R, Dandu V, Brown A, Jasti M, et al. Spectrum of neuropsychiatric manifestations in covid-19. *Brain Behav Immun* (2020) 88:71–4. doi: 10.1016/j.bbi.2020.06.020

4. Moody R, Wilson K, Flanagan KL, Jaworowski A, Plebanski M. Adaptive immunity and the risk of autoreactivity in covid-19. *Int J Mol Sci* (2021) 22 (16):8965. doi: 10.3390/ijms22168965

5. Rojas M, Rodríguez Y, Acosta-Ampudia Y, Monsalve DM, Zhu C, Li Q-Z, et al. Autoimmunity is a hallmark of post-covid syndrome. *J Trans Med* (2022) 20 (1):129. doi: 10.1186/s12967-022-03328-4

6. Acosta-Ampudia Y, Monsalve DM, Rojas M, Rodríguez Y, Zapata E, Ramírez-Santana C, et al. Persistent autoimmune activation and proinflammatory state in post-coronavirus disease 2019 syndrome. *J Infect Dis* (2022) 225:2155-62. doi: 10.1093/infdis/jiac017

7. Wallukat G, Hohberger B, Wenzel K, Fürst J, Schulze-Rothe S, Wallukat A, et al. Functional autoantibodies against G-protein coupled receptors in patients with persistent long-Covid-19 symptoms. *J Transl Autoimmun* (2021) 4:100100–. doi: 10.1016/j.jtauto.2021.100100

8. Seeßle J, Waterboer T, Hippchen T, Simon J, Kirchner M, Lim A, et al. Persistent symptoms in adult patients 1 year after coronavirus disease 2019 (Covid-19): A prospective cohort study. *Clin Infect Dis* (2021) 74(7):1191–8. doi: 10.1093/cid/ciab611

9. Masiá M, Fernández-González M, Telenti G, Agulló V, García JA, Padilla S, et al. Durable antibody response one year after hospitalization for covid-19: A longitudinal cohort study. *J Autoimmun* (2021) 123:102703–. doi: 10.1016/j.jaut.2021.102703

10. Li C, Yu D, Wu X, Liang H, Zhou Z, Xie Y, et al. Twelve-month specific igg response to sars-Cov-2 receptor-binding domain among covid-19 convalescent plasma donors in wuhan. *Nat Commun* (2021) 12(1):4144–. doi: 10.1038/s41467-021-24230-5

11. De Giorgi V, West KA, Henning AN, Chen LN, Holbrook MR, Gross R, et al. Naturally acquired sars-Cov-2 immunity persists for up to 11 months following infection. *J Infect Dis* (2021) 224(8):1294–304. doi: 10.1093/infdis/jiab295

12. Choe PG, Kang CK, Kim K-H, Yi J, Kim ES, Park SW, et al. Persistence of neutralizing antibody response up to 1 year after asymptomatic or symptomatic sars-Cov-2 infection. *J Infect Dis* (2021) 224(6):1097–9. doi: 10.1093/infdis/jiab339

13. Plūme J, Galvanovskis A, Šmite S, Romanchikova N, Zayakin P, Linē A. Early and strong antibody responses to sars-Cov-2 predict disease severity in covid-19 patients. *J Trans Med* (2022) 20(1):176. doi: 10.1186/s12967-022-03382-y

14. Nguyen-Contant P, Embong AK, Kanagaiah P, Chaves FA, Yang H, Branche AR, et al. S protein-reactive igg and memory b cell production after human sars-Cov-2 infection includes broad reactivity to the S2 subunit. *mBio* (2020) 11(5):e01991–20. doi: 10.1128/mBio.01991-20

15. Lynch KL, Whitman JD, Lacanienta NP, Beckerdite EW, Kastner SA, Shy BR, et al. Magnitude and kinetics of anti–severe acute respiratory syndrome coronavirus 2 antibody responses and their relationship to disease severity. *Clin Infect Dis* (2021) 72(2):301–8. doi: 10.1093/cid/ciaa979

16. Ryan FJ, Hope CM, Masavuli MG, Lynn MA, Mekonnen ZA, Yeow AEL, et al. Long-term perturbation of the peripheral immune system months after sars-Cov-2 infection. *BMC Med* (2022) 20(1):26. doi: 10.1186/s12916-021-02228-6

17. Dan JM, Mateus J, Kato Y, Hastie KM, Yu ED, Faliti CE, et al. Immunological memory to sars-Cov-2 assessed for up to 8 months after infection. *Science* (2021) 371(6529):eabf4063. doi: 10.1126/science.abf4063

18. Horton DB, Barrett ES, Roy J, Gennaro ML, Andrews T, Greenberg P, et al. Determinants and dynamics of sars-Cov-2 infection in a diverse population: 6-month evaluation of a prospective cohort study. *J Infect Dis* (2021) 224(8):1345–56. doi: 10.1093/infdis/jiab411

19. Marklund E, Leach S, Axelsson H, Nyström K, Norder H, Bemark M, et al. Serum-igg responses to sars-Cov-2 after mild and severe covid-19 infection and analysis of igg non-responders. *PLoS One* (2020) 15(10):e0241104–e. doi: 10.1371/journal.pone.0241104

20. Ozgocer T, Dagli ŞN, Ceylan MR, Disli F, Ucar C, Yildiz S. Analysis of long-term antibody response in covid-19 patients by symptoms grade, gender, age, bmi, and medication. *J Med Virol* (2022) 94(4):1412–8. doi: 10.1002/jmv.27452

21. Peluso MJ, Deitchman AN, Torres L, Iyer NS, Munter SE, Nixon CC, et al. Long-term sars-Cov-2-Specific immune and inflammatory responses in individuals recovering from covid-19 with and without post-acute symptoms. *Cell Rep* (2021) 36(6):109518–. doi: 10.1016/j.celrep.2021.109518

22. Hojjat Jodaylami M, Djaïleb A, Ricard P, Lavallée É, Cellier-Goetghebeur S, Parker M-F, et al. Cross-reactivity of antibodies from non-hospitalized covid-19 positive individuals against the native, B.1.351, B.1.617.2 and P.1 sars-Cov-2 spike proteins. *Sci Rep* (2021) 11(1):21601. doi: 10.1038/s41598-021-00844-z

23. Laurie MT, Liu J, Sunshine S, Peng J, Black D, Mitchell AM, et al. Sars-Cov-2 variant exposures elicit antibody responses with differential cross-neutralization of established and emerging strains including delta and omicron. *J Infect Dis* (2022) 225:jiab635. doi: 10.1093/infdis/jiab635

24. Faustini S, Shields A, Banham G, Wall N, Al-Taei S, Tanner C, et al. Cross reactivity of spike glycoprotein induced antibody against delta and omicron variants before and after third sars-Cov-2 vaccine dose in healthy and immunocompromised individuals. *J Infect* (2022) 84(4):579–613. doi: 10.1016/j.jinf.2022.01.002

25. Zhou Y, Han T, Chen J, Hou C, Hua L, He S, et al. Clinical and autoimmune characteristics of severe and critical cases of covid-19. *Clin Trans Sci* (2020) 13 (6):1077–86. doi: 10.1111/cts.12805

26. Vlachoyiannopoulos PG, Magira E, Alexopoulos H, Jahaj E, Theophilopoulou K, Kotanidou A, et al. Autoantibodies related to systemic autoimmune rheumatic diseases in severely ill patients with covid-19. *Ann Rheum Dis* (2020) 79(12):1661. doi: 10.1136/annrheumdis-2020-218009

27. Bastard P, Rosen LB, Zhang Q, Michailidis E, Hoffmann H-H, Zhang Y, et al. Autoantibodies against type I ifns in patients with life-threatening covid-19. *Science* (2020) 370(6515):eabd4585. doi: 10.1126/science.abd4585

28. Wang EY, Mao T, Klein J, Dai Y, Huck JD, Jaycox JR, et al. Diverse functional autoantibodies in patients with covid-19. *Nature* (2021) 595(7866):283–8. doi: 10.1038/s41586-021-03631-y

29. Liu Y, Ebinger JE, Mostafa R, Budde P, Gajewski J, Walker B, et al. Paradoxical sex-specific patterns of autoantibody response to sars-Cov-2 infection. *J Trans Med* (2021) 19(1):524. doi: 10.1186/s12967-021-03184-8

30. Chang SE, Feng A, Meng W, Apostolidis SA, Mack E, Artandi M, et al. New-onset igg autoantibodies in hospitalized patients with covid-19. *Nat Commun* (2021) 12(1):5417. doi: 10.1038/s41467-021-25509-3

31. Johnston F, Anderson T, Harlock M, Castree N, Parry L, Marfori T, et al. Lessons learnt from the first Large outbreak of covid-19 in health-care settings in Tasmania, Australia. *Western Pac Surveill Response J* (2021) 12(4):1-7. doi: 10.5365/wpsar.2021.12.4.884

32. Dong E, Du H LF. An interactive web-based dashboard to track covid-19 in real time. *Lancet Inf Dis* (2020) 20(5):533–4. doi: 10.1016/S1473-3099(20)30120-1

33. Mahase E. Covid-19: What do we know about omicron sublineages? *BMJ* (2022) 376:o358. doi: 10.1136/bmj.o358

34. Smatti MK, Cyprian FS, Nasrallah GK, Al Thani AA, Almishal RO, Yassine HM. Viruses and autoimmunity: A review on the potential interaction and molecular mechanisms. *Viruses* (2019) 11(8):762. doi: 10.3390/v11080762

35. Gaebler C, Wang Z, Lorenzi JCC, Muecksch F, Finkin S, Tokuyama M, et al. Evolution of antibody immunity to sars-Cov-2. *Nature* (2021) 591(7851):639–44. doi: 10.1038/s41586-021-03207-w

36. Siracusano G, Brombin C, Pastori C, Cugnata F, Noviello M, Tassi E, et al. Profiling antibody response patterns in covid-19: Spike S1-reactive iga signature in the evolution of sars-Cov-2 infection. *Front Immunol* (2021) 12:772239. doi: 10.3389/fimmu.2021.772239

37. Zhang S, Xu K, Li C, Zhou L, Kong X, Peng J, et al. Long-term kinetics of sars-Cov-2 antibodies and impact of inactivated vaccine on sars-Cov-2 antibodies based on a covid-19 patients cohort. *Front Immunol* (2022) 13:829665. doi: 10.3389/fimmu.2022.829665

38. WHO. *Who coronavirus disease (Covid-19) dashboard: World health organisation* (2020). Available at: https://covid19.who.int/.

39. Garcia-Beltran WF, St. Denis KJ, Hoelzemer A, Lam EC, Nitido AD, Sheehan ML, et al. Mrna-based covid-19 vaccine boosters induce neutralizing immunity against sars-Cov-2 omicron variant. *Cell* (2022) 185(3):457–66.e4. doi: 10.1016/j.cell.2021.12.033

40. Slight-Webb S, Lu R, Ritterhouse LL, Munroe ME, Maecker HT, Fathman CG, et al. Autoantibody-positive healthy individuals display unique immune profiles that may regulate autoimmunity. *Arthritis Rheumatol* (2016) 68 (10):2492–502. doi: 10.1002/art.39706

41. Neiman M, Hellström C, Just D, Mattsson C, Fagerberg L, Schuppe-Koistinen I, et al. Individual and stable autoantibody repertoires in healthy individuals. *Autoimmunity* (2019) 52(1):1–11. doi: 10.1080/08916934.2019.1581774

42. Shome M, Chung Y, Chavan R, Park JG, Qiu J, LaBaer J. Serum autoantibodyome reveals that healthy individuals share common autoantibodies. *Cell Rep* (2022) 39(9):110873. doi: 10.1016/j.celrep.2022.110873

43. Jukic A, Bakiri L, Wagner EF, Tilg H, Adolph TE. Calprotectin: From biomarker to biological function. *Gut* (2021) 70(10):1978. doi: 10.1136/gutjnl-2021-324855

44. Konikoff MR, Denson LA. Role of fecal calprotectin as a biomarker of intestinal inflammation in inflammatory bowel disease. *Inflammatory Bowel Dis* (2006) 12(6):524–34. doi: 10.1097/00054725-200606000-00013

45. Jarlborg M, Courvoisier DS, Lamacchia C, Martinez Prat L, Mahler M, Bentow C, et al. Serum calprotectin: A promising biomarker in rheumatoid arthritis and axial spondyloarthritis. *Arthritis Res Ther* (2020) 22(1):105. doi: 10.1186/s13075-020-02190-3

46. Stascheit F, Hotter B, Hoffmann S, Kohler S, Lehnerer S, Sputtek A, et al. Calprotectin as potential novel biomarker in myasthenia gravis. *J Transl Autoimmun* (2021) 4:100111–. doi: 10.1016/j.jtauto.2021.100111

47. Shokri-Afra H, Alikhani A, Moradipoodeh B, Noorbakhsh F, Fakheri H, Moradi-Sardareh H. Elevated fecal and serum calprotectin in covid-19 are not consistent with gastrointestinal symptoms. *Sci Rep* (2021) 11(1):22001. doi: 10.1038/s41598-021-01231-4

48. Mahler M, Meroni P-L, Infantino M, Buhler KA, Fritzler MJ. Circulating calprotectin as a biomarker of covid-19 severity. *Expert Rev Clin Immunol* (2021) 17(5):431–43. doi: 10.1080/1744666X.2021.1905526

frontiers | Frontiers in Immunology

TYPE Original Research
PUBLISHED 05 September 2022
DOI 10.3389/fimmu.2022.988125

OPEN ACCESS

EDITED BY
Moncef Zouali,
Institut National de la Santé et de la Recherche Médicale (INSERM), France

REVIEWED BY
Siriruk Changrob,
Cornell University, United States
Matteo Bulati,
Mediterranean Institute for Transplantation and Highly Specialized Therapies (ISMETT), Italy

*CORRESPONDENCE
Raul M. Torres
Raul.Torres@cuanschutz.edu

SPECIALTY SECTION
This article was submitted to B Cell Biology, a section of the journal Frontiers in Immunology

RECEIVED 06 July 2022
ACCEPTED 09 August 2022
PUBLISHED 05 September 2022

CITATION
Castleman MJ, Stumpf MM, Therrien NR, Smith MJ, Lesteberg KE, Palmer BE, Maloney JP, Janssen WJ, Mould KJ, Beckham JD, Pelanda R and Torres RM (2022) Autoantibodies elicited with SARS-CoV-2 infection are linked to alterations in double negative B cells.
Front. Immunol. 13:988125.
doi: 10.3389/fimmu.2022.988125

Autoantibodies elicited with SARS-CoV-2 infection are linked to alterations in double negative B cells

Moriah J. Castleman[1], Megan M. Stumpf[1], Nicholas R. Therrien[1], Mia J. Smith[1,2], Kelsey E. Lesteberg[1,3], Brent E. Palmer[4], James P. Maloney[5], William J. Janssen[6,7], Kara J. Mould[6,7], J. David Beckham[1,3,8], Roberta Pelanda[1] and Raul M. Torres[1]*

[1]Department of Immunology and Microbiology, University of Colorado School of Medicine, Aurora, CO, United States, [2]Barbara Davis Center for Diabetes, Department of Pediatrics, University of Colorado School of Medicine, Aurora, CO, United States, [3]Department of Medicine, Division of Infectious Disease, University of Colorado School of Medicine, Aurora, CO, United States, [4]Department of Medicine, Division of Allergy and Clinical Immunology, University of Colorado School of Medicine, Aurora, CO, United States, [5]Department of Medicine, Division of Pulmonary Sciences and Critical Care Medicine, University of Colorado School of Medicine, Aurora, CO, United States, [6]Department of Medicine, National Jewish Health, Denver, CO, United States, [7]Department of Medicine, University of Colorado, Aurora, CO, United States, [8]Rocky Mountain Regional Veterans affairs (VA), Medical Center, Aurora, CO, United States

Double negative (DN) B cells (CD27-IgD-) comprise a heterogenous population of DN1, DN2, and the recently described DN3 and DN4 subsets. In autoimmune disease, DN2 cells are reported to be precursors to autoreactive antibody secreting cells and expansion of DN2 cells is linked to elevated interferon levels. Severe SARS-CoV-2 infection is characterized by elevated systemic levels of pro-inflammatory cytokines and serum autoantibodies and expansion of the DN2 subset in severe SARS-CoV-2 infection has been reported. However, the activation status, functional capacity and contribution to virally-induced autoantibody production by DN subsets is not established. Here, we validate the finding that severe SARS-CoV-2 infection is associated with a reduction in the frequency of DN1 cells coinciding with an increase in the frequency of DN2 and DN3 cells. We further demonstrate that with severe viral infection DN subsets are at a heightened level of activation, display changes in immunoglobulin class isotype frequency and have functional BCR signaling. Increases in overall systemic inflammation (CRP), as well as specific pro-inflammatory cytokines (TNFα, IL-6, IFNγ, IL-1β), significantly correlate with the skewing of DN1, DN2 and DN3 subsets during severe SARS-CoV-2 infection. Importantly, the reduction in DN1 cell frequency and expansion of the DN3 population during severe infection significantly correlates with increased levels of serum autoantibodies. Thus, systemic

inflammation during SARS-CoV-2 infection drives changes in Double Negative subset frequency, likely impacting their contribution to generation of autoreactive antibodies.

KEYWORDS

double negative, DN1, DN2, DN3, B cells, inflammation, SARS–CoV–2, autoreactive

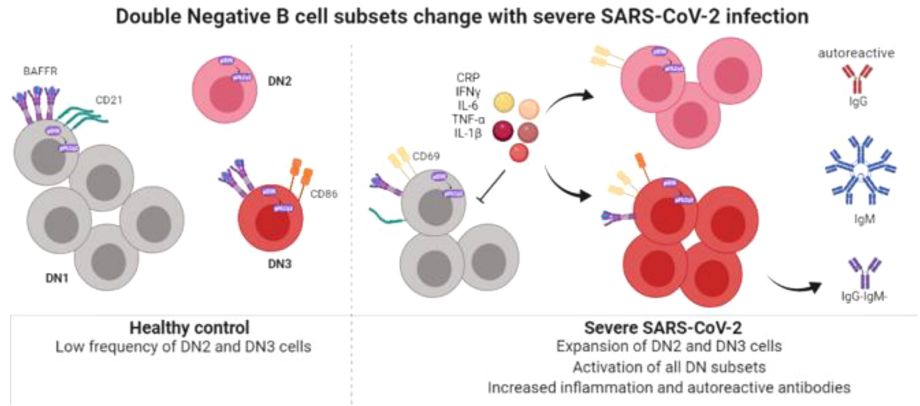

GRAPHICAL ABSTRACT
Created with BioRender.com.

Introduction

B lymphocytes from human peripheral blood can be categorized (based on the expression of IgD and CD27 surface receptors) into naive (CD27-IgD+), unswitched memory (CD27+IgD+) and Ig class-switched memory (CD27+ IgD-), or Double-Negative (DN: CD27-IgD-) B cell subsets (1, 2). DN B cells were first identified due to their expansion in patients with Systemic Lupus Erythematosus (SLE) and are considered memory B cells due to the similarity in phenotype with conventional memory B cells, presence of class-switched immunoglobulins IgG or IgA, and evidence of somatic hypermutation indicating DN cells are antigen experienced (3–5). In addition to SLE, expansion of the Double Negative population has been reported in a variety of autoimmune disorders including; Guillain-Barre syndrome, Myasthenia gravis and Multiple sclerosis (6, 7), as well as, Common Variable Immunodeficiency (CVID) where an expansion in the autoreactive VH4-34 DN population was also reported (8). Furthermore, expansion of DN B cells in SLE patients correlated with higher titers of serum VH4-34 autoreactive antibodies (4, 5). Together these reports suggest a contribution of DN cells to autoimmunity.

Further examination of SLE patients revealed that Double Negative B cells are a heterogenous population of cells comprised of DN1 and DN2 subsets identified based not only on $CD27^{-}IgD^{-}$ but also on differential expression of CD11c and CD21, whereby DN1 cells express CD21 but not CD11c ($CD21^{+}CD11c^{-}$) and DN2 cells express high levels of CD11c in the absence of CD21 ($CD21^{-}CD11c^{++}$) (2, 9). In SLE flares, there is a loss of DN1 cells with a corresponding increase in DN2 cells, with DN2 cells described as a pathogenic precursor to autoreactive antibody secreting cells (9). Single cell transcriptomic analysis of PBMCs from healthy controls has suggested the existence of two additional DN subsets called DN3 and DN4 cells, whereby DN3 cells were enriched in *IGHA2* transcripts and DN4 cells were enriched in *IGHE* transcripts (10). More recently, cellular evidence confirming the existence of a DN3 subset lacking expression of both CD11c and CD21 has been reported ($CD11c^{-}CD21^{-}$), but there is limited evidence for the existence of a DN4 subset expressing both CD11c and CD21 (11–13). The functional role of these diverse Double Negative subsets in various immune responses, particularly in the context of viral infection, and the mechanisms that promote generation of each unique subset compared to another remain to be determined.

Given their relatively recent identification, there is limited information on the B cell developmental pathways that populate the DN3 and DN4 subsets. However, for the DN2 subset a role for inflammatory cytokines in modulating their development has been established. Specifically, increased frequencies of DN2 cells in SLE patients were correlated with increased levels of IFN-γ, IFN-λ, and IFN-γ-induced cytokines including TNF-α and IL-6 (9, 14, 15). Accordingly, *in vitro* generation of DN2 cells from naive B cell precursors can be facilitated by either IFN-γ or IFN-λ in the presence of TLR7L, IL-21, BAFF and BCR stimulation, a process that could be inhibited by IL-4 and CD40L mimicking T cell help (9, 14, 15). Together, these reports suggest a role for inflammatory cytokines, such as is typically induced during viral infection, in regulating the composition of the Double Negative population.

Severe acute respiratory syndrome coronavirus 2 (SARS-CoV-2), the causative agent of the current coronavirus disease 2019 (COVID-19) has a multi-faceted immunopathology including T cell activation, increased IFN-γ, TNF-α, IL-6, IL-1β cytokines and production of autoreactive antibodies (16–20). Additionally, multiple groups have reported an expansion of the DN2 and DN3 subsets in PBMCs from severe SARS-CoV-2 infection (11, 12, 21, 22) and a concordant reduction in the DN1 subset (11, 12). Stratification of severely infected samples into those with high and low levels of C-reactive protein (CRP), an indicator of overall systemic inflammation, revealed that expansion of DN2 and DN3 cells was more predominant in high CRP samples, implicating inflammation as a driver of DN2/3 subset expansion with viral infection (21). Expansion of the DN3 subset correlated with a variety of clinical parameters including increased respiratory rate and increased levels of D-dimer and CRP (11), suggesting a possible role for DN3 cells in disease pathogenesis. Furthermore, individuals who recovered from infection had a higher frequency of DN1 cells than individuals who succumbed to infection (23), indicating DN1 cells may play a protective role in viral infection. Despite these reports on DN subset frequency and correlation with disease parameters, there is still limited information on DN cells in both healthy controls and during SARS-CoV-2 infection. Specifically, the phenotype of DN subsets with regard to activation and inhibitory receptor expression as well as responses to BCR signaling (to determine functionality of the BCR) have not been reported for DN subsets in SARS-CoV-2 infection nor has the association of DN subsets with autoreactive antibody production in viral infection been reported. Therefore, the phenotype, function and possible contribution to virally-induced autoimmunity by DN subsets, particularly the novel DN3 population, needs further characterization.

In this report, we have interrogated PBMCs and plasma from healthy controls, individuals immunized against SARS-CoV-2 by mRNA vaccines, and individuals with mild or severe SARS-CoV-2 infection. The results of these analyses confirm that there is a reduction in the frequency of DN1 cells within the Double Negative population coinciding with an increase in the frequency of DN2 and DN3 cells in severe SARS-CoV-2 patients. With severe viral infection, the B cells within each DN subset are at a heightened level of activation, display changes in immunoglobulin class isotype frequency and possess the ability to signal through the BCR. Importantly, increases in overall systemic inflammation (CRP), as well as increases in specific pro-inflammatory cytokines (TNFα, IL-6, IFNγ, IL-1β), significantly correlate with the alteration in the frequencies of DN1, DN2 and DN3 subsets during severe SARS-CoV-2 infection. Furthermore, we show that the reduction in DN1 cells and expansion of DN3 cells is significantly correlated with increases in relative titer of autoreactive antibodies during severe infection. Together these data provide evidence that systemic inflammation during SARS-CoV-2 infection likely drives changes in Double Negative subset frequency, thereby impacting their contribution to generation of autoreactive antibodies.

Materials and methods

Human peripheral blood mononuclear cells

Individuals with severe SARS-CoV-2 infection were hospitalized at the University of Colorado Hospital (UCH) or St. Joseph's Hospital (SJH). Informed consent to donate whole blood was obtained from a legally authorized representative (SJH) or by an approved waiver of consent (UCH). Subjects were 18 years of age or older and mechanically ventilated for acute respiratory distress syndrome, as defined by the Berlin Criteria, due to SARS-CoV-2. The presence of virus was confirmed by polymerase chain reaction of a nasal swab. Patients were excluded from this study if they had a history of solid organ or bone marrow transplants, chronic lung disease, hemoptysis, increased risk for bleeding, pregnancy or who were immunosuppressed. We did not actively exclude patients with a diagnose of autoimmune disease prior to acquisition of severe SARS-CoV-2 infection, however upon retrospective review of patient files, 13 out of 14 patients did not have an autoimmune disease and 1 out of 14 patients had Type 1 Diabetes Mellitus. Whole blood was collected from central venous catheters in cell preparation tubes with sodium citrate and processed per the manufacturer's instructions (BD Biosciences, San Jose, CA). Plasma was stored at -80 degrees until use. PBMCs were resuspended in 90% FBS with 10% DMSO or 90% FBS + DMEM and 10% DMSO and stored in liquid nitrogen until use.

For individuals immunized against SARS-CoV-2 by Pfizer BNT162b2-mRNA or Moderna mRNA-1273, informed consent was provided for the acquisition of whole blood as well as the dates of their primary inoculation and booster. For individuals deemed mildly infected (convalescent stage) with SARS-CoV-2, informed consent was provided for the acquisition of whole

blood, and they were included in this study if they had a positive viral qPCR test or the presence of anti-SARS-CoV2 antibodies in the absence of vaccination (samples were collected before vaccination was available to the general public) and did not require hospitalization. For these individuals, whole blood was drawn by staff at the University of Colorado Clinical and Translation Research Centers (CTRC), part of the Colorado Clinical and Translation Sciences Institute (CCTSI), in sodium heparin tubes (BD, Franklin Lakes, NJ). Whole blood was centrifuged at 1,700 rpm for 5minutes to collect plasma. Plasma was stored at -80°C until use. Cells were then diluted in 1X PBS, suspended over a Ficoll-Paque gradient and centrifuged 2,400 rpm for 25 minutes to isolate PBMCs from the buffy coat. PBMCs were washed in 1X PBS, and enumerated by hemocytometer. PBMCs were resuspended in 90% FBS with 10% DMSO and stored in liquid nitrogen until use.

For healthy control samples, plateletpheresis leukoreduction filter (LRS chambers) were purchased from Vitalant Blood Center (Denver, CO). Cells were diluted in media containing RPMI Medium 1640 (Gibco, Netherlands) with 10% FBS, 1mM sodium pyruvate (Gibco), 1X non-essential amino acids (Gibco), 1X Glutamax (Gibco) and 50uM 2-mercaptoethanol (Sigma-Aldrich, St. Louis, Missouri). Cells were then suspended over a Ficoll- Paque gradient (Cytiva, Sweden) and centrifuged 2,400 rpm for 25 minutes at RT to isolate PBMCs in the buffy coat layer. PBMCs were washed in media, the cell pellet was resuspended in 1X PBS (Corning, Glendale, Arizona) and cell count was enumerated by hemocytometer. PBMCs were resuspended in 90% FBS (Gemini, Sacramento, CA) with 10% DMSO (ATCC, Manassas, VA) and stored in liquid nitrogen until use. LRS chambers do not allow the acquisition of plasma, thus when plasma was examined in this study, the immunized individuals were used as a comparator to mild or severe SARS-CoV-2 individuals.

The Colorado Multiple Institutional Review Board (COMIRB) at the University of Colorado School of Medicine and National Jewish Health approved the use of human plasma and PBMCs, and this study was performed under the Declaration of Helsinki.

Frequency and phenotyping of B cell subsets *ex vivo* by flow cytometry

PBMCs were quickly thawed in a 37°C water bath, washed in warm media containing RPMI Medium 1640 with 25mM HEPES (Corning), centrifuged 1,500 rpm x 5min at RT, washed again and enumerated by hemocytometer. PBMCs were stained for 20min on ice in 1X PBS with the following antibodies (clone in parenthesis): CD3 (OKT3), CD19 (SJ25C1), CD27 (M-T271), IgD (IA6-2), CD21 (Bu32), CD11c (B-ly6), FcRL5 (509f6), IgM (MHM-88), CD69 (FN50), CD86 (IT2.2), CD72 (REA231), CD22 (HIB22), BAFFR (11C1) and IgG (G18-145) and in the presence of Live/Dead Blue for UV viability dye (Invitrogen, Eugene, OR). Cells were then washed in 1X PBS, centrifuged 1,500 rpm x 5 min at 4°C, fixed in 4% PFA (Fisher, Fair Lawn, NJ) for 15min at RT, washed with 1X PBS and resuspended in FACS Buffer containing 1% BSA (Fisher, Fair Lawn, NJ) + 0.05% Sodium Azide (Aldrich, St. Louis, MO) in 1X PBS.

All flow cytometry data was acquired on the Cytek Aurora. PBMCs from healthy humans were used for single color reference controls except where the use of Ultra Comp eBeads (Invitrogen) was necessary. Flow cytometry data was analyzed using FlowJo software (v 10.8.1). Within the lymphocyte single cell viable gates, DN1 cells were identified as CD3- CD19+ CD27- IgD- CD21+ CD11c-, DN2 cells were identified as CD3- CD19+ CD27- IgD- CD21- CD11c++, and DN3 cells were identified as CD3- CD19+ CD27- IgD- CD21- CD11c- in accordance with other groups (2, 11, 12). The frequency of DN1, DN2 or DN3 subsets were enumerated out of the total Double negative population (CD27-IgD-) or out of the total B cell population (CD19+). Expression of surface markers on each DN subset are reported as geometric mean fluorescent intensity (gMFI). FMOs used as staining controls are indicated in figure legends.

Assessment of BCR signaling by phospho flow cytometry

PBMCs were thawed as described above. After enumeration, PBMCs were incubated for 45min at 37°C+ 5% CO2 to reduce basal phosphorylation levels in warm serum-free RMPI Medium 1640 while in the prescence of the following antibodies (clone): CD3 (OKT3), CD19 (SJ25C1), CD27 (M-T271), CD21 (Bu32), CD11c (B-ly6), and Live/Dead Blue for UV viability dye. Cells were centrifuged 1,500 rpm x 5min at RT, resuspended in warm RPMI with 5% FBS and stimulated with either 10ug/mL Rabbit anti-human IgG (H+L) F(ab')2 (Southern Biotech, Birmingham, AL) or 75μM pervanadate (used as an experimental positive control) for 5 minutes in a 37°C water bath. After a quick centrifuge spin to pellet the cells (2,400 g x 30 seconds at RT), PBMCs were resuspended in 100uL per million cells Cytofix/ Cytoperm (BD) and incubated for 20 minutes on ice. Cells were washed in 1X Perm/Wash (BD), then incubated in the presence of this buffer for intracellular staining for 30min on ice with the following antibodies (clone): pSYK Y348 (I120-722), pPLCγ2 Y759 (K86-689.37) and IgD (IA6-2). Cells were washed with 1X Perm/Wash, centrifuged 1,500 rpm x 5min at 4°C, and resuspended in FACS Buffer containing 1% BSA (Fisher)+ 0.05% Sodium Azide (Aldrich) in 1X PBS. Data was acquired on the Cytek Aurora and cell subsets defined as described above.

Quantification of cytokines in plasma

Plasma was thawed on ice and TNFα, IL-6, IFNγ, and IL-1β were quantified by the U-PLEX Assay and CRP was quantified

using the V-PLEX Assay according to manufacturer's instructions (Meso Scale Discovery, Rockville, MD). Both assays were evaluated on the QuickPlex SQ 120 Instrument (Meso Scale Discovery).

Measurement of autoreactive IgG antibodies in plasma

Autoreactive IgG antibodies were enumerated in plasma samples as previously described (24). Briefly, 96-well Nunc-Immuno MaxiSorp plates (Thermo Fisher Scientific) were either coated for 2 hours at 37°C with 0.5ug/mL 9G4 antibody to identify VH4-34 (kind gift of Dr. John Cambier, University of Colorado School of Medicine), coated overnight at 4°C with either 15ug/mL of sonicated calf thymus DNA for chromatin (Sigma-Aldrich), 1ug/mL Smith antigen (Arotec Diagnostics), or 50ug/mL cardiolipin (Sigma-Aldrich). The 9G4 monoclonal antibody is specific to the VH4-34 idiotype and can be used to identify B cells expressing the VH4-34 BCR (25, 26). Plates were washed 3X, blocked for 1-2 hour at 37°C. To block plates for detection of anti-chromatin, anti-Smith or VH4-34 autoantibodies, a buffer of 1X PBS, 1mM EDTA, 0.05% NaN3 and 1% BSA was used. To block plates for detection of anti-cardiolipin autoantibodies a blocking buffer of 1X PBS with 1% BSA was used. For 9G4 reactivity, each plasma sample was plated starting at 1:200 in a 3-fold serial dilution across 6 dilutions and incubated for overnight at 4°C. For chromatin, Smith or cardiolipin reactivity, each plasma sample was plated starting at 1:8 in a 3-fold serial dilution across 6 dilutions and incubated for 2 hours at 37°C. Plates were washed 3X and incubated with Goat anti-human IgG (for 9G4 Goat anti-human IgG multispecies cross absorbed was used) conjugated to alkaline phosphatase (Southern Biotech) for 1 hour at 37°C. Plates were washed 3X and developed with 1 mg/ml of 4-nitrophenyl phosphate disodium salt hexahydrate (Alkaline Phosphatase Substrate; Sigma-Aldrich) diluted in developing buffer (1M diethanolamine, 8.4 mM MgCl2, and 0.02% NaN3 in water) and incubated at 37°C for 10-30 minutes. Absorbance values (O.D.) were read at 405 nm on the VersaMax ELISA reader (MDS Analytical Technologies). The dilutions were log transformed to generate a curve and the linear part of the curve was used to select a dilution at which to compare relative O.D. values for each group. For absolute titers of chromatin, Smith or cardiolipin reactivity O.D. values were compared at 1/128 dilution and for 9G4 reactivity O.D. values were compared at 1/16200 dilution. The absolute titers were then normalized by the total amount of IgG in the corresponding plasma sample (quantification of total IgG described below).

Quantification of total IgG in plasma

Levels of total IgG in plasma were quantified as previously described (24). Briefly, 96-well plates were coated with Goat anti-human IgG capture antibody (Southern Biotech) overnight at 4°C in 1X PBS. Plates were then washed 3X and blocked for 1 hour at 37°C. Plasma samples were plated starting at a 1:200 dilution in a 5-fold serial dilution across 6 points and incubated for 2 hours at 37°C. A standard curve of IgG (Southern Biotech) starting at 1pg/mL was used to quantify total levels of IgG in each plasma sample. Plates were washed 3X and incubated with Goat anti-human IgG conjugated to alkaline phosphatase (Southern Biotech) in 1X PBS for 1 hour at 37°C. Plates were washed and developed as described above. For absolute titers of IgG O.D. values were compared at 1/12500.

Data analysis

Data was graphed and analyzed using Prism Graph-Pad Software (v 9.2.0). One-way ANOVA was used to determine the significance of differences between cohorts (healthy controls, immunized samples, mild or severe infection) or between cell subsets (DN1, DN2 and DN3) as indicated in the figure legends. A Pearson correlation was used to determine the significance of differences between systemic cytokines with the frequency of DN subsets or between the frequency of DN subsets with the titer of autoreactive antibodies as indicated in figure legends. Significance was defined as $p < 0.05$. If a trend to significance $p<0.09$ was observed, then it was noted on the figure. Each human donor in a group is represented by a dot on the scatter plot and the total sample size measured for each assay is indicated in each figure legend.

Results

Altered frequencies of Double Negative B cell subsets during severe SARS-CoV-2 infection

To begin to characterize how immunization and viral infection might influence the presence of Double Negative B cell subsets, we collected human peripheral blood mononuclear cells (PBMCs) from healthy controls, individuals immunized with an mRNA vaccine against SARS-CoV-2, or individuals convalescing from a mild SARS-CoV-2 infection or subjects with severe SARS-CoV-2 infection requiring hospitalization (Supplemental Table 1). Double Negative ($CD27^{-}IgD^{-}$) B cells comprise a heterogeneous population of DN1, DN2 and DN3 subsets which are identified based on differential expression of CD11c and CD21 (Figure 1A), whereby DN1 cells express CD21 but not CD11c ($CD21^{+}CD11c^{-}$), DN2 cells expressing high levels of CD11c but not CD21 ($CD21^{-}CD11c^{++}$), and DN3 cells do not express either surface receptor ($CD21^{-}CD11c^{-}$) (2, 11, 12). A DN4 population expressing both CD11c and CD21, has been suggested based on transcriptome and phenotypic

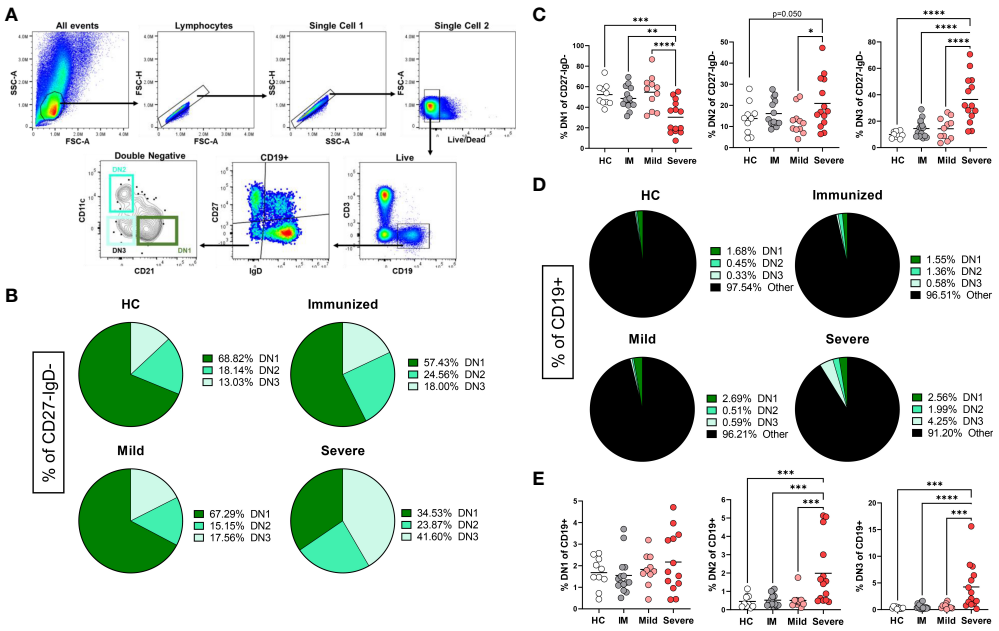

FIGURE 1
Alteration in the frequency of Double Negative subsets with Severe SARS-CoV-2 infection. **(A)** Flow plots demonstrating the gating strategy to identify DN1, DN2 and DN3 populations in human PBMCs. **(B)** Pie charts depicting the average frequency of DN1, DN2, and DN3 subsets within the total double negative population (CD27-IgD-) for healthy controls (HC), individuals immunized against SARS-CoV-2 (IM), individuals with mild or severe SARS-CoV-2 infection. **(C)** Quantification comparing the frequency of each DN subset within total double negative population (CD27-IgD-). **(D)** Pie charts depicting the average frequency of DN1, DN2, and DN3 subsets within the total B cell population (CD19+). **(E)** Quantification comparing the frequency of each DN subset within total B cells (CD19+) between healthy controls (HC, N=10), individuals immunized (IM, N=15) against SARS-CoV-2, and individuals with mild (N=11) or severe SARS-CoV-2 infection (N=14). Statistics: one-way ANOVA, *p < 0.05, **p < 0.01, ***p < 0.001, ****p < 0.0001.

analyses (10, 11), however, in our analyses we did not observe a reproducibly distinct DN4 subset ($CD21^{+}CD11c^{+}$) in all individuals, thus this population was not further characterized. As expected (9), in healthy controls within the Double Negative population, DN1 cells were the most frequent subset followed by DN2 cells with DN3 cells being the most infrequent subset (Figure 1B). A similar hierarchy of DN subsets (DN1>DN2>DN3) within the DN population was also observed in individuals immunized against SARS-CoV-2 (Figure 1B). Conversely, individuals with mild SARS-CoV-2 infection harbored similar frequencies of DN3 and DN2 cells with DN1 cells remaining as the predominant subset (Figure 1B). Importantly, for individuals with severe SARS-CoV-2 infection, DN3 cells were the most frequent subset compared to DN1 and DN2 cells within the Double Negative population (Figure 1B).

Upon comparison of the frequency of subsets within the Double Negative population between healthy controls, individuals immunized against SARS-CoV-2, and subjects with either mild or severe SARS-CoV-2 infection demonstrated that there is a significant loss of DN1 cells with severe infection (Figure 1C), in keeping with previous reports (11, 12). A significant increase in DN2 cells within the Double Negative population with severe SARS-CoV-2 infection was observed as compared to DN2 cells from mild infection (Figure 1C). Similarly, in severe infection a significant increase in DN3 cells within the Double Negative population with severe infection was observed as compared to DN3 cells from healthy controls, individuals immunized against SARS-CoV-2 and subjects with mild SARS-CoV-2 infection (Figure 1C).

DN cells are a relatively minor population within the total B cell population (Figure 1D) and quantification of the DN1 subset did not reveal any significant differences in the frequency of DN1 cells amongst CD19+ cells with severe SARS-CoV-2 infection compared to other individuals (Figure 1E). Importantly, we observed a significant increase in DN2 and DN3 cells within the total B cell population with severe SARS-CoV-2 infection compared to heathy controls, individuals immunized against SARS-CoV-2 or subjects with mild infection (Figure 1E), in accordance with previous reports (22, 23).

Overall, these data demonstrate that the Double Negative population undergoes major alterations in subset frequency with severe SARS-CoV-2 infection suggesting that viral infection regulates the composition of DN1, DN2 and DN3 B cell subsets.

Comparison of DN1, DN2, and DN3 cells in healthy individuals

To better characterize the uniqueness of B cell subsets within the Double Negative B cell population, especially the novel DN3 subset, we phenotypically compared the DN1, DN2 and DN3 subsets with each other from healthy controls. It was previously reported that DN2 cells from SLE patients express higher levels of the activation marker CD69 when compared to conventional memory B cells (9). In accord with that finding, our study revealed DN2 cells from healthy individuals have on average the highest level of CD69 expression compared to DN1 and DN3 cells in healthy controls (Figure 2), indicating DN2 cells naturally reside at a more activated state than other Double Negative subsets. In healthy controls, DN2 cells also have the highest expression level of CD86, a co-receptor that stimulates T cells (27), compared to DN1 or DN3 cells, with DN3 cells displaying a higher level of CD86 expression than DN1 cells (Figure 2). These data indicate that under normal conditions DN2 cells are poised to participate in B-T cell interactions, which was unexpected given DN2 cells are reported to participate in extrafollicular antibody responses (9), a process that includes T-cell independent antibody responses (28). Finally, our results further suggest DN3 cells are more likely to participate in activation of T cells through higher CD86 expression than DN1 cells.

Comparison of BAFFR expression, a receptor important for response to the survival cytokine BAFF (29), demonstrated that in healthy controls DN1 cells have significantly higher expression of BAFFR than DN2 and DN3 cells and DN2 cells express an intermediate level compared to the lowest BAFFR levels on DN3 cells (Figure 2). These data suggest that DN1 cells are the subset most dependent on BAFF for survival, whereas DN3 cells are the least dependent on BAFF for survival.

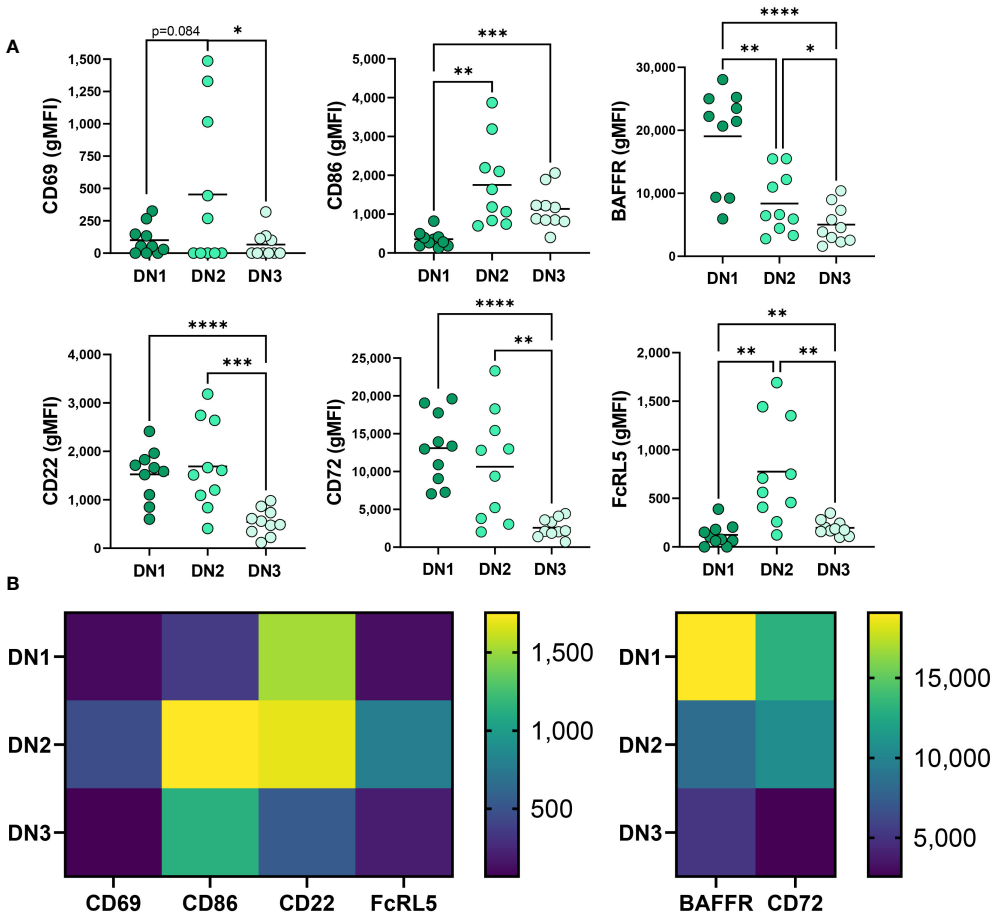

FIGURE 2
Phenotypic comparison of DN1, DN2 and DN3 cells in healthy controls. **(A)** Quantification of expression level (gMFI: geometric mean fluorescent intensity) of CD69, CD86, BAFFR, CD22, CD72 and FcRL5 on DN1, DN2 or DN3 cells from healthy controls (N=10) and **(B)** a heatmap visualizing the differences between DN1, DN2 and DN3 subsets of average gMFI values. Statistics: one-way ANOVA, *p < 0.05, **p < 0.01, ***p < 0.001, ****p < 0.0001.

We also queried expression of receptors known to inhibit BCR signaling (30–32), specifically measuring CD72, CD22 and FcRL5 inhibitory receptor expression on Double Negative B cell subsets in healthy controls. DN2 cells from SLE patients were reported to express the highest level of CD22 when compared to conventional memory cells (9). Examination of CD22 demonstrated comparable CD22 expression between DN2 and DN1 cells in healthy controls (Figure 2) whereas DN3 cells expressed the lowest level of CD22 (Figure 2), implying that DN3 cells might experience the least CD22-mediated inhibition of BCR signaling *via* the recruitment of SHP-1 (33). Examination of another inhibitory receptor, CD72, revealed that DN1 cells have the highest level of CD72 expression compared to DN2 and DN3 cells, and DN3 cells have the lowest expression level of CD72 (Figure 2). These data suggest that in healthy controls CD72 may play an important role in regulating DN1 cells compared to other Double Negative B cell subsets. Finally, we compared expression of FcRL5 on Double Negative B cell subsets and demonstrate that in healthy controls DN2 cells express the highest level of FcRL5 (Figure 2), suggesting FcRL5 uniquely regulates the DN2 subset.

Together these findings begin to characterize the novel DN3 subset phenotype relative to the better characterized DN1 and DN2 subsets in healthy individuals with key features of DN3 cells expressing the lowest levels of CD22, CD72, CD69 and BAFFR out of the DN subsets.

Phenotypic alteration in DN1 cells during severe SARS-CoV-2 infection

We next questioned how SARS-CoV-2 infection might promote a reduced frequency of DN1 cells and initially measured expression of CD21, the defining receptor on DN1 cells. This analysis revealed a significant reduction in CD21 expression on DN1 with severe SARS-CoV-2 infection as compared to DN1 cells from healthy controls, immunized individuals and those with mild SARS-CoV-2 infection (Figures 3A, B). These data suggest that with severe viral infection, loss of CD21 surface expression may account, at least in part, for the reduction in DN1 cell frequency. Examination of BAFFR on DN1 cells revealed that DN1 cells from severe SARS-CoV-2 infected subjects express significantly lower levels of BAFFR when compared to DN1 cells from healthy controls or individuals immunized against SARS-CoV-2 or with mild SARS-CoV-2 infection (Figures 3A, B). This would suggest DN1 cells inefficiently compete for BAFF and a subsequent reduction in DN1 cell survival may accompany

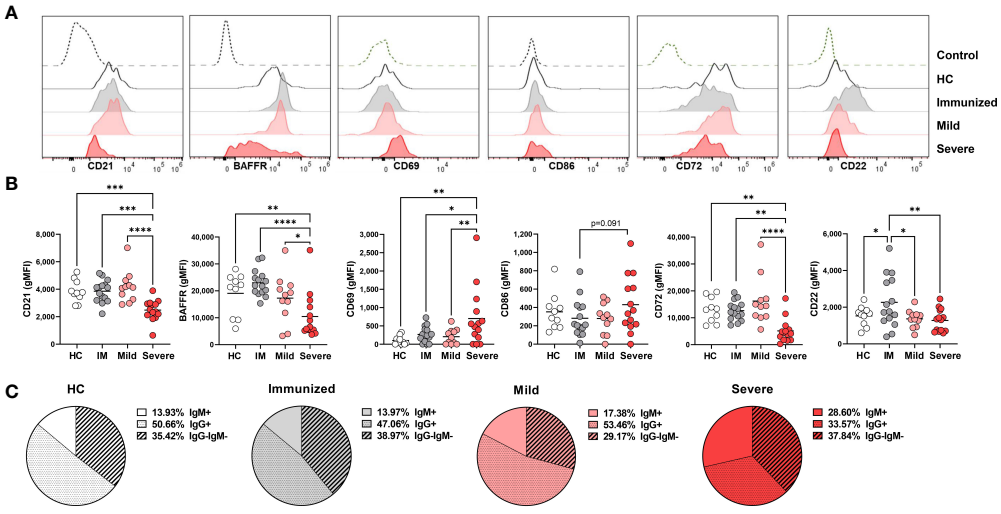

FIGURE 3
Phenotypic changes in DN1 cells with Severe SARS-CoV-2 infection. **(A)** Representative histograms depicting expression of CD21, BAFFR CD69, CD86, CD72, and CD22 on DN1 cells from a healthy control (HC), an individual immunized against SARS-CoV-2 or with mild or severe SARS-CoV-2 infection. Control dotted histogram is an FMO for CD69, CD68, CD72 and CD22. Control dotted histogram for BAFFR and CD21 is expression on CD3+ T cells from a healthy control subject. **(B)** Quantification of CD21, BAFFR, CD69, CD86, CD72, and CD22 expression (gMFI: geometric mean fluorescent intensity) on DN1 cells from healthy controls (HC), individuals immunized against SARS-CoV-2 (IM), or with mild or severe SARS-CoV-2 infection. **(C)** Pie charts depicting the average frequency of IgM+, IgG+, or IgG-IgM- DN1 cells for healthy controls (HC, N=10), individuals immunized against SARS-CoV-2 (N=15), or with mild (N=11) or severe SARS-CoV-2 infection (N=14). Statistics: one-way ANOVA, *p < 0.05, **p < 0.01, ***p < 0.001, ****p < 0.0001.

severe viral infection and further account for the diminution of the DN1 population.

To assess the influence of viral infection on DN1 B cell activation, we evaluated expression of the CD69 and CD86 activation receptors on virally infected and control individuals. These analyses revealed that there was a significant increase in expression of CD69 on DN1 cells with severe SARS-CoV-2 infection as compared to healthy controls, immunized individuals or those who had experienced mild SARS-CoV-2 infection. We also observed a trend of higher CD86 expression on DN1 cells from severe SARS-CoV-2 infection as compared to DN1 cells from individuals immunized against SARS-CoV-2 (Figures 3A, B). Together these results indicate that DN1 cells are in an activated state with viral infection.

We also measured the levels of the CD22 and CD72 inhibitory receptors on DN1 B cells as an assessment of functional capacity since both inhibitory receptors are able to negatively regulate BCR signaling (30, 31). DN1 cells from severe SARS-CoV-2 infected subjects express significantly lower levels of CD72 compared to DN1 cells from healthy controls or individuals immunized against SARS-CoV-2 or with mild SARS-CoV-2 infection (Figures 3A, B). Interestingly, immunization against SARS-CoV-2 appeared to increase expression of CD22 on DN1 cells such that DN1 cells from healthy controls and individuals with mild or severe SARS-CoV-2 infection had significantly lower levels of CD22 expression than DN1 cells from immunized subjects (Figures 3A, B). These data indicate that immunization and viral infection differentially effect inhibitory receptor expression on DN1 cells and DN1 cells in severe infection express relatively reduced levels of both the CD72 and CD22 inhibitory receptors.

Since the more broadly-defined Double Negative B population was initially described as an antigen-experienced memory B cell population lacking expression of CD27 with nearly half of the population class-switched to IgG (5), and the majority of DN1 cells from heathy controls express IgG (9), we asked whether viral infection also modified isotype class dominance in DN1, DN2 and DN3 subsets. In healthy controls, the majority of DN1 cells are IgG^+, a third of DN1 cells are IgG^-IgM^- and the remaining small portion are IgM^+ (Figure 3C). A similar breakdown of immunoglobulin isotype class was observed with DN1 cells from immunized individuals and subjects with mild SARS-CoV-2 infection (Figure 3C). Conversely, with DN1 cells from subjects with severe SARS-CoV-2 infection we observed a significant reduction in IgG^+ cells and a corresponding increase in IgM^+ DN1 cells (Figure 3C), suggesting that severe viral infection modifies immunoglobulin class type in DN1 cells.

Overall, these data demonstrate that DN1 are phenotypically altered with severe SARS-CoV-2 infection such that they are at a heightened level of activation and express reduced levels of inhibitory receptors and BAFFR and display a shift in antibody isotype class.

Activation of DN2 cells during severe SARS-CoV-2 infection

Given the increased frequency of DN2 cells with severe SARS-CoV-2 infection (Figure 1), we anticipated that these cells might exhibit enhanced survival as indicated by increased expression levels of BAFFR. However, we did not find significant differences in BAFFR expression on DN2 cells from healthy individuals or those with either mild or severe SARS-CoV-2 infection although DN2 cells from severe viral infection trended to have reduced BAFFR expression (Figures 4A, B). Notably, immunization against SARS-CoV-2 increased expression levels of BAFFR on DN2 cells (Figures 4A, B), suggesting that vaccination may modify longevity of these cells.

To determine how viral infection influenced the activation state of DN2 cells, we quantified levels of the CD69 and CD86 on this subset. DN2 cells from severely infected SARS-CoV-2 subjects had significantly higher levels of CD69 expression, but not CD86, when compared to individuals immunized against SARS-CoV-2 or those with mild infection (Figures 4A, B). Together, these data indicate that DN2 cells are more activated with severe infection.

We next again assessed if immunization or viral infection influenced inhibitory receptor expression on DN2 B cells by measuring CD72 and CD22 surface expression. The mean fluorescence intensity (MFI) of CD72 was found to be expressed at a higher level on DN2 cells from immunized individuals and those with mild viral infection compared to healthy controls (Figures 4A, B). Accordingly, CD72 was expressed at a significantly lower level on DN2 cells from severe SARS-CoV-2 infection compared to DN2 cells after immunization or those with mild infection (Figures 4A, B). Examination of CD22 revealed no significant difference in levels of expression on DN2 cells from each group, however, similar to the CD72 inhibitory receptor, the average CD22 MFI was higher on DN2 cells after immunization against SARS-CoV-2 suggesting that vaccination induces inhibitory receptor expression on DN2 cells (Figures 4A, B). DN2 cells from healthy controls and SLE patients were reported to also express the FcRL5 inhibitory receptor (9). Measurement of FcRL5 revealed that there is a wide distribution of expression on DN2 cells in all cohort populations and without significant differences in expression (Figures 4A, B). Together, these data indicate that while CD72 expression is depressed with severe SARS-CoV-2 infection, the expression of the CD22 and FCRL5 inhibitory receptors on DN2 cells does not change with severe infection. In contrast, immunization appears to elevate expression of CD22 and CD72 on DN2 B cells.

DN2 cells from healthy controls or individuals with SLE have been reported to predominantly express IgG (9). In accord, our evaluation of immunoglobulin isotype class expressed by DN2 cells reveals that the majority of DN2 cells are IgG^+,

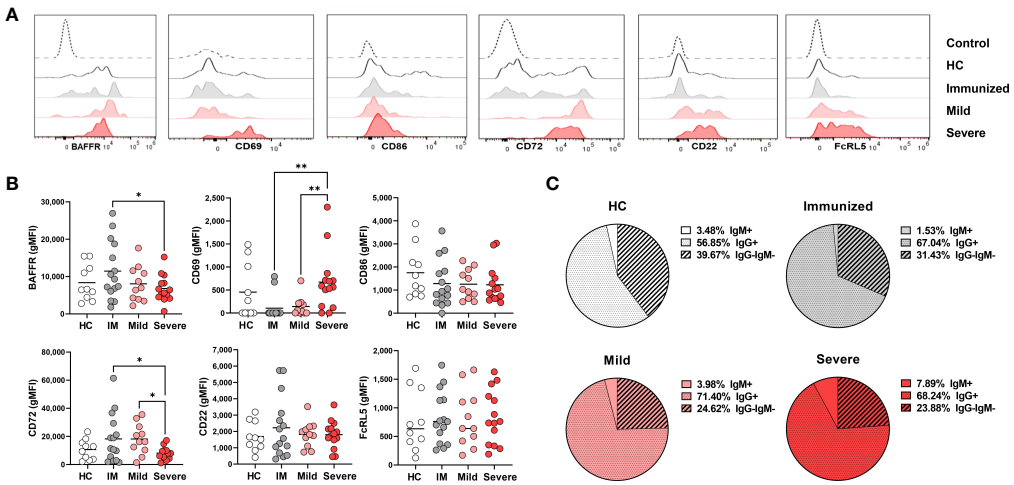

FIGURE 4
Phenotypic changes in DN2 cells with Severe SARS-CoV-2 infection. **(A)** Representative histograms depicting expression of BAFFR, CD69, CD86, CD72, CD22 and FcRL5 on DN2 cells from a healthy control (HC), individual immunized against SARS-CoV-2 or individuals with mild or severe SARS-CoV-2 infection. Control dotted histogram is an FMO for CD69, CD68, CD72 and CD22. Control dotted histogram for BAFFR and FcRL5 is expression on CD3+ T cells from a healthy control subject. **(B)** Quantification of BAFFR, CD69, CD86, CD72, CD22 and FcRL5 expression (gMFI: geometric mean fluorescent intensity) on DN2 cells from healthy controls (HC), those immunized against SARS-CoV-2 (IM), or individuals with mild or severe SARS-CoV-2 infection. **(C)** Pie charts depicting the average frequency of IgM+, IgG+, or IgG-IgM- DN2 cells for healthy controls (HC, N=10), individuals immunized against SARS-CoV-2 (N=15), and individuals with mild (N=11) or severe SARS-CoV-2 infection (N=14). Statistics: one-way ANOVA, *p < 0.05, **p < 0.01.

approximately one quarter of DN2 cells are $IgG^{-}IgM^{-}$and a smaller fraction are IgM+ (Figure 4C). Interestingly, compared to DN2 cells from healthy controls, there was a slight increase in the frequency of IgG^{+} DN2 cells after immunization against SARS-CoV-2, or in individuals with mild or severe SARS-CoV-2 infection (Figure 4C). Importantly, with severe SARS-CoV-2 infection we observed a significant increase in IgM^{+} DN2 cells compared to healthy controls and a corresponding decrease in $IgG^{-}IgM^{-}$ DN2 cells with severe infection (Figure 4C), demonstrating that viral infection alters the composition of immunoglobulin isotype expression in DN2 cells.

Together these data indicate that DN2 cells persist with severe viral infection, are more activated with minimal change in inhibitory receptor expression and slight changes in immunoglobulin isotype class.

Phenotypic characterization of the novel DN3 cells during severe SARS-CoV-2 infection

DN3 cells are a newly reported subset of the Double Negative population with an unknown phenotype (12). Given the significantly increased frequency of DN3 cells with severe SARS-CoV-2 infection (Figure 1), we anticipated that that DN3 cells might display enhanced survival resulting from increased expression levels of BAFFR. Surprisingly, DN3 cells were observed to express significantly lower levels of BAFFR with severe SARS-CoV-2 infection compared to DN3 cells from heathy controls or individuals immunized against SARS-CoV-2 (Figures 5A, B). Together these data, along with the maintenance of BAFFR expression on DN2 cells described above (Figure 4), suggests the DN2 and DN3 subsets apparently rely less on the survival cytokine BAFF with severe viral infection.

Given that DN2 cells express the FcRL5 inhibitory receptor and expression is unchanged with viral infection (Figure 4), we wondered whether DN3 cells also express this receptor. Analysis of FcRL5 expression on DN3 cells reveals that this population appears to normally express low levels of FcRL5 and expression is variably increased on DN3 cells with severe SARS-CoV-2 infection and when compared to immunized individuals or those with mild infection (Figures 5A, B). Examination of other inhibitory receptors, CD72 and CD22, revealed that there was a significant increase in expression level of CD72 on DN3 cells from mild SARS-CoV-2 compared to heathy controls, such that DN3 cells from subjects with severe SARS-CoV-2 infection have significantly lower levels of CD72 expression than from mild infection (Figures 5A, B). Expression of CD22 on DN3 cells from severe SARS-CoV-2 infection trends to a higher level of expression than DN3 cells from heathy controls and subjects with mild infection (Figures 5A, B). Together these data

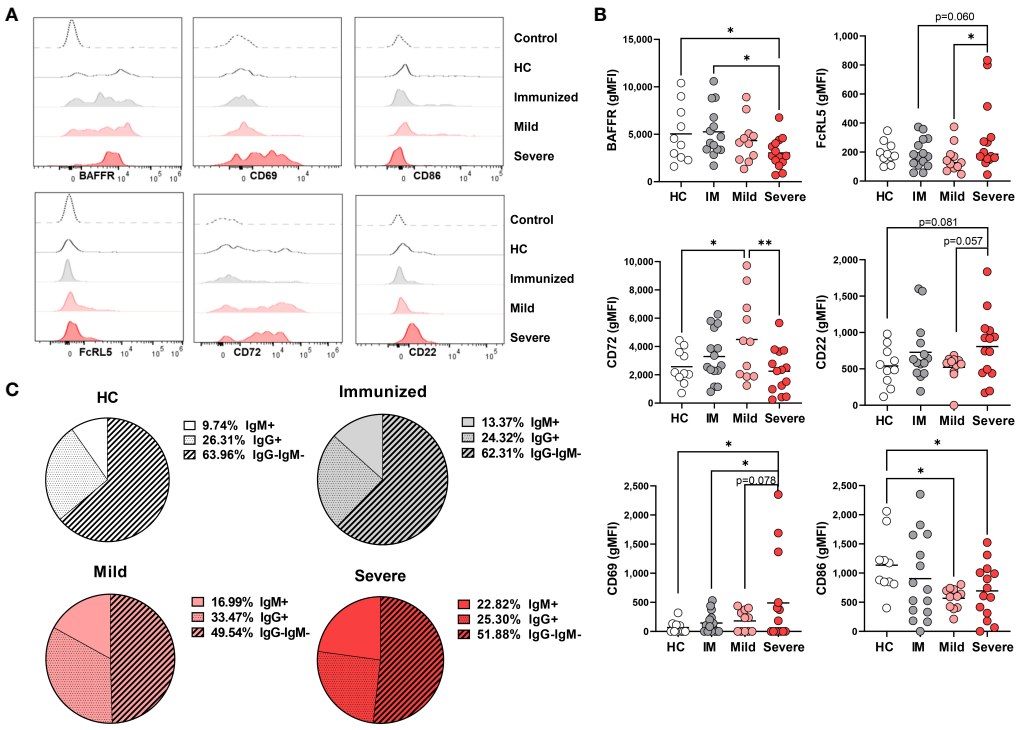

FIGURE 5
Phenotypic changes in DN3 cells with Severe SARS-CoV-2 infection. **(A)** Representative histograms depicting expression of BAFFR, CD69, CD86, FcRL5, CD72, and CD22 on DN3 cells from a healthy control (HC), a subject immunized against SARS-CoV-2, or individuals with mild or severe SARS-CoV-2 infection. Control dotted histogram is an FMO for CD69, CD68, CD72 and CD22. Control dotted histogram for BAFFR and FcRL5 is expression on CD3+ T cells from a healthy control subject. **(B)** Quantification of BAFFR, CD69, CD86, FcRL5, CD72, and CD22 expression (gMFI: geometric mean fluorescent intensity) on DN3 cells from healthy controls (HC), individuals immunized against SARS-CoV-2 (IM), or individuals with mild or severe SARS-CoV-2 infection. **(C)** Pie charts depicting the average frequency of IgM+, IgG+, or IgG-IgM- DN3 cells for healthy controls (HC, N=10), individuals immunized against SARS-CoV-2 (N=15), and individuals with mild (N=11) or severe SARS-CoV-2 infection (N=14). Statistics: one-way ANOVA, *p < 0.05, **p < 0.01.

indicate that inhibitory receptor expression on DN3 cells from severe SARS-CoV-2 infection appears modestly increased compared to DN3 cells from healthy controls.

Our analyses of DN1 and DN2 cell subsets show these populations were both highly activated with severe SARS-CoV-2 infection (Figures 3, 4). Therefore, we next asked whether DN3 cells were also activated as indicated by increased expression of the CD69 and CD86 markers. Quantification of CD69 on DN3 cells revealed that, while variable, on average there is a higher level of expression of CD69 on DN3 cells from severe SARS-CoV-2 infection compared to healthy controls, individuals immunized against SARS-CoV-2 and those with mild infection (Figures 5A, B). These results suggest severe SARS-CoV-2 infection promotes robust activation on DN3 cells. Intriguingly, expression of CD86 was significantly downregulated on DN3 cells from subjects with mild or severe SARS-CoV-2 infection compared to healthy controls, suggesting DN3 cells may have less capacity to activate T cells with viral infection (Figures 5A, B).

To the best of our knowledge, the immunoglobulin isotype class of DN3 cells has not been reported. In this study, the majority of DN3 cells from healthy controls are $IgG^{-}IgM^{-}$ (likely IgA given the reported enrichment in *IGHA2* transcripts) (10), followed by an intermediate frequency of IgG^{+} DN3 cells, with a smaller proportion of IgM^{+} DN3 cells (Figure 5C). A similar breakdown of $IgG^{-}IgM^{-}$ DN3 cells as the most frequent immunoglobulin class followed by an intermediate frequency of IgG^{+} DN3 cells and fewer IgM^{+} DN3 cells was observed in immunized individuals and those with mild or severe SARS-CoV-2 infection (Figure 5C). Importantly, with severe SARS-CoV-2 infection we again observed a significant increase in IgM^{+} DN3 cells and a trend to an increase in IgM^{+} DN3 cells with mild infection compared to DN3 cells from healthy controls (Figure 5C). These changes were concomitant with significant decreases in the frequency of $IgG^{-}IgM^{-}$ DN3 cells from mild or severe SARS-CoV-2 subjects compared to DN3 cells from healthy controls (Figure 5C). These data demonstrate that viral infection modifies isotype class dominance in the DN3 subset.

Overall, it is clear that viral infection modulates the phenotype of the novel DN3 subset such that these cells have reduced BAFFR and CD86 but elevated levels of FcRL5, CD22, and CD69 during severe disease. A summary of these findings is depicted in Supplemental Table 2.

Double negative B cells subsets maintain the ability to signal through the BCR during severe SARS-CoV-2 infection

DN2 cells from SLE patients have the ability to signal through the BCR despite expressing CD22 and FCRL5 inhibitory receptors (9), however the functional capacity of DN2 cells to respond to BCR signaling in healthy individuals or other disease states has not been reported. DN2 cells from severe SARS-CoV-2 infection also express inhibitory receptors and thus we asked whether DN2 cells maintained an ability to signal through the BCR. To address this, PBMCs from healthy controls, immunized individuals, or individuals with either mild or severe SARS-CoV-2 infection were stimulated with anti-human Ig to induce BCR signaling and DN subsets were subsequently assessed for activation of BCR signaling effector molecules as previously described (34). Specifically, we used flow cytometry to measure the mean fluorescence intensity of phospho-SYK (pSYK), a tyrosine kinase signaling molecule proximal to the BCR (34), with and without anti-Ig stimulation. The results from these analyses revealed that DN1 cells from all cohorts (heathy controls, immunized individuals and SARS-CoV-2 mild and severe infected individuals) displayed significant increases in pSYK levels after BCR stimulation (Figure 6). Similar increases in pSYK levels were observed for DN2 and DN3 cells in all cohorts (Figure 6). We further quantified levels of pPLCγ2, another BCR signaling effector molecule further downstream in the BCR signal transduction cascade. Here, we again found that the B cells within all three DN subsets, DN1, DN2 and DN3, and from each cohort, displayed significant increases in pPLCγ2 levels after BCR stimulation (Figure 6). These data indicate that despite changes in B cell inhibitory receptor expression with severe SARS-CoV-2 infection observed above, the B cells within all DN subsets maintain the ability to transduce signals originating from the BCR.

We have previously reported that severe SARS-CoV-2 infection enhances BCR signaling by B_{ND} cells, a typically functionally anergic B cell population in healthy controls (24).

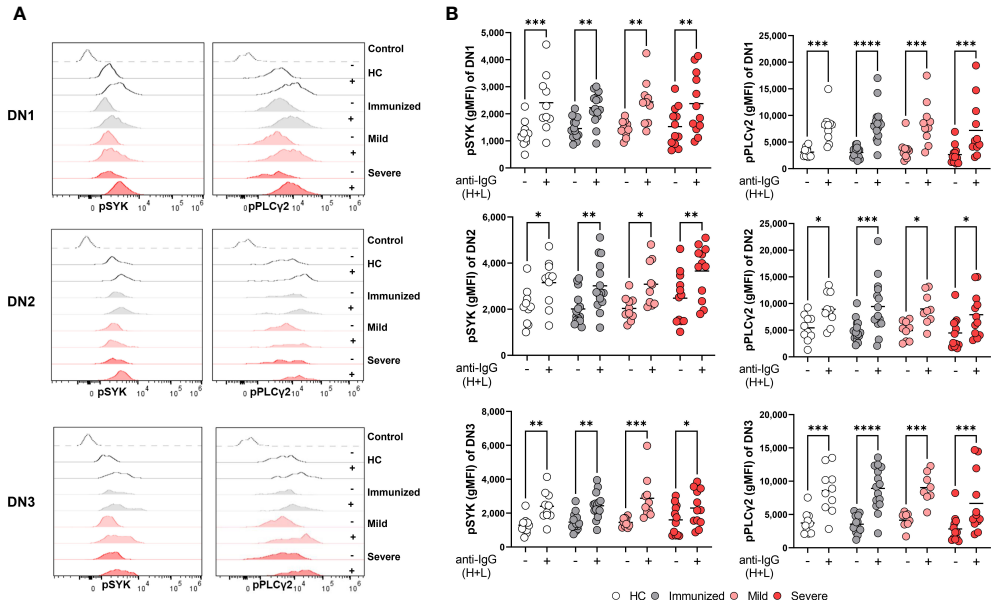

FIGURE 6
Maintenance of BCR signaling in Double Negative subsets during Severe SARS-CoV-2 infection. **(A)** Representative histograms depicting expression of pSYK and pPLCγ2 on DN1, DN2, or DN3 cells from a healthy control (HC), individual immunized against SARS-CoV-2, and individual with mild or severe SARS-CoV-2 infection without (-) or with (+) stimulation by 10μg/mL anti-IgG (H+L) F(ab')2 for 5 min. Control dotted histogram is an FMO. **(B)** Quantification of expression levels of pSYK and pPLCγ2 (gMFI: geometric mean fluorescent intensity) on DN1, DN2, or DN3 cells from healthy controls (HC, N=10), individuals immunized against SARS-CoV-2 (N=15), or individuals with mild (N=10) or severe SARS-CoV-2 infection (N=12) without **(-)** or with (+) stimulation by 10μg/mL anti-IgG (H+L) F(ab')2 for 5 min. Statistics. one-way ANOVA, *p < 0.05, **p < 0.01, ***p < 0.001, ****p < 0.0001.

To determine if DN2 or any of the B cells within the different DN subsets display enhanced BCR signaling with severe viral infection, we calculated the fold difference of pSYK and pPLγC2 between unstimulated and BCR-stimulated B cells and compared these values between cohorts. The results of these analyses did not reveal any significant enhancement in the ability of B cells from any DN subset, or cohort, to transduce BCR signals leading to SYK and PLCγ2 activation (Supplemental Figure 1). Thus, despite residing at a higher activation level as observed above (CD69), DN2 cells do not display an enhancement in BCR signaling with severe viral infection. However, we noted that DN2 cells from healthy controls, immunized individuals and individuals with mild infection displayed increased basal levels of pSYK and pPLCγ2 relative to DN1 and DN3 cells (Supplemental Figure 2). We observed a similar higher basal level of pSYK and pPLCγ2 expression in DN2 cells compared to DN1 or DN3 cells from individuals with severe SARS-CoV-2 infection (Figure 7). This suggests that DN2 cells naturally have the largest capacity to signal through the BCR compared to other DN subsets, a process which may be independent of traditional inhibitory receptors (CD22, CD72, FcRL5) and/or that the function of inhibitory receptors is impaired during viral infection.

Systemic inflammation during severe SARS-CoV-2 infection is linked to alteration in Double Negative B cell frequency

Inflammatory cytokines such as IFNλ and IFNγ are able to promote the *in vitro* generation of DN2 cells from naive B cells

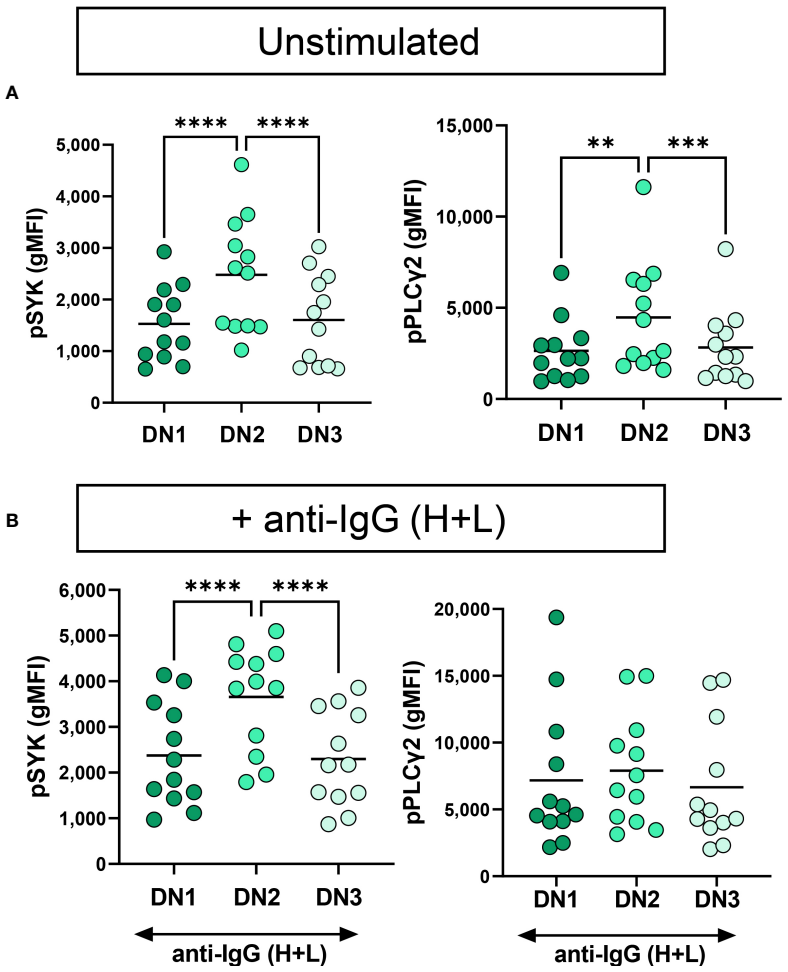

FIGURE 7
Functional comparison of DN1, DN2 and DN3 cells in severe SARS-CoV-2 infection. **(A)** Quantification of expression level of pSYK or pPLCγ2 on DN1, DN2 or DN3 cells from individuals with severe SARS-CoV-2 infection (N=12) without (unstimulated) or **(B)** with stimulation by 10μg/mL anti-IgG (H+L) F(ab')2 for 5 min. Statistics. one-way ANOVA, **p < 0.01, ***p < 0.001, ****p < 0.0001.

(9, 14, 15) and we and others have reported an increase in pro-inflammatory cytokines with severe SARS-CoV-2 infection (Supplemental Table 1) (16, 24, 35). Accordingly, we questioned whether the increased systemic inflammation associated with severe viral infection might account for the observed changes in DN subset frequencies. We began to address this by measuring levels of C-reactive protein (CRP) in plasma, an indicator of overall inflammatory state, from immunized and virally infected cohorts and as expected found that CRP levels were significantly higher in severe SARS-CoV-2 when compared to levels found in individuals immunized against SARS-CoV-2 (Supplemental Table 1). Furthermore, levels of CRP significantly correlated negatively with the frequency of DN1 cells within the Double Negative population (Figure 8A). In line with the CRP correlation, there were also significant negative correlations between the levels of TNF, IL-6, IFNγ, and IL-1β and the frequency of DN1 cells (Figure 8A). These data indicate that SARS-CoV-2 associated inflammation promotes a loss of the DN1 population. In contrast, the observed increases in the DN2 subset were significantly and positively correlated with levels of CRP as was the frequency of DN2 cells within the Double Negative population (Figure 8B), in keeping with similar previous observations (12, 21). We further observed significant positive correlations between the levels of specific cytokines including TNF, IL-6, IFNγ, and IL-1β with the increased frequency of DN2 cells (Figure 8B). These data suggest that the inflammation associated with severe SARS-CoV-2 infection likely drives expansion of the DN2 subset. Moreover, correlation of levels of CRP with the frequency of DN3 cells again demonstrated a significant positive relationship (Figure 8C), and as previously reported (11). There were again significant positive correlations between the levels of the TNF, IL-6, IFNγ, and IL-1β proinflammatory cytokines and the frequency of DN3 cells in our cohorts (Figure 8C). Overall, these data link broad systemic inflammation and specific inflammatory cytokines with the observed changes in specific DN subset frequencies during severe SARS-CoV-2 infection.

Changes in Double Negative B cell frequency are linked to increased levels of autoreactive antibodies during severe SARS-CoV-2 infection

We and others have reported an increase in systemic autoreactive antibodies during severe SARS-CoV-2 infection (Supplemental Table 1) (18–20, 24, 36), suggesting an infection-induced breach in immunological tolerance and expansion of autoreactive B cells in response to inflammation during viral infection. Whereas DN1 cells are not thought to harbor autoreactive specificities, DN2 cells were demonstrated to be enriched in cells harboring a VH4-34 specificity (9), an indicator of autoreactivity in SLE patients (26, 37). Expression of germline VH4-34 Ig heavy chain in human B cells is

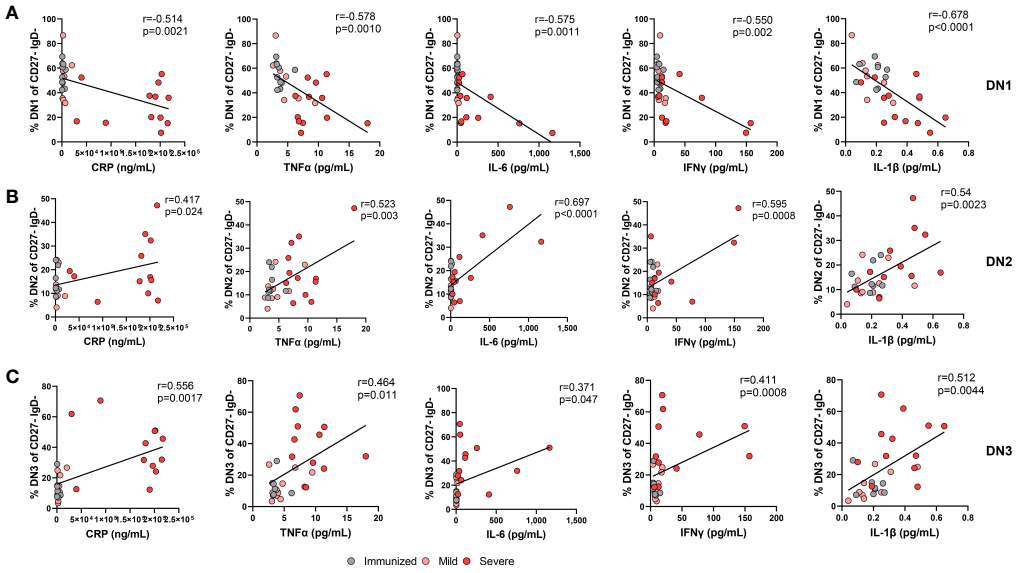

FIGURE 8
The alteration in the frequency of Double Negative populations correlates with increased systemic inflammation during Severe SARS-CoV-2 infection. **(A)** Correlation of systemic cytokine levels (CRP, TNFα, IL-6, IFNγ, IL-1β) in individuals immunized against SARS-CoV-2 (grey circles, N=8), individuals with mild (pink circle, N=9) and severe SARS-CoV-2 infection (red circle, N=12) with frequency of DN1 cells, **(B)** frequency of DN2 cells, or **(C)** frequency of DN3 cells within total double negative population (CD27-IgD-). Statistics: Pearson correlation, r and p values noted on each panel.

associated with BCRs with specificity to nuclear antigen, chromatin, CD45 and glycoproteins on red blood cells (26, 37). We and others have demonstrated that serum autoantibodies of VH4-34 origin are elevated in severe SARS-CoV-2 infection (12, 24). The specificities displayed by DN3 cells, and whether there is a similar enrichment in autoreactive specificity, has not been established. As we observe increased frequencies of both DN2 and DN3 subsets with severe viral infection, we asked whether either DN2 or DN3 subset was associated with autoantibody production during severe SARS-CoV-2 infection. Correlating of the frequency of DN1 cells within the Double Negative population with the plasma titer of VH4-34 IgG normalized to total IgG levels revealed a significant negative correlation between these parameters (Figure 9A). Similarly, we observed a significant negative correlation between the frequency of DN1 cells and the relative titer of anti-Smith IgG antibodies (Figure 9A). A trend was further observed between the correlation of the frequency of DN1 cells with the relative titers of anti-Chromatin IgG or anti-Cardiolipin IgG (Figure 9A). These data indicate that a reduction in the presence of DN1 cells with severe viral infection correlates with a rise in autoreactive antibody titers suggesting that DN1 cells may be limiting in the formation of autoantibodies.

Surprisingly, despite the reported enrichment of autoreactive specificities within the DN2 cell subset in SLE, our data did not demonstrate any significant correlation between the frequency of DN2 cells within the Double Negative population and the relative titers of VH4-34, anti-Chromatin, anti-Smith or anti-cardiolipin IgG (Figure 9B). In contrast, we instead find that a significant positive correlation exists between the frequency of DN3 cells within the Double Negative population and relative titers of VH4-34 (Figure 9C). Furthermore, the frequency of DN3 cells significantly and positively correlated with the relative titers of not only VH4-34 but also anti-chromatin IgG, anti-Smith IgG, and anti-cardiolipin IgG (Figure 9C). Importantly, there was a significant negative correlation between the frequency of DN3 and DN1 cells, whereas no correlation was observed between the frequency of DN3 and DN2 cells (Supplemental Figure 3). These data suggest that as DN3 cells expand in frequency with severe SARS-CoV-2 infection so too do the levels of autoreactive antibodies and implicating this novel cell type as a potential driver of autoimmunity. Together these data indicate a strong link between the alteration in the frequency of DN1 and DN3 subsets during severe SARS-CoV-2 infection and the development of autoreactive antibodies.

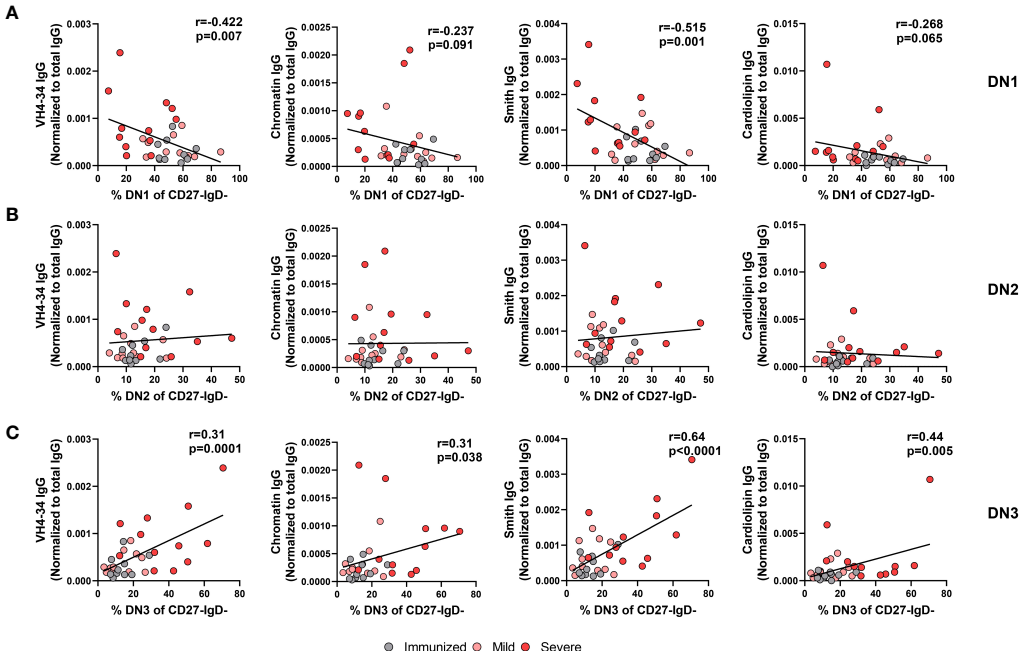

FIGURE 9
Correlation of autoreactive antibodies with changes in Double Negative subset frequencies during Severe SARS-CoV-2 infection. **(A)** Correlation of frequency of DN1 cells, **(B)** frequency of DN2 cells, or **(C)** frequency of DN3 cells within total double negative population (CD27-IgD-) with systemic levels of autoreactive IgG antibodies (VH4-34, Chromatin, Smith, cardiolipin) normalized to total IgG from individuals immunized against SARS-CoV-2 (N=10), and individuals with mild (N=11) or severe SARS-CoV-2 infection (N=13). Statistics: Pearson correlation, r and p values noted on panel.

Discussion

In this report we have interrogated the proportion, phenotype, and functional ability of DN1, DN2 and DN3 B cell subsets in healthy individuals, individuals immunized against SARS-CoV-2 and those with either mild or severe SARS-CoV-2 infection. We also quantified the level of inflammation by measurement of C-reactive protein and specific proinflammatory cytokines in plasma as well as titers of specific serum autoantibodies. From these findings we confirm a striking alteration in composition of the Double Negative population in individuals with severe SARS-CoV-2 infection such that the frequency of DN1 B cells decreases, whereas the DN2 and DN3 subset frequencies increase. We reveal by in-depth characterization of the DN subsets that B cells within each DN1, DN2, and DN3 subset with severe viral infection are highly activated, express altered frequencies of immunoglobulin isotype class, and maintain ability to signal *via* the BCR, suggesting these DN B cells are able to mount an antibody response. Importantly, an increased frequency of DN3 cells with concomitant loss of DN1 cells significantly correlated with increased systemic inflammation and autoreactive antibody production during SARS-CoV-2 infection. Thus, these data provide strong evidence that inflammatory cytokines promote alteration of the Double Negative B cell compartment during SARS-CoV-2 infection, likely contributing to the production of autoreactive antibodies with viral infection.

We present data in this study suggesting that the expansion of the DN2 and DN3 subsets and contraction of the DN1 subset in severe SARS-CoV-2 infection is driven by elevated virally-associated cytokines. Expansion of DN2 in SLE is associated with elevated levels of IFN-γ or IFN-λ (9, 14, 15). Importantly, exposure of naive B cells *in vitro* to IFN-γ or IFN-λ in the presence of TLR7L, IL-21, BAFF and BCR stimulation promotes generation of DN2 cells (9, 15, 38), demonstrating a role for inflammatory cytokines and viral ligands in driving expansion of the DN2 subset. Given these reports, and that we and others have reported increased levels of IFN-γ with SARS-CoV-2 infection (16, 24, 39), it is possible that an analogous process occurs *in vivo* during severe viral infection to promote DN2 subset expansion. As the DN3 population has only recently been identified, the B cell developmental pathway(s) leading to a DN3 cell is not clear, although trajectory analysis suggests that DN3 cells may be precursors to DN2 cells (10); in this study we confirm previous findings that elevated levels of CRP in severe SARS-CoV-2 infection is associated with an increased frequency of DN3 cells (11). Further supporting the role for viral-associated inflammation in driving expansion of the DN3 subset, we identify four specific pro-inflammatory cytokines (IFN-γ, TNF-α, IL-6, and IL-1β) that positively correlate with increased DN3 frequencies. To the best of our knowledge, no other studies have reported an expansion of DN2 or DN3 cells with other viruses. One study did report an expansion of the total DN population after immunization with live attenuated virus against tick borne encephalitis, however the exact subset(s) responsible for the increased frequency was not determined (6). Based on our data here we speculate that if systemic inflammation increases with viral infection or vaccination with whole virus so too would expansion of the DN2 and DN3 subsets. The precise mechanism(s) by which inflammatory cytokines modulate the expansion of DN3/DN2 cells and loss of DN1 cells during severe SARS-CoV-2 infection is an area of current investigation.

Here in this report, we have confirmed the expansion of DN2 and DN3 subsets associated with severe SARS-CoV-2 infection reported by others (11, 21, 22). It remains to be determined whether these subsets contribute to protective humoral responses during viral infection or contribute to COVID-19 disease pathology or both. In severe SARS-CoV-2 infection, broad immune activation of the extrafollicular B cell pathway (a dominant pathway for DN2 generation in SLE) was associated with poor clinical outcomes (12) and an elevated presence of DN3 cells has been associated with worse clinical outcomes (23), suggesting pathogenic roles for DN2 and DN3 cells. Importantly, DN2 cells are enriched in autoreactive VH4-34 clones in SLE and are precursors to autoreactive antibody secreting cells (9), and we and others have reported an increase in VH4-34 IgG levels during severe SARS-CoV-2 infection (12, 24). In this study we demonstrate that expansion of the DN3 subset positively correlates with increased levels of the specific autoreactive antibodies we tested (VH4-34, chromatin, Smith, cardiolipin) indicating that DN3 cells may contribute to autoantibody production during SARS-CoV-2 infection. Conversely, SARS-CoV-2 DN2 and DN3 cells able to bind Spike Receptor Binding Domain (RBD) have been identified, suggesting that viral infection can induce expansion of B cells with specificity to neutralizing epitopes in the Double Negative population (21, 22), although whether DN subsets have specificity to other viral antigens remains to be determined. Interestingly, a preprint study has identified an antibody with specificity to both SARS-CoV-2 and glomerular basement membrane, indicating that cross-reactive antibodies that are anti-viral and autoreactive can be produced during SARS-CoV-2 infection (Woodruff et al., 2021 medRxiv). Finally, determining if DN3 cells are a key source of autoantibodies and/or contribute to pathology observed in severe COVID-19 is an area of active investigation.

We did not address whether the expansion of the DN2 and DN3 subsets with severe viral infection was transient or durable. Our data here on the presence of these DN subsets in healthy controls, immunized individuals and those with mild viral infection would suggest that with resolution of viral-associated inflammation, the frequency of DN2 and DN3 subsets will revert back to levels that are observed in healthy controls. In support of this, a decreased frequency of RBD-specific DN2 cells was

observed 10 weeks post-infection when compared to levels during acute infection (22), suggesting that expansion of virus-specific DN2 cells is transient and resolves with infection. However, it should be noted that even five months post-recovery from severe infection, RBD-specific Double Negative B cells are still detectable (40), indicating that expansion of virally-associated DN subsets likely contracts with infection but are not lost. Furthermore, expansion of atypical memory B cells ($CD27^{-}CD21^{lo/-}$), which would include both DN2 and DN3 subsets, is resolved in patients recovered from severe SARS-CoV-2 infection (41, 42). Importantly, 6 months post-recovery from severe SARS-CoV-2 infection, one group reports a reduction in autoreactive antibody levels, suggesting a loss or contraction of the autoreactive B cell population (Woodruff et al., 2021 medRxiv). It would be of interest to determine if those who present to the clinic as COVID-19 'long-haulers' maintain expansion of DN2 and DN3 subsets to determine if these subsets play a role in remaining disease pathology.

Previous studies of atypical memory B cells ($CD27^{-}CD21^{lo/-}$), that by definition include DN2 and DN3 cells, in the context of malaria and HIV viral infection have reported these B cells to display impaired BCR signaling and proliferative responses (43, 44), a finding that has also been demonstrated in atypical memory B cells from patients with rheumatoid arthritis and Common Variable Immunodeficiency (45, 46). In this study, we do not find any evidence of defective BCR signaling in the DN1, DN2 or DN3 cells from healthy individuals or those with severe SARS-CoV-2 infection. In support of our findings, it has been shown that DN2 cells from SLE patients display intact BCR signaling as determined by levels of the BCR signaling effector, phospho-BLNK (9). Interestingly, we show that DN2 cells from severe SARS-CoV-2 infection had the highest level of pSYK expression upon BCR stimulation when compared with DN1 or DN3 cells. Overall, these findings indicate that DN1, DN2 or DN3 cells have functional BCR responses during severe SARS-CoV-2 infection. The evaluation of CD86 expression on DN subsets from healthy individuals and individuals with severe SARS-CoV-2 infection is also potentially informative given that CD86 provides a costimulatory signal to T cells. In healthy individuals, CD86 expression on DN1 cells is relatively low and compared to DN2 and DN3 suggesting that these latter populations in healthy individuals are poised to interact with T cells. In contrast, with severe viral infection, DN3 cells lose CD86 expression possibly indicating these cells may be less likely to receive T cell help.

There are limited studies examining immunoglobulin gene family usage, specifically in the Double Negative B cell subsets, during SARS-CoV-2 infection. Analysis of the V(D)J repertoire in antibody secreting cells from severe SARS-CoV-2 infection demonstrated significant oligoclonal expansion with low mutation frequencies (majority expressing germline VH genes) and autoreactive VH4-34 gene usage (12). This pattern has been associated with extrafollicular B cell activation (38), particularly in the DN2 subset during an SLE flare (9). Here in this study we demonstrate that increased frequency of DN3 cells positively correlates with the increase in VH4-34 IgG autoreactive antibodies, suggesting DN3 may be a source of autoreactive antibodies and that DN3 cells do not edit against autoreactive VH4-34 gene family usage. However, more work is needed to determine the degree of somatic hypermutation away from germline and if there is preferential immunoglobulin heavy chain family gene usage in each DN subset, including the novel DN3 cells, during viral infection.

In summary, our study provides evidence that the human Double Negative B cell compartment is altered during severe SARS-CoV-2 infection and that this change in subset type significantly correlates with inflammation and production of autoreactive antibodies. Importantly, these findings also imply that an additional B cell subset, the novel DN3 cells, may contribute to autoreactive antibody production. It remains to be determined whether these autoreactive antibodies are also cross-reactive and can mediate an anti-viral response during infection.

Data availability statement

The raw data supporting the conclusions of this article will be made available by the authors, without undue reservation.

Ethics statement

The studies involving human participants were reviewed and approved by The Colorado Multiple Institutional Review Board (COMIRB) at the University of Colorado School of Medicine and National Jewish Health approved the use of human plasma and PBMCs, and this study was performed under the Declaration of Helsinki. The patients/participants provided their written informed consent to participate in this study.

Author contributions

MC and RT designed the study, interpreted the data and wrote the manuscript. MC recruited immunized and mild SARS-CoV-2 subjects, performed experiments, and analyzed the data. MMS and NT performed experiments. MJS and RP provided expertise and samples and helped interpret results. KL, BP, JM, KM, WJ and JB provided mild or severe SARS-CoV-2 samples. All authors reviewed the manuscript. All authors contributed to the article and approved the submitted version.

Funding

The work was supported by the National Institute of Health Grant R01 AI136534 (RT), AI124474 (RP) and AI131639 (RP). The CU Anschutz CTRC/CCTSI collected whole blood and was supported by NIH/NCATS Colorado CTSA Grant Number UL1 TR002535.

Acknowledgments

We appreciate those who donated blood for this study to be conducted. We acknowledge the ImmunoMicro Flow Cytometry Shared Resource Laboratory at the University of Colorado Anschutz Medical Campus (RRID : SCR_021321), Christine Griesmer, Ayal Levi, Jazalle McClendon, and Shannon McManus for enrolling patients with severe SARS-CoV-2 and processing the biological specimens. We appreciate helpful discussions with Sophie Hillion Weber from University of Brest.

Conflict of interest

The authors declare that the research was conducted in the absence of any commercial or financial relationships that could be construed as a potential conflict of interest.

Publisher's note

All claims expressed in this article are solely those of the authors and do not necessarily represent those of their affiliated organizations, or those of the publisher, the editors and the reviewers. Any product that may be evaluated in this article, or claim that may be made by its manufacturer, is not guaranteed or endorsed by the publisher.

Supplementary material

The Supplementary Material for this article can be found online at: https://www.frontiersin.org/articles/10.3389/fimmu.2022.988125/full#supplementary-material

References

1. Kaminski DA, Wei C, Qian Y, Rosenberg AF, Sanz I. Advances in human b cell phenotypic profiling. *Front Immunol* (2012) 3:302. doi: 10.3389/fimmu.2012.00302

2. Sanz I, Wei C, Jenks SA, Cashman KS, Tipton C, Woodruff MC, et al. Challenges and opportunities for consistent classification of human b cell and plasma cell populations. *Front Immunol* (2019) 10:2458. doi: 10.3389/fimmu.2019.02458

3. Huang W, Sinha J, Newman J, Reddy B, Budhai L, Furie R, et al. The effect of anti-CD40 ligand antibody on b cells in human systemic lupus erythematosus. *Arthritis rheumatism* (2002) 46(6):1554–62. doi: 10.1002/art.10273

4. Anolik JH, Barnard J, Cappione A, Pugh-Bernard AE, Felgar RE, Looney RJ, et al. Rituximab improves peripheral b cell abnormalities in human systemic lupus erythematosus. *Arthritis rheumatism* (2004) 50(11):3580–90. doi: 10.1002/art.20592

5. Wei C, Anolik J, Cappione A, Zheng B, Pugh-Bernard A, Brooks J, et al. A new population of cells lacking expression of CD27 represents a notable component of the b cell memory compartment in systemic lupus erythematosus. *J Immunol* (2007) 178(10):6624–33. doi: 10.4049/jimmunol.178.10.6624

6. Ruschil C, Gabernet G, Lepennetier G, Heumos S, Kaminski M, Hracsko Z, et al. Specific induction of double negative b cells during protective and pathogenic immune responses. *Front Immunol* (2020) 11:606338. doi: 10.3389/fimmu.2020.606338

7. Fraussen J, Marquez S, Takata K, Beckers L, Montes Diaz G, Zografou C, et al. Phenotypic and ig repertoire analyses indicate a common origin of IgD(-)CD27(-) double negative b cells in healthy individuals and multiple sclerosis patients. *J Immunol* (2019) 203(6):1650–64. doi: 10.4049/jimmunol.1801236

8. Richardson CT, Slack MA, Dhillon G, Marcus CZ, Barnard J, Palanichamy A, et al. Failure of b cell tolerance in CVID. *Front Immunol* (2019) 10:2881. doi: 10.3389/fimmu.2019.02881

9. Jenks SA, Cashman KS, Zumaquero E, Marigorta UM, Patel AV, Wang X, et al. Distinct effector b cells induced by unregulated toll-like receptor 7 contribute to pathogenic responses in systemic lupus erythematosus. *Immunity* (2018) 49 (4):725–39.e6. doi: 10.1016/j.immuni.2018.08.015

10. Stewart A, Ng JC, Wallis G, Tsioligka V, Fraternali F, Dunn-Walters DK. Single-cell transcriptomic analyses define distinct peripheral b cell subsets and discrete development pathways. *Front Immunol* (2021) 12:602539. doi: 10.3389/fimmu.2021.602539

11. Sosa-Hernandez VA, Torres-Ruiz J, Cervantes-Diaz R, Romero-Ramirez S, Paez-Franco JC, Meza-Sanchez DE, et al. B cell subsets as severity-associated signatures in COVID-19 patients. *Front Immunol* (2020) 11:611004. doi: 10.3389/fimmu.2020.611004

12. Woodruff MC, Ramonell RP, Nguyen DC, Cashman KS, Saini AS, Haddad NS, et al. Extrafollicular b cell responses correlate with neutralizing antibodies and morbidity in COVID-19. *Nat Immunol* (2020) 21(12):1506–16. doi: 10.1038/s41590-020-00814-z

13. Jenks SA, Wei C, Bugrovsky R, Hill A, Wang X, Rossi FM, et al. B cell subset composition segments clinically and serologically distinct groups in chronic cutaneous lupus erythematosus. *Ann rheumatic dis* (2021) 80(9):1190–200. doi: 10.1136/annrheumdis-2021-220349

14. Zumaquero E, Stone SL, Scharer CD, Jenks SA, Nellore A, Mousseau B, et al. IFNgamma induces epigenetic programming of human T-bet(hi) b cells and promotes TLR7/8 and IL-21 induced differentiation. *eLife* (2019) 8:1–36. doi: 10.7554/eLife.41641

15. Barnas JL, Albrecht J, Meednu N, Alzamareh DF, Baker C, McDavid A, et al. B cell activation and plasma cell differentiation are promoted by IFN-lambda in systemic lupus erythematosus. *J Immunol* (2021) 207(11):2660–72. doi: 10.4049/jimmunol.2100339

16. Yang L, Liu S, Liu J, Zhang Z, Wan X, Huang B, et al. COVID-19: immunopathogenesis and immunotherapeutics. *Signal transduct targeted Ther* (2020) 5(1):128. doi: 10.1038/s41392-020-00243-2

17. Wang EY, Mao T, Klein J, Dai Y, Huck JD, Liu F, et al. Diverse functional autoantibodies in patients with COVID-19. *medRxiv: Preprint server Health Sci* (2021) 595:283–288. doi: 10.1101/2020.12.10.20247205

18. Bastard P, Rosen LB, Zhang Q, Michailidis E, Hoffmann HH, Zhang Y, et al. Autoantibodies against type I IFNs in patients with life-threatening COVID-19. *Science* (2020) 370(6515):1–12. doi: 10.1126/science.abd4585

19. Chang SE, Feng A, Meng W, Apostolidis SA, Mack E, Artandi M, et al. New-onset IgG autoantibodies in hospitalized patients with COVID-19. *Nat Commun* (2021) 12(1):5417. doi: 10.1038/s41467-021-25509-3

20. Xiao M, Zhang Y, Zhang S, Qin X, Xia P, Cao W, et al. Antiphospholipid antibodies in critically ill patients with COVID-19. *Arthritis Rheumatol* (2020) 72 (12):1998–2004. doi: 10.1002/art.41425

21. Kaneko N, Kuo HH, Boucau J, Farmer JR, Allard-Chamard H, Mahajan VS, et al. Loss of bcl-6-Expressing T follicular helper cells and germinal centers in COVID-19. *Cell* (2020) 183(1):143–57.e13. doi: 10.1016/j.cell.2020.08.025

22. de Campos-Mata L, Tejedor Vaquero S, Tacho-Pinot R, Pinero J, Grasset EK, Arrieta Aldea I, et al. SARS-CoV-2 sculpts the immune system to induce sustained virus-specific naive-like and memory b-cell responses. *Clin Trans Immunol* (2021) 10(9):e1339. doi: 10.1002/cti2.1339

23. Cervantes-Diaz R, Sosa-Hernandez VA, Torres-Ruiz J, Romero-Ramirez S, Canez-Hernandez M, Perez-Fragoso A, et al. Severity of SARS-CoV-2 infection is linked to double-negative (CD27(-) IgD(-)) b cell subset numbers. *Inflammation Res* (2022) 71(1):131–40. doi: 10.1007/s00011-021-01525-3

24. Castleman MJ, Stumpf MM, Therrien NR, Smith MJ, Lesteberg KE, Palmer BE, et al. SARS-CoV-2 infection relaxes peripheral b cell tolerance. *J Exp Med* (2022) 219(6):1–15. doi: 10.1084/jem.20212553

25. Isenberg D, Spellerberg M, Williams W, Griffiths M, Stevenson F. Identification of the 9G4 idiotope in systemic lupus erythematosus. *Br J Rheumatol* (1993) 32(10):876–82. doi: 10.1093/rheumatology/32.10.876

26. Richardson C, Chida AS, Adlowitz D, Silver L, Fox E, Jenks SA, et al. Molecular basis of 9G4 b cell autoreactivity in human systemic lupus erythematosus. *J Immunol* (2013) 191(10):4926–39. doi: 10.4049/jimmunol.1202263

27. Lenschow DJ, Sperling AI, Cooke MP, Freeman G, Rhee L, Decker DC, et al. Differential up-regulation of the B7-1 and B7-2 costimulatory molecules after ig receptor engagement by antigen. *J Immunol* (1994) 153(5):1990–7.

28. Jenks SA, Cashman KS, Woodruff MC, Lee FE, Sanz I. Extrafollicular responses in humans and SLE. *Immunol Rev* (2019) 288(1):136–48. doi: 10.1111/imr.12741

29. Smulski CR, Eibel H. BAFF and BAFF-receptor in b cell selection and survival. *Front Immunol* (2018) 9:2285. doi: 10.3389/fimmu.2018.02285

30. Smith KG, Tarlinton DM, Doody GM, Hibbs ML, Fearon DT. Inhibition of the b cell by CD22: a requirement for Lyn. *J Exp Med* (1998) 187(5):807–11. doi: 10.1084/jem.187.5.807

31. Adachi T, Wakabayashi C, Nakayama T, Yakura H, Tsubata T. CD72 negatively regulates signaling through the antigen receptor of b cells. *J Immunol* (2000) 164(3):1223–9. doi: 10.4049/jimmunol.164.3.1223

32. Haga CL, Ehrhardt GR, Boohaker RJ, Davis RS, Cooper MD. Fc receptor-like 5 inhibits b cell activation *via* SHP-1 tyrosine phosphatase recruitment. *Proc Natl Acad Sci United States America* (2007) 104(23):9770–5. doi: 10.1073/pnas.0703354104

33. Franks SE, Cambier JC. Putting on the brakes: Regulatory kinases and phosphatases maintaining b cell anergy. *Front Immunol* (2018) 9:665. doi: 10.3389/fimmu.2018.00665

34. Packard TA, Cambier JC. B lymphocyte antigen receptor signaling: initiation, amplification, and regulation. *F1000prime Rep* (2013) 5:40. doi: 10.12703/P5-40

35. Darif D, Hammi I, Kihel A, El Idrissi Saik I, Guessous F, Akarid K. The pro-inflammatory cytokines in COVID-19 pathogenesis: What goes wrong? *Microbial pathogenesis* (2021), 153:104799. doi: 10.1016/j.micpath.2021.104799

36. Wang EY, Mao T, Klein J, Dai Y, Huck JD, Jaycox JR, et al. Diverse functional autoantibodies in patients with COVID-19. *Nature.* (2021) 595 (7866):283–8. doi: 10.1038/s41586-021-03631-y

37. Cappione AJ, Pugh-Bernard AE, Anolik JH, Sanz I. Lupus IgG VH4.34 antibodies bind to a 220-kDa glycoform of CD45/B220 on the surface of human b lymphocytes. *J Immunol* (2004) 172(7):4298–307. doi: 10.4049/jimmunol.172.7.4298

38. Tipton CM, Fucile CF, Darce J, Chida A, Ichikawa T, Gregoretti I, et al. Diversity, cellular origin and autoreactivity of antibody-secreting cell population expansions in acute systemic lupus erythematosus. *Nat Immunol* (2015) 16(7):755–65. doi: 10.1038/ni.3175

39. Del Valle DM, Kim-Schulze S, Huang HH, Beckmann ND, Nirenberg S, Wang B, et al. An inflammatory cytokine signature predicts COVID-19 severity and survival. *Nat Med* (2020) 26(10):1636–43. doi: 10.1038/s41591-020-1051-9

40. Reyes RA, Clarke K, Gonzales SJ, Cantwell AM, Garza R, Catano G, et al. SARS-CoV-2 spike-specific memory b cells express higher levels of T-bet and FcRL5 after non-severe COVID-19 as compared to severe disease. *PloS One* (2021) 16(12):e0261656. doi: 10.1371/journal.pone.0261656

41. Oliviero B, Varchetta S, Mele D, Mantovani S, Cerino A, Perotti CG, et al. Expansion of atypical memory b cells is a prominent feature of COVID-19. *Cell Mol Immunol* (2020) 17(10):1101–3. doi: 10.1038/s41423-020-00542-2

42. Wildner NH, Ahmadi P, Schulte S, Brauneck F, Kohsar M, Lutgehetmann M, et al. B cell analysis in SARS-CoV-2 versus malaria: Increased frequencies of plasmablasts and atypical memory b cells in COVID-19. *J leukoc Biol* (2021) 109 (1):77–90. doi: 10.1002/JLB.5COVA0620-370RR

43. Moir S, Ho J, Malaspina A, Wang W, DiPoto AC, O'Shea MA, et al. Evidence for HIV-associated b cell exhaustion in a dysfunctional memory b cell compartment in HIV-infected viremic individuals. *J Exp Med* (2008) 205(8):1797–805. doi: 10.1084/jem.20072683

44. Portugal S, Tipton CM, Sohn H, Kone Y, Wang J, Li S, et al. Malaria-associated atypical memory b cells exhibit markedly reduced b cell receptor signaling and effector function. *eLife* (2015:1–21) 4. doi: 10.7554/eLife.07218

45. Rakhmanov M, Keller B, Gutenberger S, Foerster C, Hoenig M, Driessen G, et al. Circulating CD21low b cells in common variable immunodeficiency resemble tissue homing, innate-like b cells. *Proc Natl Acad Sci United States America* (2009) 106(32):13451–6. doi: 10.1073/pnas.0901984106

46. Isnardi I, Ng YS, Menard L, Meyers G, Saadoun D, Srdanovic I, et al. Complement receptor 2/CD21- human naive b cells contain mostly autoreactive unresponsive clones. *Blood.* (2010) 115(24):5026–36. doi: 10.1182/blood-2009-09-243071

frontiers | Frontiers in Immunology

TYPE Original Research
PUBLISHED 09 December 2022
DOI 10.3389/fimmu.2022.954435

OPEN ACCESS

EDITED BY
Moncef Zouali,
Institut National de la Santé et de la Recherche Médicale (INSERM), France

REVIEWED BY
Fernando Luis Barroso Da Silva,
University of São Paulo, Brazil
Sreenu Vattipally,
University of Glasgow, United Kingdom

*CORRESPONDENCE
Magdalena Plebanski
magdalena.plebanski@rmit.edu.au

SPECIALTY SECTION
This article was submitted to B Cell Biology, a section of the journal Frontiers in Immunology

RECEIVED 27 May 2022
ACCEPTED 14 November 2022
PUBLISHED 09 December 2022

CITATION
Boer JC, Pan Q, Holien JK, Nguyen T-B, Ascher DB and Plebanski M (2022) A bias of Asparagine to Lysine mutations in SARS-CoV-2 outside the receptor binding domain affects protein flexibility. *Front. Immunol.* 13:954435. doi: 10.3389/fimmu.2022.954435

A bias of Asparagine to Lysine mutations in SARS-CoV-2 outside the receptor binding domain affects protein flexibility

Jennifer C. Boer[1], Qisheng Pan[2,3], Jessica K. Holien[4], Thanh-Binh Nguyen[2,3], David B. Ascher[2,3] and Magdalena Plebanski[1]*

[1]School of Health and Biomedical Science, Royal Melbourne Institute of Technology, Melbourne, VIC, Australia, [2]School of Chemistry and Molecular Biosciences, University of Queensland, Brisbane, QLD, Australia, [3]Computational Biology and Clinical Informatics, Baker Heart and Diabetes Institute, Melbourne, VIC, Australia, [4]School of Science, Royal Melbourne Institute of Technology (RMIT) University, Melbourne, VIC, Australia

Introduction: COVID-19 pandemic has been threatening public health and economic development worldwide for over two years. Compared with the original SARS-CoV-2 strain reported in 2019, the Omicron variant (B.1.1.529.1) is more transmissible. This variant has 34 mutations in its Spike protein, 15 of which are present in the Receptor Binding Domain (RBD), facilitating viral internalization via binding to the angiotensin-converting enzyme 2 (ACE2) receptor on endothelial cells as well as promoting increased immune evasion capacity.

Methods: Herein we compared SARS-CoV-2 proteins (including ORF3a, ORF7, ORF8, Nucleoprotein (N), membrane protein (M) and Spike (S) proteins) from multiple ancestral strains. We included the currently designated original Variant of Concern (VOC) Omicron, its subsequent emerged variants BA.1, BA2, BA3, BA.4, BA.5, the two currently emerging variants BQ.1 and BBX.1, and compared these with the previously circulating VOCs Alpha, Beta, Gamma, and Delta, to better understand the nature and potential impact of Omicron specific mutations.

Results: Only in Omicron and its subvariants, a bias toward an Asparagine to Lysine (N to K) mutation was evident within the Spike protein, including regions outside the RBD domain, while none of the regions outside the Spike protein domain were characterized by this mutational bias. Computational structural analysis revealed that three of these specific mutations located in the central core region, contribute to a preference for the alteration of conformations of the Spike protein. Several mutations in the RBD which have circulated across most Omicron subvariants were also analysed, and these showed more potential for immune escape.

Conclusion: This study emphasizes the importance of understanding how specific N to K mutations outside of the RBD region affect SARS-CoV-2

conformational changes and the need for neutralizing antibodies for Omicron to target a subset of conformationally dependent B cell epitopes.

KEYWORDS

molecular modelling, Omicron, infectiousness, mutation, SARS-CoV-2

Introduction

SARS-CoV-2 is part of the *Betacoronavirus* genus, a highly diverse group of viruses characterized by positive-sense, single-strand RNA (1), which can infect many mammalian and avian species. SARS-CoV-2 infection occurs mainly *via* the Spike protein (2–4), which is structurally characterized by an S1 subunit and an S2 subunit. The S1 contains the receptor binding domain (RBD), while the S2 region drives the membrane fusion (5).

Binding of the human ACE2 receptor to RBD is a critical step for initiation of target cell entry and can occur with high affinity even at very low molar ranges of viral proteins (6). The RBD undergoes conformational changes that fluctuate between configurations identified as "up" (or open) and "down" (or closed) states. The "up" configuration allows accessibility to the ACE2 receptor binding site, while in the "down" state it remains hidden (4, 7). In addition, the binding of RBD to ACE2 receptor exposes the viral S2 domain allowing it to insert the fusion peptide into the target cell membrane (8, 9). Studies like these are a strong indication that residues outside of the Spike protein RBD area can also play a critical role in viral pathogenesis and underpin the abilty of the virus to dock onto host cells.

As the rapid evolution of SARS-CoV-2 continues, new variants like Omicron (B.1.1.529.1 or BA.1) and its subvariants (BA.2, BA.3, BA.4, BA.5, BQ.1 and BBX.1) have emerged, which contain an alarming number of Spike protein mutations. A total of 34 mutations have been identified in the Spike protein of Omicron, when compared to the original Wuhan strain (10). Mutations are mostly found in the RBD and N-terminal domain, which at the same time, are also both major targets for neutralizing antibodies. The high number of mutations present in Omicron is also a great cause of concern for the efficacy of existing vaccines as well as immune-therapeutics and has led Pfizer to formulate a new vaccine targeted against Omicron, which passed Phase III trials (11). Many attempts have been made to better understand the SARS-CoV-2 neutralizing antibody binding properties and how these have evolved to compromise protection provided by vaccination or prior infection. For instance, through the use of an artificially constructed neutralization resistant virus expressing the Omicron Spike protein variant, authors showed that Omicron and the neutralization resistant Spike construct, were both 30-180 fold more resistant to neuralization by convalescent plasma, compared to the original Wuhan sequence (12).

Meanwhile, a molecule-based data-driven type of analysis compared the binding free energy (BFE) of Omicron against Wuhan RBD complexes, to 132 known antibody specificities (13). The results showed that the mutations present in Omicron had a considerable impact on antibody binding to the virus and suggested an ongoing natural evolutionary pressure of the SARS-CoV-2 virus to direct its antigenic drift towards evading human immune response. Most importantly, the authors concluded that the emerging Omicron mutations, enable the virus to escape antibody immunity induced by current vaccines (13).

The repercussions of an evolutionary pressure that directs specific point mutations of SARS-CoV-2 toward antibody evasion is of considerable importance and requires robust investigation. Understanding the mutations that could affect conformational stability, antibody docking and recognition of these types of B cell epitopes, is imperative for successful vaccine design, and will help foster strategies able to promote effective production of neutralizing antibodies in response to vaccination, correlated with long-term protective immunity against viral infection.

In this paper, we investigated mutations specifically occurring in Omicron and it's subvariants, across several proteins when compared to all the other prominent ancestral variants. Of these mutations, a vast majority appeared to be an N to K mutation occurring specifically in the Spike protein region. Although the N to K mutations occur mainly outside of the RBD region, they are potential key contributors to the change of the RBD conformations of the Spike protein. Further to that, several mutations in the RBD of Omicron's subvariants were also analysed, which showed a stronger potential of immune escape, compared to the prototype. These results emphasize the understanding of how mutations outside of the RBD area can affect structural organization of the virus and can help further our knowledge of B cell epitope recognition, which is crucial for the advancement of peptide-based future vaccine design strategies.

Materials and methods

In this work, we first performed the alignments on the full-spectrum of SARS-CoV-2 proteins of all the current and past VOCs, followed by computational structural analysis to investigate the effects of residue mutation specifically on Omicron and its subvariants. Additional *in-silico* experiments

were performed on the mutations in RBD to explore the infectiousness and immune escape properties of Omicron Spike variants directly.

SARS-CoV-2 variant alignment

For SARS-CoV-2 variants protein alignment, we used the original Omicron, 5 different subvarariants, two emerging variants and the original Wuhan sequence (Table 1). The FASTA sequences were retrieved from the GISAID database (https://www.gisaid.org/) (14–16). In the EpiCov search section of GISAID there is an available tab that allows for the selection of the major circulating variants. Of these, we selected the current VOC Omicron (including its subvariants BA.1, BA.2, BA.3, BA.4, BA.5 plus XBB.1 and BQ.1, the two variants predicted to emerge as dominant variants) and previously circulating VOCs (Alpha, Beta, Gamma, and Delta). The virus names listed below are GISAID nomenclature and the specific viruses were selected based on various conditions: for all variants we selected the conditions in which the sequence was complete and excluding sequences with low coverage. Variants were chosen based on their historical appearance. The specific amino acid sequences of the various genomic regions were obtained from the selected variants with FASTA sequence on GISAID and searched using BlastN (17, 18). Within the cross-platform sequence alignment editor Jalview (19), we performed Multiple Sequence Alignment using Fast Fourier (MAFFS) (20) which is a high-speed multiple sequence alignment algorithm utilizing the Fast Fourier Transform to optimize protein alignments based on the amino acidic physical properties (19). We further aligned the amino acid sequences for the surface glycoprotein, membrane protein and nucleoprotein, ORF3a, ORF7 and ORF8 areas of Alpha, Beta, Gamma, Delta and Omicron variants plus the original Wuhan sequence, and set the latter as a reference genome.

Spike protein structure curation *via* homology modelling

To build the complete structure for the following *in-silico* structural analysis, homology modelling was performed to build the missing regions in the experimental structures using MODELLER version 10.2 (21). We built the Spike protein trimer to obtain a comprehensive 3D insight, rather than only model the crucial region, such as the RBD (22–24). The different templates used to model were listed in Table 2.

Two apo trimeric Spike protein systems, all RBD-up and all RBD-down, were prepared for this work. Alignment for modelling Omicron Spike protein was based on protein sequence change in Omicron to reduce human artefacts (25). For the RBD-down system, we employed a cryo-EM-determined structure with three RBD being down state (PDB ID: 7DWY) (26) to model the Spike folding. For the RBD-up system, we used the Spike-Ab complex having all monomers in up position with missing region from residues 827 to 854 (PDB ID: 7CZZ) (27) and Spike protein (PDB ID: 7KRR) (28) having only 1 monomer in up position (chain A) without missing region from residues 827 to 854 as templates. Similar to the modelling of the apo Spike RBD-up system, the Spike-ACE2 and Spike-Ab models were built using the template complex Spike-ACE2 (PDB ID: 7KJ4 (29) and Spike-Ab (PDB ID: 7CZZ), respectively. The missing region from both templates were built using up conformation of Spike monomer (PDB ID: 7KRR).

TABLE 1 SARS-CoV-2 prototype and Variants of Concern.

Nr	Virus name GISAID nomenclature	Equivalent NCBI accession nr	Clade	Lineage	% sequence Identity GISAID vs NCBI	Variant
1	hCoV-19/Wuhan/WIV04/2019	MN996528.1	Original	Original	100%	Wuhan
2	hCoV-19/England/205041766/2020	MZ005945.1	FRY	B1.1.7	99%	Alpha
3	hCoV-19/Japan/IC-0564/2021	MW988204.1	GR	P.1	100%	Gamma
4	hCoV-19/SouthAfrica/KRISP-EC-K004574/2020	MW981442.1	GH	B.1.351	99%	Beta
5	hCoV-19/India/MH-NCCS-BJ1/2021	MZ023220.1	G	B1.1617	99%	Delta
6	hCoV-19/USA/NM-CDC-QDX32337620/2021	OM202878.1	GRA	B.1.1.529.1	99%	Omicron
7	hCoV-19/Botswana/R165B92_BHP_AAC32282/2021	ON375778.1	GRA	BA.1	99%	Omicron
8	hCoV-19/USA/CA-ASC-210844543/2022	ON080219.1	GRA	BA.2	99%	Omicron
9	hCoV-19/Denmark/DCGC-392185/2022	OP170269.1	GRA	BA.3	99%	Omicron
10	hCoV-19/USA/NY-Wadsworth-22042624-01/2022	OP147180.1	GRA	BA.4	99%	Omicron
11	hCoV-19/Denmark/DCGC-588045/2022	OX278505.1	GRA	BA.5	100%	Omicron
12	hCoV-19/Malaysia/IMR_OS6350/2022	ON674677.1	GRA	BA.2.12.1	99%	Omicron
13	hCoV-19/Australia/NSW-ICPMR-35588/2022	OP661948.1	GRA	BA.2.75	100%	Omicron
14	hCoV-19/USA/AZ-ASU92993/2022	OP607549.1	GRA	BQ.1	99%	Omicron
15	hCoV-19/India/TN-CDFD-O-162/2022	OP659449.1	GRA	BBX.1	99%	Omicron

The model with lowest Discrete Optimized Protein Energy (DOPE) score (30) was chosen. Structural difference was measured using all-atom Root mean square deviation (RMSD) calculated by superimposing the homology models with the main templates (PDB ID: 7DWY, 7CZZ, and 7KJ4) for different systems (Table 2). Our models showed low structural deviation with the experimental structures (Table 2) and the AlphaFold2 models (RMSD: 0.55 Å) (22). Final models for Spike protein with both open and closed conformation were available in the Supplementary Materials for detailed comparison. The PyMol Molecular Graphics System, Version 2.0 (31), was used to visualise the protein structures and generate the figures.

Mutation analysis

Mutational tolerance was explored using the COVID-3D resource (32).

The effects of the mutations on protein thermodynamic stability and dynamics were calculated using SDM (33), mCSM-Stability (34), DUET (35), ENCoM (36), mCSM-membrance (37), DynaMut (38), and DynaMut2 (39). The effects of the mutations on the protomers interaction as well as the Spike-ACE2 interaction were evaluated using mCSM-PPI (34), mCSM-PPI2 (40), and mmCSM-PPI (40); which have been previously shown to correlate strongly with experimental data on this complex (41). The effects of the mutations on antibody binding were analysed using the protein models described above of the S protein bound to the monoclonal antibody from COVID-19 convalescent patients P5A-2F11 (PDB:7CZZ). These calculations were conducted using mCSM-AB (42), mCSM-AB2 (43), and mmCSM-AB (44). Each method outputs the change in Gibb's free energy (ΔΔG) of thermodynamics or affinity (in Kcal/mol). The inputs of these structure-based predictors were the homology models described previously. Since these homology models are more structurally similar to the actual experimental structures, these we utilized instead of adopting the snapshots derived by our MD. This provides more accurate and informative results in a single, easy to compare value.

All atomic MD simulations of the prototype and Omicron variants in the open and closed forms were performed using GROMACS (version 2020) for 20 ns in triplicate. Amber ff99SB-ILDN (45) force field and TIP3P water model (46) were applied to the systems. Detailed information on MD simulations can be found here (47). In short, the system was neutralized and solvated in a periodic cubic box with its wall being 1nm away from the complex atoms. The system was first minimized for 50,000 steps using the steepest descent algorithm, followed by the equilibration over 100 ps each at the constant volume and the constant pressure of 1 atm. Weak harmonic positional restraints on the complex atoms with a force constant were imposed during the minimization and these initial equilibration steps. The system was then carried out for 20 ns at 300 K in the constant pressure (NPT) ensemble in triplicate without the constraints of all the complex atoms. Hydrogen bond (Hbond) interaction was analysed using a cutoff distance of 3.5 Å. C-alpha RMSD for Spike-ACE2 and Spike-Ab of prototype and Omicron Spike proteins were calcualted to monitor the simulation (Figure S6).

Results

Multiple sequence alignment between VOCs in SARS-CoV-2

Despite the high numbers of mutations present in Omicron, evidence from phylogenetic trees, has so far shown no intermediate branches of evolution when comparing Omicron to previous VOCs (48, 49). When investigating the alignments we specifically examined the ones that showed amino acid conservation across all other variants and exhibited change only in Omicron. A total of 34 mutations are present in Omicron. Of these, there are 24 mutations consisting in amino acid mutations that have occurred only in Omicron (Figure 1 and Figures S1A–C) whilst remaining consistent throughout the other variants. Of the 24 Omicron specific mutations, 14 are specific to Omicron as well as all its subvariants. Of these 14, four are N to K mutations (30%), while the remaining mutations only occurred in one (7,6%) instances (Figure 2). Interestingly when looking at other SARS-CoV-2 regions of interest like N, ORF3a, ORF7 and ORF8 (Figure S2–5), none of these regions showed a specific bias towards N to K mutations, indicating that although it is occurring outside of the

TABLE 2 The templates in homology modelling.

Variant	Form	Binding partner	Template (PDB code)	RMSD to template (Å)
Prototype	down (closed)	apo	7DWY* (27)	0.34
Prototype	up (open)	apo	7CZZ* (28), 7KRR (29)	0.69
Prototype	up (open)	ACE2	7KJ4* (30), 7KRR (29)	1.92
Prototype	up (open)	P5A-2F11 (antibody)	7CZZ* (28,27), 7KRR	1.27
Omicron	down (closed)	apo	7DWY* (27)	0.50
Omicron	up (open)	apo	7CZZ* (28), 7KRR (29)	0.72
Omicron	up (open)	ACE2	7KJ4* (30), 7KRR (29)	1.29
Omicron	up (open)	P5A-2F11 (antibody)	7CZZ* (28), 7KRR (29)	1.18

*All atom RMSD was calculated based on this template.

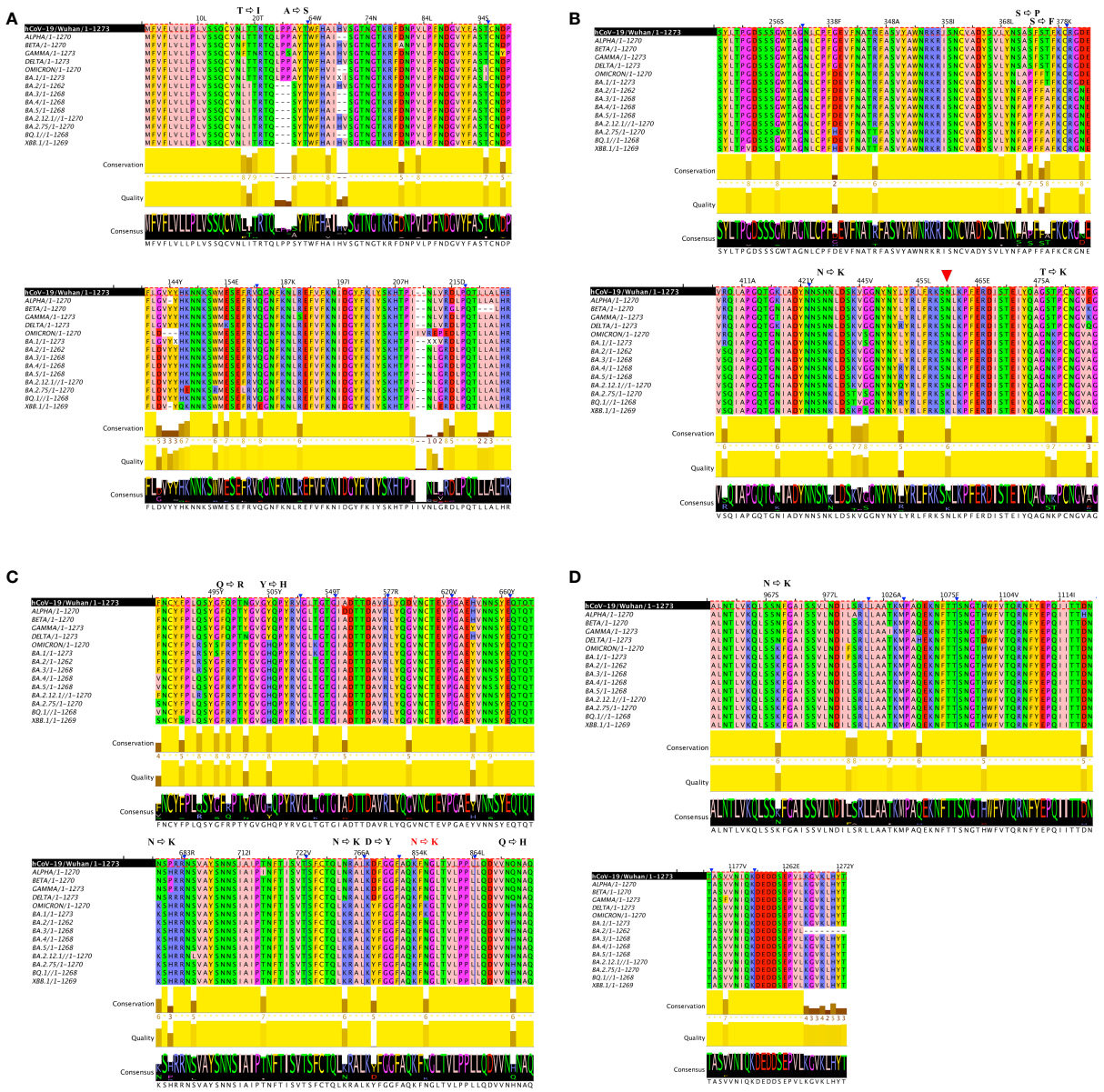

FIGURE 1
Multiple alignments in 6 VOC strains. Multiple sequence alignment of full-length Spike proteins of Alpha, Beta, Gamma, Delta and Omicron SARS-CoV-2 VOCs including it's subvariants (BA.1, BA.2, BA.3, BA.4, BA.5) as well as currently emerging variants (BQ.1 and BBX.1) show a distinct preference for N to K transition in the Spike region. **(A)** is first portion of the Spike protein **(B)** second portion of the Spike protein, red arrow indicates another NtoK transition acquired **(C)** third portion of the Spike protein, NtoK in red indicates a lost mutation **(D)** final portion of the Spike protein. In order to facilitate localization of where mutations have occurred, in **(A-C)** a truncated Spike protein is depicted, blue arrows and lines indicate the sites where a portion of the amino acid sequence is not visible. Full length Omicron protein with annotated mutations can be viewed in Figure S1A–C.

RBD region, this genetic variation is still highly specific to the Spike protein sequence.

Furthermore, missense tolerance ratio (MTR) of all 30 missense mutations reported in Omicron Spike protein were obtained using COVID-3D tools (Table S1). Only three mutations (A67V, G446S, and L981F) were located at intolerant positions, indicating that they were not under purifying selection.

Mutation analysis on three N to K mutations on the thermodynamics stability and protomer interaction of Spike protein apo structure

Given the highly skewed N to K mutations taking place in the Spike protein area, we next investigated these specific

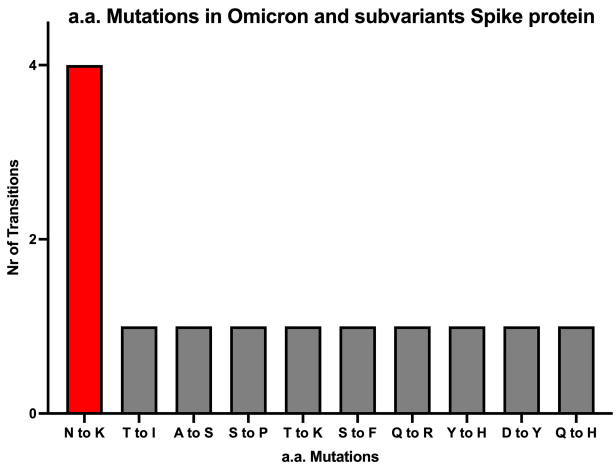

FIGURE 2
All amino acid mutations in Omicron Spike protein. The numbers of N to K mutations are about 4-fold higher compared to 9 other mutations occurring in the SARS-CoV-2 Spike region of Omicron and it's subvariants.

mutations. Both N764K and N969K mutations were highly conserved in all the Omicron subvariants (BA.1 - BA.5) and emerging subvariants (BQ.1, BBX.1), while N856K was only reported in the main variant (BA.1) (Figures 1A–D). Both N440K and N679K have previously been described, with N440K located in RBD reported to affect the interaction of Spike protein with antibody (50), and N679K likely to increase the virus infection by enhancing the cleavage of S1 and S2 subunits (51). Thus, we focussed on the remaining three N to K mutations (N764K, N856K and N969K), which are all located in the central core region of the S2 subunit of Spike protein, to explore the potential molecular consequences on the change of RBD conformation.

These three mutations, N764K, N856K, and N969K, were predicted to mildly destabilise the structure by mCSM-Stability, SDM, DUET, ENCoM, DynaMut1, mCSM-Membrance (single-site mutation predictions, Table S2), and DynaMut2 (multiple-site mutation predictions, Tables 3, S2), consistent with the prediction of I-Mutant 3.0 (52). Previous work (53) has shown that using homology models as inputs for these predictors was reliable with DynaMut2 showing the best consistency. Furthermore, only DynaMut2 accepts multiple-site mutations. Thus, only the results from this predictor were presented in the main text. Only N856K in open conformation has a mild positive prediction on the Spike protein. The degree of deleterious effects on Spike thermodynamics stability was slightly stronger on open conformation of Spike (down:up = -1.87 Kcal/mol:-2.00 Kcal/mol, average on all protomers, Table 3), indicating that the weaker destabilisation of the closed conformations would potentially account for the preference of RBD conformation by these three N to K mutations.

TABLE 3 The effects of Omicron multiple-site mutations on protein thermostability and stability of the trimeric Spike protein.

Mutations	Protomer ID	DynaMut2 (Kcal/mol) - closed conformation	DynaMut2 (Kcal/mol) - open conformation	mmCSM-PPI (Kcal/mol) - closed conformation	mmCSM-PPI (Kcal/mol) - open conformation
N764K	A/B/C	-1.62	-1.89	-0.60	-0.72
N856K	A/B/C	-1.75	0.85	-1.57	-2.28
N969K	A/B/C	-1.9	-1.86	-0.60	-0.48
N764K/ N856K/ N969K	A	-1.86	-2.05	-0.70	-0.79
N764K/ N856K/ N969K	B	-1.83	-1.93	-0.84	-1.12
N764K/ N856K/ N969K	C	-1.93	-2.02	-1.05	-0.73

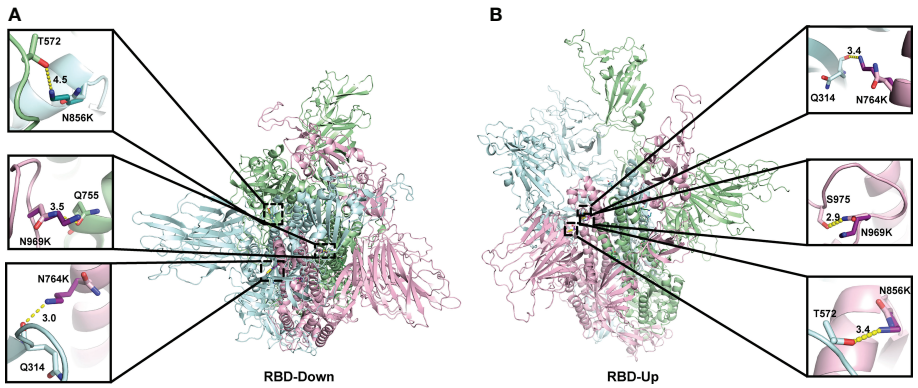

FIGURE 3
Location of three N to K mutations in the central core region of the homology model of Spike protein. The monomers of the Spike proteins in open **(A)** and closed **(B)** were shown in ribbons with different colours (pink, green, cyan). Side chain atoms of both prototype and Omicron residues were shown in sticks with the Carbon atoms in light and dark colours, respectively. The residues making Hydrogen bond interactions with prototype and Omicron residues are shown in sticks. Hydrogen bond interaction was shown in yellow dash line. The zoom-in versions of the interactions were shown next to the Spike protein.

The effects of these three mutations on the affinity of the trimeric Spike was also evaluated by measuring how the global stability on the Spike complex contributes to the interaction between each protomer. All three mutations showed a comparable destabilising effect on the Spike trimer when either the open or closed conformation was analysed (down:up = -0.86 Kcal/mol:-0.88 Kcal/mol, average on all protomers, Table 3). Single-site mutation effect predictions are displayed in the (Table S3). Of all N to K mutants, N856K mutation of both the open and closed conformations showed the strongest destabilising effect.

When analysing the structural changes, for the N764K mutation, the side chain of K764 in the model of both the open and closed conformations, forms an additional hydrogen bond with Q314 (Figures 3A–B). For N856K, the side chain of K856 in Omicron model in open conformation forms an additional hydrogen bond with T572 (Figure 3B). Both of these are in agreement with previous studies (10, 54, 55). The similar polar contacts between protomers may account for similar mutation effects on two conformations.

Mutation effects on the Spike-ACE2 complex

Four mutations (S477N, Q493R, Q498R, and N501Y) located on the binding surface of RBD in the Spike protein, which were nominated based on previous studies (55) and were consistently observed in different Omicron subvariants, were identified by mCSM-PPI, mCSM-PPI2, and mmCSM-PPI to have mild effects on the affinity of the interaction between Spike protein and human ACE2 receptor protein (Table 4). While Q493R and Q498R were predicted to decrease binding affinity, consistent with the introduction of a larger charged residue, S477N and N501Y were predicted to stabilise the interaction. The calculation of the change of binding affinity caused by N501Y is also consistent with a previous MD study (56).

A more comprehensive study on multiple-site mutation effects was examined using mmCSM-PPI. This also supported the mild change of Spike-ACE2 binding. The new polar contacts formed by the Omicron mutant residues, including R493 (Spike) with D30 (ACE2), R498 (Spike) with Y41 and

TABLE 4 Mutation effects on the Spike-ACE2 complex.

Mutations	Distance to surface (Å)*	mCSM-PPI (Kcal/mol)	mCSM-PPI2 (Kcal/mol)	mmCSM-PPI (Kcal/mol)	Outcome
S477N	5.63	0.42	0.12	0.12	Increased affinity
Q493R	2.85	-1.86	-0.71	-0.71	Decreased affinity
Q498R	3.18	-2.86	-1.11	-1.11	Decreased affinity
N501Y	3.43	-1.79	0.52	0.52	Increased affinty
S477N/Q493R/Q498R/N501Y	/	/	/	-0.92	Descreased affinity

*Distance to surface is a measurement from the wild-type residue to the binding interface between Spike and ACE2 in the homology model, to indicate the biochemical property of the mutation, which is not used to measure of the binding.

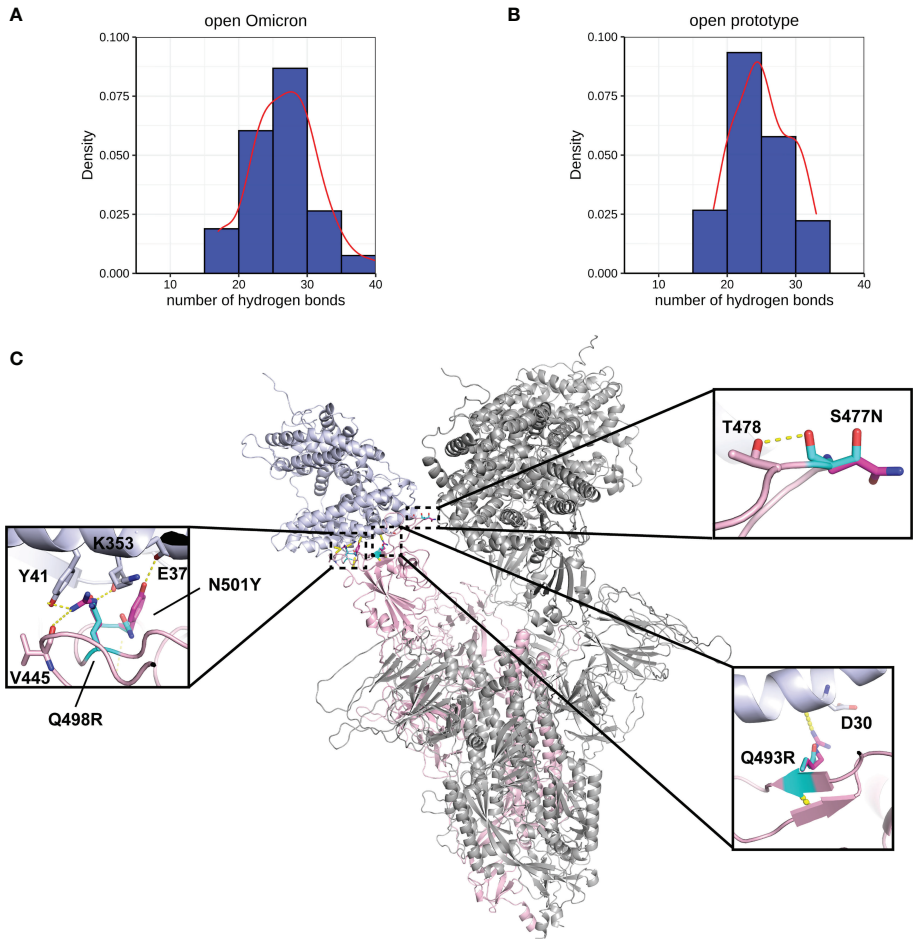

FIGURE 4
Interactions between Spike and ACE2. Hydrogen bond interaction distribution between residues in Spike (residues 332-527) and ACE2 proteins during 20 ns of triplicate MD simulations in **(A)** open Omicron and **(B)** open prototype variants are shown in blue histogram with its smoothed density line shown in red. These both represent RBD-up conformation of Omicron and Prototype Spike proteins. Density on y axis refers to the Kernel density, the image depicts the probability density function of the variable. The Spike protein was presented in ribbon with three RBD all binding to ACE2 **(C)**. Four mutations in the receptor binding interface were zoom-in. Both prototype (cyan) and Omicron residues (magenta) were shown in sticks with the Carbon atoms on Spike-ACE2 complex (pink-blue). Hydrogen bond was shown in yellow dash line.

K353 (ACE2), and Y501 (Spike) with E37 (ACE2), can provide potential explanations for this (Figure 4C). To further explore this, we ran a short MD simulation on both the prototype and Omicron Spike and analysed the effect of each variant on Spike-ACE2 complexes. The distribution of the number of Hbond interactions between Spike (residues 332-527) and ACE2 proteins (Figures 4A, B) was measured and shown that the open form of Omicron has majority of the number of Hbond interactions 25 to 30, while the prototype has majority of the number of Hbond interactions between 20 and 25. It showed that Omicron has a stronger interaction in majority of the cases comparing to the prototype. This observation is consistent with our structural predictions (Table 4) where few of the mutations increase the binding affinity between Omicron and ACE2.

Mutation effects on the Spike-antibody complex

Another four mutations (S477N, T478K, E484A, and Q493R), located on the RBD-antibody interface, were nominated based on previous works (57, 58) and were repetitively observed in different Omicron subvariants. P5A-2F11 is one of the neutralizing monoclonal antibodies derived from the COVID-19 convalescent patients (27), which presents strong compatibility with ACE2. The effects of the mutations on the recognition by the P5A-2F11 antibody were analysed as a representative to better understand the immune evasion of Omicron, especially for repetitive positive cases reported in the post-COVID age.

We performed MD of these systems and obtained snapshots of the Spike proteins. The distribution of the number of Hbond

10.3389/fimmu.2022.954435

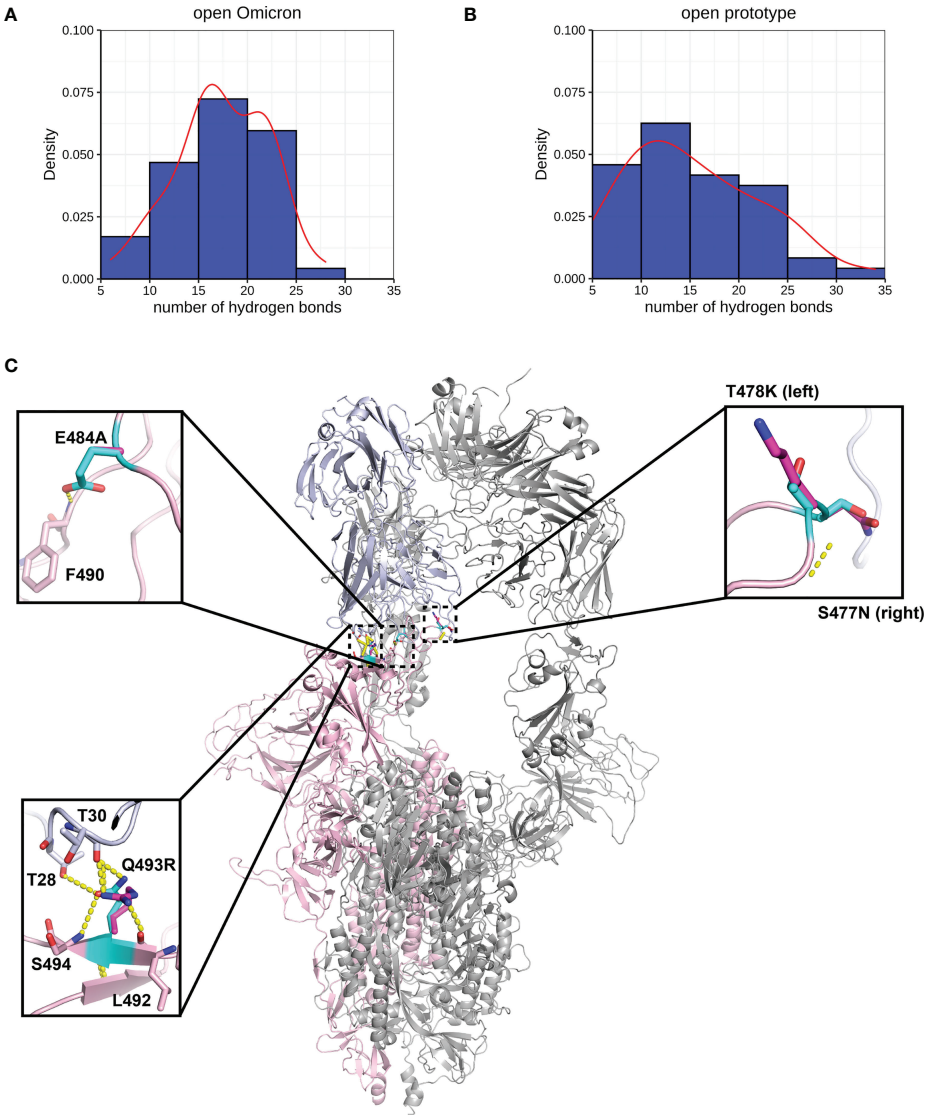

FIGURE 5
Interactions between Spike and antibody (P5A-2F11). Hydrogen bond interaction distribution between residues in Spike (residues 332-527) and antibody proteins during 20 ns of triplicate MD simulations in **(A)** Omicron and **(B)** prototype variants are shown in blue histogram with its smoothed density line shown in red. Both represent RBD-up conformation of Omicron and Prototype Spike proteins. Density on y axis refers to the Kernel density, the image depicts the probability density function of the variable The Spike protein was presented in ribbon with three RBD all binding to P5A-2F11 **(C)**. Both prototype (cyan) and Omicron residues (magenta) were shown in sticks with the Carbon atoms on Spike-P5A-2F11 complex (pink-blue). Hydrogen bond was shown in yellow dash line.

interactions between Spike (residues 332-527) and antibody proteins (Figures 5A, B) were measured and showed that the prototype has more portion of Hbond interaction from 25 to 35 than the Omicron. Although the difference is small because of the short MD simulations, it showed that Omicron has a tendency to have weaker interaction to AB than the prototype. All of these four mutations, located at the Spike-P5A-2F11 interface, were individually predicted by mCSM-AB, mCSM-AB2, and mmCSM-AB to decrease the binding affinity of the complex. These four individual mutations were predicted to mildly reduce the binding between Spike and P5A-2F11, (Table 5) consistent with previous *in-silico* work on epitopes (59), while the combination of these mutations was predicted to have a much larger reduction in recognition by P5A-2F11, consistent with earlier work on other neutralizing antibodies (10). The deteoriation of Spike-P5A-2F11 binding is likely due to the change of polar contacts of these mutants (Figure 5C). Our results indicated the mutations reported in the Omicron subvariants could potentially decrease the neutralizing effect of antibodies, even on patients recovering from the infection,

TABLE 5 Mutation effects on the Spike-Ab complex.

Mutations	Distance to surface (Å)*	mCSM-AB (Kcal/mol)	mCSM-AB2 (Kcal/mol)	mmCSM-AB (Kcal/mol)	Outcome
S477N	2.91	0.80	-0.01	-0.14	Decreased affinity
T478K	4.88	-0.11	-0.32	-0.15	Decreased affinity
E484A	4.01	-0.59	-0.42	-0.02	Decreased affinity
Q493R	2.7	0.76	-0.39	-0.49	Decreased affinity
S477N/T478K/E484A/Q493R	/	/	/	-0.80	Decreased affinity

*Distance to surface is a measurement from the wild-type residue to the binding interface between Spike and Ab in the homology model, to indicate the biochemical property of the mutation, which is not used to measure of the binding.

which could underpin the observed connection between the high infectiousness and immune escape properties of Omicron.

Discussion

Understanding the evasion of humoral responses by viruses and the critical consequences for antibody immunotherapies as well as vaccine design, are extremely important for the identification of novel treatments. As the SARS-CoV-2 virus continues its ever-changing journey, it becomes increasingly important to unravel the complex molecular aspects of increased transmissibility as well as the viral modality of genetic drift.

Much focus has been dedicated to investigating key mutations, including the mutations of K417 and E484 in RBD (60), and dominant mutations like the N501Y and D614G (61), which present themself across a majority of variants. Others have even looked at antibody evasion properties of Omicron subvariants (62) as well as the use of deep mutational scanning to identify mutationally constrained areas in the RBD regions, which represent ideal targets for antibodies (63, 64). Further to that, it has been established that the RBD constitutes a key functional component of the S1 subunit, responsible for SARS-CoV-2 binding to lung cells through ACE2 (6, 55–58). Although a highly pursued avenue has been studying the combination of various mutations (65), to date there haven't been studies in which the authors have investigated a skew towards one type of specific mutation, like the N to K mutations, and specifically investigated the viral properties solely in this context.

Using a range of bioinformatic tools, here we showed for the first time a skew towards N to K mutation both inside and outside the RBD region, but only present in the Spike protein of SARS-CoV-2. Out of the four N to K mutations, three (N764K, N856K, and N969K) are located in the trimerization region and exhibit mild negative contributions to the protein folding and the interactions of Spike protomers. Interestingly, we also noticed that these three N to K mutations on the three RBD-down conformation are more energetically stable, suggesting the trimeric Omicron Spike protein with all RBD-down state may benefit from these residue substitutions. This may subsequently promote the escape of recognition from antibodies. Furthermore, the stronger mild destabilising effects caused by mutations for RBD-up conformation may potentially provide the flexibility for the Spike structure. The negative effects on Spike thermodynamics stability caused by these three N to K mutations were consistent with the predictions from I-Mutant 3.0 (52). The missing loop from residue 824 to 854 in our homology models was structurally similar to the cryo-EM determined structure (66), but some local residue environment might still differ from ones determined from experimental structures (10, 55), presenting a larger molecular distance between K856 and T572 in the closed conformation (Figure 3A).

The RBD undergoes changes in the conformation that can either expose the binding site or not. These "up" and "down" conformational alterations pose an interesting problem for SARS-CoV viruses as immune recognition is less efficient when RBD is hidden in a down conformation compared to when it is exposed. Conversely hidden RBD may lead to inefficient host cell interaction and host cell entry. Previous studies using cryo-EM structures and constant-pH Monte Carlo simulations showed that enhanced virulence could also be a consequence of an improved viral stability of the trimeric Spike in the open state with the better RBD availability to ACE2, rather than only through the alteration in the RBD-ACE2 interaction itself (10, 67, 68). Meanwhile, more research revealed that the Spike protein of Omicron is more likely to have one RBD-up conformation, not only maintaining the interaction with ACE2 but also restricting the recognition of antibody (69, 70). In our *in-silico* work, we identified that three N to K mutations reported in Omicron and its subvariants may contribute to a mild preference of all the RBD-down conformation, compared to the prototype Spike protein. Although our results were not directly comparable with the previous studies, both showed that the ever-changing COVID Spike protein may adopt a strategy to restrict less RBD-up conformation to facilitate immune evasion (71). We showed a new insight of the Omicron mutations outside RBD which could contribute to this conformational alteration. Two of these three N to K mutations (N764K and N969K) have been circulating in Omicron BA.1 to the latest dominant BA.5, and we, hence, expected this N to K bias may be kept in the new dominant variant, which attracts attention on the dynamics of the Spike protein.

The preference of the alteration of RBD conformation is crucial for the availability of the interaction with ACE2 and antibody. The change of the binding of Spike-ACE2 and Spike-

Ab upon Omicron mutations in RBD, however, play a vital role on the infection of Omicron. Four different mutations on the binding interface of Spike-ACE2 and Spike-Ab were investigated according to the distance of the wild-type residue to the interface and previous studies. In addition, from our alignments, we observed that the selected mutations remain consistent in all the subsequently emerged variants to date. Previous studies informed a stronger binding between Omicron Spike protein and ACE2 (23, 56, 72) and a reduction of binding between Omicron Spike protein and Abs (52, 58, 70). The predictive increased binding affinity caused by N501Y was consistent with these findings, while the other calculations may slightly differ. However, we based our results on homology models, which may vary from the actual experimental structures. The prototype Spike-ACE2 model has the largest structural difference (Table 2) with the experimental one. Since the prediction tools used in our study are sensitive to the input structure (53), these factors may affect the measurement of the change of binding. Overall there have been substantial studies on antibody neutralization effect of Omicron subvariants (73–75). We further selected one Spike-Ab, derived from convalescent patient as a proof of principle. Previous studies have extensively identified individual mutation patterns without focusing on specific amino acid mutations (10, 52, 55, 60–62, 64, 65). So far, the N to K mutation N440K is the only one located within the RBD area of the Omicron variant. For instance, SARS-CoV-2 Omicron G339D and N440K mutations are located in a neighbouring site called antigenic site IV, which in turn is a known recognition site by the S309 mAb (76). Interestingly, previous studies have shown that the Lysine side chain introduced by the N440K substitution does not affect binding of S309 (77), while others have demonstrated that K417N mutation both alone or in combination with other mutations, produces a greater ACE2 affinity than a K417T mutation either alone or in combination with other mutations (60).

Another important aspect to consider is whether this genetic drift could potentially be the result of gene editing inherent to the virus rather than an evolutionary pressure driven by circulating vaccines. Interestingly, the predilection of N to K mutations over other mutations cannot be explained by viral RNA editing enzymes like Adenosine Deaminases that Act on RNA (ADARs). ADARs are RNA editing enzymes that play an important role in regulating transcriptome and proteome diversity. This type of editing can have important roles that function in favour or against viral survival and can even change over the course of an infection (78). However, ADARs are known to exhibit a preference for adenosine to inosine (A to I) transition, where the inosine modification will subsequently be read as guanosine (G). Therefore, when looking at the Asparagine (AAT and AAC) and Lysine (AAG and AAA) codons, as both last codons of Asparagine are not an A, the Asparagine to Lysine (N to K) variation is unlikely due to ADAR preference in mutation. It is, therefore, more likely that these genetic variations are vaccine-driven rather than a mutational preference in the viral replication machinery.

In our studies, this emphasized the importance of using molecular dynamics (MD) simulations and computational mutation analysis methods to understand SARS-CoV-2 evolution, since antigenic drifting could have large implications to the preference of RBD conformation, which is associated with studies on B cell epitopes and vaccine design. A particular point of concern for Omicron is its phylogenetically different lineage which is highly distinct from all the previously dominant SARS-CoV-2 variants. Although the mutations on the RBD may not significantly improve the binding of ACE2, they could most likely be the result of evolutionary pressure driving the virus to change specific antibody binding sites. In this study we have shown that the number of mutations in Omicron and its subvariants is highly skewed towards an N to K substitution and that this characteristic is typical for Omicron and its subsequently emerged and dominant subvariants, solely occurs in the Spike protein region. Furthermore, our studies also show that altogether these mutations may potentially contribute to differences in stochastic movements (up *vs* down) and that the N to K mutation bias may potentially contribute to the alteration of RBD conformation. This type of mutation should therefore be considered in future vaccine design.

Data availability statement

The original contributions presented in the study are included in the article/Supplementary Material. Further inquiries can be directed to the corresponding author.

Author contributions

JB wrote first draft of the paper. JB and MP contributed with conceptualization of paper, data generation, writing and editing. QP, T-BN, DA and JH contributed with data generation, text editing. All authors contributed to the article and approved the submitted version.

Funding

JH is a Vice Chancellors Research Fellow, funded by RMIT University. DA is supported by an National Health and Medical Research Council of Australia Investigator grant (GNT1174405) and the Victorian Government's Operational Infrastructure Support Program. MP is an NHMRC Senior Fellow. MP is an NHMRC SRFB Senior Fellow.

Conflict of interest

The authors declare that the research was conducted in the absence of any commercial or financial relationships that could be construed as a potential conflict of interest.

Publisher's note

All claims expressed in this article are solely those of the authors and do not necessarily represent those of their

affiliated organizations, or those of the publisher, the editors and the reviewers. Any product that may be evaluated in this article, or claim that may be made by its manufacturer, is not guaranteed or endorsed by the publisher.

Supplementary material

The Supplementary Material for this article can be found online at: https://www.frontiersin.org/articles/10.3389/fimmu.2022.954435/full#supplementary-material

References

1. Xu X, Chen P, Wang J, Feng J, Zhou H, Li X, et al. Evolution of the novel coronavirus from the ongoing wuhan outbreak and modeling of its spike protein for risk of human transmission. *Sci China Life Sci* (2020) 63(3):457–60. doi: 10.1007/s11427-020-1637-5

2. Hoffmann M, Kleine-Weber H, Schroeder S, Krüger N, Herrler T, Erichsen S, et al. SARS-CoV-2 cell entry depends on ACE2 and TMPRSS2 and is blocked by a clinically proven protease inhibitor. *Cell* (2020) 181(2):271–80. doi: 10.1016/j.cell.2020.02.052

3. Letko M, Marzi A, Munster V. Functional assessment of cell entry and receptor usage for SARS-CoV-2 and other lineage b betacoronaviruses. *Nat Microbiol* (2020) 5(4):562–9. doi: 10.1038/s41564-020-0688-y

4. Walls AC, Park YJ, Tortorici MA, Wall A, McGuire AT, Veesler D. Structure, function, and antigenicity of the SARS-CoV-2 spike glycoprotein. *Cell* (2020) 181 (2):281–92. doi: 10.1016/j.cell.2020.02.058

5. Xia S, Zhu Y, Liu M, Lan Q, Xu W, Wu Y, et al. Fusion mechanism of 2019-nCoV and fusion inhibitors targeting HR1 domain in spike protein. *Cell Mol Immunol* (2020) 17(7):765–7. doi: 10.1038/s41423-020-0374-2

6. Lan J, Ge J, Yu J, Shan S, Zhou H, Fan S, et al. Structure of the SARS-CoV-2 spike receptor-binding domain bound to the ACE2 receptor. *Nature* (2020) 581 (7807):215–20. doi: 10.1038/s41586-020-2180-5

7. Wrapp D, Wang N, Corbett KS, Goldsmith JA, Hsieh CL, Abiona O, et al. Cryo-EM structure of the 2019-nCoV spike in the prefusion conformation. *Science* (2020) 367(6483):1260–63. doi: 10.1126/science.abb2507

8. Gui M, Song W, Zhou H, Xu J, Chen S, Xiang Y, et al. Cryo-electron microscopy structures of the SARS-CoV spike glycoprotein reveal a prerequisite conformational state for receptor binding. *Cell Res* (2017) 27(1):119–29. doi: 10.1038/cr.2016.152

9. Hofmann H, Pöhlmann S. Cellular entry of the SARS coronavirus. *Trends Microbiol* (2004) 12(10):466–72. doi: 10.1016/j.tim.2004.08.008

10. Cerutti G, Guo Y, Liu L, Liu L, Zhang Z, Luo Y, et al. Cryo-EM structure of the SARS-CoV-2 omicron spike. *Cell Rep* (2022) 38(9):110428. doi: 10.1016/j.celrep.2022.110428

11. Chalkias S, Harper C, Vrbicky K, Walsh SR, Essink B, Brosz A, et al. A bivalent omicron-containing booster vaccine against covid-19. *N Engl J Med* (2022) 387(14):1279–91. doi: 10.1056/NEJMoa2208343

12. Schmidt F, Muecksch F, Weisblum Y, Da Silva J, Bednarski E, Cho A, et al. Plasma neutralization properties of the SARS-CoV-2 omicron variant. *N Engl J Med* (2022) 386(6):599–601. doi: 10.1056/NEJMc2119641

13. Chen J, Wang R, Gilby NB, Wei GW. Omicron variant (B.1.1.529): Infectivity, vaccine breakthrough, and antibody resistance. *J Chem Inf Model* (2022) 62(2):412–22. doi: 10.1021/acs.jcim.1c01451

14. Elbe S, Buckland-Merrett G. Data, disease and diplomacy: GISAID's innovative contribution to global health. *Glob Chall Hoboken NJ* (2017) 1(1):33–46. doi: 10.1002/gch2.1018

15. Shu Y, McCauley J. GISAID: Global initiative on sharing all influenza data - from vision to reality. *Euro Surveill Bull Eur Sur Mal Transm Eur Commun Dis Bull* (2017) 22(13):30494. doi: 10.2807/1560-7917.ES.2017.22.13.30494

16. Khare S, Gurry C, Freitas L, Schultz MB, Bach G, Diallo A, et al. GISAID's role in pandemic response. *China CDC Wkly* (2021) 3(49):1049–51. doi: 10.46234/ccdcw2021.255

17. Altschul SF, Gish W, Miller W, Myers EW, Lipman DJ. Basic local alignment search tool. *J Mol Biol* (1990) 215(3):403–10. doi: 10.1016/S0022-2836(05)80360-2

18. Camacho C, Coulouris G, Avagyan V, Ma N, Papadopoulos J, Bealer K, et al. BLAST+: architecture and applications. *BMC Bioinf* (2009) 10:421. doi: 10.1186/1471-2105-10-421

19. Waterhouse AM, Procter JB, Martin DMA, Clamp M, Barton GJ. Jalview version 2–a multiple sequence alignment editor and analysis workbench. *Bioinform Oxf Engl* (2009) 25(9):1189–91. doi: 10.1093/bioinformatics/btp033

20. Katoh K, Standley DM. MAFFT multiple sequence alignment software version 7: improvements in performance and usability. *Mol Biol Evol* (2013) 30 (4):772–80. doi: 10.1093/molbev/mst010

21. Webb B, Sali A. Comparative protein structure modeling using MODELLER. *Curr Protoc Bioinform* (2016) 54:5.6.1–5.6.37. doi: 10.1002/cpbi.3

22. Ford CT, Jacob Machado D, Janies DA. Predictions of the SARS-CoV-2 omicron variant (B.1.1.529) spike protein receptor-binding domain structure and neutralizing antibody interactions. *Front Virol* (2022) 2:830202. doi: 10.3389/fviro.2022.830202

23. Lan J, He X, Ren Y, Wang Z, Zhou H, Fan S, et al. Structural insights into the SARS-CoV-2 omicron RBD-ACE2 interaction. *Cell Res* (2022) 32(6):593–5. doi: 10.1038/s41422-022-00644-8

24. Yuan M, Liu H, Wu NC, Lee CCD, Zhu X, Zhao F, et al. Structural basis of a shared antibody response to SARS-CoV-2. *Science* (2020) 369(6507):1119–23. doi: 10.1126/science.abd2321

25. Mannar D, Saville JW, Zhu X, Srivastava SS, Berezuk AM, Tuttle KS, et al. SARS-CoV-2 omicron variant: Antibody evasion and cryo-EM structure of spike protein–ACE2 complex. *Science* (2022) 375(6582):760–4. doi: 10.1126/science.abn7760

26. Yan R, Zhang Y, Li Y, Ye F, Guo Y, Xia L, et al. Structural basis for the different states of the spike protein of SARS-CoV-2 in complex with ACE2. *Cell Res* (2021) 31(6):717–9. doi: 10.1038/s41422-021-00490-0

27. Yan R, Wang R, Ju B, Yu J, Zhang Y, Liu N, et al. Structural basis for bivalent binding and inhibition of SARS-CoV-2 infection by human potent neutralizing antibodies. *Cell Res* (2021) 31(5):517–25. doi: 10.1038/s41422-021-00487-9

28. Zhang J, Cai Y, Xiao T, Lu J, Peng H, Sterling SM, et al. Structural impact on SARS-CoV-2 spike protein by D614G substitution. *Science* (2021) 372(6541):525–30. doi: 10.1126/science.abf2303

29. Xiao T, Lu J, Zhang J, Johnson RI, McKay LGA, Storm N, et al. A trimeric human angiotensin-converting enzyme 2 as an anti-SARS-CoV-2 agent. *Nat Struct Mol Biol* (2021) 28(2):202–9. doi: 10.1038/s41594-020-00549-3

30. Shen M, Sali A. Statistical potential for assessment and prediction of protein structures. *Protein Sci* (2006) 15(11):2507–24. doi: 10.1110/ps.062416606

31. Schrödinger LLC. *The PyMOL molecular graphics system, version 1.8*. Schrödinger: LLC (2015).

32. Portelli S, Olshansky M, Rodrigues CHM, D'Souza EN, Myung Y, Silk M, et al. Exploring the structural distribution of genetic variation in SARS-CoV-2 with the COVID-3D online resource. *Nat Genet* (2020) 52(10):999–1001. doi: 10.1038/s41588-020-0693-3

33. Worth CL, Preissner R, Blundell TL. SDM–a server for predicting effects of mutations on protein stability and malfunction. *Nucleic Acids Res* (2011) 39(Web Server issue):W215–222. doi: 10.1093/nar/gkr363

34. Pires DEV, Ascher DB, Blundell TL. mCSM: predicting the effects of mutations in proteins using graph-based signatures. *Bioinform Oxf Engl* (2014) 30(3):335–42. doi: 10.1093/bioinformatics/btt691

35. Pires DEV, Ascher DB, Blundell TL. DUET: a server for predicting effects of mutations on protein stability using an integrated computational approach. *Nucleic Acids Res* (2014) 42(Web Server issue):W314–319. doi: 10.1093/nar/gku411

36. Frappier V, Chartier M, Najmanovich RJ. ENCoM server: exploring protein conformational space and the effect of mutations on protein function and stability. *Nucleic Acids Res* (2015) 43(W1):W395–400. doi: 10.1093/nar/gkv343

37. Pires DEV, Rodrigues CHM, Ascher DB. mCSM-membrane: predicting the effects of mutations on transmembrane proteins. *Nucleic Acids Res* (2020) 48(W1): W147–53. doi: 10.1093/nar/gkaa416

38. Rodrigues CH, Pires DE, Ascher DB. DynaMut: predicting the impact of mutations on protein conformation, flexibility and stability. *Nucleic Acids Res* (2018) 46(W1):W350–5. doi: 10.1093/nar/gky300

39. Rodrigues CHM, Pires DEV, Ascher DB. DynaMut2: Assessing changes in stability and flexibility upon single and multiple point missense mutations. *Protein Sci Publ Protein Soc* (2021) 30(1):60–9. doi: 10.1002/pro.3942

40. Rodrigues CHM, Myung Y, Pires DEV, Ascher DB. mCSM-PPI2: predicting the effects of mutations on protein-protein interactions. *Nucleic Acids Res* (2019) 47 (W1):W338–44. doi: 10.1093/nar/gkz383

41. MacGowan SA, Barton MI, Kutuzov M, Dushek O, van der Merwe PA, Barton GJ. Missense variants in human ACE2 strongly affect binding to SARS-CoV-2 spike providing a mechanism for ACE2 mediated genetic risk in covid-19: A case study in affinity predictions of interface variants. *PloS Comput Biol* (2022) 18 (3):e1009922. doi: 10.1371/journal.pcbi.1009922

42. Pires DEV, Ascher DB. mCSM-AB: a web server for predicting antibody-antigen affinity changes upon mutation with graph-based signatures. *Nucleic Acids Res* (2016) 44(W1):W469–473. doi: 10.1093/nar/gkw458

43. Myung Y, Rodrigues CHM, Ascher DB, Pires DEV. mCSM-AB2: guiding rational antibody design using graph-based signatures. *Bioinform Oxf Engl* (2020) 36(5):1453–9. doi: 10.1093/bioinformatics/btz779

44. Myung Y, Pires DEV, Ascher DB. mmCSM-AB: guiding rational antibody engineering through multiple point mutations. *Nucleic Acids Res* (2020) 48(W1): W125–31. doi: 10.1093/nar/gkaa389

45. Lindorff-Larsen K, Piana S, Palmo K, Maragakis P, Klepeis JL, Dror RO, et al. Improved side-chain torsion potentials for the amber ff99SB protein force field. *Proteins* (2010) 78(8):1950–8. doi: 10.1002/prot.22711

46. Jorgensen WL, Chandrasekhar J, Madura JD, Impey RW, Klein ML. Comparison of simple potential functions for simulating liquid water. *J Chem Phys* (1983) 79(2):926–35. doi: 10.1063/1.445869

47. Zhan J, Harrison AR, Portelli S, Nguyen TB, Kojima I, Zheng S, et al. Definition of the immune evasion-replication interface of rabies virus p protein. *PloS Pathog* (2021) 17(7):e1009729. doi: 10.1371/journal.ppat.1009729

48. Kandeel M, Mohamed MEM, Abd El-Lateef HM, Venugopala KN, El-Beltagi HS. Omicron variant genome evolution and phylogenetics. *J Med Virol* (2022) 94(4):1627–32. doi: 10.1002/jmv.27515

49. Sun Y, Lin W, Dong W, Xu J. Origin and evolutionary analysis of the SARS-CoV-2 omicron variant. *J Biosaf Biosecurity* (2022) 4(1):33–7. doi: 10.1016/j.jobb.2021.12.001

50. Liu L, Iketani S, Guo Y, Chan JFW, Wang M, Liu L, et al. Striking antibody evasion manifested by the omicron variant of SARS-CoV-2. *Nature* (2022) 602 (7898):676–81. doi: 10.1038/s41586-021-04388-0

51. He X, Hong W, Pan X, Lu G, Wei X. SARS-CoV-2 omicron variant: Characteristics and prevention. *MedComm* (2021) 2(4):838–45. doi: 10.1002/mco2.110

52. Kumar S, Thambiraja TS, Karuppanan K, Subramaniam G. Omicron and delta variant of SARS-CoV-2: A comparative computational study of spike protein. *J Med Virol* (2022) 94(4):1641–9. doi: 10.1002/jmv.27526

53. Pan Q, Nguyen TB, Ascher DB, Pires DEV. Systematic evaluation of computational tools to predict the effects of mutations on protein stability in the absence of experimental structures. *Brief Bioinform* (2022) 23(2):bbac025. doi: 10.1093/bib/bbac025

54. Zeng C, Evans JP, Qu P, Faraone J, Zheng YM, Carlin C, et al. Neutralization and stability of SARS-CoV-2 omicron variant. *BioRxiv Prepr Serv Biol* (2021):2021.12.16.472934. doi: 10.1101/2021.12.16.472934

55. Hong Q, Han W, Li J, Xu S, Wang Y, Xu C, et al. Molecular basis of receptor binding and antibody neutralization of omicron. *Nature* (2022) 604(7906):546–52. doi: 10.1038/s41586-022-04581-9

56. Jawad B, Adhikari P, Podgornik R, Ching WY. Binding interactions between receptor-binding domain of spike protein and human angiotensin converting enzyme-2 in omicron variant. *J Phys Chem Lett* (2022) 13(17):3915–21. doi: 10.1021/acs.jpclett.2c00423

57. Cao Y, Wang J, Jian F, Xiao T, Song W, Yisimayi A, et al. Omicron escapes the majority of existing SARS-CoV-2 neutralizing antibodies. *Nature* (2022) 602 (7898):657–63. doi: 10.1038/s41586-021-04385-3

58. Shah M, Woo HG. Omicron: A heavily mutated SARS-CoV-2 variant exhibits stronger binding to ACE2 and potently escapes approved COVID-19 therapeutic antibodies. *Front Immunol* (2021) 12:830527. doi: 10.3389/fimmu.2021.830527

59. Hu YF, Hu JC, Chu H, Yau T, Zhang BZ, Huang JD. In-silico analysis of monoclonal antibodies against SARS-CoV-2 omicron. *Viruses* (2022) 14(2):390. doi: 10.3390/v14020390

60. Mannar D, Saville JW, Zhu X, Srivastava SS, Berezuk AM, Zhou S, et al. Structural analysis of receptor binding domain mutations in SARS-CoV-2 variants of concern that modulate ACE2 and antibody binding. *Cell Rep* (2021) 37 (12):110156. doi: 10.1016/j.celrep.2021.110156

61. Kaleta T, Kern L, Hong SL, Hölzer M, Kochs G, Beer J, et al. Antibody escape and global spread of SARS-CoV-2 lineage A.27. *Nat Commun* (2022) 13 (1):1152. doi: 10.1038/s41467-022-28766-y

62. Iketani S, Liu L, Guo Y, Liu L, Chan JFW, Huang Y, et al. Antibody evasion properties of SARS-CoV-2 omicron sublineages. *Nature* (2022) 604(7906):553–6. doi: 10.1038/s41586-022-04594-4

63. Starr TN, Greaney AJ, Stewart CM, Walls AC, Hannon WW, Veesler D, et al. Deep mutational scans for ACE2 binding, RBD expression, and antibody escape in the SARS-CoV-2 omicron BA.1 and BA.2 receptor-binding domains [Internet]. *PLoS Pathog* (2022) 8(11):e1010951. doi: 10.1371/journal.ppat.1010951

64. Starr TN, Greaney AJ, Hilton SK, Ellis D, Crawford KHD, Dingens AS, et al. Deep mutational scanning of SARS-CoV-2 receptor binding domain reveals constraints on folding and ACE2 binding. *Cell* (2020) 182(5):1295–1310.e20. doi: 10.1016/j.cell.2020.08.012

65. Hendy M, Kaufman S, Ponga M. Molecular strategies for antibody binding and escape of SARS-CoV-2 and its mutations. *Sci Rep* (2021) 11(1):21735. doi: 10.1038/s41598-021-01081-0

66. Ye G, Liu B, Li F. Cryo-EM structure of a SARS-CoV-2 omicron spike protein ectodomain. *Nat Commun* (2022) 13(1):1214. doi: 10.1038/s41467-022-28882-9

67. Giron CC, Laaksonen A, Barroso da Silva FL. Up state of the SARS-COV-2 spike homotrimer favors an increased virulence for new variants. *Front Med Technol* (2021) 3:694347. doi: 10.3389/fmedt.2021.694347

68. Wang P, Casner RG, Nair MS, Wang M, Yu J, Cerutti G, et al. Increased resistance of SARS-CoV-2 variant P.1 to antibody neutralization. *Cell Host Microbe* (2021) 29(5):747–751.e4. doi: 10.1016/j.chom.2021.04.007

69. Yin W, Xu Y, Xu P, Cao X, Wu C, Gu C, et al. Structures of the omicron spike trimer with ACE2 and an anti-omicron antibody. *Science* (2022) 375 (6584):1048–53. doi: 10.1126/science.abn8863

70. Zhao Z, Zhou J, Tian M, Huang M, Liu S, Xie Y, et al. Omicron SARS-CoV-2 mutations stabilize spike up-RBD conformation and lead to a non-RBM-binding monoclonal antibody escape. *Nat Commun* (2022) 13(1):4958. doi: 10.1038/s41467-022-32665-7

71. Yang TJ, Yu PY, Chang YC, Chang NE, Tsai YX, Liang KH, et al. Structure-activity relationships of B.1.617 and other SARS-CoV-2 spike variants [Internet]. *bioRxiv* (2021). doi: 10.1101/2021.09.12.459978v1

72. Li L, Liao H, Meng Y, Li W, Han P, Liu K, et al. Structural basis of human ACE2 higher binding affinity to currently circulating omicron SARS-CoV-2 sub-variants BA.2 and BA.1.1. *Cell* (2022) 185(16):2952–2960.e10. doi: 10.1016/j.cell.2022.06.023

73. Yu J, Collier ARY, Rowe M, Mardas F, Ventura JD, Wan H, et al. Neutralization of the SARS-CoV-2 omicron BA.1 and BA.2 variants. *N Engl J Med* (2022) 386(16):1579–80. doi: 10.1056/NEJMc2201849

74. Duan LJ, Jiang WG, Wang ZY, Yao L, Zhu KL, Meng QC, et al. Neutralizing immunity against SARS-CoV-2 omicron BA.1 by infection and vaccination. *iScience* (2022) 25(9):104886. doi: 10.1016/j.isci.2022.104886

75. Viana R, Moyo S, Amoako DG, Tegally H, Scheepers C, Althaus CL, et al. Rapid epidemic expansion of the SARS-CoV-2 omicron variant in southern Africa. *Nature* (2022) 603(7902):679–86. doi: 10.1038/s41586-022-04411-y

76. Pinto D, Park YJ, Beltramello M, Walls AC, Tortorici MA, Bianchi S, et al. Cross-neutralization of SARS-CoV-2 by a human monoclonal SARS-CoV antibody. *Nature* (2020) 583(7815):290–5. doi: 10.1038/s41586-020-2349-y

77. McCallum M, Czudnochowski N, Rosen LE, Zepeda SK, Bowen JE, Walls AC, et al. Structural basis of SARS-CoV-2 omicron immune evasion and receptor engagement. *Science* (2022) 375(6583):864–8. doi: 10.1126/science.abn8652

78. Piontkivska H, Wales-McGrath B, Miyamoto M, Wayne ML. ADAR editing in viruses: An evolutionary force to reckon with. *Genome Biol Evol* (2021) 13(11): evab240. doi: 10.1093/gbe/evab240

Frontiers in Immunology

Explores novel approaches and diagnoses to treat immune disorders.

The official journal of the International Union of Immunological Societies (IUIS) and the most cited in its field, leading the way for research across basic, translational and clinical immunology.

Discover the latest Research Topics

See more →

Frontiers

Avenue du Tribunal-Fédéral 34
1005 Lausanne, Switzerland
frontiersin.org

Contact us

+41 (0)21 510 17 00
frontiersin.org/about/contact